Dissertation
submitted to the
Combined Faculties for the Natural Sciences and for Mathematics of the
Ruperto-Carola University of Heidelberg, Germany
for the degree of
Doctor of Natural Sciences

Put forward by
Dipl.-Phys. Mario Ruckelshausen
born in Gießen
Oral examination: 25. 07. 2013

Cold-water corals: A paleoceanographic archive

Tracing past ocean circulation changes in the mid-depth subtropical western South Atlantic off Brazil for the last 40 ka BP

Reviewer: **Prof. Dr. Augusto Mangini**
Prof. Dr. Werner Aeschbach-Hertig

Contents

Zusammenfassung

Verschiedene Studien zeigen, dass die ozeanischen Zwischenwassermassen während des letzten Deglazials ungewöhnlich stark im ^{14}C abgereichert waren. Die ^{14}C-Alter liegen bei mehreren tausend Jahren im Vergleich zur Atmosphäre jener Zeit. Als mögliche Erklärung wird die Existenz eines isolierten Tiefenwasserreservoirs im Südlichen Ozean während des letzten glazialen Maximums postuliert, dessen Auflösung im Deglazial zudem große Mengen ^{14}C-armen Kohlenstoffs in Form von CO_2 in die Atmosphäre freisetzte. Die Idee eines hypothetischen Tiefenreservoirs aufgreifend werden in dieser Arbeit subfossile Kaltwasserkorallen aus dem subtropischen südwestlichen Atlantik vor Brasilien untersucht. Gekoppelte $^{230}Th/U$ und ^{14}C-Messungen ermöglichen die Rekonstruktion der Radiokohlenstoffverteilung in intermediären Tiefen für die letzten ∼40 ka BP. Die Ergebnisse zeigen, dass stark ^{14}C-abgereicherte Wassermassen auch während des mittleren Holozäns und zu glazialen Zeiten vor Beginn des Deglazials auftreten mit vergleichbaren ^{14}C-Altern anderer Studien. Des Weiteren folgt der ^{14}C-Abfall in diesen Phasen scheinbar der Zerfallskurve und untermauert die Idee einer aus dem Süden kommenden isolierten Wassermasse. Lokale Phänomene, etwa durch Austritte von kohlenwasserstoffhaltigen Fluiden am Kontinentalrand als eine mögliche Quelle geologisch alten Kohlenstoffs, können anhand stabiler Isotopenmessungen ausgeschlossen werden. Messungen der Neodymisotopie unterstreichen die südliche Herkunft des Wassers für die letzten mindestens 37 ka BP an den tiefergelegenen Korallenstandorten. Für die Korallen aus den flacheren Gebieten werden bemerkenswert große Schwankungen in der Neodymisotopie beobachtet, die mit dem Beginn der deglazialen Phase zusammenfallen aber sehr wahrscheinlich lokalen Ursprungs sind.

Abstract

Marine radiocarbon reconstructions from different intermediate depths reveal large depletions exceeding several thousand ^{14}C years compared to the contemporaneous atmosphere during the last termination. It is suggested that very old waters from a radiocarbon-deficient abyssal reservoir previously well isolated from the atmosphere during the last glacial maximum was mixed back to the upper ocean and atmosphere during the deglaciation thereby raising atmospheric CO_2. In pursuing the idea of a hypothesized isolated reservoir, measurements on sub-fossilized cold-water corals from intermediate depths off Brazil are performed. Coupled $^{230}Th/U$ and ^{14}C dates allow reconstruction of the $\Delta^{14}C$ history of the ambient seawater for the past ∼40 ka BP. It becomes apparent that large depletions in the radiocarbon content of these depths are not a phenomenon restricted to the last termination. Injection of very old waters appear during the mid-Holocene and glacial period before the onset of the last termination with depletions comparable to other studies. Local hydrocarbon seepage activity as a possible source of ^{14}C-dead carbon can be precluded as indicated by stable isotope measurements. Interestingly, ^{14}C activity decrease apparently following in part the decay curve one would expect for a closed system pointing to an isolated and continuously ageing water mass, which bathed the corals. ε_{Nd} isotopic composition indicate no significant changes of the water mass composition for the deeper coral sites for the last 37 ka BP supporting the assumption of a southern origin of the water also at times of large depletions in ^{14}C. For the shallower corals, however, ε_{Nd} exhibits large variations. It is suggested that local boundary exchange processes have altered the original Nd isotopic signature in these depths.

1

Motivation

Understanding the interplay between Earth's different compartments (ocean, cryosphere, marine and terrestrial biosphere, atmosphere etc.) is of great importance in grasping current and past climates and climate changes. As revealed by paleodata, Earth's climate was significantly distinct during the last glacial period from that of the Holocene epoch. Punctuated by millennial-scale climate shifts the last glacial period was characterized by unstable and cooler conditions compared to the relatively warm and stable Holocene (e.g. Grootes et al., 1993; Monnin et al., 2001; Jouzel et al., 2007). The reasons are manifold. Complex intertwining physical processes and feedback mechanisms are rendering the climate system tightly coupled, which behaves to a high degree non-linear. Unequivocal identification of the triggers driving the system is thus difficult (Randall et al., 2007). In addition to the ongoing proxy research and their applications to the real world, climate models have been developed. Though their future projections seem to give satisfactory outcomes in the first place, modeling attempts into the past have proven much more tedious and often did not match paleoproxy records. The reasons for that might be in part today's limited computing power, ill-constrained boundary conditions or even further physical mechanisms being not or only insufficiently described in the models (Robinson and Siddall, 2012). Providing reliable boundary conditions elicited from the paleorecords is tough but fundamental in the attempt to model aspects of Earth's climate and to gain a better understanding of the relationships governing this system. Of special interest for many paleoclimatologists is the time period of the most recent termination of the last glacial period between $\sim$11$-$19 ka BP. This vivid transition was accompanied by a sharp rise of atmospheric CO_2 concentrations concomitantly followed by a steep drop of the atmospheric $\Delta^{14}C$ among others. There is common sense that CO_2 was released from the ocean, but despite decades of paleoclimate research the exact mechanism how CO_2 was stored in the glacial ocean and deliberated again remains an unresolved issue. Previous studies have inferred a vital role for the Southern Ocean as a possible locus for the deglacial CO_2 release (e.g. Francois et al., 1997; Sigman and Boyle, 2000; Anderson et al., 2009). Discovered ^{14}C

anomalies in intermediate-depth waters at various locations seem to have witnessed the demise of a poorly ventilated abyssal reservoir presumably located in the Southern Ocean region (Marchitto et al., 2007; Bryan et al., 2010; Mangini et al., 2010). Disintegration of a formerly isolated carbon-rich reservoir could have been in part responsible for the observed ^{14}C anomalies as well as for the rise in atmospheric CO_2 (Broecker and Barker, 2007). But this idea is far from being accepted and there is a lot of controversy about the existence of such a reservoir during glacial times (see Hain et al. (2011) and references therein).

In pursuing the reservoir hypothesis this thesis provides paleoceanographic data obtained on cold-water corals from intermediate depths off Brazil covering the last ∼40 ka BP. Most cold-water coral studies stem from the North Atlantic, whereas the South Atlantic/ Atlantic sector of the Southern Ocean was put in second place for many years. Our picture from the paleoceanography in this region is, therefore, by far more incomplete than for the north. Corals have proven to be suitable archives for paleoceanographic studies since their aragonitic skeletons allow precise dating with $^{230}Th/U$ and record a wealth of distinct proxies and water mass tracers among them ^{14}C and neodymium. The intermediate-depth location off Brazil was chosen as a promising place to study the history of different water mass tracers as this depth is in the direct reach of southerly-derived Antarctic Intermediate Water. Variations in circulation and/or changes of the water mass composition within the Southern Ocean are expected to reveal also off Brazil. Previous ^{14}C investigations on cold-water corals from Brazil have shown large depletions in the ^{14}C content of the ambient water between ∼8−27 ka BP. But not all questions in this study could be addressed: Are there further ^{14}C anomalies before 8 ka BP or beyond 27 ka BP? If so, are they related in timing to major climate events? How long lasted the observed ^{14}C depletions in the intermediate depth? Were these times accompanied by low oxygen levels even anoxic conditions in the surrounding seawater? How large was the water depleted in ^{14}C in respect to the atmospheric ^{14}C record? Is the timing of the ^{14}C depletions in accordance to other ^{14}C studies from intermediate depths? Did the depleted water off Brazil contributed to the rise in atmospheric CO_2. What can be derived about the origin of the in part extremely ^{14}C-depleted water? Is the idea of an alleged deep-ocean reservoir flushing the mid-depth off Brazil viable? To tackle all these questions properly, it would be necessary to substantially increase the number of coral samples from this oceanic region to obtain a precise picture of the ^{14}C history in the intermediate water. Additional Nd isotope measurements on the corals will deliver supporting informations on the characteristics of the ambient water during coral formation and will potentially allow to determine the origin of the water especially at times of massive ^{14}C depletions. This multi-proxy approach will help refining our current understanding of the past oceanography in this region and will hopefully deliver some further insights about the unresolved issue regarding deep-water reservoirs on a glacial-interglacial timescale.

Part I

Introduction

„What we know is a drop, what we don't know is an ocean. "

Isaac Newton

2

Ocean circulation

The world ocean constitutes an important key in grasping Earth's climate system. It is able to store and transport huge amounts of heat, nutrients, and also carbon thereby modulating climate. As the largest carbon reservoir it poses a crucial sink and source for the most important greenhouse gas, videlicet CO_2. By sequestering and storing CO_2 in the deep ocean interior for centuries or even thousands of years and the subsequently release, the ocean is able to significantly modulate atmospheric CO_2 concentrations. As revealed in Antarctic ice cores, atmospheric CO_2 dramatically fluctuated over the past several hundred thousand years in close concert with glacial-interglacial cycles. The last glacial termination, for instance, was accompanied by a CO_2 increase of about 80 ppmv indicating substantial variances in the marine carbon cycle intimately linked with changes in ocean circulation. The ocean circulation is playing an important role in influencing Earth's climate by redistributing large amounts of heat stored in the water. This is shown by many paleorecords suggesting severe shifts in atmospheric circulation with dramatic consequences in Indian and African monsoon rainfall or changes in climate for Western Europe. For that reason some word must be said about ocean circulation.

About 71% of Earth's surface is covered by ocean water, that is, most of the energy Earth received from the sun is withhold in the upper ocean. As water has a five to sixfold higher heat capacity than the continents (consisting of rocks), the ocean constitute an seemingly inexhaustible heat reservoir. To emphasize the importance of this reservoir it is pointed out that the total amount of thermal energy within the first two to three meters of the ocean surface is equal or larger than the total energy stored in the atmosphere! This heat is continuously redistributed by ocean currents at all latitudes over thousand of kilometers and for the most part released back in form of latent heat (Rahmstorf, 2002). To illustrate the effects: the temperature difference between summer and winter in the mid-latitudes is about 8 °C across the sea compared to several 10 °C within the continental interior (Rahmstorf, 2002). Europe, in particular, benefits from this energy redistribution.

The power, Europe gains from the Gulf Stream and the North Atlantic Current, respectively continuing the Gulf Stream northeast, is on the order of 1 PW (peaking with 1.2 ± 0.3 PW at 24 °N) contributing to the mild climate in northwestern Europe (Ganachaud and Wunsch, 2000). The heat is released and transported by winds across the European continent leading to temperature rises by as much as 10 °C as compared to other locations on the same latitude (Rahmstorf, 2002). But not only the regional climate would be affected by absence of any heat transport into the north. As a consequence enhanced formation of sea ice in the North Atlantic could take place and by this might alter Earth's albedo and thus the global radiation budget.

2.1 Atlantic meridional overturning circulation

The large-scale ocean circulation consists of a series of currents driven either directly by wind stress, exerted on the ocean surface reaching down to a couple of hundred meters or currents driven by density gradients created by transport of surface heat and freshwater into the ocean interior and subsequent turbulent mixing of heat and salt (Rahmstorf, 2002). A third driving force arises from the gravitational pull of the Moon and the Sun. In the Atlantic Ocean surface currents like the Gulf Stream and the North Atlantic Drift continuing the Gulf Stream eastward, transport warm and saline water from the tropical and subtropical region poleward into the high North Atlantic region. On its way to the north the surface water gradually cools thereby becomes denser though freshwater input due to precipitation takes place en route. The Norwegian and Greenland Sea north of Iceland are considered to be important deep water formation areas where surface water is losing its neutral buoyancy and eventually sinks to large depths forming North Atlantic Deep Water (NADW). This water mass overflows the Greenland-Scotland ridge and spreads as a deep western boundary current towards the South Atlantic (Dickson and Brown, 1994). As it moves it is supplemented by deep water formation in the Labrador and Mediterranean Sea (Sarmiento and Gruber, 2006) (Fig. 2.1). The geometry of this NADW is quite impressive: depending on the location where to look it can reach a thickness of up to 2 km and widths of up to 800 km. Average velocities are in the range of several centimeters per second (Viana et al., 1998). Among other properties NADW stands out as a tongue of water of high salinity and oxygen concentration, low nutrient content, and a high $^{14}C/^{12}C$ ratio (Broecker, 1991). Further contributing factors driving the circulation in the Atlantic basin is the wind-induced Ekman upwelling in the Southern Ocean allowing deep water to reach at or near the ocean surface. Taken together, the establishing overturning circulation cell in the Atlantic is commonly known as Atlantic meridional overturning circulation (AMOC) and constitutes an important part of the considerably larger global conveyor circulation. See Fig. 2.1 for a schematic view of the circulation on a global scale operating in today's ocean. Though the driving forces of the AMOC are adequately known they are interacting in a non-linear way so that no unique decomposition exists (Rahmstorf, 2002). Hence, the AMOC is usually depicted as a meridional cut representing a zonally averaged water mass

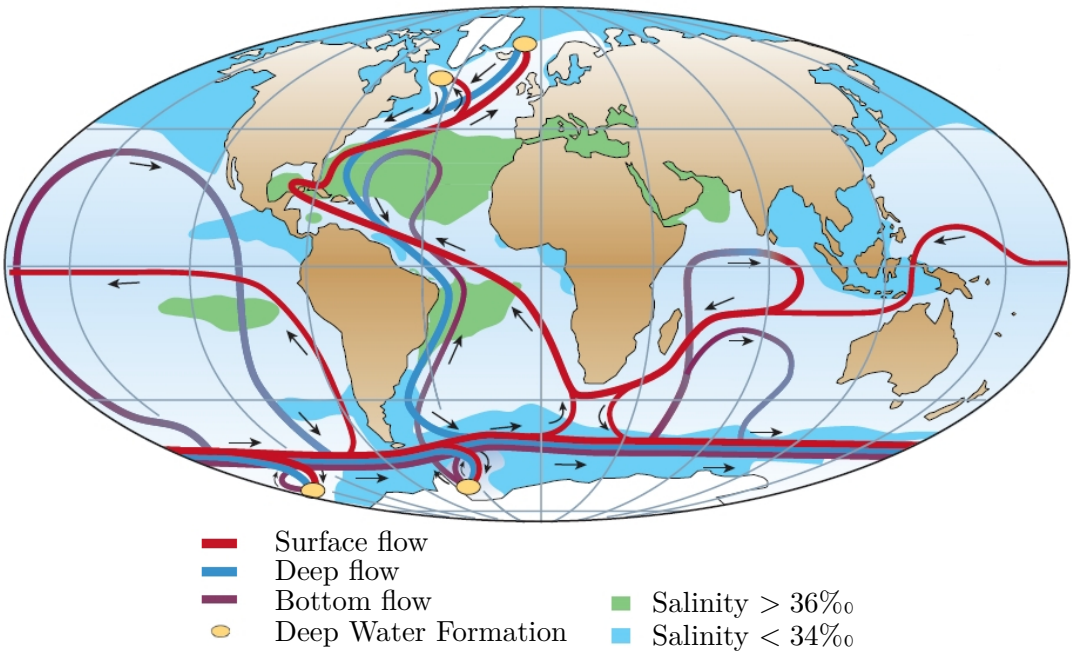

Fig. 2.1: Simplified representation of the global conveyor circulation. Surface currents are shown in red, deep water in light blue and bottom water in dark blue. Arrows indicate flow directions. Note the higher saline water in the Atlantic compared to the Pacific Ocean resulting in absent deep-water formation in the North Pacific. The Indian Ocean is restricted to the north by the Indian subcontinent which impedes deep-water formation as well. A recent study from Fukamachi et al. (2010) has shown a further formation site of deep water east of the Kerguelen islands, not shown. Also forming deep water in the Mediterranean Sea is contributing to the shallower part of NADW, not shown either. Figure modified from Rahmstorf (2002).

comprising a superposition of wind-driven and thermohaline components as shown in Fig. 2.2 (Kuhlbrodt et al., 2007). Another deep-water formation area driving the AMOC is located around the Antarctic continent. Deep water is descending within the Weddell and Ross Sea forming so-called Antarctic Bottom Water (AABW) occupying the deepest parts of the Southern Ocean, which spreads along the seafloor of all ocean basins (Killworth, 1983). In the Indian Ocean, for instance, AABW returns a little later as a near surface water flowing in part back as a surface current into the Atlantic (Fig. 2.1). Different from the genesis of NADW, AABW originates either to intensive evaporation usually taking place within so-called polynyas (areas of open water surrounded by sea ice) or more typically during sea ice formation fractionating salt by brine rejection, which lead to high seawater salinity (Adkins et al., 2002b). All branches of the conveyor circulation also dubbed as thermohaline circulation are connected with the fast moving Antarctic Circumpolar Current (ACC) encircling the Southern Ocean. The ACC is acting as a giant blender strongly mixing the various joining water masses in a short period of time until they cannot be distinguished any more. For instance, NADW has lost its distinct water mass properties

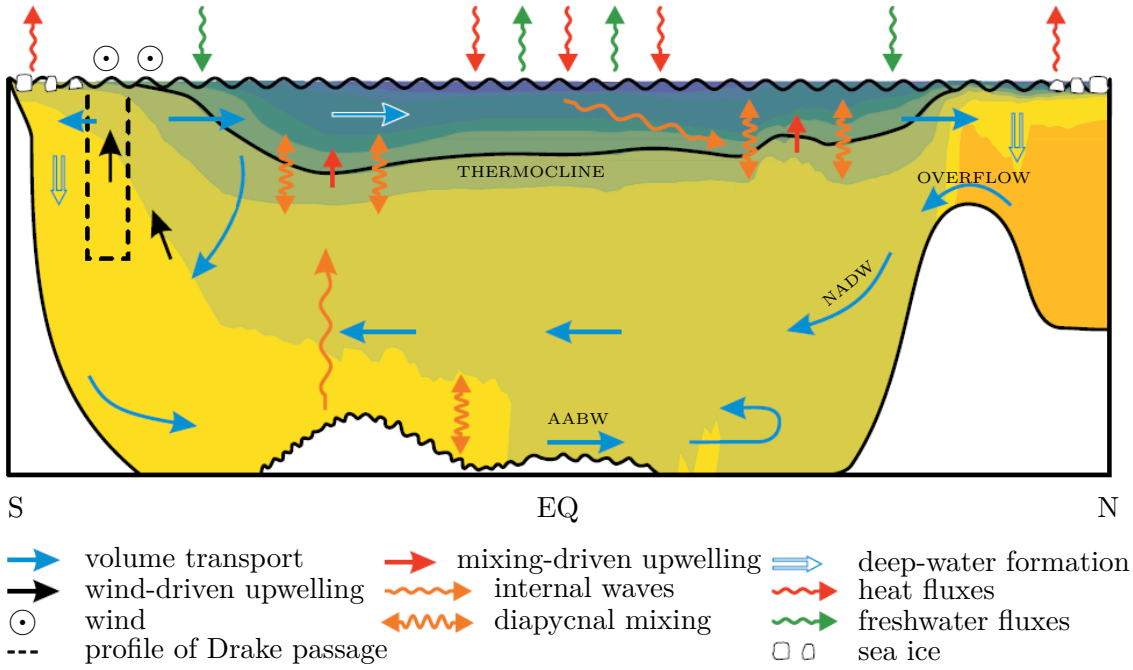

Fig. 2.2: Blue arrows show the flow directions of the AMOC. Color shading illustrates the density stratification of the seawater, zonally averaged from observational data with AABW (yellow) being the densest water mass and lightest water in blue. The most important fluxes and mixing processes are shown. In the Southern Ocean, westerly winds cause northward oriented Ekman transport resulting in upwelling of deep waters. Figure modified from Kuhlbrodt et al. (2007). See Kuhlbrodt et al. (2007) for a more comprehensive description.

after it half encircled the Antarctic continent (Broecker, 1991). All discrete locations of deep water formation are the only ones existing in today's ocean. The Pacific lacks any comparable deep water as the sluggish flowing NADW. A possible reasons for that might be the apparent twice as high observed evaporation rate in the Atlantic compared to the Pacific as assessed by Baumgartner and Reichel (1975) (103 cm/year versus 55 cm/year) and the concomitant salinity contrast between North Atlantic surface water to those at comparable latitudes in the North Pacific (the difference in salinity amounts to 2−3 g/l). As pointed out by Broecker (1991) this salinity contrast is so severe that even North Pacific water if cooled to near its freezing point (−1.8 °C), would sink only to depths of several hundred meters making it impossible to form deep water. In the Indian Ocean, simply the location of the Indian subcontinent in the subtropics prevents any deep water formation (Brown et al., 1989). It is important to note that the concept of a conveyor circulation envisioned in Fig. 2.1 is hardly likely. There is no simple and closed world-spanning circulation which can easily traced back by tracer experiments. There are a lot of circulation branches not shown in this picture on which extensive mixing processes with the ambient seawater might occur, not to mention intersecting currents. Though aspect of this global circulation might be

true many aspects are until today subject to current research and are not well understood.

2.2 AMOC during the last glacial period

As outlined above the highest surface densities in the ocean are reached where water becomes densest. The AMOC is primarily thermally driven despite the lower salinity of the surface water in the deep water formation regions compared to the subtropical area (Fig. 2.1). Nevertheless, the salinity is playing an important role because it lead to a surprising non-linearity behavior of the overturning circulation. Changes in salinity accounts for a positive feedback in the sense that more saline surface water in the formation regions is amplifying the circulation strength thereby transporting even more saline waters

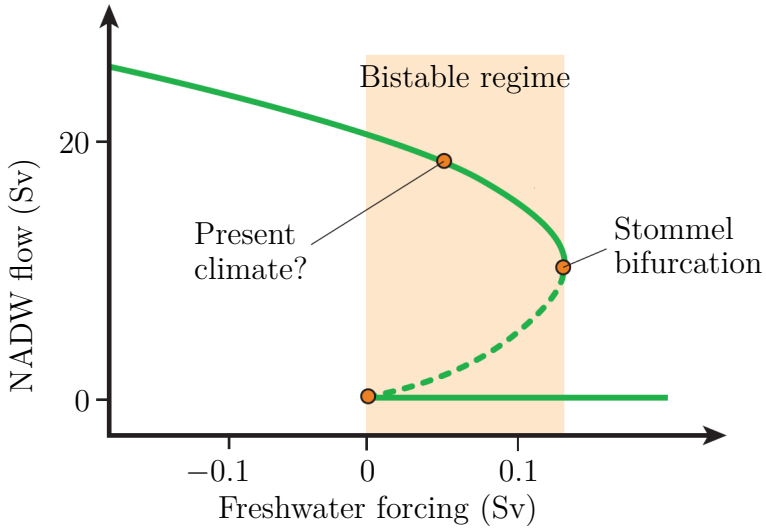

Fig. 2.3: Steady-state thermohaline driven circulation strength (flow rate) of NADW as a function of the freshwater input (forcing) into the North Atlantic as a solution of simple box model considerations of Rahmstorf (1996). The dashed line is an unstable solution. Pushing the freshwater input beyond a critical point (Stommel bifurcation) lead to two stable equilibrium states, with and without NADW formation, posing the question of the stability of current deep water circulation in the Atlantic. Figure modified from Rahmstorf (2002).

in these regions (Rahmstorf, 2002). As deep water formation areas are characterized by a net precipitation, freshwater at the surface would accumulate and salinity would drop if circulation slowed down or stopped. A more thoroughly investigation of this thought experiment culminates into a mathematical relation connecting the freshwater input (forcing) with the circulation strength of the NADW. The solutions of this quadratic equation suggest that the circulation strength behaves nonlinearly and can take on two possible equilibrium states, with and without NADW with a well defined

threshold in between (Stommel bifurcation) (Fig. 2.3) (e.g. Stommel, 1961; Manabe and Stouffer, 1993; Rahmstorf, 2002). This interesting feature of the thermohaline part of the AMOC has been confirmed and extensively investigated in various climate models and might play a crucial role in understanding and explaining past climate changes. A wealth of ocenographic data from paleorecords suggests that past circulation in the Atlantic Ocean has significantly changed during the glacial period. The existing paleoceanographic data allow to draw a picture of three distinct modes of circulation, which prevailed in the last 120,000 years in the Atlantic. These modes have been dubbed as interstadial, stadial, and Heinrich mode (Rahmstorf, 2002). Fig. 2.4 illustrates the three modes. The rise in the bottom topography in Fig. 2.4 marks the shallow Greenland-Scotland ridge. Today's circulation is equal to the interstadial mode or modern mode (Warm). Deep-water formation takes place in the deep basins to the north of Iceland (Nordic Seas) through open-ocean convection followed by overflowing of the shallow sill. AABW is penetrating the deeper parts of the Atlantic towards north. However, the situation was much different during the glacial times (Cold), when deep water formation zones presumably have shifted towards the subpolar Atlantic region south to Iceland (Irminger Sea). NADW was replaced by shallow Glacial North Atlantic Intermediate Water (GNAIW), which occupied depths less than 2,500 m (Labeyrie, 1992) thereby allowed AABW to shallow significantly. During the Heinrich mode (Off), NADW formation presumably ceased due to iceberg surges and associated freshwater input from the Laurentide ice sheet through Hudson Strait, which is thought to have destabilized deep-water formation. As a consequence, dominant southern-sourced water (AABW) filled the deep Atlantic basin to depths as shallow as 1,000 m (Sarnthein et al., 1994; Rahmstorf, 2002).

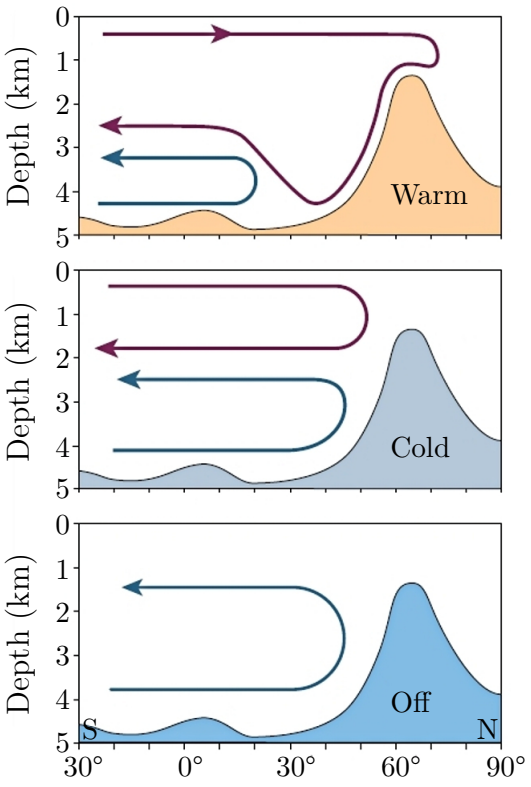

Fig. 2.4: Prevailing circulation modes in the Atlantic Ocean during the last 120 ka. Picture modified from Rahmstorf (2002).

2.3 Heinrich events

Heinrich events are characterized by enhanced ice-rafted detritus (IRD) found in North Atlantic sediment cores. Their timing is in good accordance to the pattern of millennial scale climate fluctuations of the last glacial period as derived from ice cores and other paleorecords (Bond et al., 1993). Heinrich events show an apparent cyclicity of about 6,000−7,000 years (Kirby and Andrews, 1999) and usually lasted about 500 ± 250 years (Hemming, 2004). During these events large amounts of icebergs, presumably released from the Laurentide ice shield (LIS) were transported across the northeast Atlantic Ocean (Heinrich, 1988; Bond et al., 1992). The detritus trapped within the ice were carried along across the Atlantic and deposited to the ocean sediments when ice melted. Geochemical investigations of the sediment layers point to the region around the Hudson Strait as the major trough draining the eastern portion of the LIS by releasing an "iceberg armada" (Broecker et al., 1992; Hemming, 2004). But the cause of these iceberg discharges restricted to the last glacial is still a matter of debate. One explanation attempt put forward by MacAyeal (1993) is the binge-purge model. According to this hypothesis, the LIS reached a critical volume due to ongoing accumulation of ice. At some point the ice volume was thick enough so that geothermal heat penetrating the ice from the bottom could not escaped into the atmosphere anymore, which led to melting ice at the bottom of the ice shield. Lubrication by water facilitated the collapse of the LIS or parts of it, which finally lead to the release of icebergs into the North Atlantic. Fig. 2.5 depicts an example of three sediment cores from the North Atlantic showing distinct Heinrich layers (ice-rafted debris (IRD). The thickness of these layers usually increase in the direction of the Hudson Strait from typically ∼1 cm in the eastern North Atlantic up to ∼50 cm near the Hudson Bay (Andrews et al., 1994). So far, six distinct layers have been identified in North Atlantic sediments, which are attributed to Heinrich events, labeled H1-H6 from youngest to oldest (Bond et al., 1992). Some authors consider the Younger Dryas (YD) as a further Heinrich event (H0)

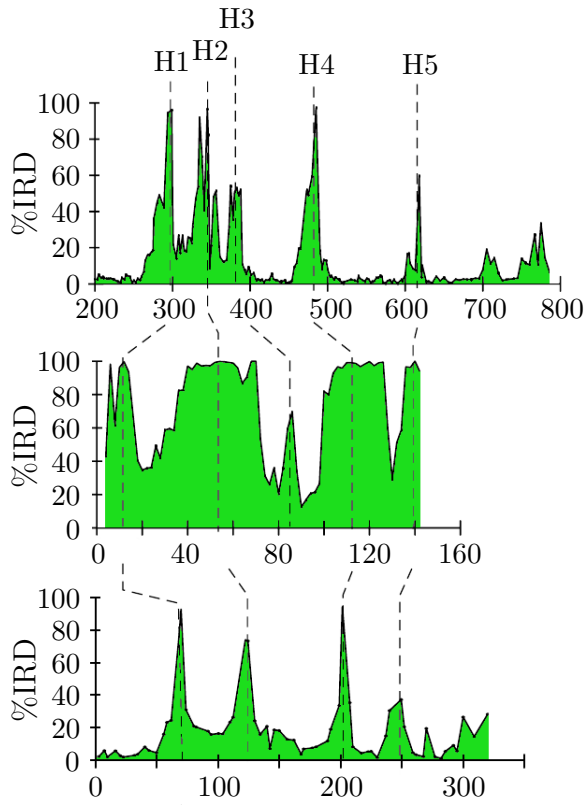

Fig. 2.5: Stratigraphy of some North Atlantic sediment cores exhibiting Heinrich layers (H1-H5). %IRD here is defined as the ratio of lithic grains (> 150 μm) to the total number of entities in the sediment. Picture modified from Hemming (2004).

(Andrews et al., 1994; Broecker, 1994) even though it does not show up in Fig. 2.5. During these extreme events, a staggering amount of fresh water was introduced into the glacial ocean and very likely helped to destabilize deep water formation. According to model estimates the fresh water flux during H4 has been estimated to 0.29 ± 0.05 Sv (Roche et al., 2004). Several dynamical ocean model results give reason to surmise that the AMOC is sensitive to freshwater perturbations on the order of only 0.1 Sv (Stocker and Wright, 1991; Manabe and Stouffer, 1997).

3

Cold-water corals

3.1 Habitat and distribution

In the last three decades it has become apparent that corals, once thought to be restricted to shallow waters in tropical and subtropical regions, are ubiquitous in all oceans on virtually all latitudes and depths (Wilson, 1979a). This discovery, well beyond the reach of scuba diving, was made possible by using new underwater techniques. Remotely operating vehicles and manned submersibles are allowing exploration of never before seen deep-water environments, where so-called cold-water corals thrive. Corals belong to the class anthozoa, a subset within the phylum cnidaria. Most corals are sessile and colony-forming animals of which the order scleractinia (scler = hard, actinia = ray; stony corals) is for the purpose of this work the most important one to mention. Scleractinia are able to form skeletons composed of calciumcarbonate forming reefs or reef-like structures both in shallow and deep waters. Warm-water corals can build vast reefs structures, which sometimes can be seen even from outer space.

These reefs are usually confined within the 20 degree centigrade isotherms between ∼30° N and ∼30° S. Cold-water corals, however, do not show this spatial restriction (see Fig. 3.1). Over 5,100 coral species today are known to inhabit the world's ocean of which about 65% live in cold-water environments (Cairns, 2007; Roberts et al., 2009). Their depth distribution is eurybathic ranging from the relatively cold and shallow waters (40 m) of the high northern and southern latitudes to the abyssal ocean (6,328 m) (Keller, 1976; Cairns and Stanley, 1981). Because they usually live below the photic zone they are also referred to as deep-water corals. In contrast to warm-water corals cold-water corals do not harbor any endosymbiotic and phototrophic algae (zooxanthellae) living inside the cells of the polyp's gastroderm. Tropical shallow-water corals benefit from the symbiotic relationship with the algae, which provides the coral with nutrients and helps facilitating the biomineralization of its skeleton (Gattuso et al., 1999). The magnificent colors tropical corals exhibit are a side

product of this connection. By contrast, cold-water corals do not exhibit such a variety of colors. The polyps of cold-water corals can reach sizes up to several centimeters in diameter living at the outermost part of the skeletons on top of a cup-like structure called a corallite. According to Sherwood (2007, p. 495), the corallite is 'supported by a thin horizontal plate called the dissepiment' and '... is lengthened by periodic uplift of the polyp and formation of a new dissepiment.' Like their tropical-living counterparts they are also able to grow large three-dimensional reef-like structures even if the majority are non-constructing and solitary living species. One major framework builder is the cosmopolitan cold-water coral *Lophelia pertusa*. Fig. 3.2 depicts a large *L. pertusa* framework in its natural environment

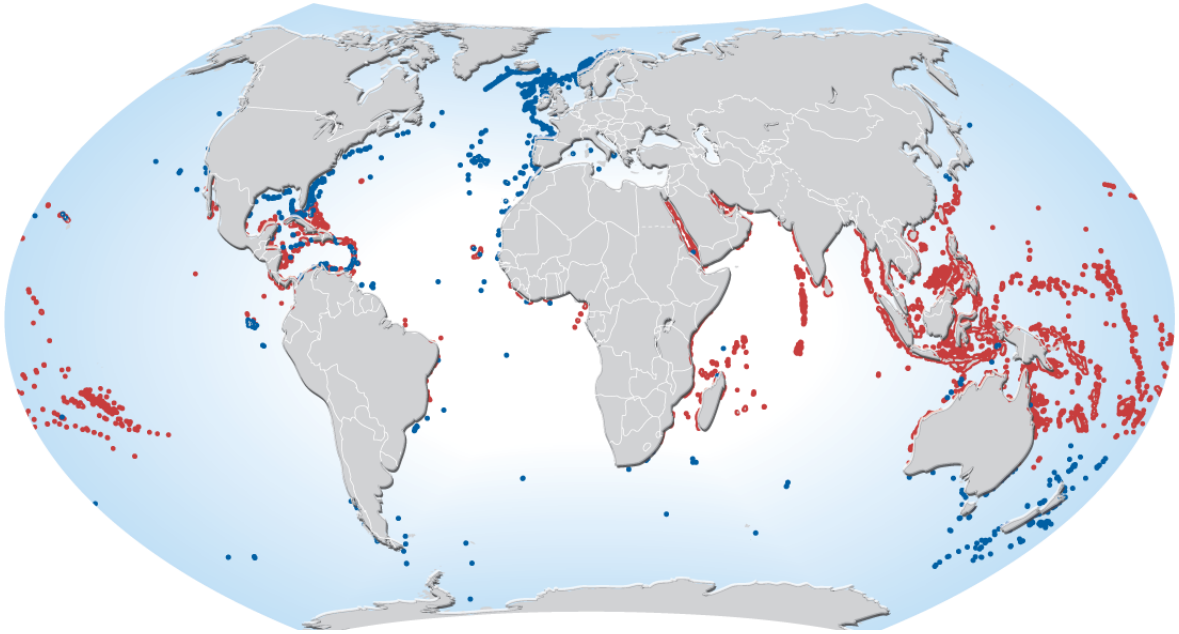

Fig. 3.1: Recent distribution of warm-water (●) and cold-water corals (●). Warm-water reefs are usually confined within the 20 degree centigrade isotherms between ∼30° N and ∼30° S. Cold-water corals, however, do not show this spatial restriction. Picture available online at `http://www.grida.no/graphicslib/detail/distribution-of-coldwater-and-tropical-coral-reefs_1153`, UNEP World Conservation Monitoring Center (2013), Hugo Ahlenius, UNEP/GRID-Arendal. Accessed 2013/4/23.

occurring at the Blake Plateau off the southeastern coast of the US in 450−1,000 m water depth. The largest coherent *L. pertusa* structure discovered so far in 2002 has an expanse of ∼120 km^2 located west of Røst island in the Lofoten archipelago, which beats the previous record holder covering already ∼100 km^2 (Wilson, 1979b). Reef-like cold-water frameworks are usually found along continental slopes, shelf breaks, fjords, bedrock outcrops, volcanic mid-ocean ridges, offshore submarine banks, and artificial structures like oil rigs (Rogers, 1999). Only the uppermost part of such a reef-like structure is alive and covered with living

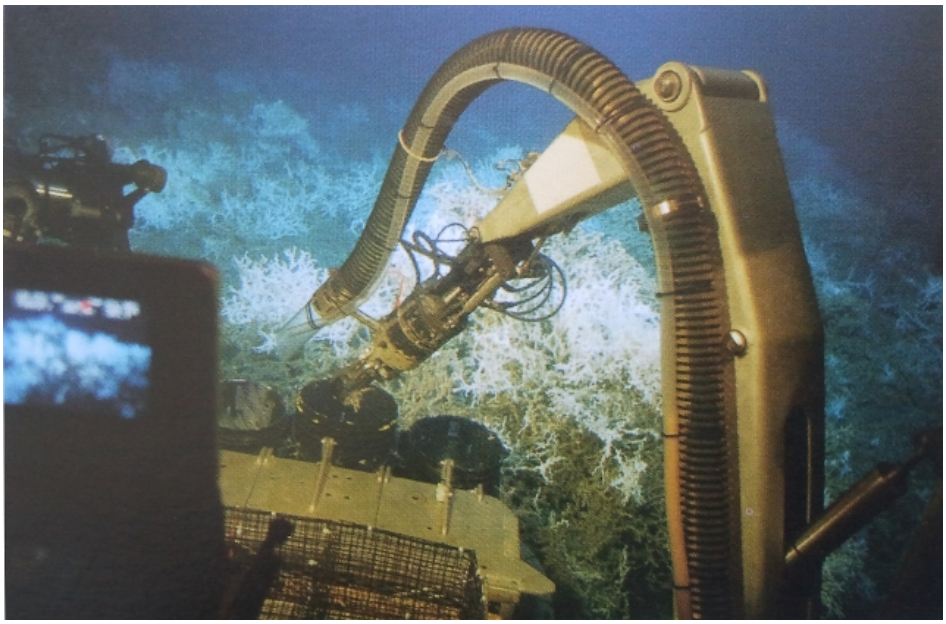

Fig. 3.2: Manned submersible taking samples from a *L. pertusa* framework at the Blake Plateau off Florida. Only the uppermost part of this coral framework is alive (white parts) and covered with living tissue hosting thousands of polyps. Picture from Roberts et al. (2009).

tissue hosting thousands of polyps (cf. Fig.3.2 the white parts of the *L. pertusa* framework), the lower sections are dead (brown) and are exposed to erosion. The dead coral scaffold often acts as a sediment trap strengthening the whole structure further while the living part grows aloft reaching heights up to several hundred meters (DeMol et al., 2002). This build-up is a steady process which takes up to several millennia. The resulting structure is then called a carbonate mound. Though some cold-water coral species are becoming rather old, a couple of hundred years (Andrews et al., 2002; Risk et al., 2002), their growth rate is much slower than for the tropical ones. Observed rates are roughly between 0.24−25 mm/a (Mortensen and Rapp, 1998; Brooke and Young, 2009) versus 100−200 mm/a for branching tropical species (Buddemeier and Kienze, 1976). Even though deep-water coral ecosystems are apparently discontinuously distributed and more patchy than the tropical reefs, their predicted global coverage exceeds by far the tropical ones (Freiwald and Roberts, 2005). Also, deep-water ecosystems seem to be biodiversity hotspots forming valuable nursing grounds and provide shelter for many marine species (Roberts et al., 2006). Cold-water reef systems are in this respect in no way inferior to their tropical counterparts.

3.2 Environmental controls on coral growth

Still little is known concerning the environmental controls responsible for the distribution of scleractinian cold-water corals. It appears that a variety of parameters such as temperature, salinity, current strength, local geomorphic setting, food supply, and even the substrate of the seafloor are influencing the distribution (Hovland et al., 2002). The oxygen and nutrient availability and supply have a major impact as well as the aragonite saturation. Hydrostatic pressure, however, seems to play a secondary role. This becomes evident for some species, which have been found in rather shallow water (< 40 m) in high latitude regions, rendering other aspects seemingly more important than pressure (Freiwald et al., 2004). A recent study from Dullo et al. (2008), however, indicates that (potential) density might have after all an impact on the distribution of species *L. pertusa* in the northeast Atlantic region. The study has shown *L. pertusa* frameworks on the Celtic and Norwegian margin thrive in waters with a potential density range between $\sigma_\Theta = 27.35-27.65$ kg/m^3 Dullo et al. (2008). The authors argue that this potential density range might be a basic prerequisite for reef development along the continental margin as this potential density range appears to promote larvae dispersal of *L. pertusa* (Dullo et al., 2008). This idea is picked up in section 6.6.2. Cold-water corals are suspension feeders equipped with tentacles nourishing from food particles they capture from the ambient water. Fig. 3.3 shows a close-up of a *L. pertusa* colony with expanded tentacles. Though their diet is mostly uncertain they presumably live on organic matter and zooplankton even small pelagic crustaceans (Henrich et al., 1997). Enhanced currents in these environments seem to play a crucial role in generating preferred conditions for a possible coral settlement. On the one hand currents are responsible for the food supply on the other hand hamper fast sediment smothering (Roberts et al., 2009). Known cold-water coral species are stenothermic, tolerating temperatures only between $4-13$ °C but are able to tolerate lower temperatures for short periods of time (Bett, 2001; Freiwald, 2002). In contrast, they are able to tolerate relatively wide salinity ranges comprising $32-38.8$ psu, which are observed in the Ionian Sea and in Scandinavian fjords (Taviani et al., 2005).

Fig. 3.3: Close-up of a living colored variety of a *L. pertusa* colony with expanded tentacles actively catching organic matter and zooplankton. The color is caused by the coral's organic tissue. Figure from (Roberts et al., 2009).

3.3 Corals as a paleoceanographic archive

In the last two decades cold-water corals have become an indispensable mean in paleoceanography and paleoclimate research. This success comes not by chance. Whether or not marine sediments or shell-secreting organisms, like corals, come into question as a paleo-environmental archive depends on if they faithfully record environmental signals of climatic significance. A wide geographical distribution is also useful as well as an insensitivity for external perturbations. Unlike marine sediments, which can be smeared by the activity of ocean bottom dwellers, making it at times impossible to get reliable proxy data, corals do not show this drawback. They provide a paramount archive for a whole variety of (geo)chemical tracers and proxy informations (to name but a few: ^{14}C, ^{143}Nd/^{144}Nd, Cd/Ca, ^{13}C, ^{18}O, Li/Mg, Sr/Ca, Mg/Ca etc.) preserved in their calcareous skeletons. Their annual to decadal resolution, spanning several centuries for solitary and several decades for branching scleractinians such as for *L. pertusa* (Druffel et al., 1990; Freiwald et al., 2004) facilitate to document even rapid climate changes (Adkins et al., 1998; Robinson et al., 2005). For instance, like the annual rings in trees, tropical reef corals and some cold-water species show visual growth bandings deposited annually. Even growth rings at a finer scale have been documented, which are apparently related to the lunar cycle. The growth layers for cold-water corals can be rather narrow (10−100 μm (Lazier et al., 1999)) making sampling on an annual level difficult. Since they usually have a more complicated morphology than their shallow-water counterparts ring discrimination is in addition more catchier. Fig. 3.4 depicts an example of annually deposited incremental growth rings in a young (∼30 year old) skeleton from a *Primnoa resedaeformis* cold-water coral colony collected in the northwest Atlantic from depths between 250 m and 475 m (Sherwood et al., 2005). The arborescent skeleton composes of calcite and gorgonin[1] rather than aragonite. It was possible to sample single growth rings for ^{14}C analysis from *P. resedaeformis* from seven different colonies. The results are shown in Fig. 3.5 as Δ^{14}C plotted against the counted ring age. The sharp rise in the mid-ocean's Δ^{14}C distribution at this location due to atmospheric input of ^{14}C through aerial A- and H-bomb testing in the 1950s to mid-1960s are clearly visible. As a matter of fairness, however, it must be mentioned that interpretation of growth banding in

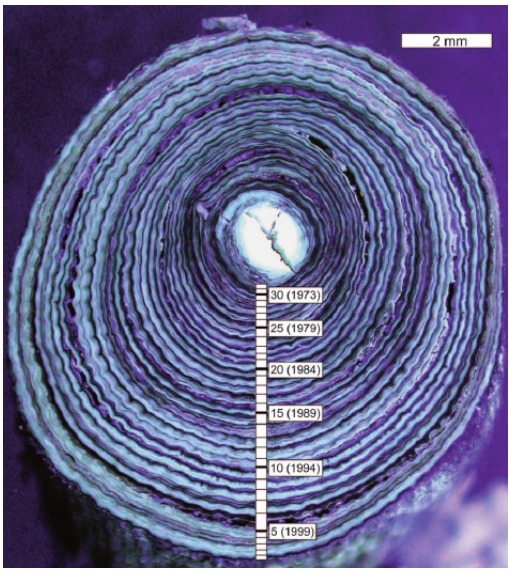

Fig. 3.4: Annual growth rings in a young (∼30 year old) *P. resedaeformis* cold-water coral. Picture from (Sherwood et al., 2005).

[1]Gorgonin is a skleroprotein, which helps to stabilize the skeleton.

cold-water corals is not always that easy and a reliable chronometer since many species do not show a visual banding, which is in part due to the lack of a strong seasonality in the deep-water environments. Hence, ring growth is mostly far less pronounced than in shallow-water corals (Adkins et al., 2004). This being the case, radiometric dating methods will still be the first choice in establishing absolute ages or chronologies. In recent years a wealth of other tools have been developed especially for reconstructing past sea surface temperatures (SST), the key holder in understanding climate and climate changes. In the early 1950s, Epstein et al. (1953) demonstrated that during secretion of carbonate skeletons of some marine invertebrates like molluscs, isotopic oxygen composition is the same as if precipitation had occurred inorganically under equilibrium conditions. During this process oxygen isotopes (^{18}O, ^{17}O, ^{16}O) become slightly fractionated when precipitating from a calcifying fluid compared to the ambient seawater isotopic composition. This fractionation[2] is on the order of several per mille and closely related to seawater temperature and its isotopic composition. In general, δ^{18}O of marine carbonates increases with decreasing seawater temperatures and vice versa (Mook and de Vries, 2000). The isotopic variations in δ^{18}O can be measured with high precision and are used to reconstruct paleo-seawater temperatures (e.g. McCrea, 1950; Emiliani, 1955; Shackleton, 1974). This method, however, is limited by the variability of the surface seawater δ^{18}O, usually relatively constant during the course of a year, can significantly be influenced in areas of high rainfall or evaporation and river input. Though, this technique works in principle for shallow-water corals and deep-sea corals too, it is more difficult to obtain reliable data. Applicability of the isotopic thermometer for scleractinians is marred by the fact that precipitation of $CaCO_3$ is moreover influenced by the metabolism of the polyp, which is accountable for an observed disequilibrium in the aragonite δ^{18}O relative to inorganically precipitated aragonite (Mikkelsen et al., 1982; Spiro et al., 2000). Thus stable oxygen isotope values are not directly linked to temperatures. This feature is referred to as vital-effect and is not well understood until today (Shirai et al., 2005). In any case species dependent calibration slopes of temperature-δ^{18}O-isotopic-fractionations under experimental conditions and/or in field experiments must be carried out. As deep-water environments show relatively stable conditions oxygen isotope ratios of

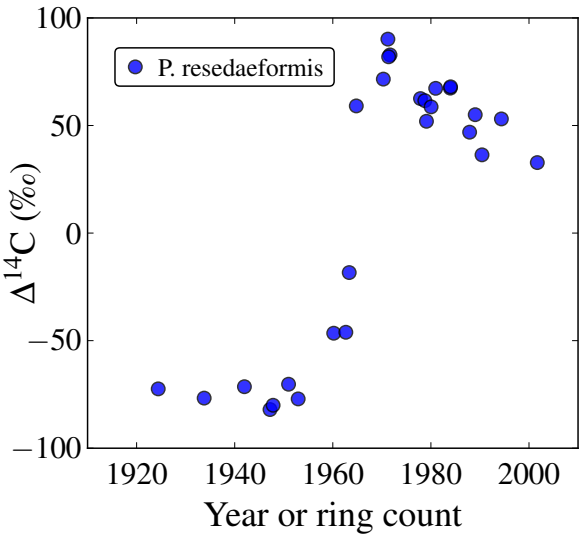

Fig. 3.5: Recorded bomb-^{14}C versus age in cold-water corals from the northwest Atlantic. Figure modified from Sherwood et al. (2005).

[2]... normally expressed as $\delta^{18}\mathrm{O} = (({}^{18}\mathrm{O}/{}^{16}\mathrm{O})_{\mathrm{coral}}/({}^{18}\mathrm{O}/{}^{16}\mathrm{O})_{\mathrm{VPDB}} - 1) \cdot 1000$ ‰.

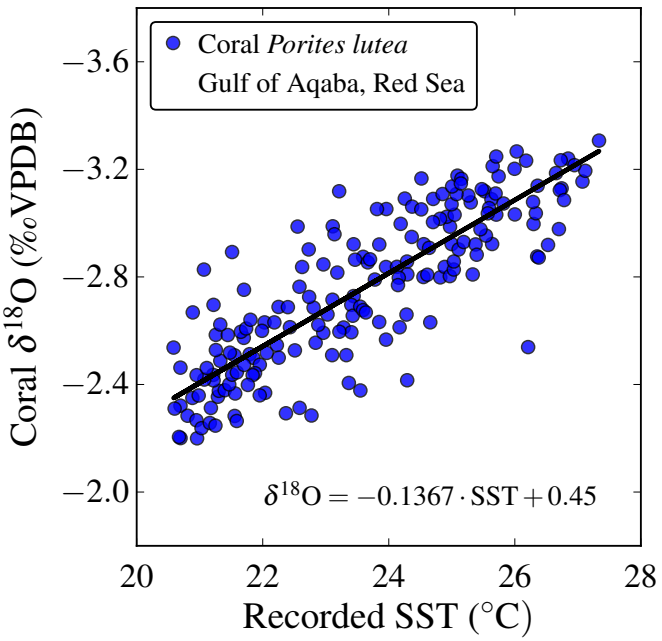

Fig. 3.6: Relation between SST and skeletal $\delta^{18}O$ from shallow-water corals of species *Porites lutea* together with regression line. Picture modified from Al-Rousan et al. (2007).

cold-water corals are even more influenced by vital effects (Rollion-Bard et al., 2010). For illustration Fig. 3.6 shows an example of a measured calibration curve for the warm-water coral *Porites lutea* from the northern Gulf of Aqaba (Red Sea), which reveals a linear relationship between SST and the skeletal $\delta^{18}O$ (Al-Rousan et al., 2007). In recent years trace and minor element compositions like Mg/Ca, Sr/Ca, U/Ca, Li/Mg, the $\delta^{13}C/\delta^{18}O$-line-technique and others have been investigated as additional potential temperature proxies to validate and reconstruct temperatures independently and to find the most trustworthy method. The above briefly described applications are just two examples of a large selection of different techniques developed to get reliable proxy informations from a coral skeleton. The reader is referred to the comprehensive literature in this field.

4

Tools and methods

4.1 Uranium-series disequilibrium

There are many radionuclides in our environment. Some of them have been produced by human activity through artificial nuclear reactions in the past 65 years or so. Hazarding the consequences, for example, mankind intentionally liberated more than 200 different artificial radionuclides into the atmosphere during the A- and H-bomb testing era in the 1950s to mid 60's resulting in a global fallout of these nuclides thereafter, which can be measured until today (Board on Health Care Services, 1999; Froehlich, 2010). Another large group of radionuclides are cosmogenic produced. Earth's atmosphere is continuously bombarded by cosmic rays from outer space forming radionuclides with half lives from days up to 10^6 years. Among them ^{14}C and ^{10}Be, which are important dating tools. See section 4.3.1 for more information about the production and use of radiocarbon. A third origin of radionuclides widely used today as a geochronological tool for the reconstruction of different timescales and discrete episodes in earth history are the primordial nuclides. These include the long-lived ^{238}U, ^{235}U and ^{232}Th, the

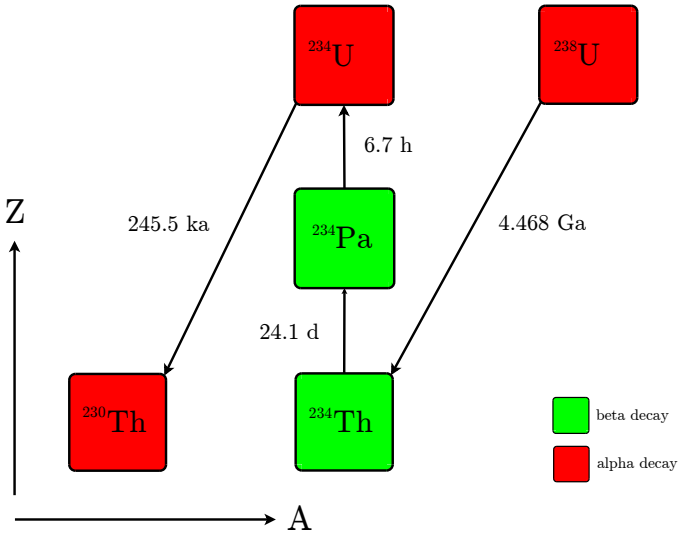

Fig. 4.1: Excerpt of the uranium-radium decay series. Numbers denote the corresponding half-lives.

starting points of the three so-called natural decay chains, which have existed in their current form since before Earth was formed ∼4.6 Ga ago and are still present. Fig. 4.1 exhibits a few decay steps of the ^{238}U series ultimately ending in lead ^{206}Pb. Especially for the ^{238}U decay chain all intermediate products show half-lives being much smaller than for ^{238}U. Therefore, one would reason that radioactive equilibrium between these intermediate products should have established a long time ago throughout the environment rendering dating attempts impossible. This is not the case as will be outlined in the next section.

4.2 Nature of radioactive disequilibrium

Natural processes such as phase changes, adsorption, partial melting, degassing, crystallization, oxidation/reduction and many more cause chemical fractionation among different elements (nuclides) of a decay chain producing a transient state of parent-daughter disequilibrium. This radioactive disequilibrium can be used to determine the age of the material (Bourdon et al., 2003). For instance, uranium usually exists in two oxidation states mainly U^{4+} and U^{6+}. During weathering processes uranium is in its hexavalent oxidation state forming a whole variety of uranyl complexes among them the quite soluble uranyl carbonate $UO_2(CO_3)_3^{-4}$ (Starik and Kolyadin, 1957; Langmuir, 1978)[1] In a reducing environment, however, uranium is in its U^{4+} state where it is insoluble and thus far less mobile than U^{6+} (Ivanovich and Harmon, 1992). In contrast to uranium, thorium, which exists in natural waters in its quadrivalent Th^{4+} state, is insoluble and is efficiently stripped from the water column by adsorption and reverse scavenging processes onto mineral surfaces of biogenic and terrigenic origin or precipitated as a hydrolysate (Koczy et al., 1957). The ocean surface water in particular has a negligible specific thorium activity compared to uranium. During organically or inorganically mediated precipitation of calcium carbonate from an aqueous solution thorium will not be incorporated, which results in a Th/U disequilibrium as observed in corals or speleothems (Scholz, 2005).

Another totally unrelated process to that described above occurs in low-temperature environments contributing to the disequilibrium at all phase boundaries is owed to the decay itself. During the α-decay of ^{238}U, ^{234}Th is dislocated in the crystal lattice by around 20 nm (depending on the substrate) (Kigoshi, 1971). This in turn gives rise to a preferred leaching of the ^{234}U during chemical weathering. This phenomenon is known as α-recoil-effect. In rivers the ^{234}U/^{238}U activity ratios are usually larger than one and exhibit large deviations from secular equilibrium up to several hundred per mille (Henderson, 2002). As a result ocean seawater is also slightly enriched in ^{234}U with activity ratios of ^{234}U/^{238}U = 1.1468 (Anderson and Carr, 2010), normally expressed as δ^{234}U = 146.8‰[2]. This ocean value is

[1] The variety of different uranyl species is depending on the temperature and pH of the water, the above mentioned uranyl complex is the dominant form for a pH level of ∼8 (seawater).

[2] The δ^{234}U activity of a sample is defined as the relative deviation from a standard given as parts per thousand, $\delta^{234}\mathrm{U} = (^{234}\mathrm{U}/^{238}\mathrm{U})/(^{234}\mathrm{U}/^{238}\mathrm{U})_{\mathrm{eq}} - 1) \cdot 1000$. In case of reporting δ^{234}U to atomic ratios

governed by a fragile balance between input and output of uranium isotopes and is thought to have been stable for the last 400,000 years (Henderson, 2002).

4.2.1 ^{230}Th/U-dating of corals

In 1956 the important discovery was made that the ^{238}U decay series in newly formed coral carbonate shows a systematically radioactive disequilibrium (Barnes et al., 1956). Further investigations approved that this is also the case for a broad variety of marine carbonates (e.g. molluscs, foraminifera, coccoliths). This paved the way for a prolific era of age determination, which continues until today thereby allowing the reconstruction of various marine processes within the Quaternary period. As outlined in chapter 3 corals are able to biogenically precipitate $CaCO_3$ from seawater. The exact mechanism is a matter of debate, though. In the end the chemical conditions most likely within the coral endoderm determines which dissolved large anion is precipitated from the aqueous medium.

The dominant species, which is coming into question is the uranyl carbonate $UO_2(CO_3)_3^{-4}$ (Shen and Dunbar, 1995). Due to the octahedral configuration of this uranyl complex, uranium is more compatible with the orthorhombic conformation of aragonite than the rhombohedral form of calcite (Reeder et al., 2001). The result are lower uranium concentrations in the latter one. Uranium concentrations range from 0.02−0.05 ppmw for foraminifera calcite to 2−5 ppmw for aragonitic corals (Ku, 1965; Russell et al., 1994). Since almost all coral skeletons, shallow-water as well as cold-water corals, compose of aragonite, uranium measurements can precisely be conducted with different proved mass spectrometer techniques (Edwards et al., 1986/87).

4.2.2 ^{230}Th/U age calculation

U-series decay equations are a set of differential equations describing the decay rate of a certain nuclide with respect to the preceding nuclides of the same decay chain.

$$\frac{dN_{238}}{dt} + \lambda_{238} N_{238} = 0 \tag{4.1}$$

$$\frac{dN_{234}}{dt} + \lambda_{234} N_{234} - \lambda_{238} N_{238} = 0 \tag{4.2}$$

$$\frac{dN_{230}}{dt} + \lambda_{230} N_{230} - \lambda_{234} N_{234} = 0 \tag{4.3}$$

$$\vdots$$

rather than activities, $^{234}U/^{238}U_{eq}$ is equal to $\lambda_{238}/\lambda_{234} = 5.472 \cdot 10^{-5}$.

The equations for the short-lived intermediate daughters ^{234}Th and ^{234}Pa are neglected. By successively solving these equations from top to down by applying the Laplace transformation

$$\mathcal{L}(N(t)) = \mathcal{N}(s) = \int_0^\infty e^{-st} N(t) dt$$

to these equations one will obtain simple linear expressions that can be solved for the Laplace transformed $\mathcal{N}(s)$. One example to illustrate the approach: Applying the Laplace transformation to the first equation on both sides yields

$$s\mathcal{N}(s) - \mathcal{N}^0 + \lambda\mathcal{N}(s) = 0 \quad \text{with} \quad \mathcal{N}^0 = N^0 \quad \text{the initial value of } {}^{238}U$$

Solving this equation gives

$$\mathcal{N}(s) = \frac{\mathcal{N}^0}{\lambda + s}$$

Inverting this expression by inverting the Laplace transformation using tables or by hand one will find the time-dependent solution we are looking for

$$N(t) = \mathcal{L}^{-1}\{\mathcal{N}(s)\} = \mathcal{L}^{-1}\left\{\frac{\mathcal{N}^0}{\lambda + s}\right\}$$

$$N_{238}(t) = N^0_{238} \cdot e^{-\lambda_{238} \cdot t}$$

The solution to the second equation is given in addition

$$\mathcal{N}_2(s) = \frac{\mathcal{N}^0_2}{\lambda_2 + s} + \frac{\lambda_1 \mathcal{N}^0_1}{(\lambda_2 + s)(\lambda_1 + s)}$$

After applying partial fraction decomposition, $\lambda_j + s$ then can easily be transformed back by replacing them with $exp(\lambda_j \cdot t)$

$$\frac{1}{(\lambda_1 + s)(\lambda_2 + s) \cdot \ldots \cdot (\lambda_{i-1} + s)} = \sum_j^i \frac{1}{\lambda_j + s} \cdot \frac{1}{\prod^i_{\substack{k=1,\\ k\neq j}} (\lambda_k - \lambda_j)}$$

Thus for ^{234}U

$$N_{234}(t) = N^0_{234} \cdot e^{-\lambda_{234} \cdot t} + N^0_{238} \frac{\lambda_1}{\lambda_2 - \lambda_1} (e^{-\lambda_1 \cdot t} - e^{-\lambda_2 \cdot t})$$

In doing so for the third equation and by converting it to an activity expression[3] and making some approximations $\lambda_{234} \wedge \lambda_{230} \gg \lambda_{238}$, one will finally find the **marine age equation** used in this thesis.

$$\frac{^{230}Th}{^{238}U} = 1 + \left(\left(\frac{^{230}Th}{^{238}U} \right)_0 - 1 \right) e^{-\lambda_{230} \cdot t} + \frac{\delta^{234}U}{1000} \left(\frac{\lambda_{230}}{\lambda_{230} - \lambda_{234}} \right) (1 - e^{(\lambda_{234} - \lambda_{230}) \cdot t}) \qquad (4.4)$$

This equation is transcendental in t and can be solved numerically, e.g. with the Newton-Raphson method. I refer the interested reader to the appendix A for an alternative and more detailed derivation of this last equation using no Laplace transformation. Information about this topic can be found in (e.g. Bateman, 1910; Ivanovich and Harmon, 1992; Schiff, 1999). Fig.4.2 is showing the time evolution of the different isotopic activity ratios of a closed system and their heading back towards secular equilibrium. This behavior is typical

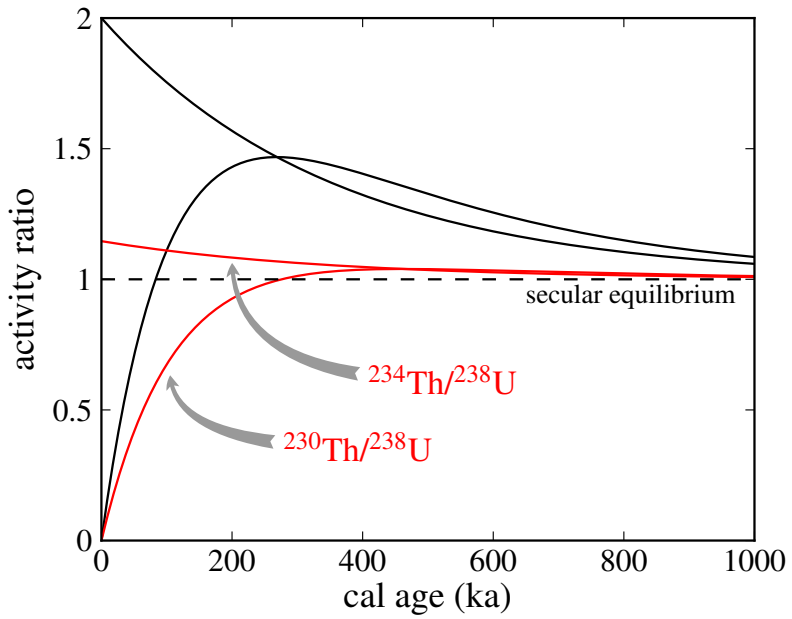

Fig. 4.2: Time evolution of the different isotopic activity ratios in a closed system with no initial ^{230}Th. Red and black lines indicate different starting values in ^{234}Th/^{238}U.

for marine carbonates like shallow-water corals. Since ^{230}Th is effectively stripped from the water column the initial $^{230}Th_0$ activity found in surface waters is virtually zero. This is not the case for deep-water corals as thorium concentrations increase with water depth. As a consequence, cold-water corals may incorporate so-called unsupported or non-radiogenic

[3]To obtain activities rather than atomic ratios, the above equation is simply multiplied by the decay constant of ^{230}Th.

thorium leading to older apparent ^{230}Th/U ages. I will discuss this topic in-length in the next section. The scope of the uranium-thorium dating method is between 400−600 ka depending on the initial $(^{234}U/^{238}U)_0$, sample size, and measurement precision.

4.2.3 The necessity to correct for initial ^{230}Th

4.2.3.1 Hydrogenous and detrital derived thorium

A few words must be said about the correction for non-zero initial ^{230}Th in cold water corals since the ability to precisely account for initial thorium has a relatively large impact on the ^{230}Th/U dating. Several sources contribute to a possible incorporation of ^{230}Th during the live span of a coral. Dissolved ^{230}Th concentrations increase with water depth and have mostly negligible values at the water surface (Fig.4.3) (Anderson et al., 1983; Roy-Barman et al., 1996). This is a common feature in water where ^{230}Th is continuously being produced from the decay of dissolved ^{238}U, which is homogenously distributed in the open ocean water having a residence time of about 400,000 years (Mangini et al., 1979). The adjusting concentration gradient with depth is expressing the high particle reactivity of thorium. The increase with depth can be explained with the reverse-scavenging model proposing a successively adsorption and desorption of dissolved ^{230}Th on sedimenting particles (Bacon and Anderson, 1982; Nozaki et al., 1987). This observation also holds for ^{232}Th with the difference that ^{232}Th is not being continuously produced since it is the starting point of the ^{232}Th decay chain. Sources for ^{232}Th are continental derived detrital weathering products, which are transported into the ocean mainly by river runoff or wind-borne dust. The concentration gradient for particulate ^{230}Th is on average much less pronounced exhibiting concentrations in part much lower than for dissolved ^{230}Th (Fig.4.3). Therefore, deep-living corals bathing in elevated thorium concentrations and show higher than expected thorium concentrations in their skeletons[4]. Detrital clay in secular equilibrium, however, exhibit ^{230}Th/^{232}Th atomic ratios close to the bulk earth value of $4 \cdot 10^{-6}$ based on a

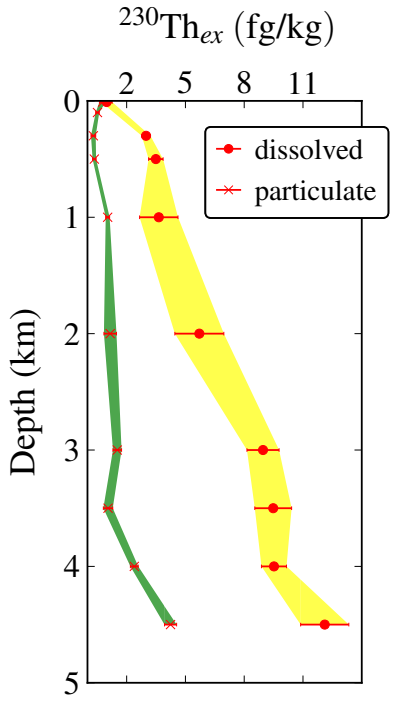

Fig. 4.3: ^{230}Th concentration profile from the eastern North Atlantic. Picture after (Vogler et al., 1998)).

[4]Surface water has dissolved atomic ^{230}Th/^{230}Th ratios smaller than $5-10 \cdot 10^{-6}$ compared to deeper water with ratios larger than $700 \cdot 10^{-6}$ (Moore, 1981).

mean $^{232}Th/^{238}U$ concentration in Earth's crust of 3.8 (Taylor and McLennan, 1985; Cheng et al., 2000a). Thus, for deep-water corals a mixture between both $^{230}Th/^{232}Th$ sources and their end-members can be expected to be found in the skeleton (Cheng et al., 2000a).

4.2.3.2 Coating derived thorium and uranium

Another effect that influences $^{230}Th/U$ dating of cold-water corals are metallic coatings the inner and outer surface of the a skeleton acquire usually after death due to direct exposure to the seawater. During the live span of a coral with its varies living polyps, the calcareous exoskeleton is covered with living tissue called coenosarc, which spreads along the surface connecting the different polyps. After their death, though, this mucus-like layer corrodes exposing the corals' skeleton to the surrounding seawater making it vulnerable to chemical alteration and/or external biological activity. As a consequence one will often find the surface of sub-fossilized corals littered with the housing remains of epifaunal living organisms like the calcitic tubes of serpulid worms. Borings from endolithic organisms like tiny sponges might also modify the Th concentrations, since they can become partially filled with sediment and/or secondary precipitated aragonite. But if the corals' skeleton is longer exposed to the ambient seawater, dissolved Fe-Mn oxyhydroxides will constantly precipitate on the surface of a coral covering it with time with a thin[5], amorphic metallic coating (Fig. 4.4) (Bayon et al., 2004). This authigenic coa-

Fig. 4.4: Heavily coated calyx from the North Atlantic region. Picture from Lomitschka (1999).

ting incorporates usually a large number of trace elements formerly dissolved in the seawater, among them uranium and thorium, whose concentrations largely exceeds the genuine skeletal concentrations of U and Th (Lomitschka and Mangini, 1999). Several minimal invasive methods have been described in the literature to get rid of these coatings and to receive enough pristine material for accurate dating (Shen and Boyle, 1988; Stein et al., 1991; Lomitschka and Mangini, 1999). For instance, one method involves removal of the coatings

[5]The coating phase on average is several 100 μm thick and often visible as a black layer (Fig.4.4).

with ascorbic acid and subsequent use of a Na_2EDTA solution preventing the coatings' constituents to readsorp onto the coral skeleton again (Lomitschka and Mangini, 1999). This strategy may be useful in cases where only little material is left. For larger samples though, a more rigorous mechanical cleaning procedure is often more beneficial.

4.2.4 Correcting for initial ^{230}Th

To cut the matter short, there is no way to precisely correct for initial ^{230}Th in corals. For the marine age equation (Eq. 4.4) the activity ratio

$$\left(\frac{^{230}\mathrm{Th}}{^{238}\mathrm{U}}\right)_0 \quad \text{can be substituted by} \quad \left(\frac{^{232}\mathrm{Th}}{^{238}\mathrm{U}}\right)\left(\frac{^{230}\mathrm{Th}}{^{232}\mathrm{Th}}\right)_0$$

The measured ^{232}Th/^{238}U activity in the carbonate serves as an indicator-ratio to assess the incorporated initial ^{230}Th. This is possible as both isotopes have fairly large half-lives (^{232}Th: $1.4{\cdot}10^{10}$ years, ^{238}U: $4.46{\cdot}10^{9}$ years), thus the ratio does not change on the short timescales we are looking at ($< 50,000$ years). The problem shifts toward estimating the initial water ratio of $(^{230}\mathrm{Th}/^{232}\mathrm{Th})_0$ at the location of the corals at times the corals grew. Since there is no known fractionation occurring between the different thorium isotopes during sklerogenesis, the thorium ratio in water should be equal to the corals' aragonite ratio. Water column measurements of dissolved ^{230}Th and ^{232}Th have been measured in great numbers. Data from the eastern North Atlantic (Vogler et al., 1998) for instance depicted values of 10 ± 4 and Moran et al. (1997) reported results from the Labrador Sea with 8.6 ± 4.3. Overall, reported values range from 0−30 (Cheng et al., 2000a) (0−400 m water depth). There has also been efforts to model the ^{230}Th distribution in the oceans with an OGCM (Ocean General Circulation Model) (Henderson et al., 1999), which yield a good fit to today's water column measurements of ^{230}Th suggesting that the model is advecting and removing ^{230}Th within the ocean realistically. Model runs have been performed along a meridional transect through the West Atlantic with different ocean flow patterns thought to have prevailed during the Holocene and LGM (Last Glacial Maximum ∼22−19 ka BP) (Fig. 4.5). The model

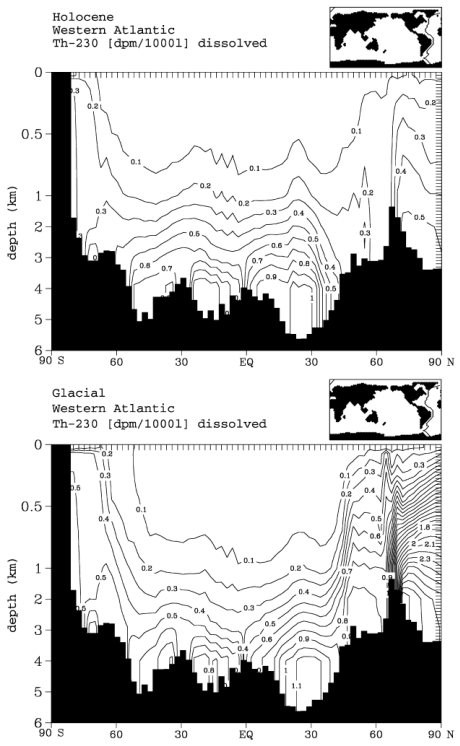

Fig. 4.5: Modeled dissolved ^{230}Th during the preindustrial Holocene and LGM (Henderson et al., 1999).

values can be used for a first order approach to correct for an initial ^{230}Th concentration. As there are no modeled ^{232}Th concentrations one must be content with present water column measurements. A published seawater ^{232}Th profile closest to the location of the investigated corals in this thesis can be found in Chen et al. (1986). Differences in the modeled ^{230}Th seawater activity during the LGM and Holocene are not significant for the depth range of interest (600−800 m) and are not affecting the coral dating.

4.2.5 Sensitivity check

After the substitution in section 4.2.4 the marine age equation is now dependent on the initial $(^{230}\mathrm{Th}/^{232}\mathrm{Th})_0$ activity ratio. Though reported water values for this ratio exhibit a relatively wide range between 0−30 (Cheng et al., 2000a), the measured ^{232}Th concentration (respectively activity ratio) within the coral is actually the dominant factor for the age and error calculation. Fig. 4.6 illustrates this sensitivity after having applied a first order Gaussian error propagation of equation 4.4. A higher measured ^{232}Th concentration in a coral results in a larger absolute age uncertainty and concurrently lowers the age of a coral. The single white dot stands for the uncorrected age for a specific coral measured in this thesis (age 27.1 ka BP) with a 2σ error of 243 years. The colored dots show the course of the age and error development after corrections have been made for initial ^{230}Th. The measured ^{232}Th concentration for the yellow dots is chosen to be constant to 1 ppbw (1 ng/g), while the initial water value was changed in thirty one steps between 0−30. The red dots are showing the same situation but with a fixed ^{232}Th concentration of 2 ppbw and a varying initial water ratio between 0−30 again. Lastly, for the blue dots the $(^{230}\mathrm{Th}/^{232}\mathrm{Th})_0$ is set to 8 (arbitrarily chosen) and the ^{232}Th concentration varies between 0−30. As one can see from Fig. 4.6 the ^{232}Th content of a coral has the largest impact on its age and error despite the fact that we do not know the initial water ratio $(^{230}\mathrm{Th}/^{232}\mathrm{Th})_0$ precisely. It is clear from this point of view that a rigorous cleaning technique is necessary to keep the ^{232}Th concentration as small as possible. While older corals are relatively impervious for initial ^{230}Th, for very young corals the error is dominated by the initial Th correction. In this work the initial water

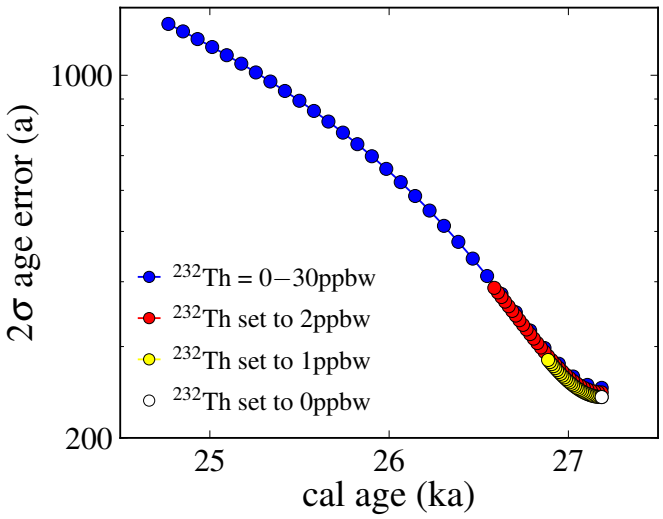

Fig. 4.6: Correlation between coral age and age error as a function of measured ^{232}Th and estimated $(^{230}\mathrm{Th}/^{232}\mathrm{Th})_0$ ratio. Curves have been slightly shifted in y-direction for better visibility. See text for further description.

$(^{230}Th/^{232}Th)_0$ value in 600−800 m water depth off Brazil is set to 8 with an appraised uncertainty of 50%.

4.2.6 Diagenesis

Originally borrowed from geology and oceanography the term diagenesis describes 'physical, chemical, and biological changes occurring in sediments during and after the period of initial deposition, including lithification, but excluding surficial alteration (weathering) and metamorphism'(Geyh and Schleicher, 1990). Regarding corals diagenesis comprises alterations of the skeleton induced by carbonate dissolution, secondary aragonite precipitation, pore filling, and conversion from aragonite to calcite potentially happening after the death of the polyps. All of these effects lead to a gradual exchange of uranium and/or thorium with the environment. These processes are obviously important as they can affect the accuracy of the uranium-series clock. One approach to test corals for post-depositional diagenesis is to measure their uranium concentrations. Modern corals exhibit concentrations ranging between 2−3.5 ppmw (Shen and Dunbar, 1995). The observed scatter has been attributed in part to a number of slightly changing environmental parameters such as seawater temperature, pH, Ca^{2+} ion concentration and variations in salinity. Identifying one single cause for this variation is hampered by the fact that the biological activity of the polyp affects the carbonate precipitation and with that the uranium concentration as well. This is known as vital-effect (Gvirtzman et al., 1973). Furthermore, borings from endolithic organisms like tiny sponges may also modify the U content of the skeleton. These borings can become partially filled with sediment and/or secondary precipitated aragonite. Less intuitive processes show that even dead, non-bioeroded corals can become enriched in uranium along the skeletal margins and trabecular centers when exposed to concentrated uranium solutions from the surroundings (Swart and Hubbard, 1982; Robinson et al., 2006). Another process involves potentially filling of the coral's porous aragonitic skeleton within 1,000 years after its death with aragonite enriched in uranium relative to the original coral. The corals' porosity is thereby reduced by 5% leading to an apparent

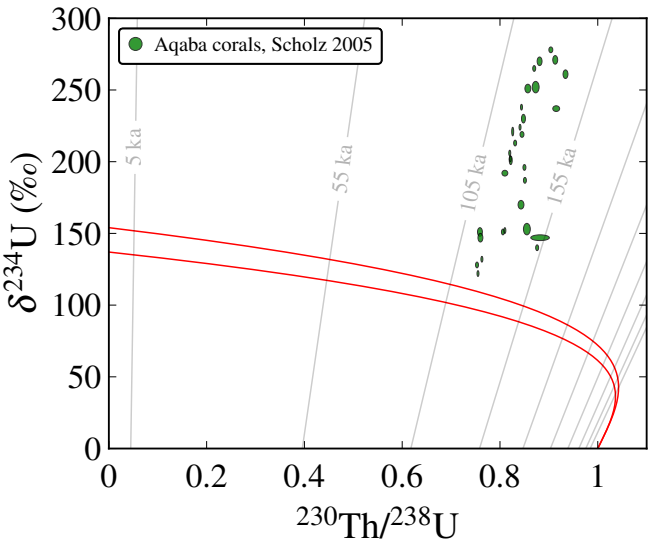

Fig. 4.7: The solid red lines show the isotopic evolution of a closed system starting with a mean $\delta^{234}U$ of 146‰ and a zero $^{230}Th/^{238}U$ activity. Deviations from this span are symptomatic of diagenetic alteration as indicated by the green error ellipses from Scholz (2005).

age rejuvenation of 7% with no measurable effect on the calculated initial uranium isotopic composition (Lazar et al., 2004; Robinson et al., 2006). When speaking about the initial uranium isotopic composition a second gauge to check diagenetic activity is to measure the uranium isotopic activity ratio $^{234}U/^{238}U$. First shown by Broecker and Takahashi (1966), marine carbonates incorporate the isotopic composition of the surrounding seawater. The present-day open-ocean seawater $\delta^{234}U$ is $\sim$147‰, as recently pointed out by Anderson and Carr (2010) and Robinson et al. (2004) and is conservative within at least the upper 2,000 m (Cheng et al., 2000b) with only variations in the sub-‰ level (Anderson and Carr, 2010). Some older studies by contrast report more variable values with a lower bound as small as 139.5 ± 3.5‰ (Chen et al., 1986) and an upper bound going as high as 149.6 ± 1‰ (Delanghe et al., 2002). All reported $^{234}U/^{238}U$ measurements consider already the newly determined decay constant of ^{234}U (Cheng et al., 2000a).

It is not just that very recent corals indeed build in this isotopic signature (Szabo et al., 1994), they as well verify the assumed constancy of the measured water values to within 10‰ over the last several hundred thousand years (e.g. Henderson et al., 1993; Gallup et al., 1994; Stirling et al., 1995; Henderson, 2002). If the coral's skeleton behaved as a closed system its initial $\delta^{234}U_i$ ($= \delta^{234}U \cdot e^{\lambda_{234} \cdot t}$) should be identical to that of today's ocean (Edwards et al., 1986/87). Fig 4.7 demonstrates the isotopic evolution of a closed system (solid red lines) starting with a mean $\delta^{234}U$ of 146.8^{+6}_{-10}‰ and an initial $^{230}Th/^{232}Th$ activity of zero. Deviations from this span are symptomatic of diagenetic alteration. Gray lines are isochrones (isotopic pairs of values giving the same age). For illustration the data from Scholz (2005) from last interglacial shallow-water corals from Barbados is plotted as well (Fig 4.7). Corals feature strong diagenetic alterations making them unsuitable for conventional age determination according to the marine age equation (Eq. 4.4).

4.2.6.1 X-ray diffraction (XRD)

Another potential pitfall is the post-depositional diagenetic alteration of aragonite to calcite (McGregor and Gagan, 2003). As already mentioned in the beginning of this section, aragonite is a metastable polymorph of calcium carbonate and gradually transforms into the much more stable modification calcite. This process lead to an opening of the carbonate system and allows the exchange of different isotopes compromising $^{230}Th/U$ dating. The X-ray diffraction technique allows to analyze the crystal structure of a variety of minerals and moreover provides a quantitative evaluation of its composition. Fig. 4.8 exemplarily shows a section of a typically measured X-ray diffractogram of a 65 ka old coral sample, which in this case can be entirely explained by just one present mineral phase videlicet aragonite. This finding is a strong evidence supporting the assumption that no alteration from aragonite to calcite in this specific sample happened. It must be emphasized that all these indicators used to test the closed system behavior of the coral carbonate are often not meaningful when viewed alone.

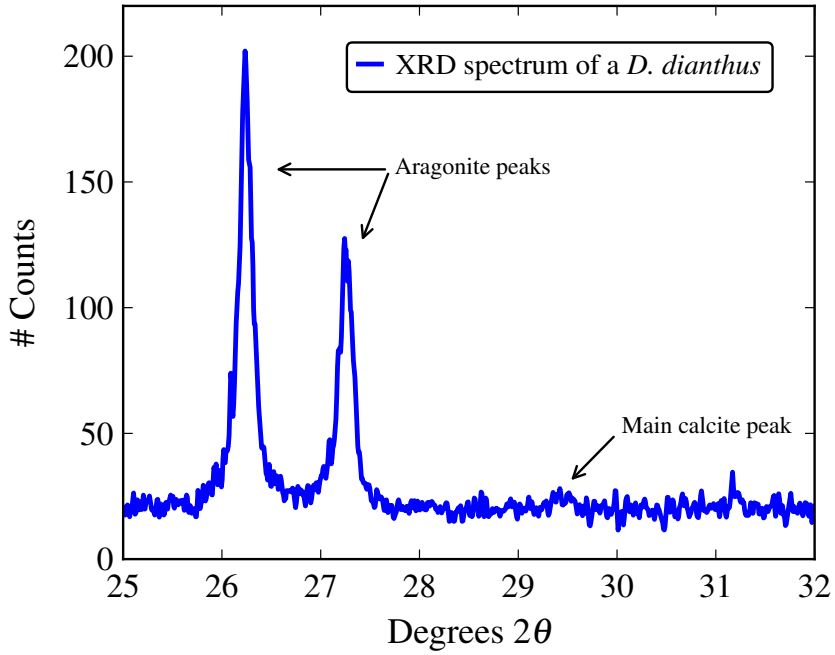

Fig. 4.8: X-ray diffractogram of a *Desmophyllum dianthus* (∼65 ka old) with distinct aragonite peaks and no detectable calcite. Picture adapted from Adkins (1998).

4.3 Radiocarbon dating

4.3.1 ^{14}C production

The ^{14}C age method has undoubtedly become more acquainted to the general public than any other dating tool. Inextricably linked with this important dating technique is the name of Willard Frank Libby who, as a pioneer in isotope research, was awarded the Nobel Prize in chemistry in 1960 for his contributions in this field. ^{14}C is one of the so-called cosmogenic radionuclides which are being continuously produced in the upper layers of the atmosphere. The locus of peak production of ^{14}C is above 15 km, where the energy deposition of galactic cosmic rays (GCR) is highest. GCR mainly consists of protons (89%), alpha particles (10%), and is galactic in origin (Mursula and Usoskin, 2003). GCRs usually have energies of the order of ∼1 GeV and show a flux of about 1,000 particles/m^2/s. These high energy particles induce spallation processes through collisions with the atmosphere's molecules, mainly nitrogen (most abundant). High energy particles released in this way in turn produce cascading secondary particles down the atmosphere including (thermal) neutrons, myons, and electrons until the kinetic energy of this particle shower is too small. The ^{14}C production equation is schematically shown in Fig. 4.9, which is often abbreviated as ^{14}N(n, p)^{14}C. For this to work ^{14}N must capture a neutron within a relatively narrow energy range (Korff and Clarke, 1942). The resulting intermediate compound particle is unstable and immediately decays into ^{14}C emitting a single proton. ^{14}C spontaneously decays back by β^- decay into ^{14}N with a half life of $5,730 \pm 30$ years, the so-called Cambridge half life[6]. The above particle reaction is the main source of ^{14}C in the atmosphere and contributes to more than 99% of the total ^{14}C-production rate. Our sun emits also relatively high energy particles namely solar cosmic rays (SCR), whose production rate is usually below a percent of the GCR and is therefore negligible (Masarik and Beer, 2009). ^{14}C production moreover exhibits large variations with increasing atmospheric depth as well as a latitudinal dependence due to the geomagnetic shielding. Owing to the dipole character of Earth's magnetic field, neglecting higher magnetic multipoles, there is a five times higher secondary neutron flux at the poles than at the equator resulting in a latitudinal ^{14}C gradient which vanishes rapidly through mixing between the stratosphere and the well-mixed troposphere (Harkness, 1970). Two

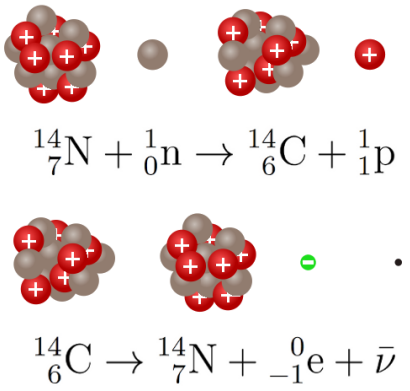

Fig. 4.9: Production and decay scheme for ^{14}C.

[6]It is thanks to a fail measurement from Libby and coworkers in the beginning of radiocarbon dating that all age calculations are performed with a wrong half life of 5,568 years instead of the more precise half life of 5,730 years.

third of the ^{14}C production takes place in the stratosphere only one third in the troposphere (e.g. Lal and Peters, 1967; O'Brien, 1979). After that, ^{14}C is rapidly oxidized to ^{14}CO with a mean life time of about days to months and is subsequently further oxidized to $^{14}CO_2$ showing a longer residence time in the atmosphere of about 5 years.

4.3.2 Carbon reservoirs

^{14}C-tagged atmospheric CO_2 finally enters the Earth's carbon cycle, one of Earth's biogeochemical cycles, which consists of different reservoirs within those carbon in its various molecular forms is exchanged, subsequently recycled, and reused on different timescales. The reservoirs of the carbon cycle encompass the ocean, atmosphere, biosphere, and terrestrial hydrosphere from which the ocean is by far the largest and most important one (Froehlich, 2010). For instance, today's atmosphere CO_2 inventory is about 750 GtC (1 GtC = 10^9 metric tons of carbon) with a CO_2 residence time of 5 years. Consequently 20% of the CO_2 inventory are annually exchanged with the biosphere (ca. 60 GtC per year) and the ocean surface waters (ca. 90 GtC per year) (Schimel et al., 1995). See Fig. 4.10 for a highly simplified picture exhibiting carbon inventories and exchange fluxes across the reservoirs' common boundaries. The given numbers in Fig. 4.10 are still under debate. Natural sources and sinks of CO_2 are the living and dead biosphere and the ocean. Plants, for instance, consume the gaseous carbon dioxide in a photosynthetic process fixating carbon to build carbohydrates both on land and as dwelling phytoplankton in the sunlit surface of the ocean. On the other hand CO_2 is also released through plant and root respiration, and rotting of organic material. Hence the short exchange time of CO_2 on the order of a few years at least between the atmosphere and biosphere. Once CO_2 is dissolved in the ocean water it stays there. The likelihood to get back soon to the atmosphere is slim. The exchange time between the atmosphere and ocean is on the order of a millennium. A complicating factor is that CO_2, once dissolved, forms different chemical species (carbonic acid (H_2CO_3), bicarbonate (HCO_3^-), and carbonate (CO_3^{2-})) in different portions depending on the pH and the alkalinity of the seawater. It subsequently mixes within the deeper water and is vertically and laterally transported via ocean currents.

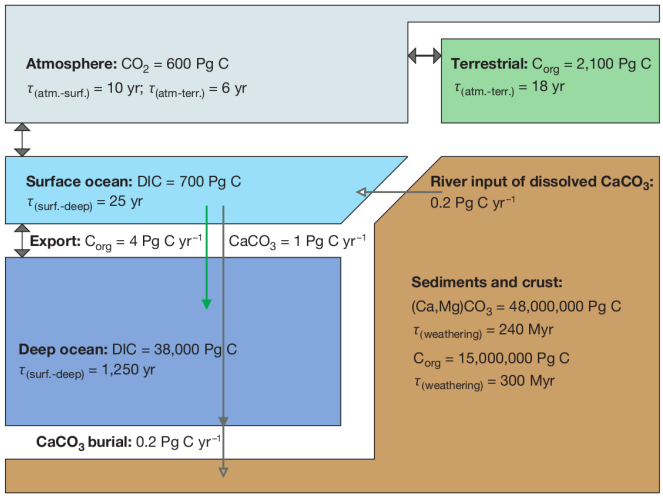

Fig. 4.10: Earth carbon inventories and their associated exchange fluxes and residence times. Picture from Sigman and Boyle (2000).

Since the ocean is the largest carbon reservoir with an inventory ∼60 times the atmosphere, minor changes in its chemical state are thought to be sufficient to have a huge impact on atmospheric CO_2 concentration. Variations in the ocean carbonate chemistry could lead to outgassing of molecular CO_2 between the ocean-atmosphere boundary, which is a promising mechanism to explain the observed ups and downs of atmospheric CO_2 during the course of glacial and interglacial cycles (Broecker, 1982). Since carbon ^{14}C is reasonably well mixed in these different reservoirs, but not totally, especially not in the ocean during the average lifetime for a ^{14}C atom to decay, renders it a very valuable tool to disentangle the complex processes of the carbon cycle enlightening the spatial and temporal variability of carbon sources and sinks. For example by measuring the ^{14}C deficiency per unit of ordinary carbon in a reservoir one is able to use it as a tracer to determine the turnover time of seawater in the ocean or of soil organic matter (Levin and Hesshaimer, 2000).

4.3.3 Measurements

The isotopic concentrations for the three naturally-occurring carbon isotopes are 98.89% for ^{12}C, 1.11% for ^{13}C, and less than 10^{-9} % for ^{14}C (Nier, 1950). These values are not fixed and must be regarded as median values because isotopic fractionation and decay during transfer of carbon between different geochemical phases lead to slight but significant changes in these concentrations. To give the reader a better impression of how small Earth's ^{14}C inventory actually is, let us consider a steady-state case where radiocarbon production equals its decay. From this it follows:

$$P_{^{14}C} \cdot A = \overbrace{\lambda_{^{14}C} \cdot N_{^{14}C}}^{\text{decay}}$$

with P being the production rate of ∼2.05 ^{14}C atoms cm^{-2} s^{-1} (global average: integrated over the depth of the Earth's atmosphere and all latitudes) (Masarik and Beer, 2009) and A representing the Earth's surface, the whole ^{14}C budget would be no more than ∼63 metric tons. The annually ^{14}C production is ∼7.6 kg and is distributed over all active carbon reservoirs leading to a mean specific activity in organic matter of around 15 dpm/gC (dpm/gC decays per minute per gram carbon) (Anderson and Libby, 1951). When plants die off the steady uptake of radiocarbon in the form of $^{14}CO_2$ grinds to a halt. In the course of time the specific activity is decreasing by ^{14}C decay. The age of a sample is then calculated simply by measuring the residual ^{14}C activity (or equivalently the $^{14}C/^{12}C$ isotopic ratio) followed by normalization to the atmospheric reference level and applying of the exponential law governing the decay. In the pioneering time of radiocarbon measurements in the 1950s Libby and coworkers used a beta-counting technique to count single decays, but the background to signal ratio (16 : 1) eliminated the possibility of meaningful measurements in the first place. The masterly performance was to shield the setup with a bundle of anticoincidence-cosmic-ray-guard counters, which significantly reduced the background

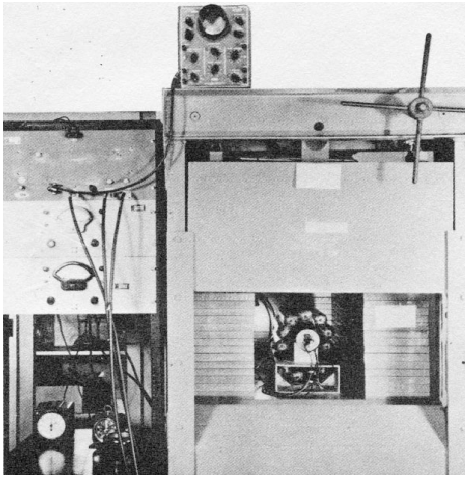

Fig. 4.11: First ^{14}C counting apparatus built by Libby, which smoothed the way for radiocarbon dating. Picture taken from Currie (2004).

signal coming from μ^- radiation (Currie, 2004) (Fig. 4.11). Even today ^{14}C measurements are conducted with this counting technique. Though advances in shielding technique have been made, which improved counting precision to as low as ∼0.2% (Poisson relative standard deviation) compared to Libby's 1−5% uncertainties in the beginning of 1950, the technique is dying breed and is replaced bit by bit by accelerator mass spectrometer techniques (AMS).

4.3.4 Age calculation

There are three critical assumptions for ^{14}C dating that need to be fulfilled in order to get reliable absolute ages: 1. A constant ^{14}C production by cosmic rays over the applicable time range of this method (about 10 half-lives ∼50 ka). 2. The sizes of the exchangeable carbon reservoirs should be constant on average for many thousands of years. 3. A uniform global distribution of ^{14}C is required shortly after its production. Early on it was realized that atmospheric $^{14}CO_2$ is well mixed within the atmosphere and without significant deviations from an uniform global distribution (Anderson and Libby, 1951). Unfortunately, the former two assumptions have proven false. It has been shown that ^{14}C production rate in the past was subject to short-term changes in Earth's magnetic shielding, modulated by the magnetic field carried along by the solar wind filling the interplanetary space. The suns magnetic field, however, just plays an indirect role and is mostly confined to the immediate vicinity around the sun (e.g. de Vries, 1958; Stuiver, 1961; Stuiver and Quary, 1980). On a long term basis (> than several hundred years), ^{14}C production is besides influenced through changes in the geomagnetic dipole field (Damon et al., 1978). Reconstructions based on paleomagnetic records suggest that the Earth's magnetic-field strength has continuously in-

creased over the past 40 ka BP (Laj et al., 2002), thereby lowering the ^{14}C production rate. The flux and modulation of galactic protons, however, are thought to have been constant in time and should not influence the ^{14}C age calculation. Also the sizes of the active carbon reservoirs, like the atmosphere, have been changed during the past, especially during transition between glacial-interglacial periods rendering absolute age determination completely impossible. To overcome these problems calculated ^{14}C ages need to be calibrated in oder to get absolute ages. Fig. 4.12 depicts the ^{14}C calibration curve for the last 10 ka BP derived by ^{14}C dating of tree rings of known calendar ages. Since absolute age calibration is not the subject of this thesis, the reader is referred to the extensive literature about this topic. ^{14}C ages have been calculated in this thesis following the equation:

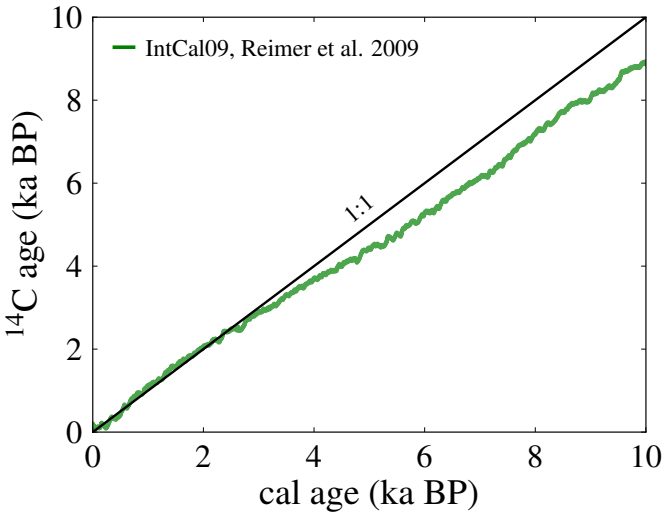

Fig. 4.12: Cut-out from the tree ring calibration curve from Reimer et al. (2009) illustrating the deviations between ^{14}C ages and calendar ages.

$$^{14}\mathrm{C\ age} = \frac{1}{\lambda} \cdot \ln\left(\mathrm{F_m}\right), \quad \text{with } \mathrm{F_m} \text{ being the measured ratio } \frac{(^{14}\mathrm{C}/^{12}\mathrm{C})_{\mathrm{sample}}}{(^{14}\mathrm{C}/^{12}\mathrm{C})_{\mathrm{standard}}} \tag{4.5}$$

By definition the ^{14}C decay constant λ is chosen to be corresponding to the Libby half life rather than the "true" half life. The reference activity $^{14}\mathrm{R}_{\mathrm{standard}} = (^{14}\mathrm{C}/^{12}\mathrm{C})$ is based on the activity of wood from AD 1890, which is thought to have been in equilibrium with the atmosphere, corrected for decay to 1950. This specific activity was selected to represent the last time atmospheric radiocarbon activity was undisturbed by human activities. By convention the year 1950 is set 0 BP in radiocarbon dating.

4.3.4.1 ^{13}C correction

Radiocarbon measurements must be corrected for isotopic fractionation since the lighter carbon isotopes are preferentially taken up in any biological pathway. This can lead to spurious ^{14}C ages for contemporary existing material. This phenomenon is known since the mid-1950s, when Harmon Craig first identified that certain biochemical processes alter the equilibrium between the carbon isotopes in the different reservoirs (Craig, 1953). During photosynthesis, plants, depending of which photosynthetic pathway they use, discriminate the lighter carbon isotope ^{12}C in favor of ^{13}C and ^{14}C resulting in a deficiency of the last ones giving the samples an apparently older radiocarbon age. The discrimination process is in good agreement twice as much for ^{14}C than for ^{13}C.

Luckily, the ratio between the stable ^{13}C and ^{12}C atoms can be used to correct for the initial depletion or enrichment of ^{14}C, this correction is called normalization (Taylor, 1987). Some figures for illustration: after assimilation of carbon, C_3 plants deriving their CO_2 directly from the atmosphere are depleted in $^{13}C/^{12}C$ by as much as 15‰ relative to the atmosphere's CO_2 (Harkness and Wilson, 1979) and therefore appear to be 240 years older. In an non-biological process the situation can even be inversed: the ocean surface is about 7‰ enriched in DI^{13}C making the water apparently younger than the atmosphere. Normally a ^{13}C depletion or enrichment is given as relative deviation from a ^{13}C standard called VPDB and expressed as δ^{13}C:

$$\delta^{13}\mathrm{C} = \left(\frac{(^{13}\mathrm{C}/^{12}\mathrm{C})_{\mathrm{sample}}}{(^{13}\mathrm{C}/^{12}\mathrm{C})_{\mathrm{VPDB}}} - 1 \right) \cdot 1000‰$$

The measured $^{14}C/^{12}C$ isotope ratio is then normalized to an arbitrary set value of $\delta^{13}C = -25‰$, the mean value of wood, to insure that contemporary existing material has the same radiocarbon age. Every per mille unaccounted for fractionation that is not normalized to $-25‰$, will cause an age offset of ∼16 years. For organic material this correction is as large as 80 years and for marine shells accounts to up to 400 years. As ^{13}C is routinely measured during the data acquisition in an accelerator mass spectrometer all measurements in this thesis have been corrected for fractionation following the equations below usually applied for AMS dating:

$$^{14}\mathrm{R}_{\mathrm{sample,\ n}} = {}^{14}\mathrm{R}_{\mathrm{sample}} \cdot \left(1 - \frac{2 \cdot (25 + \delta^{13}\mathrm{C}_{\mathrm{sample}})}{1000} \right)$$

Also the ^{14}C standard is normalized:

$$^{14}\mathrm{R}_{\mathrm{standard,\ n}} = {}^{14}\mathrm{R}_{\mathrm{standard}} \cdot 0.7459 \cdot \left(1 - \frac{2 \cdot (25 + \delta^{13}\mathrm{C}_{\mathrm{standard}})}{1000} \right)$$

The fraction modern (F_m) then is:

$$F_m = \frac{^{14}R_{sample} \cdot (1 - 2 \cdot (25 + \delta^{13}C_{sample})/1000)}{0.7459 \cdot {}^{14}R_{standard} \cdot (1 - 2 \cdot (25 + \delta^{13}C_{standard})/1000)}$$

Inserted in Eq. 4.5 delivers the ^{14}C age. More information about calculating and reporting ^{14}C ages can be found for example in Froehlich (2010) and Stuiver and Polach (1977).

4.3.5 The use of ^{14}C as a water mass tracer

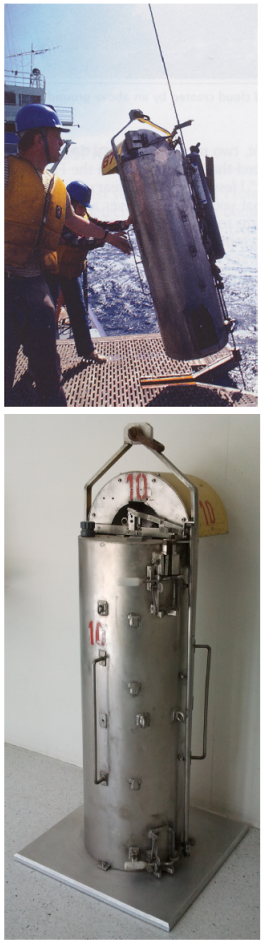

Fig. 4.13: Gerard barrels used for ^{14}C sampling.

Early on in the history of ^{14}C dating it has become clear that radiocarbon has also the potential to age ocean water as well as to determine ocean ventilation rates. This is made possible because $^{14}CO_2$, after being formed in the atmosphere, becomes dispersed throughout the Earth's active carbon reservoirs. When entering the ocean surface it is subject to a series of chemical reactions as mentioned above. Being cut off from the atmosphere, the ^{14}C-tagged carbonate species then mix with deeper water layers either by turbulent mixing or transport by ocean currents and by this means are spread throughout the ocean. Chance brought it about that the ^{14}C half life is on the one hand long enough to mix well with the ocean interior but on the other hand is short enough to prevent completely mixing. It is this characteristic that makes ^{14}C the preferential tracer to divulge residence times and renewal rates for ocean water. Subsequently, large-scale programs in oceanography were carried out to probe today's ^{14}C distribution. Before the mid-1980s large volumes of water were required to get enough DIC[7] for the radiocarbon measurements by the decay counting method. Fig. 4.13 on the left-hand side illustrates a typical water sampler (Gerard barrel) used to get water samples for radiocarbon measurements. Above: Gerard barrel during collection on the high seas. Below: scrapped water sampler in the entrance hall at the Institute of Environmental Physics. With the advent of accelerator mass spectrometry (AMS) in the mid-1980s, which directly allowed counting of ^{14}C atoms samples sizes were significantly reduced (factor of ∼1,000). This improvement opened the door to reconstruct past ocean ventilation rates by measuring calcite shells from foraminifera deposited within the marine sediments. Ever since

[7] By definition, the sum of all dissolved inorganic carbonate species ($CO_2^{aq} + H_2CO_3 + HCO_3^- + CO_3^{2-}$) is referred to as ΣCO_2 or simply DIC.

the strategy has been to measure the ^{14}C age difference between coexisting benthic and planktic foraminifera (called B.P. age) from the same depth horizon in deep-sea cores. At the best, this ^{14}C age difference provide a measure of the time elapsed for the surface water to attain the same ^{14}C signature as the bottom water. Relatively low B.P. ages indicate a rapid overturning whereas high values indicate a more sluggish ocean ventilation. In a very simplistic view, in the presence of a single moving water parcel and a constant atmospheric radiocarbon activity over time, the B.P. age is equal to a true transport time. But those requirements are usually not fulfilled in the real atmosphere-ocean system and B.P. ages do not represent a transport time.

An alternative method to reconstruct paleo deep-water ventilation histories is by using the projection-age concept first proposed by Adkins and Boyle (1997) and Mangini et al. (1998). Rather than to calculate simply the ^{14}C age difference between planktic and benthic living foraminifera, which can lead to spurious ventilation ages under a changing atmospheric $\Delta^{14}C$ as shown by Adkins (1998), projection ages are inferred by decay-correcting the measured benthic's ^{14}C activity or $\Delta^{14}C$ (obtained from deep-water corals, benthic-dwelling foraminfera or some other shell-bearing organism) back in time until it intersects with the reconstructed atmospheric $\Delta^{14}C$ record. The difference between the calendar age of the sample and the time (calendar age) of intersection of the atmospheric record yields the so-called projection age. To get true paleoventilation ages, however, one need to correct for an ocean surface reservoir offset. Since surface reservoir ages a poorly constrained especially for the past ocean only projection ages can be obtained. As a consequence projection ages always provide an upper estimate of the true ventilation age. This method circumvent the problem of a changing atmosphere's radiocarbon inventory but also cannot account for changes in the surface reservoir age nor complicated mixing histories between different water masses with different ^{14}C ages. By definition $\Delta^{14}C$ is calculated according to the following equation:

$$\Delta^{14}C_{\text{deep water}} = \left(\frac{\left(\frac{^{14}C}{^{12}C}\right)_{\text{deep water}} - \left(\frac{^{14}C}{^{12}C}\right)_{\text{standard}}}{\left(\frac{^{14}C}{^{12}C}\right)_{\text{standard}}} \right) \cdot 1000‰ \tag{4.6}$$

$$\Delta^{14}C_{\text{deep water}} = \left(\frac{e^{\text{cal age}/8266}}{e^{^{14}\text{C age}/8033}} - 1 \right) \cdot 1000‰ \tag{4.7}$$

This equation can be rewritten to Eq. 4.7 to become more manageable since the dependences of the calendar age and ^{14}C age are now apparent, see Adkins and Boyle (1997) for derivation. For more information about calculating the projection ages and results, see chapter 6. In conclusion, both presented methods allow reconstruction of paleoventilation rates as best

as possible. Once reconstructed it can be compared with the $\Delta^{14}C$ (tantamount ^{14}C age) distribution in the modern ocean to grasp past ocean circulation and circulation changes on a regional and global level as well as on different timescales. Fig. 4.14 illustrates an example of how the ^{14}C distribution looks like in the current ocean as inferred from measurements on water samples. The age distribution at a depth of 3,500 m directly reflects the large-scale meridional overturning circulation showing that the Atlantic Ocean is much better ventilated than other ocean basins like the Pacific. As explained in chapter 2, deep-water forms north of Iceland (predecessor of NADW), which penetrates until ∼3,500 m and spreads as mature NADW towards the South Atlantic indicated by increasing ages due to decay of ^{14}C along its way. The radiocarbon activity of NADW today is the highest in the whole deep ocean. Not depicted in Fig. 4.14, the eastern part of the deep Atlantic is slightly older than the western part suggesting the outflow of NADW primarily happens as a western boundary

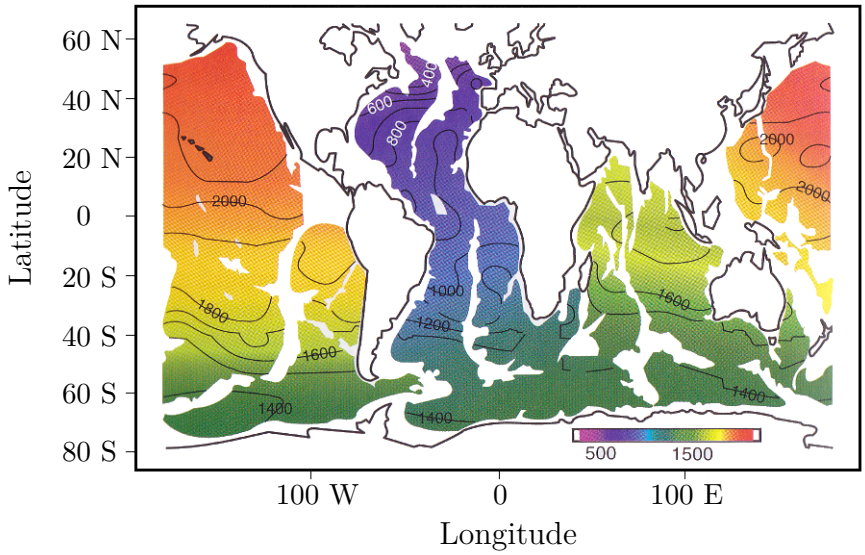

Fig. 4.14: Mapped conventional ^{14}C ages of natural radiocarbon (bomb-corrected) as measured on DIC at 3,500 m water depth. The age distribution directly reflects the large-scale overturning circulation pattern. Young deep water forming in the North Atlantic (∼400 years) spreads throughout all ocean basins driving the conveyor circulation. Age contours reflect ageing of the water by decay as well as mixing of water with different ages. The oldest deep water is found in the North Pacific in ($> 2,000$ years). Figure modified from Matsumoto and Key (2004).

current (Sarmiento and Gruber, 2006). It is important to mention that the radiocarbon ages in the South Atlantic at this depth level cannot simply be interpreted as an ageing by ^{14}C decay alone as older AABW penetrates to the north and mixes with the younger NADW lying above. Apart from these difficulties various water masses with distinct ventilation histories meet in the Southern Ocean joining the ACC eastward, which is visible

by increasing ages in the Indian Ocean and Pacific Ocean, respectively. The reader is referred to the more pictorial Fig. 2.1 for direct comparison of the large-scale deep-ocean circulation pattern. Comprehensive overviews, different depth layer, and discussions can be found in the literature (e.g. Key et al., 2004; Matsumoto and Key, 2004; Sarmiento and Gruber, 2006). Alternatively to ^{14}C as an oceanic tracer stable $^{13}C/^{12}C$ can be used as well. But it turns out the $^{13}C/^{12}C$ isotopic composition of the water shows a much smaller dynamic range (only several per mille). Thus, the $^{13}C/^{12}C$ distribution is much more complex, especially in shallow waters, where CO_2 exchange with the atmosphere and thermocline takes place, which can significantly alter the isotopic composition (e.g. Kroopnick, 1980, 1985; Marchitto et al., 2007). Moreover, $^{13}C/^{12}C$ is subject to fractionation during photosynthesis in the surface water. Deep water $^{13}C/^{12}C$ mostly do not show these drawbacks as it is decoupled from the atmosphere and direct biological activity (Duplessy et al., 1988).

4.4 Neodymium

4.4.1 Origin of neodymium

Initially used to address geological problems in the field of geochronology as a dating tool and to investigate geochemical processes in mantle and continental rock evolution on long time-scales it has been used recently as a tracer tool in paleoceanography to unriddle past ocean circulation (Frank, 2002). This is made possible due to the high resilience of the samarium-neodymium isotope system against possible remobilisation during metamorphism or weathering processes compared to other isotope systems within a rock (White, 2003). Neodymium belongs to the group of the 14 naturally occurring rare earth elements (REE), comprising the lanthanides supplemented by the two transition metals scandium and yttrium. Neodymium (Nd) comes in seven natural isotopes ranging in mass from 142−150 u. In paleoceanographic studies only the neodymium isotopic composition $^{143}Nd/^{144}Nd$ in seawater is of interest. The stable radiogenic ^{143}Nd isotope is being continuously formed by α-decay from the long-lived samarium ^{147}Sm ($T_{1/2} = (1.06 \pm 0.04) \cdot 10^{11}$ years) constituting ∼15% of the natural Sm abundance (Begemann et al., 2001). Primordial ^{144}Nd is used for normalization purposes and quasi stable ($T_{1/2} \sim 2.29 \cdot 10^{15}$ years). Though ^{148}Sm is also unstable it is not contributing to the natural abundance level of ^{144}Nd due to its much longer half life of $\sim 7 \cdot 10^{15}$ years (O'Nions et al., 1979). Before Earth was formed ∼4.5 Ga ago (Rudge et al., 2010), the Sm/Nd element concentration ratio in the solar nebula is thought to have been constant with ^{143}Nd concentrations increasing in time through decay of ^{147}Sm (Fig. 4.15). During the accretion of the Earth from the solar nebula (SN) at time t_c the Sm/Nd ratio, however, became fractionated, changing towards a lower Sm/Nd concentration thereby altering the ingrowth rate of ^{143}Nd of the newly formed Earth compared to the previous rates in the SN. This chemical differentiation between Sm and Nd is mainly a consequence of their different atomic radii (Boynton, 1975) and determines the concentrations in subsequent melting events of Earth' mantle. Nd is

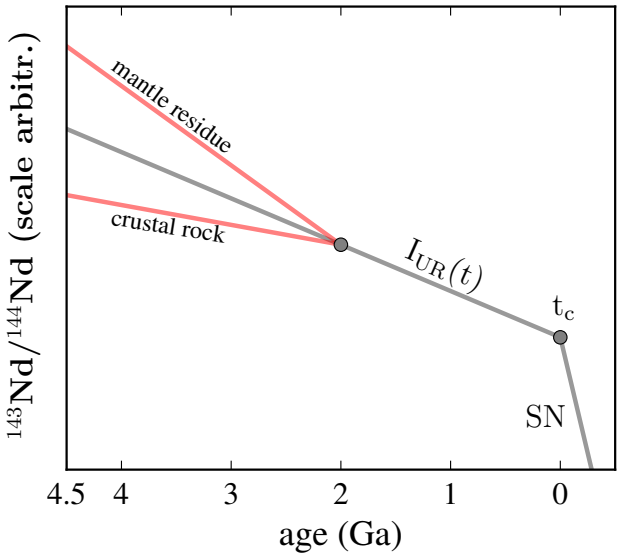

Fig. 4.15: Evolution of the Nd isotopic composition of the bulk Earth ($I_{UR}(t)$, UR: Uniform Reservoir) subsequently after its formation from the SN. Every melting event in Earth mantle fractionates Sm and Nd causing different Nd isotopic compositions in the continental crust and the residual mantle. Picture after DePaolo and Wasserburg (1976).

accommodated more easily into the partial melt of the mantle rock than Sm leading to more depleted Sm/Nd concentrations in the continental crust compared to the residual mantle (Fig. 4.15) (Goldstein and Hemming, 2003). The gray line describes the neodymium isotopic evolution of the $^{143}Nd/^{144}Nd$ ratio in time of the hypothetical uniform reservoir (bulk Earth). This bulk-earth evolution line also called as CHUR (Chrondritic Uniform Reservoir) and serves as a model for the isotopic evolution of Earth's primitive mantle. The red lines show different isotopic histories after chemical differentiation caused by a melting event as described. Continental- and mantle composition can be clearly distinguished. The initial bulk Nd isotopic composition of Earth can be obtained from chrondritic meteorites, which simultaneously originated from the SN as Earth. The accepted $^{143}Nd/^{144}Nd$ ratio in today's chrondrites is 0.512638, defining the standard value against all $^{143}Nd/^{144}Nd$ measurements are reported (Jacobsen and Wasserburg, 1980). The Nd ratios are conveniently expressed as ε_{Nd} (the relative deviation of a sample's $^{143}Nd/^{144}Nd$ isotopic ratio to the standard value expressed in parts per 10^4 (‰)) Piepgras and Wasserburg (1980) following the equation:

$$\varepsilon_{Nd} = \left(\frac{(^{143}Nd/^{144}Nd)_{sample}}{(^{143}Nd/^{144}Nd)_{CHUR}} - 1 \right) \cdot 10000‰ \tag{4.8}$$

4.4.2 Continental distribution of neodymium

Sm/Nd concentrations of the continental crust are always lower than the hypothetical chrondritic uniform reservoir, thus, ε_{Nd} tend to be predominantly negative. Conversely, positive values are expected to come from mantle rock relatively enriched in neodymium. The observed large heterogeneity in ε_{Nd} of the continental crust is the product of the different Sm/Nd concentrations and their various ages. Besides, complex and long lasting reshuffling processes of this crustal material through plate tectonics increases this heterogeneity even further. This observed heterogeneity in the neodymium isotopic composition is the basis for tracing sources and transport routes with ε_{Nd} (Goldstein and Hemming, 2003). As illustrated in Fig. 4.16, ε_{Nd} exhibits a wide range encompassing basaltic rocks from the mid-ocean ridges showing values up to +12 to old granitic cratons (continental rocks) giving values by as much as −45 (Lacan and Jeandel, 2005). This wide range in ε_{Nd} is of special interest for tracing ocean currents as outlined in the next section.

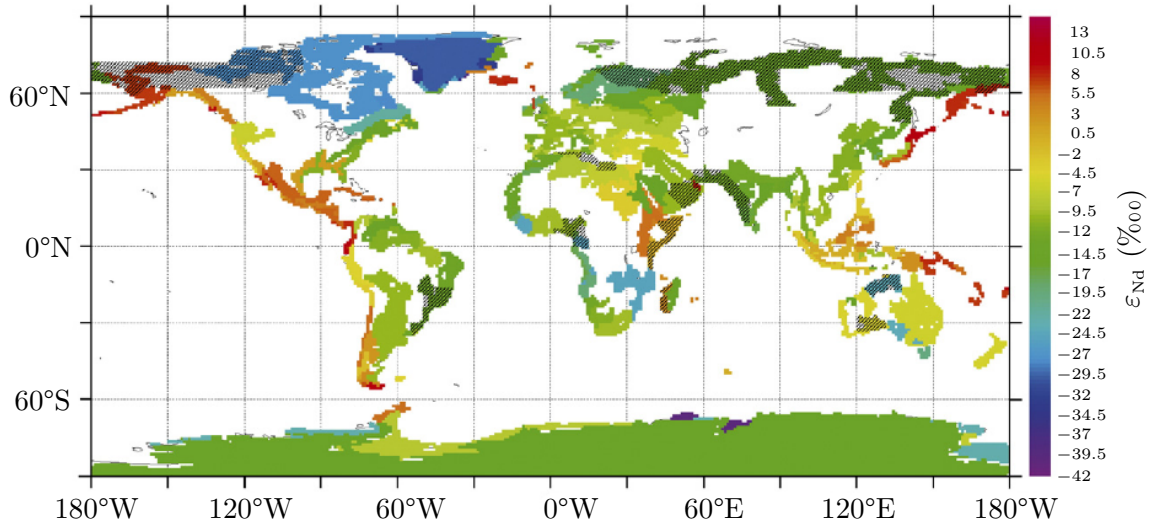

Fig. 4.16: This figure is an overview illustrating the large continental heterogeneity of the $^{143}Nd/^{144}Nd$ isotopes expressed as ε_{Nd} of the margins surrounding the oceans. Hatched areas indicate regions where ε_{Nd} were estimated due to insufficient data. Picture modified from Jeandel et al. (2007).

4.4.3 Neodymium as oceanic tracer

The following is abstracted and briefly summarized from the review articles of Frank (2002) and Goldstein and Hemming (2003). The reader is cautioned to these extensive sources for further reading. The neodymium isotopes dissolved in seawater enter the ocean mainly by river run off and aeolian dust from weathering and erosion of continental rocks and through particle-seawater interaction. Further suggested sources of neodymium are the mid-ocean ridges as well as submarine volcanoes. The exact mechanism, however, how ocean currents acquire their different Nd-isotope signatures is not well understood. 90−95% of the neodymium in the ocean persists dissolved in seawater exclusively in the +3 state in oxygenated seawater and is stabilized mostly in the form of Nd-carbonate ($NdCO_3^+$) or Nd-sulfate ($NdSO_4^+$) with traces of Nd^{3+} (Jeandel et al., 1995; Frank, 2002). Predominantly negative ε_{Nd} values in ocean water point to a continental origin of the Nd isotopes. Concentrations in seawater range between 2−7 pg/g (Fig. 4.17) which is about 10^6 to 10^7 smaller than the average Nd concentration in continental or oceanic rocks suggesting a short residence time for this REE. Responsible for this effective removing from the water column are adsorption (scavenging) onto particles affecting all rare earths. This behavior is explained by their equal valence state in oxygenated seawater. Reported residence times range between 500−1,000 years, which is relatively short compared to the oceanic mixing time of ∼1,500 years (Tachikawa et al., 2003). High Nd concentrations in the Atlantic Ocean are mainly derived from the surrounding continents by higher river run off. This is different in the Pacific Ocean where most of the Nd is supposably contributed from basaltic

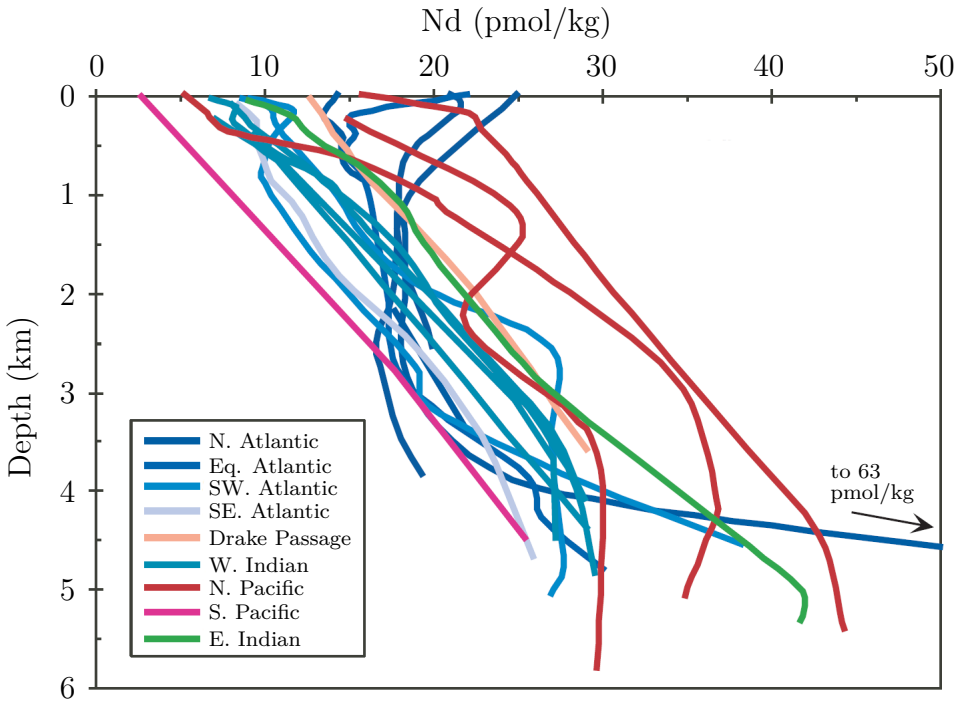

Fig. 4.17: Nd concentration measurements from all ocean basins. Apparently, Nd concentrations increase with depth and vary with between different ocean basins. Largest Nd values are found in the deep North Atlantic and deep North Pacific (> 40 pmol/kg). Lowest surface values are found in the South Pacific (< 5 pmol/kg). and the lowest values in the South Pacific respectively North Atlantic. This increase with depth is a consequence of particle scavenging steadily happening in the water column. There are some exceptions from this view, e.g. in the North Atlantic, where other factors obviously play a role. Modified from Goldstein and Hemming (2003).

material as a result of volcanic activity. Hydrothermal sources of Nd seem to play a secondary role in the Nd budget of the Pacific as it is quickly removed from the water by scavenging on hydrothermal precipitates. Observed $\varepsilon_{\mathrm{Nd}}$ in seawater differ between -26 (Baffin Bay surrounded by the old canadian craton) to high radiogenic $+20$ (island arc rocks around the Pacific Ocean) and vary due to the systematic geographic variability within the ocean provinces. Different from other marine tracers like δ^{13}C or Cd/Ca, neodymium, once dissolved, is not thought to be altered by biological processes and thus behave conservative making them a valuable tracer for paleoceanography. This conservation is strictly speaking only fulfilled in the absence of any lithogenic input along the flow path of a water mass. ^{143}Nd/^{144}Nd ratios are then not altered as long as no mixing of different water masses or other input (riverine, aeolian) with distinct Nd ratios occur altering the original isotopic Nd composition. For example, North Atlantic Deep Water (NADW) is fed in part from water originated from north of Iceland (69° N) in a region which persists of young mantle rock (high $\varepsilon_{\mathrm{Nd}}$ values). This preformed NADW water mixes farther south with the quite

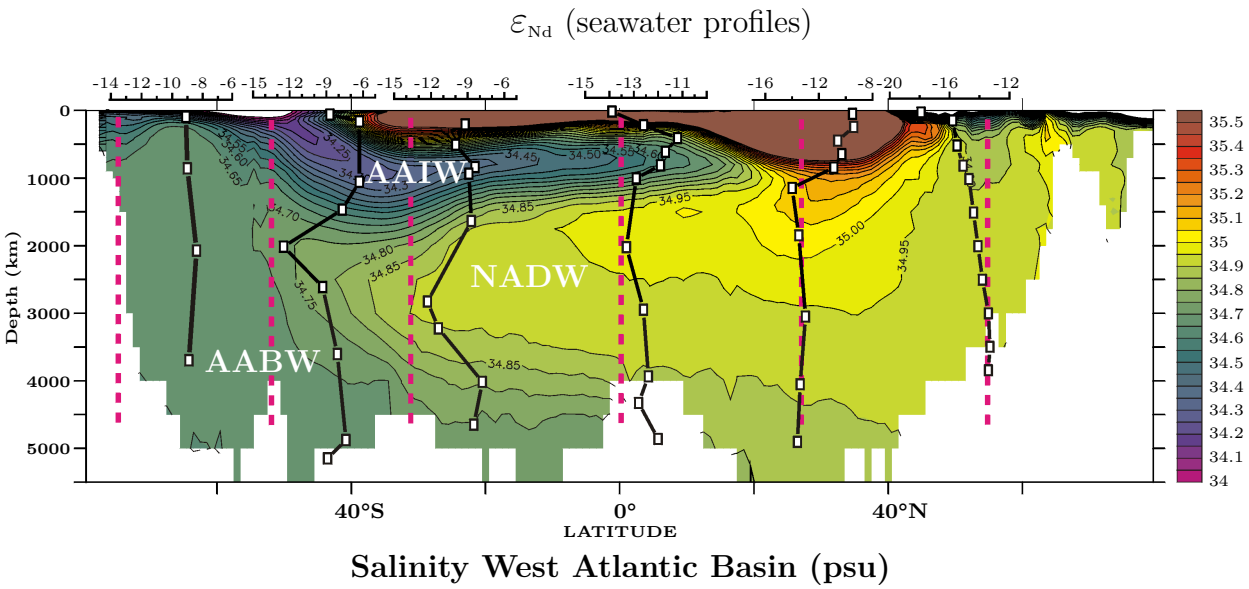

Fig. 4.18: NADW flow in the West Atlantic is oriented to the south and characterized by a high salinity. Water column Nd measurements are superimposed (open squares and black lines), and resembles this salinity field. Pink dashed lines show the modern NADW value of −13.5. Picture modified from von Blanckenburg (1999).

non-radiogenic water from the Labrador Sea from the Buffin Bay to form mature NADW with a present-day ε_{Nd} of −13.5, which can be traced several thousand kilometers without essentially changing its isotopic signature. In Fig. 4.18 NADW flow in the Atlantic is illustrated, visible on its relatively high salinities. The salinity transect from north to south is superimposed by ε_{Nd} water-column measurements (squares and black lines) that nicely track the salinity distribution of NADW. Pink dashed lines depict the modern-day average NADW value of −13.5. The southward flow of NADW is compensated by two other water masses penetrating the Atlantic from south to north videlicet Antarctic Intermediate Water (AAIW) and Antarctic Bottom Watter (AABW), both originating in the Southern Ocean, which sandwich NADW. AAIW and AABW are clearly distinguishable from the NADW water by their higher ε_{Nd} values between −7 to −9 and also their lower salinity. The NADW signature finally disappears at around 49 °S when it enters the realm of the Antarctic Circumpolar Current. The applicability of this radiogenic isotope system has been extended in recent years to many other marine archives. These include leaching of ferromanganese coatings of bulk sediments, which form at the sediment-water interface incorporating the ambient seawater Nd isotope signature. Also, cold water corals have been proven to be a reliable archive for modern and past seawater Nd isotopic composition, which is incorporated during the precipitation of their skeletons. Since their Nd concentrations are usually very low extraction of Nd from aragonite is more complicated than for sediments and requires more diligence during prior physical and chemical cleaning. Unlike sediments corals have the advantage of being absolutely datable by the ^{230}Th/U method (van de

Flierdt and Frank, 2010). Other potential marine archives shown to incorporate neodymium of surface and deep water are fish teeth, fish debris, and formaminifera.

4.5 $(^{231}Pa/^{230}Th)_{xs}$ as a paleocirculation proxy

Some $^{231}Pa/^{230}Th$ measurements have been performed in the course of this thesis. The results are presented in appendix B.2 together with a short discussion. This being the case, a few words must be spent on this issue especially since some results from other authors are presented and discussed. The decay-corrected sedimentary excess ratio $^{231}Pa/^{230}Th$ (hereafter Pa/Th) has been proposed as a promising isotopic tool for paleoceanographers to infer past ocean circulation (Yu et al., 1996). Unlike the geochemical water mass tracer $^{143}Nd/^{144}Nd$ and several nutrient proxies such as $\delta^{13}C$ and Cd/Ca (e.g. Boyle and Keigwin, 1987; von Blanckenburg, 1999; Goldstein and Hemming, 2003; Curry and Oppo, 2005) that only allow differentiating between various water masses, the marine sediment Pa/Th ratio taken by itself makes a qualitative point about the rate of overturning. This kinematic proxy is owing its application to the fact that production of ^{231}Pa and ^{230}Th in the ocean is constant and well established simplifying the interpretation of its distribution compared to other marine trace elements. The isotopes ^{230}Th and ^{231}Pa[8] are produced by uranium decay at uniform rates throughout the world's ocean. The production rates are: $\beta_{Pa} = 2.45 \pm 0.05 \cdot 10^{-3}$ dpm m^{-3} a^{-1} for protactinium and $\beta_{Th} = 2.62 \pm 0.05 \cdot 10^{-2}$ dpm m^{-3} a^{-1} for thorium. The resultant activity ratio is $\beta_{Pa}/\beta_{Th} \sim 0.093$ at every point in the water column (Turekian and Chan, 1971).

As mentioned in chapter 4 thorium once dissolved is highly particle reactive. The same applies to protactinium, which in aqueous environments is found in its pentavalent state. Even though these isotopes show a different chemical behavior, both adsorb quickly onto the surface of sinking particles and are in this way removed from the water column into the underlying sediments by reverse particle scavenging. This rapidly removal is mirrored by their very low seawater activities, which, without scavenging, would have the same activity as the parent uranium isotopes (^{234}U, ^{235}U) (Moore and Sackett, 1964). Nevertheless, as shown in Fig. 4.19 the isotopes' mean residence times are different: 50−200 years for ^{231}Pa and just 0−40 years for ^{230}Th (van der Loeff and Berger, 1993). Since ^{230}Th is an order of magnitude more particle reactive than ^{231}Pa, the former is virtually not advected horizontally. In contrast, the ^{231}Pa residence time is similar to the one for the modern deep-water in the Atlantic. As a result about 50% of the dissolved ^{231}Pa in the Atlantic is exported to the Southern Ocean where ^{231}Pa is then preferentially scavenged from the water column due to the relatively high affinity to existing biogenic opal (particulate silica) (Asmus et al., 1999; Chase et al., 2002). This is a potential pitfall because it means that

[8] Pa-231 is the daughter product of ^{235}U the starting point of the actinium series. Its half life is 32.71 ± 0.11 ka (Robert et al., 1969), whereas ^{230}Th originates from the uranium series having a half life of 75.38 ka.

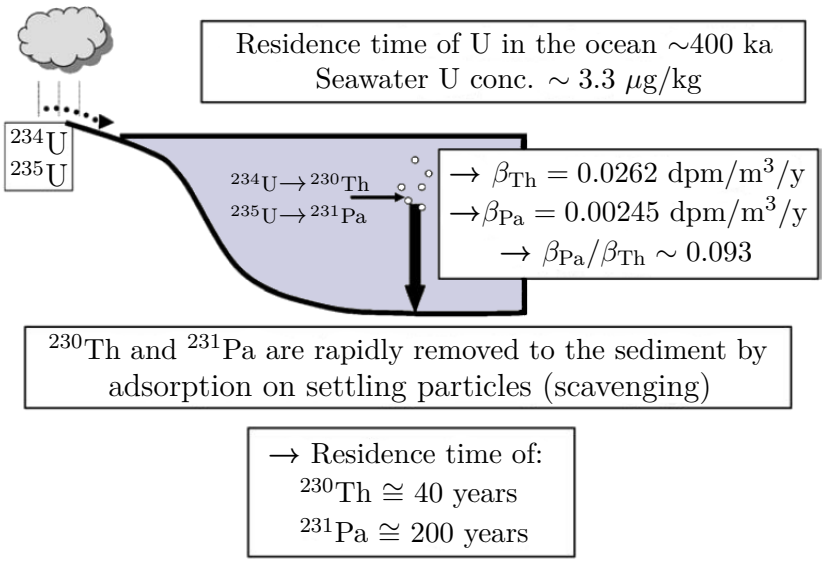

Fig. 4.19: ^{231}Pa and ^{230}Th is constantly produced in ocean waters by decay of dissolved uranium entering the ocean mainly by river runoff. Picture modified from François (2007).

Pa/Th close to the production ratio do not necessary reflect circulation changes (Bradtmiller et al., 2007; Keigwin and Boyle, 2008). Thus, checking the sediment for opal concentration is an integral part of every Pa/Th measurement. In case of a circulating water mass the Pa/Th activity ratio, decay-corrected to the time of deposition, should therefore be lower than the expected production ratio of 0.093. The greater the overturning strength (for instance in the Atlantic Ocean) the lower the ratio is compared to the production value, and the lower the overturning strength the closer this value is to 0.093. In the past decade Pa/Th has been widely used in paleoceanography to reconstruct changes mainly in the export of Atlantic deep-water (McManus et al., 2004; Gherardi et al., 2009). But this method has been challenged when it became clear that also other parameters influence the fractionation of Pa and Th in ocean water, namely particle flux (Anderson et al., 1983), particle composition (Geibert and Usbeck, 2004) and even particle size (Kretschmer et al., 2008). In such a case no easy interpretation of the Pa/Th ratio is on hand. Even though, much research efforts have been spent in understanding the behavior of this semi-quantitative proxy, further development of this ratio as a proxy for paleocirculation strength is needed. Most notably to get additional insights of the interaction between particle scavenging and ocean circulation in controlling the distribution of Pa/Th in the marine sediments. Fig. 4.20 exhibits measurements of Pa/Th on two cores from off Bermuda Rise (water depth ~4,500 m) encompassing the last 35 ka BP. Ratios for the Holocene deep Atlantic on average oscillate around 0.055 ± 0.006 and show no serious changes in deep water strength for the last 10 ka BP. The situation was much different during the last glacial period and deglaciation, respectively, when Pa/Th ratios reached almost production

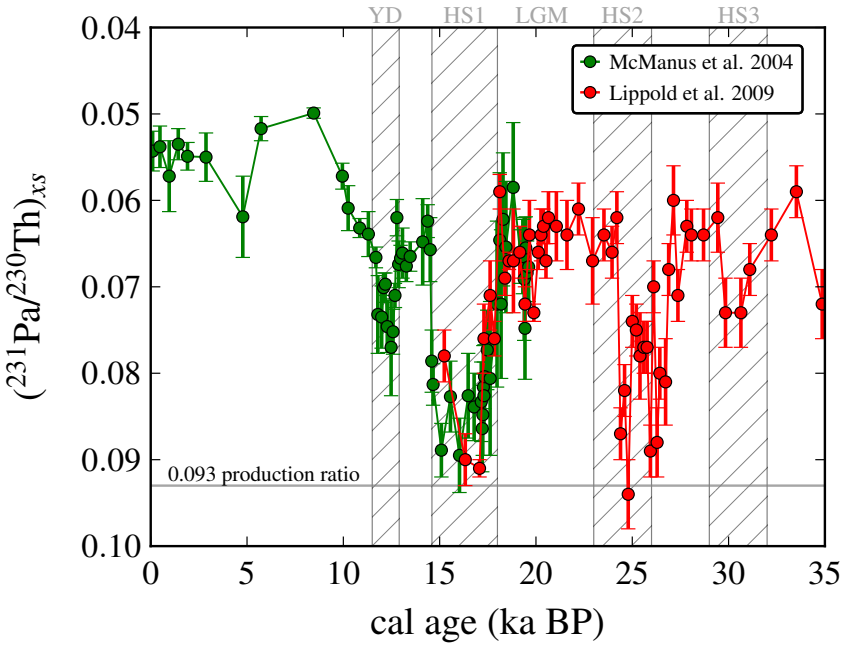

Fig. 4.20: Pa/Th ratios from two adjacent North Atlantic sediment cores for the past 35 ka BP. High values in Pa/Th near the production ratio indicate a theoretical cessation of the Atlantic meridional overturning circulation.

values, indicating severe changes in the Atlantic meridional overturning circulation coinciding with intense cooling throughout the North Atlantic realm (Denton et al., 2010). For clarification, the abbreviation HS in Fig. 4.20 stands for Heinrich stadial. The difference between Heinrich events and Heinrich stadials are not precisely defined in the literature. Heinrich events are thought to be the trigger of the subsequently followed period of colder conditions (stadials), which lasted up to several thousand years, but the exact relationship between Heinrich events and and Heinrich stadials is unclear until today.

5 Coral study area

5.1 Sediment core location

Four sediment cores have been retrieved within the framework of geological prospections conducted by the Brazilian oil company Petrobras (Petróleo Brasileiro S.A.) by means of the piston coring technique. The cores stem from the continental margin of southeast Brazil located in the Brazilian Basin south of the Vitória-Trindade-Seamount-Chain from the Campos and Santos Basin. Both are adjacent coastal sedimentary basins out of fifteen, which divide the ∼7,000 km long Brazilian shoreline. The Campos Basin is located on the southeastern Brazilian margin between 24 °S (Cabo Frio High) and 20.5 °S (Vitória High) occupying a total area of ∼100,000 km^2, mostly off-shore. The adjoining South Brazilian Bight (São Paulo Bight), hosting the Santos Basin, extends between 24 °S (Cabo Frio High) and 28 °S (Florianópolis Platform) constituting an area of over 200,000 km^2 and harbors the most examined and prolific Brazilian off-shore petroleum fields (Cainelli et al., 1999; Sumida et al., 2004).

The continental shelf in this region is on average 70−230 km wide. The shelf break is found in depth between 120−180 m (da Silveira, 1999; de Mahiques et al., 2010). Both areas are known for their oil wealth and are currently being extensively exploited by off-shore oil rigs making them the most prolific basins in the western South Atlantic (Mohriak et al., 1990). PC-ENG-111 and K-GLC-PPT-06 hereafter C1 and KGLC stem from the Campos Basin respectively the Papa-Terra field in the southern Campos Basin about 350 km (beeline) to the east of Rio from water depths between 621 m and 626 m. PC-21210009 and MXL-030 hereafter C2 and MXL stem from the Santos Basin ∼150 km south-southwest of Rio from a water depths of 781 m and 808 m, respectively (R. Kowsmann 2010, pers. comm.) (Fig. 5.1). All four sediment cores are situated within the domain of the middle slope spanning over 40 km in width at an average gradient of ∼2.5 ° (Arantes et al., 2009).

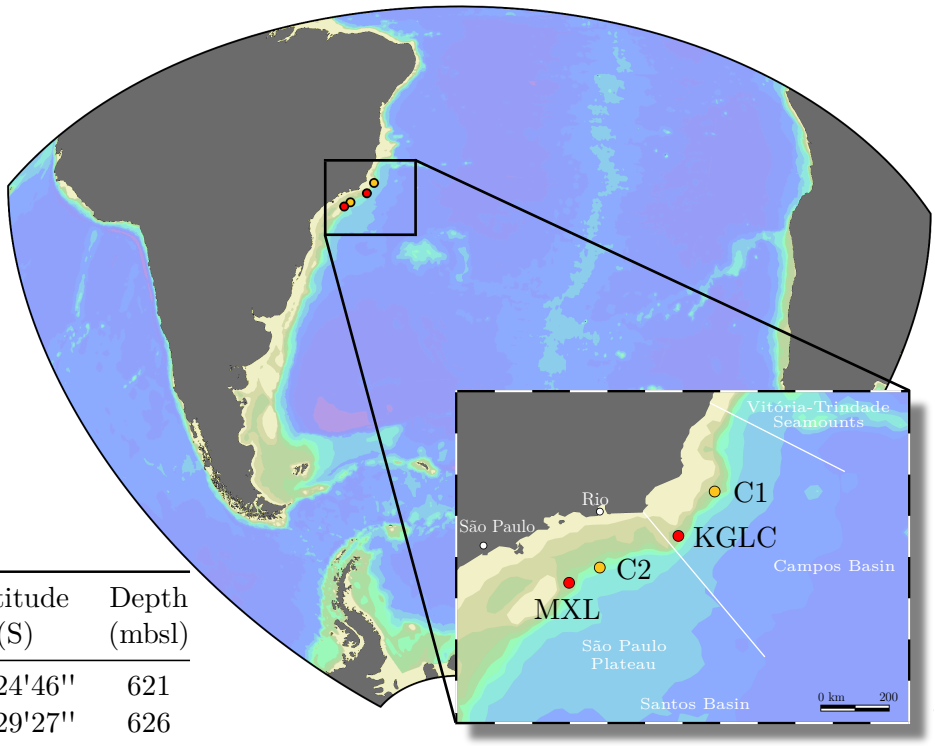

ID #	Longitude (W)	Latitude (S)	Depth (mbsl)
C1	40°08'41''	22°24'46''	621
KGLC	41°06'40''	23°29'27''	626
C2	43°12'06''	24°15'24''	781
MXL	44°01'09''	24°37'34''	808

Fig. 5.1: Location of investigated sediment cores C1, KGLC from the Campos Basin and C2, MXL from the Santos Basin retrieved from off the Brazilian margin. Also indicated on the figure are some regional physiographic features: the Vitória-Trindade seamount chain in the north and the São Paulo Plateau in the south.

5.1.1 Sedimentology of the core sites

The following is a direct quote from Viana et al. (1998), p.147 summarizing the sedimentological main characteristics of the core location as follows:

> The middle slope 550−1200 m is characterized by iron-rich laminated indurated fine sands and deep-water coral mounds that overlie a thick, metres to tens of metres, package of silty-mud to sandy laminated mud (Caddah et al., 1998), in some places disrupted by mass-flow processes. The iron-rich surface encrusted layer is generally 10 cm thick, comprising siliciclastic and biogenic fine silty sands (Caddah et al., 1994). They are yellowish brown, more rarely reddish ('rusty'). They show planar lamination marked by intercalations of fine sand and silt layers, sometimes masked by Planolites-type bioturbation (Caddah et

al., 1998). AAIW oxygen-rich flow probably oxidises the ocean bottom creating iron-rich sandy crusts, and carries ahermatipic coral larvae (Viana, 1994). These larvae grasp the gentle topographic mounds inherited from Late Pleistocene mass movements (Kowsmann et al., 1994; Viana et al., 1994) and develop coral banks elongated down-current.

5.2 Cold-water coral occurrences off southeast Brazil

There are several reports of fossil *L. pertusa* occurrences from Campos Basin (120 km off the coastline) near the location where C1 and KGLC have been retrieved. *L. pertusa* are found in this area on elongated carbonate mounds exhibiting varying widths of several tens of meters and heights up to 10−15 m. They cover an estimated area of 600 km^2 (Hovland, 2008). Fossil coral banks are found in this area in water depths between 570 to more than 850 m (Viana et al., 1998). As a side note 59 azooxanthellate species are known to live in Brazilian waters (status 2007). This number is probably a lower estimate, biased by the small number of research campaigns conducted so far. On the contrary the number for zooxanthellate shallow-water corals in the southernly Brazilian coastal area is even more sparse with only 15 known scleractinian species compared to ∼130 in the Caribbean. It is believed that the freshwater run-off of the mighty Amazon River farther north forms a geographic barrier making coral migration from north to south difficult (Kitahara, 2007). Fig. 5.2 shows typical specimens of dead coral rubble collected from sediment from the bottom of Santos Basin exhibiting different scleractinian skeletons (Sumida et al., 2004). Sediment cores C2 and MXL have been acquired from the edge of so-called pockmarks, which are described as circular or near-circular crater-like depressions in the ambient seabed, generally 10−200 m in diameter and up to 35 m deep with exceptions proving the rule (Pilcher and Argent, 2007). Pockmarks are common on continental margins with hydrocarbon-rich sedimentary basins. The current explanation points to expulsion of hydrocarbon-rich fluids escaping from fine-grained sediments. The source of this fluid are deep oil-bearing deposits beneath the continental margins which are million of years old. Bacteria living within the sediment decompose those hydrocarbons to lighter species like methane, which then migrates slowly by pore water diffusion to shallower sediment

Fig. 5.2: Cleaned fossil cold-water coral rubble collected from sediment of Santos Basin (Sumida et al., 2004).

horizons where it would stop and accumulates. If these methane-bubbles reach a critical threshold in gas concentrations respectively pressure they may burst leaving behind these crater-like depressions (Hovland et al., 1993; Figueiredo et al., 1999). Especially Santos Basin is littered with pockmarks (Fig. 5.3). Cold-water communities preferentially developed and grouped around the edges of these pockmarks indicating a close relationship between hydrocarbon seepage and coral settlement in this area. Santos Basin still host the most southerly known cold-water reef-like structures in the Atlantic Ocean (Hovland, 2008). Known fossil carbonate mounds in the Santos Basin reach heights of 20 m and are several hundred meters long (Sumida et al., 2004).

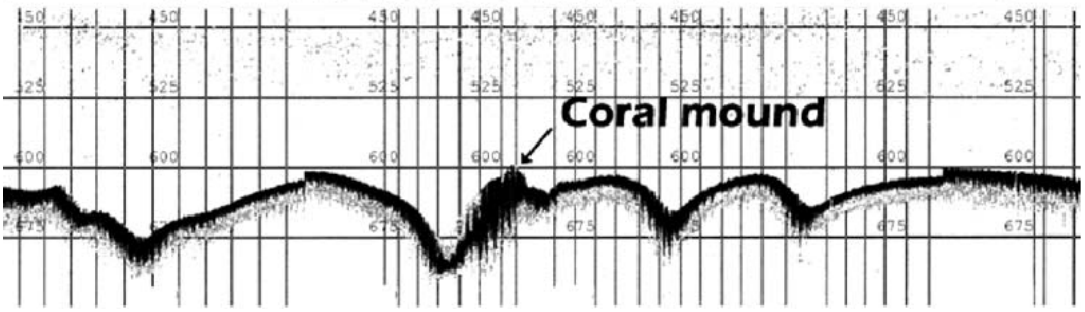

Fig. 5.3: Hydroacoustic assessment of the bottom topography in the Santos Basin showing profiles of some pockmarks. Also visible is a huge coral mound up to 20 m height on the edge of one of these pockmarks. Numbers denote water depth (Sumida et al., 2004).

5.3 Piston cores

5.3.1 C1 and KGLC

Pictured are the 380 cm and 406 cm long piston cores C1 and KGLC. Seismic data conducted by Petrobras show that KGLC was taken on an intercanyon ridge on a slope carved by numerous canyons (R. Kowsmann 2011, pers. comm.). Fossil corallites from C1 are comprised mainly of the framework builders *L. pertusa* and to a minor extent of *S. variabilis* in the lower sections of the core. Coral rubble is found in the first 300 cm of C1 followed by apparent darker sediment filling the core to the bottom (380 cm). A more pre-

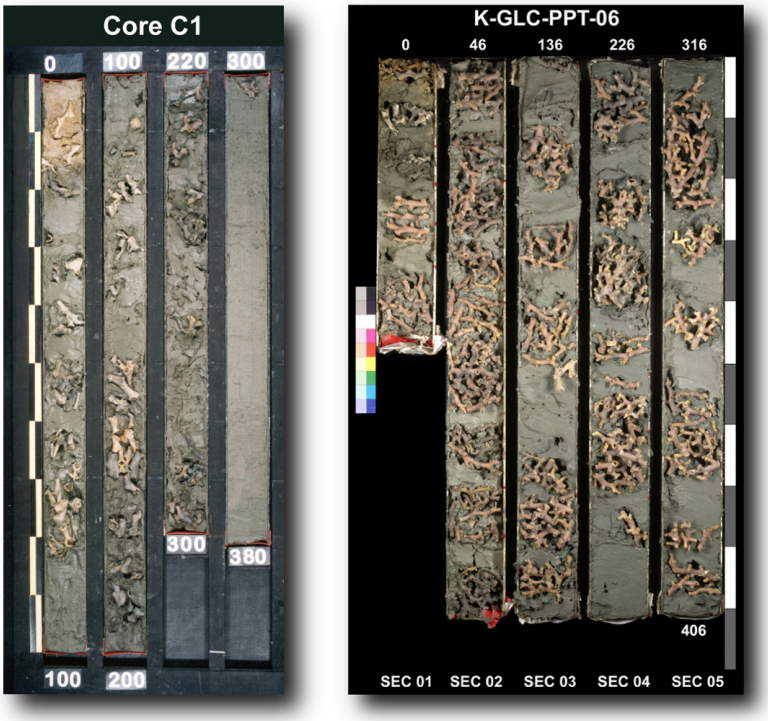

Fig. 5.4: Piston cores C1 and KGLC showing coral rubble and even whole coral branches mainly of the species *L. pertusa* and *S. variabilis*.

cise determination of the species filling KGLC revealed that the core top (∼10 cm) is harbored by *L. pertusa*, the downcore sections, however, is exclusively crammed with whole branches of fossil *S. variabilis* (R. Kowsmann 2010, pers. comm.). Interestingly, no living corals from this species have been found on the Brazilian margin so far. Coral rubble and whole branches in both cores acquire sizes up to 10 cm. Possible changes of ecological significance will be discussed in chapter 6 section 6.6. It seems reasonable to assume that all corals from the four sediment cores are autochthon in origin as to the

proximity of the described fossilized reef-like structures in those areas. All coral fragments in both cores are in a good state of preservation with no obvious signs of iron-manganese coatings nor any, at least, visual a change that must be of evident diagenetic alterations of their skeletons except for some endolithic borings every so often. Also the septa, a characteristic morphologic feature within the calyx of those corals, are well preserved. Especially the corals in KGLC look fresh and pristine. Former ^{230}Th/U dating on corals of C1 (Ruckelshausen, 2009; Mangini et al., 2010) gave ages between ∼8,500 a BP[1] for the youngest and about 20,500 a BP for the oldest samples. Fragments from KGLC on the other hand stretch the ages between 18,000−27,700 a BP with one single exception with an age of ∼4,700 a BP. They, hence, constitute a record of ∼27,000 a of the Brazilian oceanographic history. The stratigraphic order[2] one would usually expect for sediment cores taken from the plane abyssal ocean floor is disrupted in all four investigated cores pointing to complex depositional processes, which is not that unusual for that kind of oceanic environments like the continental slope. Nevertheless, a rough sedimentation rate can be calculated from the corals. For C1 a sedimentation rate of ∼40 cm/1,000 years is obtained, which is by a factor of ∼2.5 smaller than the rate deduced by the foraminiferal zonation scheme. For biozone Y1B ∼15,000−40,000 a BP a sedimentation rate of around 100 cm/1,000 a can be derived (R. Kowsmann 2011, pers. comm.) (cf. chapter 6 section 6.5). The 20 cm long gap in C1 between 200 cm and 220 cm is due to the on-board sampling technique.

5.3.2 C2 and MXL

Figure 5.5 shows C2 with a core length of 363 cm beside the 419 cm long MXL core which have been retrieved with the same coring technique. Both locations are ∼160−185 m deeper than the sites in the Campos Basin. Also seismic data compiled by Petrobras show MXL-30 was taken on a lower slope, in a narrow linear depression riddled by pockmarks and adjacent highs (resembling an egg carton) (R. Kowsmann 2011, pers. comm.). As well as the cores from Campos Basin they both hold a high abundance of coral. The first 70 cm of core C2 consist of coral rubble of species *L. pertusa* followed by a grayish colored section between 70 cm and 220 cm with virtually no corals at all. After that, corals appear again until the end of the core but with only occasional occurrences of *L. pertusa* and some *S. variabilis*. The taxonomic rank of the remaining fragments in this section could not be determined due to bad preservation. Previous ^{230}Th/U-age screenings from this section yielded ages of 370,000 years and older (A. Mangini 2008, pers. comm.). Most probably, if not certainly, post depositional diagenetic alteration of the aragonite skeletons occurred so that calendar ages cannot be regarded as reliable. This view is encouraged by investigations on planktonic foraminifera assemblages on the core's sediment, conducted by M. A. Vicalvi who placed this core section within the X-zone, after the foraminiferal zonation scheme by

[1] All given ages in this thesis are reported as BP (Before Present) where "Present" is defined as AD 1950.

[2] The law of superposition in geology states that sedimentary layers are deposited in a time sequence, with the oldest on the bottom and the youngest on the top.

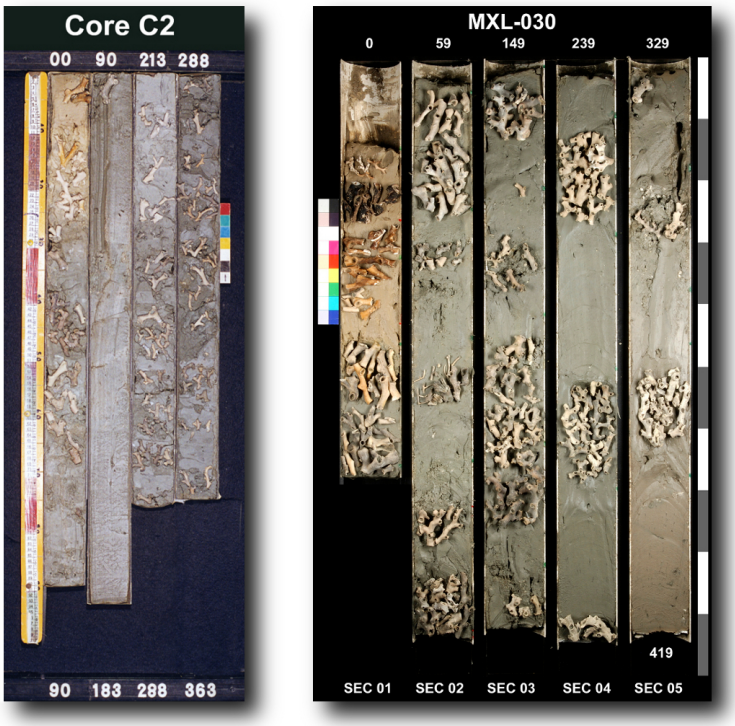

Fig. 5.5: Piston cores C2 and MXL showing coral rubble and even whole coral branches mainly of the species *L. pertusa* and *S. variabilis*.

Ericson and Wollin (1968), encompassing the Last Interglacial period (Mangini et al., 2010). Coral ages determined within the uppermost 5−70 cm are between 10,500−29,300 a BP (Ruckelshausen, 2009; Mangini et al., 2010). In sediment core MXL corals group in clusters with gaps up to 30 cm wide. The genera in this core could not be determined as easily as in KGLC as to the in parts small fragments found in this core. Only the core section between 24−82 cm predominantly hosts *L. pertusa*, the remainder could not be determined (R. Kowsmann 2010, pers. comm.). Coral fragments in C2 and MXL both look a bit more corroded and worn, not as pristine as in C1 and KGLC, but nevertheless are relatively good preserved. Age measurements range between ∼10,735−90,000 a BP in MXL. Only for MXL a rough sedimentation rate could be estimated yielding ∼35 cm/1,000 a comparable with those of C1. Many age inversions in C2 made sedimentation rate assessment impossible. The sediment gap between 183 cm and 213 cm is also due to on-board sampling technique.

5.4 Modern hydrographic setting

The sources of the surface and deep South Atlantic water masses are manifold. Being fed by the North Atlantic, the Pacific, via the Drake Passage, the Weddell Sea in the Southern Ocean and the Indian Ocean by the western extent of the Agulhas Current, as a common feature, all these water masses initially originated from the surface water in these regions carrying the specific characteristic with them, which can be traced over long distances. Our current understanding of global ocean circulation stems mainly from direct observations of water mass tracers like salinity, temperature and nutrient distribution to name but a few, without going into detail about various mixing processes between different oceanic currents and biological activity within a specific water mass, however alter the original tracer signatures. Nonetheless, recognizing these different ocean currents is possible (Reid et al., 1977). Fig. 5.6 illustrates by means of the dissolved nutrient phosphate how water masses can be distinguished by their different phosphate content, showing the major water masses flowing alongside the indicated transect encompassing the Brazilian coastal region. Every single dot on the picture marks a measurement. See the next section for a more elaborate description of the hydrographic setting of this region. The following elucidates the different water masses being found in the area of interest today. Physiographic features, which are numerous in this region and are essential in delivering boundary conditions for controlling modern circulation patterns are not going to be discussed. See Johnson (2007) and Torres et al. (2010) for a description about the physiography in the Brazilian Basin.

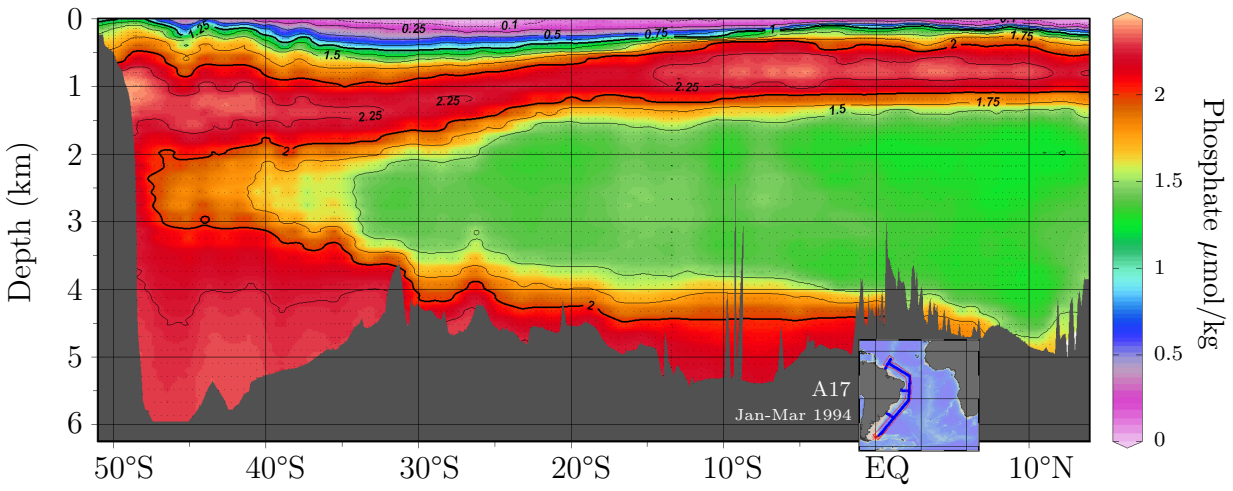

Fig. 5.6: Phosphate distribution along the transect A17 of the World Ocean Circulation Experiment (WOCE). Picture available online at `http://www.ewoce.org` (Schlitzer, 2012). Accessed 2013/4/23.

5.4.1 Local hydrography off Brazil

The surface water at the core locations is governed by the Brazil Current (BC), a 300 km wide and weak western oligotrophic surface boundary current in the South Atlantic most widely confined to the Brazilian coast between ∼20 °S and 30 °S carrying warm subtropical water from north to south (Schmid et al., 1995; Viana et al., 1998). The BC is purely wind-driven. Wind stress exerted to the ocean surface by the persistent anticyclone gyre located in the subtropical South Atlantic leads to a levorotatory geostrophic evasion movement of the water in the same direction. At ∼22 °S the BC bifurcates into a component flowing eastward, the residual continues to flow in southward direction along the coastal area until its scent finally lose (between 33−38 °S) when it collides with the north-flowing Malvinas (Falkland) Current (Olson et al., 1988). The BC consists of Superficial Tropical Water (STW), which itself is actually a mixture of three water types videlicet Tropical Water, Littoral Water and periodic contributions from upwelling South Atlantic Central Water (SACW) lying below the STW Viana et al. (1998). The BC moves the STW as depicted

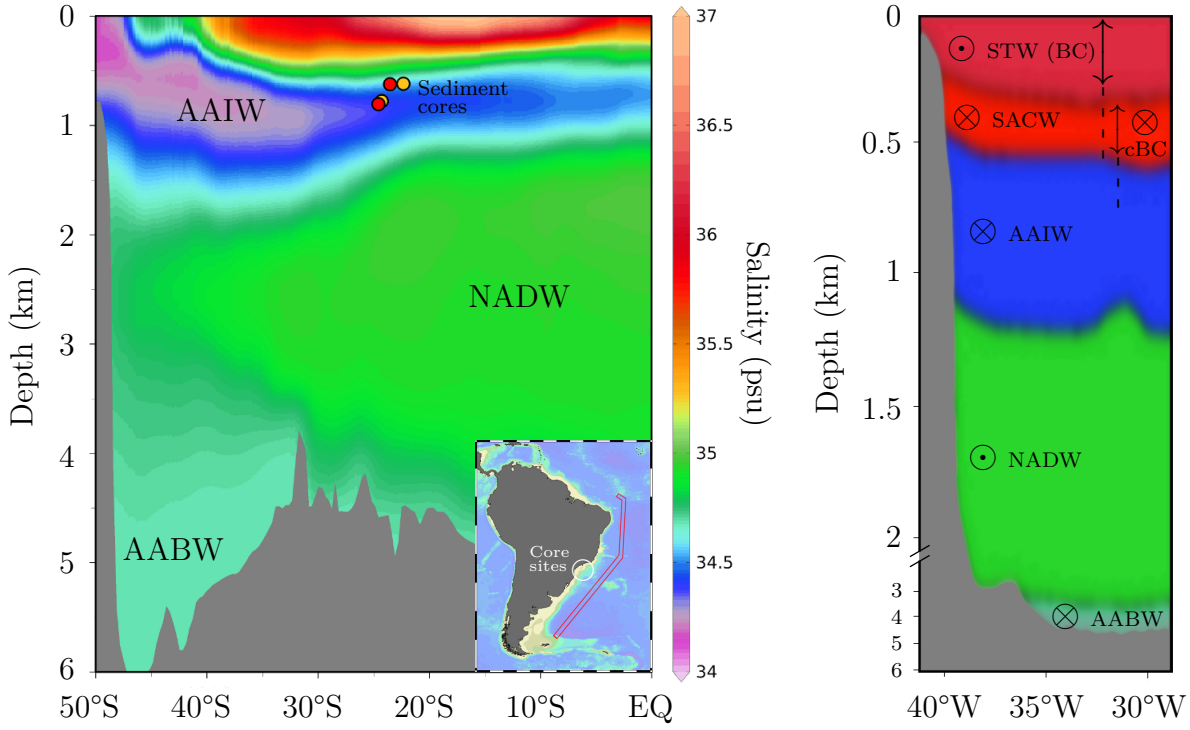

Fig. 5.7: Left: Meridional profile of the salinity distribution along the shown transect (inlay) off the South American east coast. Data from the WOCE hydrographic program. Right: Vertical stratification of water in the location area at around 22 °S. Picture modified from Viana et al. (1998). The transition between the different water masses depicted in the right-hand figure is smoother than indicated. Symbols ⊗ and ⊙ refer to water flowing in and out the drawing plane.

in the schematic representation of the right image of Fig. 5.7 accommodating the upper 250−300 m (Signorini, 1978; Evans et al., 1983). The BC thickens 50 km offshore to more than 500 m (Lima, 1992). Now and then reaching depth of up to 3,000 m in the Confluence Zone[3] at ∼38 °S (Reid et al., 1977; Saraceno et al., 2004). The subjacent Brazil Countercurrent (cBC) flows in the opposite direction that is from south to north entraining water from the so-called South Atlantic Central Water mass (SACW) occupying the depths between 300−550 m. Though the current's provenance is controversial some authors think it might be the upper and warmer branch of the Antarctic Intermediate Water (AAIW) (Sverdrup et al., 1942).

5.4.2 Antarctic Intermediate Water

Today AAIW almost entirely fills the intermediate depth of the South Atlantic and tropical oceans reaching out as far as 25 °N where it becomes indistinguishable of the quite saline Mediterranean Outflow Water (MOW) (Worthington, 1976). This water mass also irrigates the Brazilian slope within the Campos and Santos Basin isobaths between 550 m and 1,200 m reaching velocities at around 0.5 m/s (e.g. Viana, 1994; Müller et al., 1998; Viana et al., 1998; Hovland, 2008). It is characterized and recognized among others by its high dissolved-oxygen content, its unique low salinity and relatively high nutrient content (Reid et al., 1977). Newer research has shown that present-day AAIW enters the Brazil Basin between 20−28 °S from the east, bifurcating into a northward and southward flowing branch as it meets the continental break off Brazil (Müller et al., 1998). To put it in a nutshell, the AAIW formation region lies just south to the Subantarctic Front (SAF) within the Polar Frontal Zone (PFZ, 50−60 °S), a sharp transition zone separating water coming from different hydrological regions namely the cold and fresher polar surface waters, to the south, from the warmer and saltier surface waters in the Subantarctic Zone (SAZ). For the sake of completeness, the SAZ itself is a transition zone encircled by two more water fronts, the just mentioned SAF and the northerly so-called Subtropical Front. Generally speaking, where these different water masses encounter or more precisely converge, usually the colder and hence denser water subducts under the less dense water which is than being transported towards the north. By this means several water masses among them AAIW and the Subantarctic Mode Water (SAMW) have their origin in this naturally occurring water boundary system continuously encircling the Southern Ocean around Antarctica (see Sarmiento and Gruber (2006) and references therein). All four core locations are bathed today within the northward flowing AAIW. The shallower two cores from Campos Basin may be additionally influenced by the lower part of the SACW, see Fig. 5.7 (left) showing the salinity distribution along the same transect as shown in Fig. 5.6 covering the latitudes from the equator to 50 °S and depths between 0−6 km. The AAIW is clearly distinguishable from the surrounding water masses by its relatively low salinity.

[3]In oceanography a confluence zone is defined as the region where currents are flowing together and/or separates from the continent.

5.4.3 North Atlantic Deep Water

Directly below the AAIW is the North Atlantic Deep Water (NADW) flowing towards south. As discussed in chapter 2 it has its origin in the northern North Atlantic traversing as a strong deep western boundary current most of the Atlantic Ocean. It can be nicely traced by their distinct layers of dissolved-oxygen within the NADW tongue or by its relatively high salinity or low nutrient content to name but a few (Reid, 1989). Farther south at around 50−55 °S NADW finally heads to the east joining the Antarctic Circumpolar current (ACC), the largest known water current in the oceans surrounding Antarctica in easterly direction. By then at the latest, the NADW has irrevocably lost its distinction. It is an up to 800 km wide and at the core location about 2 km thick water mass flowing between 1,200 m and 3,500 m (Viana et al., 1998). To make things more complicated it should be mentioned that Circumpolar Deep Water (CPDW) (not shown in Fig. 5.7) which has its origin also in Antarctic water bifurcates at 55 °S into an upper and lower part which sandwich the southward flowing NADW (Reid, 1989).

5.4.4 Antarctic Bottom Water

Finally one will find the so-called Antarctic Bottom Water (AABW) in the deepest regions of Campos and Santos Basin reaching down not less than 3,500 m also moving in north direction. Similar to the AAIW, AABW spreads throughout all ocean basins but being the coldest and densest water mass in the world ocean and therefore usually found at its bottom, hence the name. Flowing along the bottom of the ocean, the bathymetry significantly prescribes the AABW's distribution in the different ocean basins. It is believed that AABW owes its origin in part to ultra-cold katabatic winds blowing offshore Antarctica forming mesoscale open water areas not covered with sea or only thin ice called polynyas where surface water becomes fairly chilly and brine rejection due to enhanced sea ice formation cause the water to sink (Smith et al., 1990). Another source which contributes to the upper part of the AABW is found in the ACC consisting of old deep water (Reid, 1989). Main formation areas are the Ross- and Weddell Sea. After formation and circulating around the southernmost continent in east direction one branch separates flowing into the South Atlantic basin towards north (Fig. 5.7).

Part II

Results and discussion

„For every complex problem, there is a solution that is clear, simple and wrong. “

Henry L. Mencken

6

Results and Discussion: ^{230}Th/U

6.1 Preface

In this thesis corals of different cold-water species from four sediment cores from off the Brazilian slope have been investigated. Two of these cores, namely C1 and C2, have already been examined in part for their ^{230}Th/U and ^{14}C in my diploma thesis (see Ruckelshausen (2009). Results have also been published in Mangini et al. (2010). Here, I present a variety of newly conducted measurements comprising all four sediment cores. Measurements involve ^{230}Th/U, ^{14}C, ^{143}Nd/^{144}Nd, ^{13}C, ^{18}O, and XRD complemented by some concentration measurements of neodymium and manganese. Additionally, some ^{231}Pa/^{230}Th measurements on the sediment fraction have been done as well as a few ^{143}Nd/^{144}Nd measurements of the sediment's Fe-Mn oxyhydroxide coating. Unless otherwise stated all presented and discussed results are yet unpublished. As all core locations lie in close vicinity to each other they quite likely host complement paleoceanographic information. It is therefore crucial and necessary to compare this new dataset together with the former results obtained from my diploma thesis.

6.2 ^{230}Th/U measurements

Uranium and thorium isotopes were chromatographically separated and purified from the coralline material for each sample following the chemical methodology described in my diploma thesis covering also information about the preceding sample preparation (see Ruckelshausen (2009)). A very concise overview of the chemical separation and purification procedure is summarized as a flowchart in appendix C. After the chemistry uranium and thorium were reduced to a single droplet of ~3 μl and loaded onto a rhenium filament. Measurements were carried out on the thermal ionisation mass spectrometer (TIMS,

Finnigan MAT 262 RPQ) at the Institut für Umweltphysik (IUP) at Heidelberg University. The TIMS has been run with the double filament technique allowing for higher ionisation rates than the single filament technique. The sample evaporates from the evaporation filament and is subsequently ionized from the adjacent ionisation band. Ionisation of the atoms takes place in the gas phase, which is more efficient than evaporation from the surface of the Re filament. Isotopes were measured as single charged oxides (UO^+ and ThO^+) rather than in their charged elemental form to increase the counting statistic. More information about the measurement technique and machine configuration (Faraday cups, ion counter etc.) as well as the subsequently applied machine-related correction procedures can be found elsewhere (e.g. Bollhöfer, 1996; Frank, 1997; Neff, 2001). Before calculating the final ages all samples in this work have been corrected for a total procedural ^{234}U, ^{238}U, ^{230}Th, ^{232}Th blank, which was regularly measured during this thesis (see Fig. B.1 for the procedural blank development and Tab. D.3 for used mean values).

6.3 ^{230}Th/U results

Most coral samples came out as glacial in age. Only seven samples out of fifty stem from the Holocene epoch the rest were dated back up to ∼90 ka BP with the majority covering the last glacial until ∼45 ka BP implying that most samples seem to be potentially suitable for ^{14}C dating too. Calculated activity ratios and ^{230}Th/U ages can be found in Tab. D.1 and Tab. D.2. In the following pages detailed results are presented and discussed with emphasis on the reliability of the dataset. This is crucial since all drawn inferences in this thesis depend highly on correct absolute ages.

6.3.1 Check for diagenesis

Owing to the relatively young ^{230}Th/U ages for most corals investigated one would expect diagenetic alterations having played a minor role and at best can be neglected. Nonetheless, whether diagenesis on the coralline hard parts have occurred or not must be evaluated for each sample. In Fig. 6.1 the measured δ^{234}U against the ^{230}Th/^{238}U activity ratio for each coral sample is plotted along with the previous results from cores C1 and C2 from my diploma thesis (Ruckelshausen, 2009) (two samples (M-119 and M-189) were omitted due to their large errors). Vertical lines in light gray are isochrons indicating isotopic pairs giving the same calendar age. The solid red line illustrates the time evolution of the activities for a closed system starting with the present-day open ocean seawater δ^{234}U and a zero thorium content. Latest δ^{234}U measurements on open ocean seawater from different authors show activity ratios level out at $146.8 \pm 0.1‰$ (Robinson et al., 2004; Andersen et al., 2010) and have been quite stable for the last ∼360 ka with deviations not exceeding 15‰ from the modern value as shown on U-rich slope sediments from the Bahamas (Henderson, 2002). Corals, however, often exhibit a much wider range in δ^{234}U thought to be the result of dia-

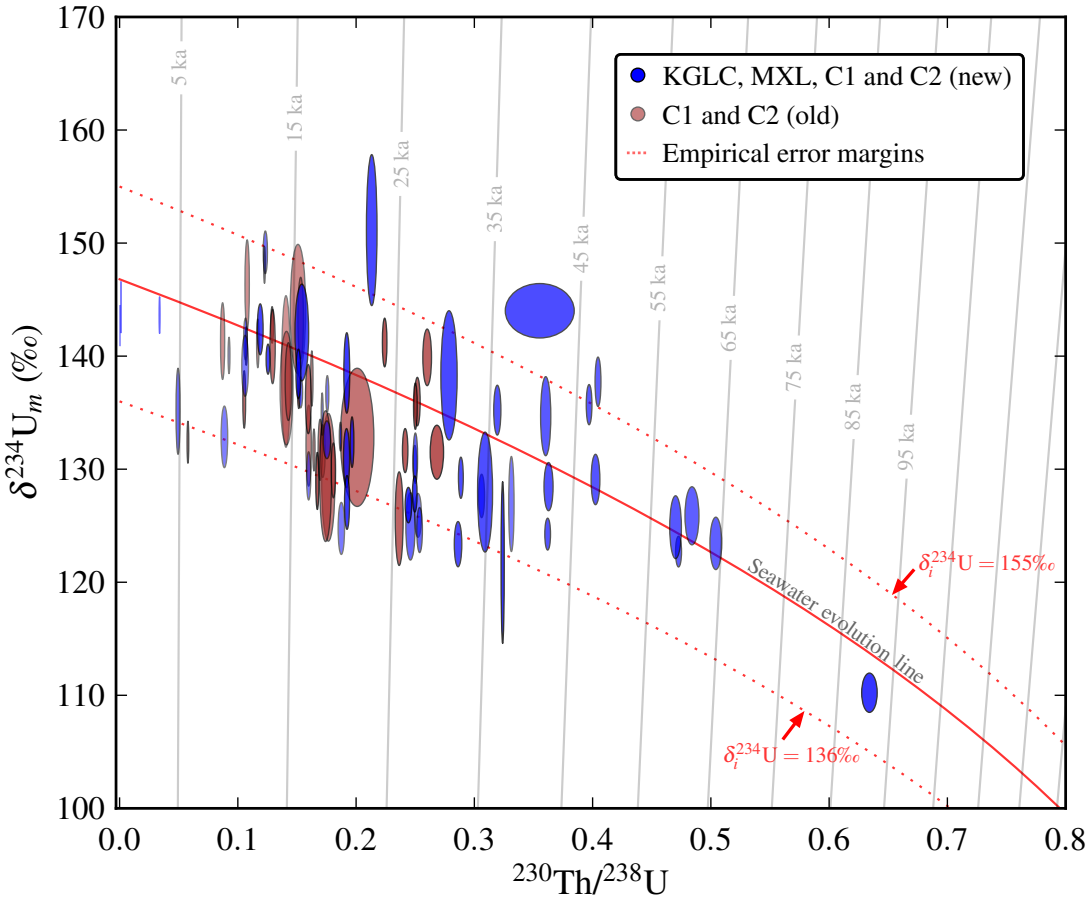

Fig. 6.1: Displayed are the measured δ^{234}U and ^{230}Th/^{238}U activity ratios for all coral samples. Vertical lines are isochrons showing calendar ages. The red solid line shows the closed system seawater evolution for a present-day δ^{234}U of 146.8‰ (Andersen et al., 2010). Most samples lie within the empirical error margin but reveal relatively large scatter. All error ellipses represent 2σ uncertainties, which, due to multivariate statistics, translate into a confidence level of ~86.5% rather than ~95.4%.

genetic activity. The dotted red lines in Fig. 6.1 give the "acceptable" error margin. Samples within this band have only experienced minor diagenesis leaving their ^{230}Th/U ages mostly unaffected. Corals deviating from this range are discarded and are not used for further studies. Unfortunately, there is no consensus about where to place exactly an upper and lower bound for the coral δ^{234}U. Fig. 6.2 summarizes some δ^{234}U measurements from various authors on seawater and corals collected either alive or from very recent colonies with ages less than 2.35 ka BP dated by ^{230}Th/U or by ring counting (Delanghe et al., 2002). Undoubtedly, with improving mass spectrometer techniques, especially with the advent of multicollector ICPMS, seawater and coral ^{234}U/^{238}U activity measurements have obviously become more and more precise. But this diagram also shows that every hard definition of an upper and lower bound for modern δ^{234}U in corals being reliable or being not trustworthy is

somewhat artificial and does not go without a certain arbitrariness. Two very recent coral samples, namely L606 and S612 from the Campos Basin, which were dated in this thesis and plotted in Fig. 6.2 too, are illustrating this problem. The exact location from where these corals were retrieved is not known, however. Both corals have ages of −26 a BP and 34 a BP and failed to record the measured seawater ratio within their respective 2σ uncertainties even though their preservation state is excellent (see Fig 6.6). As a consequence and contrary to popular belief it is suggested that local processes occurring at the Brazilian slope might be capable of slightly changing the $^{234}U/^{238}U$ activity ratio questioning the applicability of $\delta^{234}U$ as a strict means of quality control. This issue is further discussed in section 6.4. This observation might apply also for the older corals examined in this thesis. Despite this issue, most corals in Fig. 6.1 scatter within the acceptable $\delta^{234}U$ range with the upper bound set to 155‰ and the lower bound set to 136‰. As shown by (Cutler et al., 2003), coupled $^{231}Pa/^{235}U$ and $^{230}Th/U$ measurements on corals affected by diagenesis yield discordant ages while showing the expected $^{234}U/^{238}U$ of seawater and vice versa suggesting that further criteria should be taken into consideration when testing coral specimens for open system behavior.

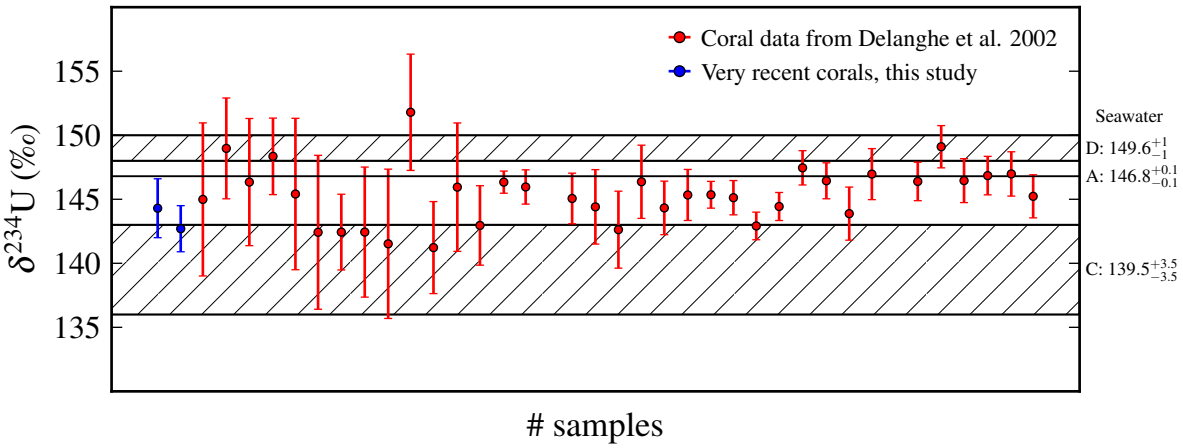

Fig. 6.2: This figure is a compilation of $\delta^{234}U$ data from modern corals from various authors, see Delanghe et al. (2002) and references therein, along with $\delta^{234}U$ seawater measurements (hatched bars). In blue are the very recent coral samples L606 and S612 with ages of only −26 a BP and 34 a BP. Both samples failed to record the latest measured seawater activity from Andersen et al. (2010). Today's seawater values are from D: Delanghe et al. (2002), A: Andersen et al. (2010), C: Chen et al. (1986). Error bars on corals denote $2\sigma_m$ uncertainties. Seawater errors are ±1SD. Picture modified from Delanghe et al. (2002).

6.3.2 Uranium concentrations of the coral samples

A further test to check the quality of the data is to look at the uranium content of each sample. Collected data of uranium concentrations in modern and fossil corals have shown prevalent values are between 2−3.5 ppmw going as high as 4 ppmw. Observed variations in the concentration have been attributed in part to a number of slightly changing environmental parameters such as seawater temperature, pH, Ca^{2+} concentration, variations in salinity as well as through the biological activity of the polyp of the coral itself (Ku, 1977; Shen and Dunbar, 1995). For example, changing the salinity from 34‰ to 38‰ is accompanied by an increase in the U concentration of the seawater by as much as 12%. The average seawater concentration is 3.3 ppbw (Chen et al., 1986). Commonly, habitats where cold-water corals thrive exhibit only small variations in their environmental parameters compared to shallow-water areas. Relatively large changes in salinity within a single water mass are therefore expected to be unlikely. But special hydrodynamic features occurring in the Campos and Santos Basin, very likely, render the intermediate-depth environment more susceptible for perturbations than at other intermediate-depth locations. Mesoscale surface eddy activity is able to stir up the water colum in this region up to depth of ∼800 m and might have impacted the salinity in this depth as well. The hydrodynamic features will be discussed in section 6.6.1 of this chapter. Because changes in seawater salinity for the core sites cannot be ruled out a new U concentration boundary has been stipulated to 4.6 ppmw.

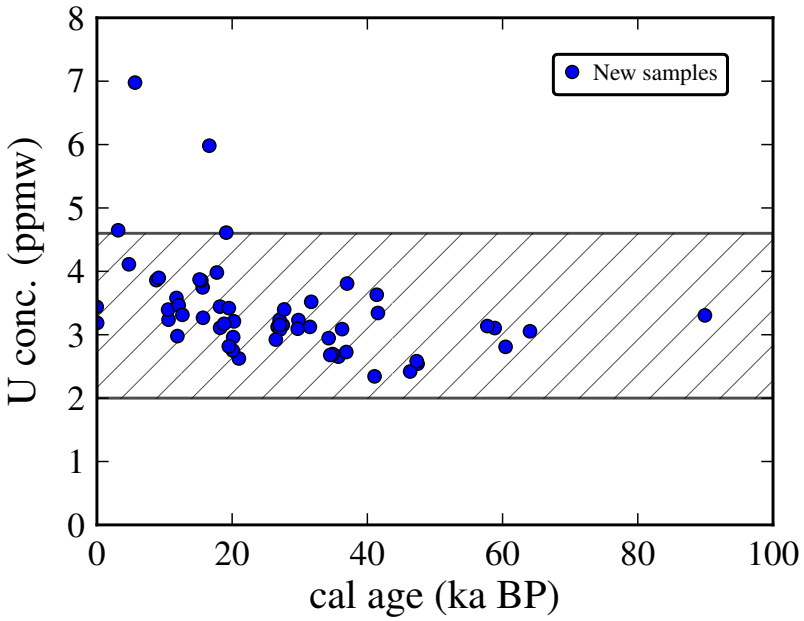

Fig. 6.3: Uranium concentrations of new samples as a function of their calendar age. Most corals display U concentrations between 2 and 4.6 ppmw. Uncertainties of the concentrations are smaller than dot size. Calendar age errors have been omitted.

Fig. 6.3 depicts the uranium concentrations of all measured samples against their calendar ages. Uncertainties are smaller than the denoted dot size. Errors in calendar ages are not shown. Most samples exhibit a concentration range within the hatched range and seem to be suited for further investigations. Interestingly, a few samples younger than 20 ka BP feature a larger scatter than the older ones. Usually one would expect the opposite to be true, since the older a sample the more likely it is that diagenesis has altered the initial U concentration. The impact of a possible diagenetic alteration on the ^{230}Th/U age can often be severe. For instance, coral S1032 from Tab D.2 (age ∼3.14 ka BP) shows a somewhat elevated U content of ∼4.6 ppmw. For simplicity, considering that the coral gained extra uranium from the water column without 1. changing the aragonite δ^{234}U and 2. not adding or losing any thorium. Correcting the seemingly elevated U concentration from ∼4.6 ppmw to 4 ppmw makes this specific sample older by around 500 years! Diagenetic exchange processes are still poorly understood and subject of ongoing research. Anyhow, this simple

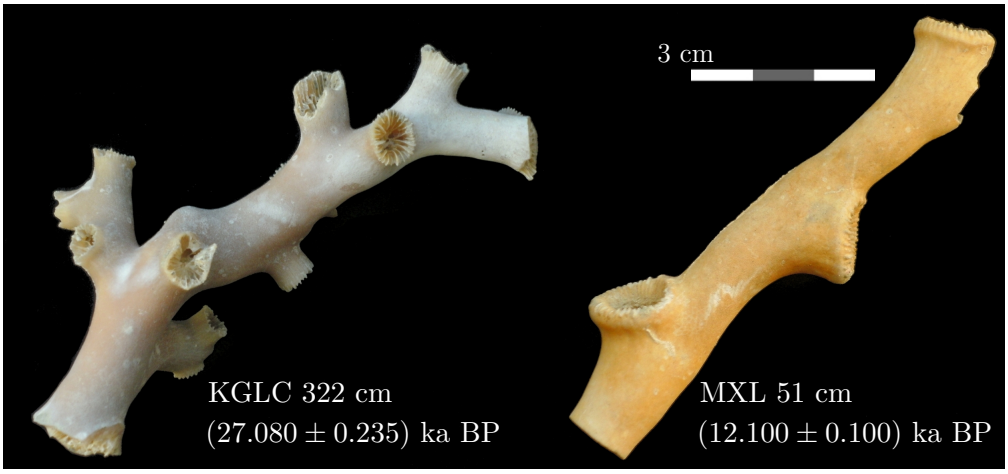

Fig. 6.4: Close-up of two coral fragments from cores KGLC and MXL representatively showing the excellent preservation state for the most samples.

example illustrates that caution should be exercised when using questionable samples especially when it comes to reconstructing rapid climate change on the order of decades or several centuries. The overall small scatter in Fig. 6.3 is indicative for a good preservation state of the aragonitic samples. This may be due to the location of the sediment cores, which is the continental slope where sedimentation rates are usually high. Coral fragments once lying at the bottom are quickly buried and are thus no longer exposed to the corrosive seawater. This is supported by the observation that nearly all corals, especially from cores MXL and KGLC are free of any obvious metallic coatings on the outer and inner surface they would usually acquire from the water column if the coral rubble are exposed on the sediment surface just long enough. Only samples within the first 10 cm of the MXL core show a black staining probably coating from Fe–Mn oxyhydroxides (see Fig. 5.5). Fig 6.4

shows a close-up of a *S. variabilis* branch from the KGLC core, which looks quite fresh even after ∼27 ka BP. On the right-hand side a *L. pertusa* specimen from core MXL is shown too. The yellow appearance is probably some form of organic tissue sticking on the coral's surface.

6.3.3 ^{232}Th content in coral samples

Another aspect which could have a large impact on the ages as well as age uncertainties of a coral is the amount of initially incorporated ^{230}Th in the aragonite lattice. As described in-depth in section 4.2.3.1 the amount of non-radiogenic ^{230}Th is estimated by assuming a reasonable initial seawater ^{230}Th/^{232}Th activity multiplied by the amount of the measured ^{232}Th within a sample (see Eq. 4.4 for recap). It is clear from this point of view that a rigorous cleaning technique is necessary to keep the ^{232}Th, fetched from sediment residues among others, as small as possible to ensure reliable ^{230}Th/U ages. Experience suggests that a sample's ^{232}Th concentration should not exceed 10 ppbw in order to get viable ages. Fig. 6.5 displays the measured ^{232}Th concentrations of all new samples plotted against their ages. Uncertainties in the ^{232}Th concentrations are smaller than dot sizes. To avoid clutter calendar age errors have been omitted. Except for one exceptional concentration exceeding

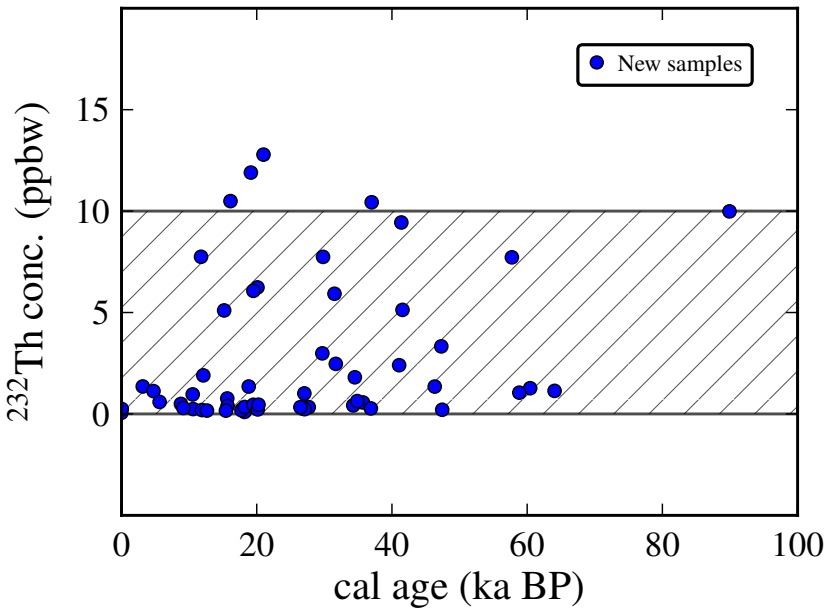

Fig. 6.5: ^{232}Th concentration of all new samples as a function of their calendar age. Most samples are within the hatched area ranging from 0−10 ppbw. Uncertainties in the ^{232}Th concentrations are smaller than dot sizes. To avoid clutter, calendar age errors have been omitted.

∼50 ng/g (not shown) only four more measurements do not fulfill this criteria and are not considered for further studies. In principle, past ^{230}Th/^{232}Th seawater activities are unknown. All calendar ages in this thesis have been corrected with an estimated initial ^{230}Th/^{232}Th seawater activity ratio of eight considering a relative uncertainty of 50% (see section 4.2.5). But the question arises how representative this initial ratio of eight really is. A modern coral from off Brazil sheds light on this issue. Repeated ^{14}C measurements on samples L606 and S612 have given much too young ^{14}C ages as one would expect to find in this environment (depths ∼600 m) (see Tab. E.2). The expected pre-bomb ^{14}C reservoir offset for this depth is on the order of ∼600 ^{14}C years (Key et al., 2004). The only reasonable explanation to think of is in-situ contamination with bomb ^{14}C from stratospheric hydrogen bomb testings conducted mainly during the 1960s. This finding would suggest that the calendar ages should not be older than ∼50 years from the time of measuring for both corals. This age is constrained by the time delay from the moment of ^{14}C release into the atmosphere and the time needed for the intermediate-depth ocean water to reach the core sites off Brazil. Vertical transport of ^{14}C via diffusion across the thermocline is negligible due to the relatively small diffusion coefficient[1]. Lateral water mass transport by ocean currents is a much more likely scenario for the observed excess ^{14}C measured in the corals. Accurate ^{230}Th/U age determination of such young samples by means of mass spectrometer techniques alone is often difficult to handle because of the corals' very small ^{230}Th content that even blank corrections subsequently carried out could have a significant influence on the ages. For L606 both ages ^{14}C and ^{230}Th/U ages agree well with the scenario of bomb ^{14}C reaching the site earliest during the 1960's. An exact determination of the arrival of the anthropogenic ^{14}C signal at this site is not possible, though. For the second coral (*S. variabilis*, S612) also a very young ^{14}C age has been measured suggesting that this coral cannot be older than about 50 years. Although the ^{230}Th/U age came out a little bit older (34 ± 15 a BP) than the ^{14}C age would suggest this age discrepancy can be reconciled with a somewhat higher applied initial seawater ^{230}Th/^{232}Th ratio of 12. This is an accordance to the applied initial ^{230}Th/^{232}Th activity ratio of 8 ± 4 used for correcting the calendar age calculations. Nonetheless, this qualitative exercise yields only an estimate for one specific time interval. It is reasonable to assume that this ratio has not been constant in time and could have varied significantly as suggested by a GCM modeling

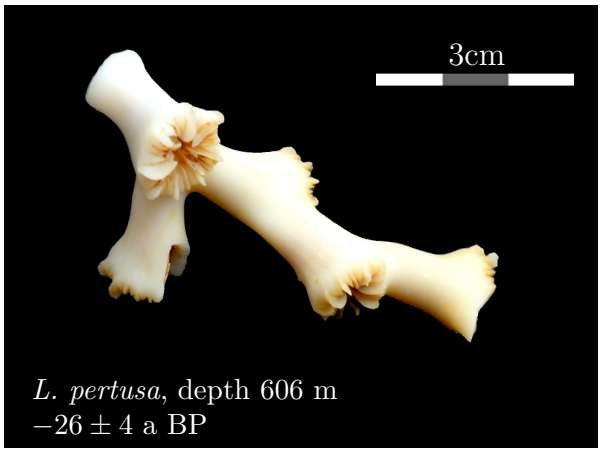

Fig. 6.6: Close-up of a *L. pertusa* (L606) coral from Campos Basin showing clear signs of contamination with bomb ^{14}C.

[1]The diffussion coefficient for the thermocline is roughly on the order of 10^{-5} m^2/s.

approach deriving dissolved ^{230}Th specific activities for the Western Atlantic Ocean during the Holocene and the LGM (Henderson et al., 1999).

6.3.4 X-ray diffraction analysis (XRD)

X-ray diffraction analyses were performed to investigate the aragonite and calcite content of the coral samples. As outlined in section 4.2.6.1 this method allows a quantitative evaluation of the composition of a variety of minerals, among others calcium carbonate. For that thirteen samples have been selected with the emphasis on specimens exhibiting relatively high and low values in δ^{234}U. This analysis can be understood as complementary to the previous checks being able to hint to open system behavior. The following syllabus is a methodological description of the performed XRD analysis from C. Vogt 2011, personal communication.

The X-ray diffraction pattern analyses were conducted in the laboratories of the research group Crystallography (University of Bremen, Central Laboratory for Crystallography and Applied Material Sciences, ZEKAM, Dept. of Geosciences). Dried bulk samples were grounded to a fine powder (< 20 μm particle size). A thorough preparation commonly increases reproducibility of the results, however, the standard deviation given by Moore and Reynolds (1989) of $\pm 5\%$ can be considered as a general guideline for mineral groups with $> 20\%$ clay fraction. In addition, the determination of well crystallized minerals like quartz, calcite or aragonite can be done with better standard deviations (Tucker, 1988; Vogt et al., 2002). The measurements were done as a continuous scan from $3-85\,^{\circ}$ 2θ, with a calculated step size of $0.016\,^{\circ}$ 2θ. Mineral identification were done by means of the Philips software X'Pert HighScore™ [...] followed by full quantification of the mineral assemblage of the bulk fraction via the QUAX full pattern method (cf. Vogt et al. (2002).

In Fig. 6.7 the initial $\delta^{234}U_i$ (decay corrected according to Eq. A.4) for all new corals versus the calendar age is plotted. The obtained $\delta^{234}U_i$ of each sample should lie within the empirical error margin explained in section 6.3.1. To avoid clutter the error ellipses which are outside the hatched area after decay correction have been removed and are not used for further analysis. The red ellipses indicate the samples on which XRD analysis were performed. It becomes apparent that all thirteen XRD samples are being devoid of any calcite. The aragonite content for most corals is 100% (mass fraction) considering a 1% uncertainty (1σ). There is no need to explain the measured diffractograms with a further mineral phase other than aragonite. Only three samples show a reduced aragonite content (96-98%) with admixtures of other mineral phases like anatase or monazite-(Ce) but all samples do not show any traces of calcite (see Tab. G.2). In conclusion, the somewhat higher and lower δ^{234}U values observed in these samples suggest that diagenesis probably cannot be called on for an explanation. This strengthens the previously made assumption that instead localized variations in the seawater $^{234}U/^{238}U$ could have played a role. A possible explanation attempt is discussed in the following section.

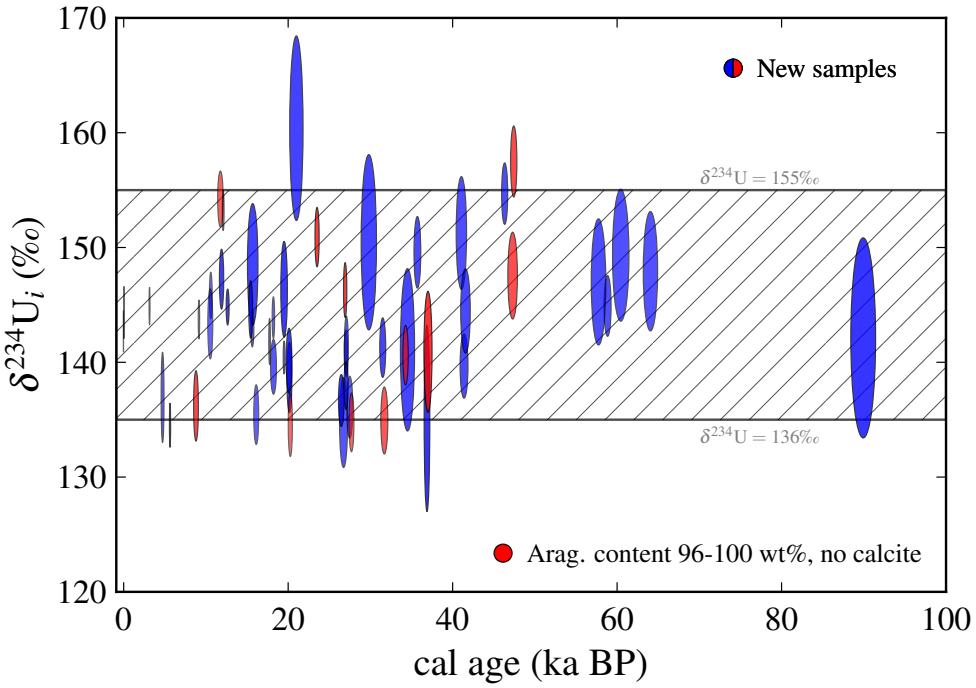

Fig. 6.7: This figure illustrates the initial (age corrected) δ^{234}U of the dataset. Samples with initial δ^{234}U lying within the hatched area are considered reliable if there are no other contradicting indications (high uranium or thorium concentrations). To avoid clutter error ellipses, which fall outside the hatched area after correction for decay have been removed. For ellipses in red the aragonite content has been measured. Error ellipses are 2σ.

6.4 Possible influences on the coral δ^{234}U

As proposed previously the relatively large scatter observed in the coral δ^{234}U cannot be accounted for by diagenetic activity alone. It is hard to imagine what kind of processes other than diagenesis might have influenced the coral $^{234}U/^{238}U$ activity ratio especially on such short timescales. As mentioned above the incorporated uranium concentration of the coral skeletons can change in the course of changing environmental parameters. Also, changes of the whole ocean uranium inventory are imaginable to have happened over longer periods of time but could not be assessed yet and probably would not affect the seawater's $^{234}U/^{238}U$ activity. In addition, there is no mechanism in corals capable of fractionating ^{234}U over ^{238}U during biomineralization of the skeleton. Compiled data from tropical corals covering the last two interglacial periods revealed that seawater δ^{234}U fluctuated significantly over the course of tens of thousands of years with an apparent rate of $\sim$1‰ per 1 ka during glacial to interglacial transitions (Esat and Yokoyama, 2006).

Attempts to explain these fluctuations led to mass balance model calculations conducted by Russell et al. (1996) calling on inflated riverine transport with elevated ^{234}U/^{238}U activities (between 1.2 and 1.3) to the ocean as a result of intense glacial-interglacial weathering. But the model output suggest only a 7‰ change in the oceanic δ^{234}U from a presumed seawater value of 144‰ over a time period of ∼30 ka, assuming that the worldwide river runoff has at maximum doubled as suggested by other indications (see Russell et al. (1996) and references therein). Hence, this mechanism is too slow to account for the observed increase in the seawater's δ^{234}U during glacial to interglacial transitions and is also too slow for the short-term variations seen in the coral data off Brazil, which show nearly simultaneous variations in δ^{234}U comprising up to ∼19‰ (Fig. 6.7).

Another mechanism put forward by Esat and Yokoyama (2006) to explain the seemingly increase of oceanic ^{234}U/^{238}U during deglaciations considers accumulation of U enriched in ^{234}U from riverine inflow previously deposited under reducing conditions during interglacials and high sea-levels stand in near shore areas in anoxic and suboxic sediments, in salt marshes and mangroves, in estuaries, and in continental margins. Throughout glacial times, however, accompanied by low a low sea level the previously accumulated uranium was subsequently oxidized to a soluble form and liberated again during times of seawater transgressions. Model calculations suggest that this mechanism is a viable candidate to explain the observed rate of change in δ^{234}U of about 1‰ per 1 ka for glacial to interglacial transitions. It is noticeable in Fig. 6.1, depicting the overview of all samples including the old results from cores C1 and C2 that during the LGM, when ice sheets had reached their maximum extend and sea level stand had had a minimum, the δ^{234}U activity seem to be conspicuously lower and subsequently rose again over the course of the last deglaciation reaching a plateau roughly 10 ka BP ago. The changes in the coral δ^{234}U amount to ∼10‰ and are apparently accompanied by the global sea level rise during that time. This observation might be indicative of an increased release of ^{234}U from the Brazilian margin into the ocean during deglacial sea level rise. Other rapid ups and downs of the δ^{234}U in Fig. 6.1, for instance during the time interval between 30−25 ka BP cannot be explained with a rising sea level. Furthermore, the short-term scatter in the dataset cannot be explained by this hypothesis. An alternative explanation involves fluid discharges from the Brazilian margin. As outlined by Esat and Yokoyama (2006)

Fig. 6.8: This picture was taken by a ROV showing a carbonate chimney lying on the seabed of the middle to lower portions of the continental slope ∼1100 mbsl of the Campos Basin. Length of the central chimney ∼40 cm (Wirsig et al., 2012). Photo by courtesy of Petrobras.

coral growth close to shorelines can be influenced directly by outflow of ^{234}U enriched fluids. Whether the corals investigated in this thesis, originating from the continental slope, are affected by groundwater discharge, commonly known to happen in immediate coastal regions is questionable, but cannot be excluded. There is, however, evidence that fluid seepage rich in hydrocarbons occurs at the passive continental margins off Brazil. These water discharges, also known as cold seeps, often manifest as authigenic carbonate formations in the form of chimneys or crusts found in the sediments or at the sediment surface (Miller and Kowsmann, 2009; Wirsig et al., 2012) (Fig. 6.8). Authigenic carbonates consisting of aragonite, calcite or even dolomite form only under conditions where escaping CH_4 is oxidized anaerobically via sulfate reduction (Ferrell and Aharon, 1994; Peckmann et al., 2001). The fluids originate from pressurized pore fluids from deep beneath the Brazilian margins supported by breakdowns in the sedimentary column, which allow migrating to shallower sediment horizons (Figueiredo et al., 1999; Teichert et al., 2003).

These emanating fluids show a somewhat lower uranium concentration than typical for seawater and are enriched in $\delta^{234}U$. There are only a few reported $\delta^{234}U$ measurements from such venting sites exhibiting values between $166-168‰$ (Teichert et al., 2003). It is conceivable that corals growing in such a region can directly incorporate such ^{234}U enriched fluids diffusing out of the margins prior to complete mixing with the bulk ocean (Esat and Yokoyama, 2006). But little is known about the recent and past seepage or venting activity from cold seeps off Brazil leaving room for speculation. Summarized, there is the possibility that the reconstructed short-term variations in $\delta^{234}U$ observed for the coral locations are not reflecting the open ocean seawater uranium composition rather than being locally influenced by yet unspecified processes occurring at the Brazilian margin. There is a growing tendency to reject all corals with initial $^{234}U/^{238}U$ activities, which deviate more than a few per mil from the modern seawater value. This criterion might be in error and may, in fact, lead to the rejection of corals that have remained a closed system.

6.5 Stratigraphy of the sediment cores

For an open ocean environment one would expect sediment to be deposited in a stratigraphic order, that is, with the oldest parts downcore and the youngest at the top. A brief glance on the age-depth relationships for the four sediment cores (Fig. 6.9 and Fig. 6.10) from the slope region reveals that this is not the case. As described in section 5.3 sediment core KGLC was taken on an intercanyon ridge on a slope carved by numerous canyons. A disturbed age-depth relation for this core should thus not come as a surprise and was expected. Deposition of coral fragments in this core happened in three steps resembling a staircase, which are explicitly segregated from each other by several-millennia enduring hiatuses. The core covers the last ~16,200 years of the last glacial period. The lowermost section of KGLC between ~1.8 m to ~4.0 m was seemingly deposited quasi simultaneously followed by a ~6,600 year hiatus. Deposition of coral branches started again ~20,000 a BP

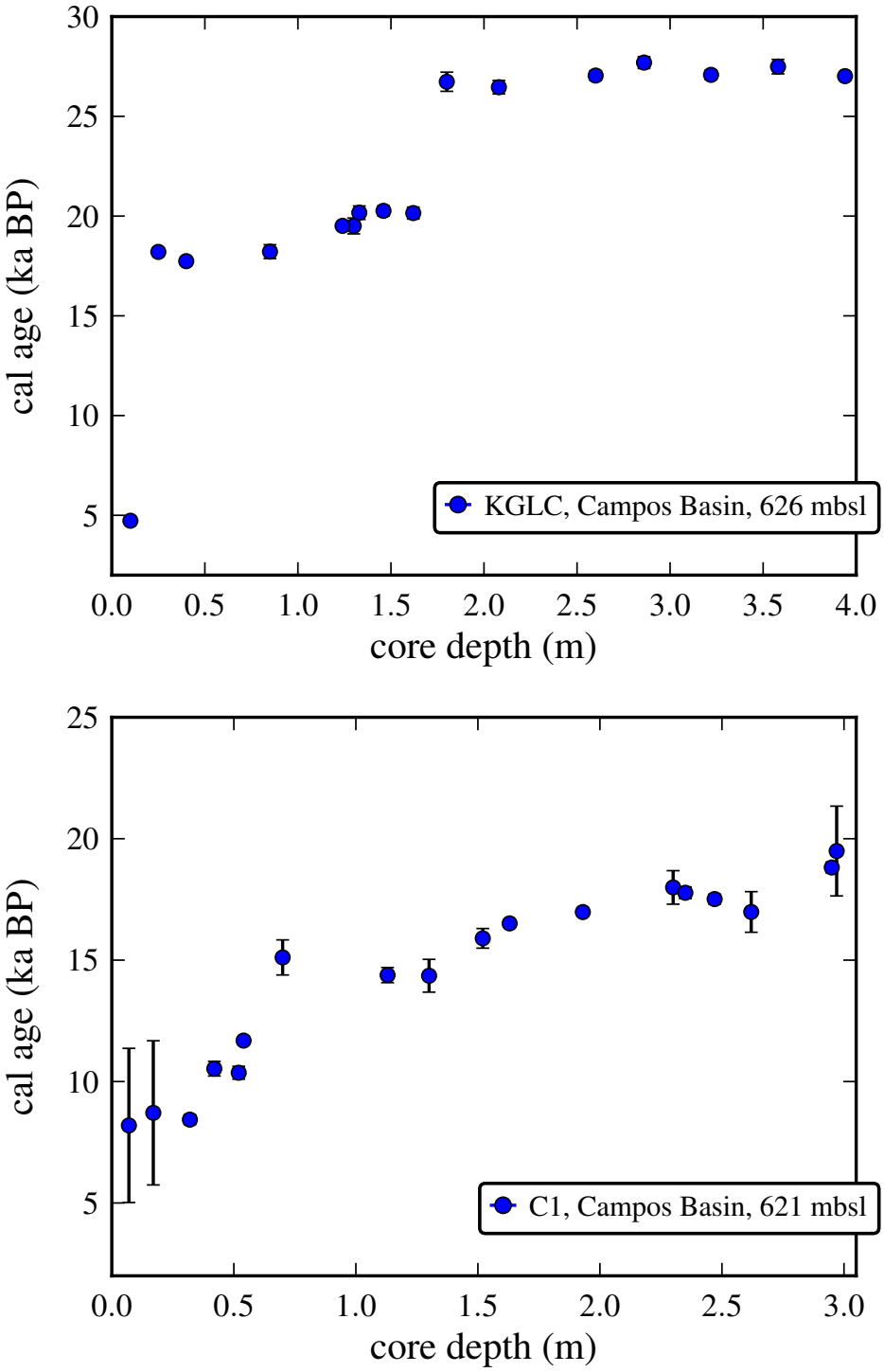

Fig. 6.9: Age-depth-relation inferred from the corals within the two sediment cores from Campos Basin. Especially core KGLC reveals an unusual sedimentation pattern, see text for more information.

ago during the LGM, lasting roughly 2,500 years before it was again interrupted by a further hiatus persisting another ∼13,500 years. The uppermost coral found in this core is 4,727 a BP old. It is worth noting that all coral specimens from KGLC are of the species *S. variabilis* with the exception of one single *L. pertusa* being the uppermost sample. The sedimentary environment at the continental slope is complex due to strong bottom water currents in this region. The dominant water mass today occupying the middle slope region is the vigorous flowing AAIW. The sedimentary record, therefore, might often be incomplete and full of stratigraphic breaks as can be seen by the two hiatuses in the KGLC core (several tens of centimeters of sediment is missing). This is where corals come in handy as they allow to detect such hiatuses often invisible in the sedimentary record. The surrounding sediment is usually not of similar age as the deposited coral rubble since the sediment can be of different origin comprising lateral and vertical sources. There are no geophysical data to confirm that some tens of centimeters of sediment are missing in the KGLC core. Unfortunately, no multi-sensor core logger or any other type of profiler was run along the core (neither the other cores) to verify whether there is a break in sedimentation.

Action from bottom currents seem to be more likely to have removed those sediment layers than mass movement along the slope as indicated by the lack of breaks in the degree of sediment consolidation, which otherwise would indicate a sedimentary unconformity caused by mass movement. A possible explanation for this unusual age-depth relation considers the area around the KGLC core as a rubble plate zone, a zone where coral rubble or whole branches of corals accumulate, fed by a steadily growing cold-water reef above this area. Times of intense reef growth and times of degradation may led to significant deposition of coral rubble/branches. The adjacent core C1 separated only ∼100 km from the KGLC location exhibits a totally different sedimentation history. This core has been sedimented more or less steadily up to its whole length of ∼3 m without any reversals in the coral ages within their denoted 2σ dating errors. C1 covers the time period from the early to mid-Holocene to the end of the LGM. The uppermost 70 cm show a lower mean sedimentation rate of about 9 cm/1,000 a than the rest of the core, which has a higher sedimentation rate of approximately 36 cm/1,000 a covering the age interval from ∼14,400−19,500 a BP.

The MXL core from Santos Basin was taken on a lower slope, in a narrow linear depression riddled by pockmarks and adjacent highs (resembling an egg carton) (see section 5.3.2). MXL is the only core covering three quarters of the last glacial period up to 89,000 a BP. It depicts also a continuous deposition of sediment and coral rubble with increasing ages downcore, but unlike C1 exhibits some age reversals which cannot be reconciled with the 2σ dating error. A possible source of error that might be in part responsible for those age inversions and also for possible inversions in all four cores could stem from core preparation at Petrobras when coral branches/rubble were individually pulled out of the mud, washed and then placed on the other core half for photography during core description. Some of them may have been displaced from their original position (R. Kowsmann 2011, pers. comm.). A rough sedimentation rate for MXL yields 35 cm/1,000 a. Core C2 encompasses

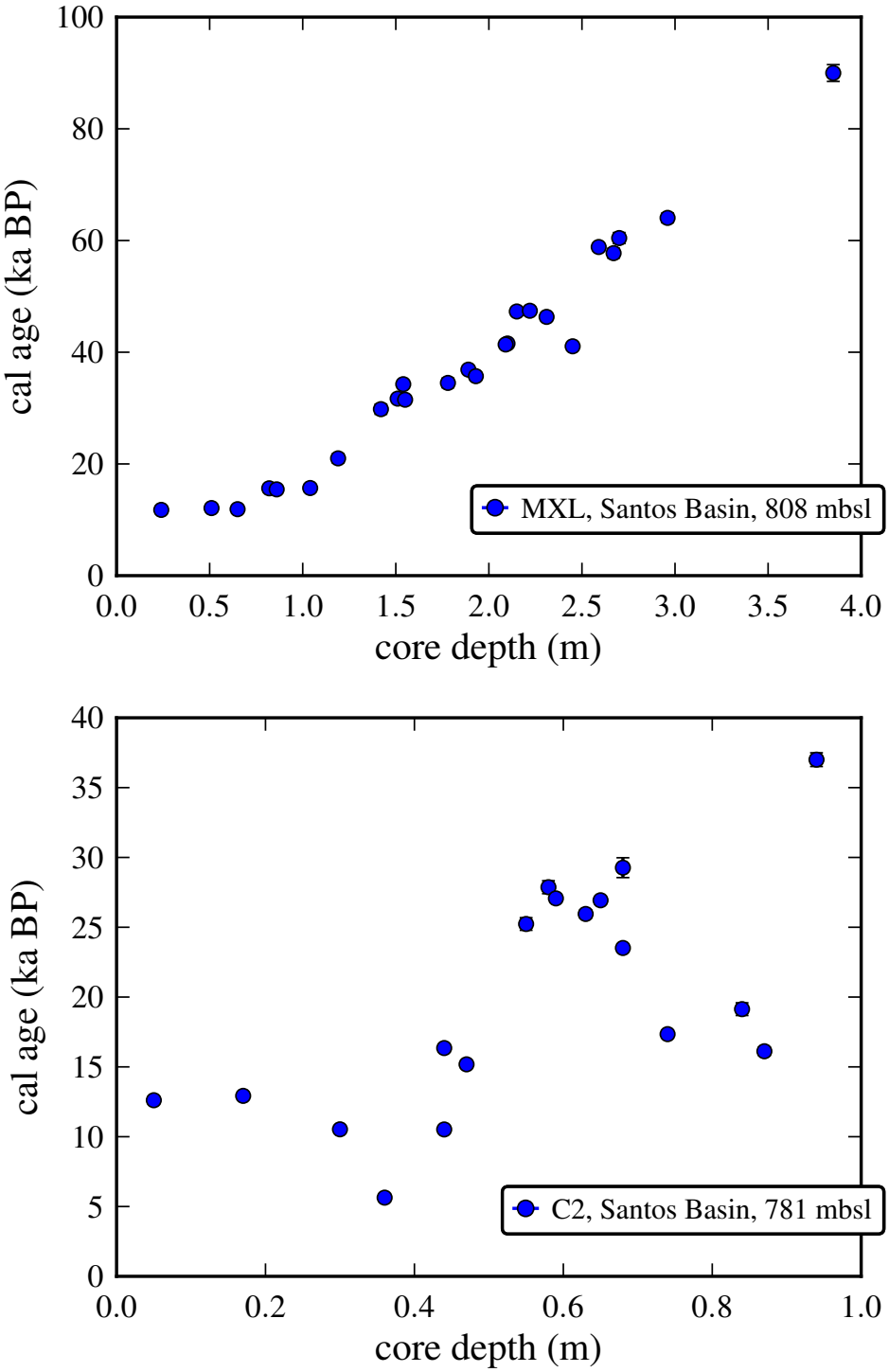

Fig. 6.10: Stratigraphic age-depth-relation inferred from the corals within the two sediment cores retrieved from the Santos Basin. Coral sedimentation pattern for C2 is complex and reflects the harsh marine setting of the slope region in this area.

around 37,000 years confined in just 100 cm sediment but unfortunately has the most complicated stratigraphic order. The many age reversals in C2 are indicative of a rough sedimentary environment rather than man-made errors during core description. A meaningful sedimentation rate for C2 cannot be given. All indicated sedimentation rates are coarse estimates, however, and associated with large uncertainties. Reported rates from the Campos Basin from the middle to lower portions of the continental slope (550−1200 mbsl) give values between 120 cm/1,000 a and 70 cm/1,000 a for the southern parts of this basin (Viana et al., 1998). By comparison, mean open ocean sedimentation rates do not exceed several millimeters per thousand years. The stratigraphic order is not important for the kind of investigations conducted in this thesis as ^{230}Th/U dating gives the absolute age of the corals. But age-depth relations can serve additional informations like sedimentation rates or might give us insights about preferred times of coral reef growth or reef degradation associated with major climate changes. The last point will be discussed in the following section.

6.6 Preferred periods of coral growth

In what follows the question is posed whether preferred periods of cold-water coral growth took place at the continental slope off Brazil in the past. Fig. 6.11 shows the previously presented age-depth relations summarized in one single picture to allow direct comparisons. Also indicated are several major climate events and their appropriate durations from which it is believed that they might have had an impact on the cold-water ecosystem off Brazil. A closer look at Fig. 6.11 hint to apparently elevated occurrences of corals during times of documented major climate events. Corals from all four cores group around Heinrich stadial 1 (HS1) and its associated so-called precursor event (PC1), which is characterized by enhanced iceberg calving from the Fennoscandian and Icelandic ice sheets preceding the sediment pulses of Heinrich event 1 (Grousset et al., 2000; Jaeschke et al., 2007).

Especially corals from C1, mostly of *L. pertusa*, seem to have proliferated during this time period, which started ∼20 ka BP and ended with the start of the Bølling-Allerød ∼14.6 ka BP ago. Before that, only sediment accumulated in C1 another ∼80 cm until the end of the core. Applying a mean sedimentation rate of ∼40 cm/1 ka for this core section, yield a ∼2.1 ka year long time interval for those 80 cm to form. Hence, C1 did not cover the time period of HS2 between ∼23−26 ka BP. Whether *L. pertusa* growth took place in the Campos Basin during HS2 and before cannot be decided. There is a noticeable gap between ∼20−23 ka BP where no coral accumulation has been recorded at all four core locations. Interestingly enough, this time period falls together with the approximate duration of the LGM (19−23 ka BP). The KGLC core next to C1 exhibits a similar behavior although intense deposition of coral rubble and even whole coral branches of the species *S. variabilis* seem to have occurred during three distinct time periods, namely PC2, PC1, and HS1. The coral ages in the ∼4 m long KGLC core suggest that *S. variabilis* settled this specific Bra-

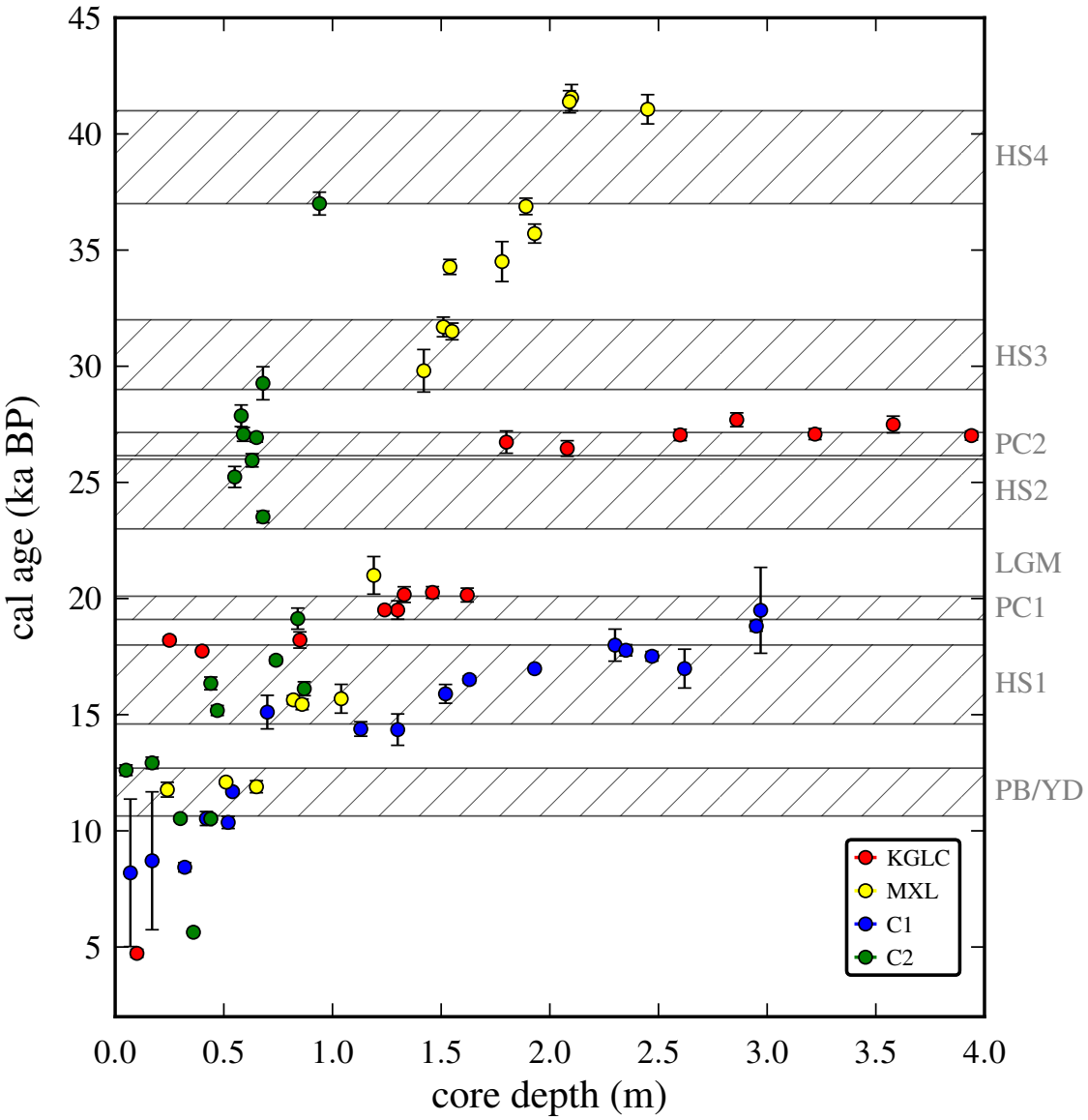

Fig. 6.11: Merged age-depth relation of all four cores revealing times of enhanced coral growth together with major climate events. Timing and duration of Heinrich stadials and the YD were adopted from various authors (e.g. Bard et al., 2000; Jaeschke et al., 2007; Pahnke et al., 2008; Barker et al., 2009).

zilian slope region at least since ∼27 ka BP. Followed by a ∼6.6 ka BP lasting hiatus in the coral deposition, separating the precursor events PC2 and PC1, *S. variabilis* growth reinstated ∼20 ka BP and ended apparently at the beginning of HS1 (∼18 ka BP). The uppermost sample in this core is of species *L. pertusa* (∼4.7 ka BP). Supposing that KGLC delivers an unbiased view of the distribution of the *S. variabilis'* flourish and demise in the Campos Basin region, reef growth for this species was rather episodic and could not

be restored until today implying conditions changed severely during the course of the last glacial period. Drawing inferences about earlier growth stages for this species are not possible due to the limited length of the core. To my knowledge, up to this day there are no documented occurrences of living *S. variabilis* reefs in this region. However, the significance of this statement is marred by the fact that sampling of the cores is rather patchy with barely enough samples to give a representative and unbiased view of the past distributions of the species *S. variabilis*. The same applies for the *L. pertusa* distribution in this region. Therefore, every interpretation given in this section regarding preferred coral growth needs to be treated with caution. Corals from cores C2 and MXL, predominantly of the species *L. pertusa*, from larger water depths are featuring a similar behavior as their shallower counterparts. C2 is the only core whose corals cover nearly all major climate events grouping around the YD, HS1, and HS2.

In contrast to C2, MXL did not record any coral deposition during HS2 and PC2 but on the other hand is the only core that exhibits occurrences reaching back as far as HS3 and HS4 thereby ignoring the fact that cores C1 and KGLC could also exhibit coral occurrences but are just not long enough to cover this earlier period. In the overall picture *L. pertusa*, in contrast to *S. variabilis*, seem to have inhabited the Brazilian slope almost continuously for at least the last 40 ka BP with only some minor gaps in between (during HS4 and the LGM). It is a priori not clear if the marked major climate events in Fig. 6.11 actually had an impact on the southwestern Atlantic region. There are several studies indicating indeed strong terrestrial and marine responses at times of Heinrich events and during the YD in this region. Two sediment records, for instance, from the northeastern Brazilian margin clearly show elevated Ti/Ca ratios during those events. The $CaCO_3$-rich sediments are interrupted by layers where the calcium content dropped significantly and were being replaced by continental-derived titan (Fig. 6.12). The titan-rich layers mark periods of enhanced river runoff from the Brazilian hinterland into the Atlantic Ocean and hint to increased precipitation during times of Heinrich events as a consequence of large southward shifts of the Intertropical Convergence Zone (ITCZ) (Arz, 1998). Increased Ti/Ca ratios are escorted by cooling events in the sea surface temperature (SST) off Brazil derived from alkenone-unsaturation ratios (Jaeschke et al., 2007) (Fig. 6.12).

The question arises if those events have facilitated enhanced coral growth in the intermediate-depth water off Brazil. As described in section 2.2 a weakening or apparent absence of NADW production in the high North Atlantic during HS2, HS1 and the Younger Dryas is thought to have resulted in the intrusion of nutrient-rich water derived from the deep South Atlantic reaching far into the North Atlantic basin. $^{231}Pa/^{230}Th$ measurements covering the LGM, for instance, suggest that the meridional overturning strength was reduced by 30−40% compared to today (McManus et al., 2004). $\delta^{13}C$ reconstructions on benthic-dwelling foraminifera from sediment cores from the western central Atlantic during the LGM indicate that nutrient-rich AABW has invaded the Atlantic basin up to ∼2,000 m being traceable up to 60 °N (Rickaby and Elderfield, 2005; Lynch-Stieglitz et al., 2007) (Fig. 6.13). Whether this antarctic-derived water mass had reached the oligotrophic mixed

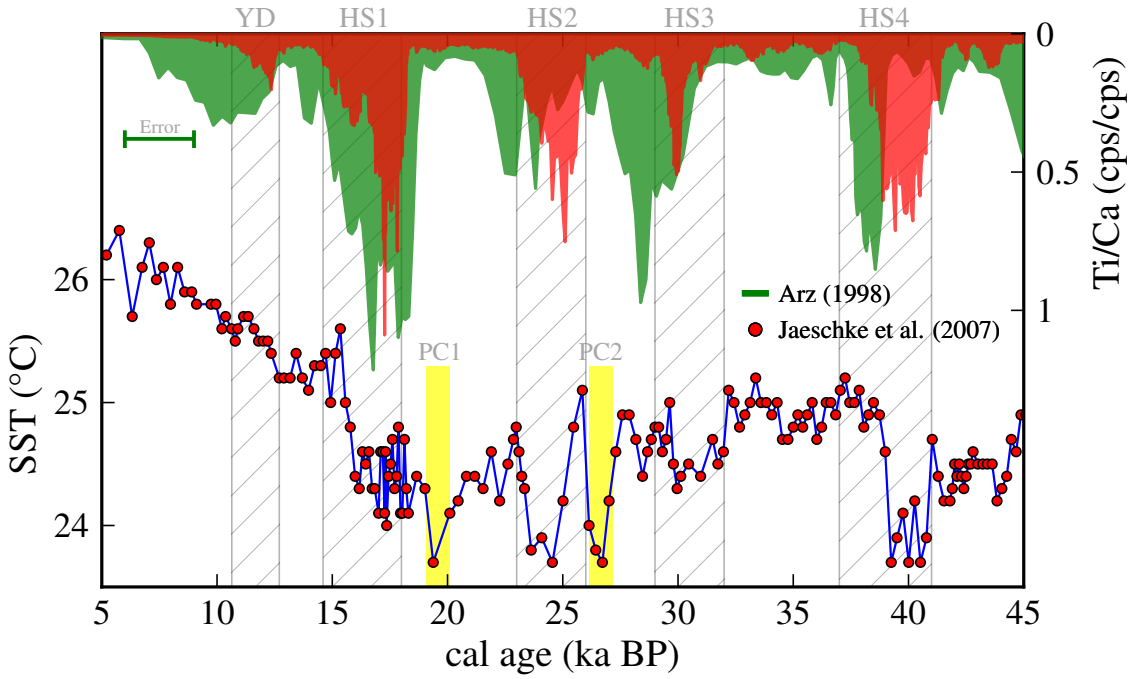

Fig. 6.12: Reconstructed alkenone-based SST and X-ray fluorescence Ti/Ca ratios from two glacial sediment deposits from off northeastern Brazil. Apparently, during Heinrich stadials Ti/Ca increased significantly and drooped in between. Titan-rich layers mark periods of enhanced river runoff from the Brazilian hinterland as a result of increased precipitation during times of Heinrich events (Arz, 1998; Jaeschke et al., 2007). Concomitantly, sea surface temperatures dropped as well as a consequence of large southward shifts of the Intertropical Convergence Zone (ITCZ). Yellow boxes indicate also drops in SST at times of the precursor events, which preceded the major sediment pulses of the Heinrich events H2 and H1 (Jaeschke et al., 2007). Note the large dating error in the Ti/Ca from Arz (1998).

layer zone of the southwestern Atlantic and stimulated enhanced phytoplankton production remains elusive. A look at Fig. 6.11 exhibits that no coral growth was recorded in all four sediment cores during the LGM (apart from corals during the brief precursor event PC1) implying that despite the great shallowing of the nutrient rich AABW, it likely did not reach the surface ocean. It is my opinion that this holds true also during the HSs and YD, even though coral growth during these times was apparently enhanced. On the one hand mixing processes across the thermocline have been in general greatly suppressed during glacial times as is the case in the temperate latitudes of today's ocean. Penetrating a further ∼2,000 m thick water layer seems to be an unjustifiable scenario. On the other hand, during the LGM, NADW was replaced by an adjusting water mass from the north filling the shallower depth of the Atlantic basin, namely the southward flowing Glacial North Atlantic Intermediate Water (GNAIW) (see 6.13). This relatively nutrient low water

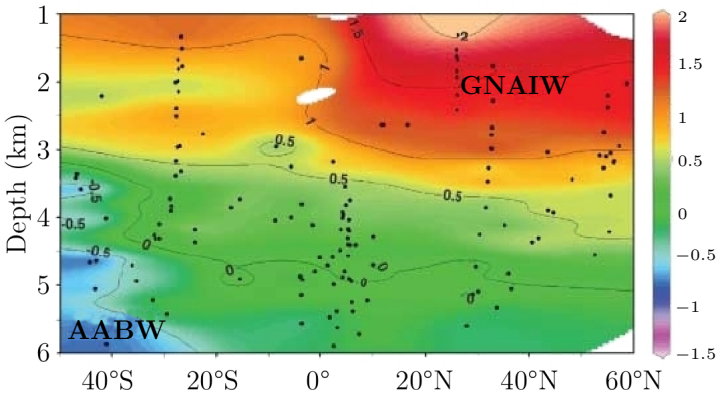

Fig. 6.13: Compiled δ^{13}C carbon isotopic data (color-coded) from the western and central Atlantic Ocean during the LGM. NADW is replaced by GNAIW and a AABW-derived water mass filling large parts of deep to mid-depth Atlantic basin. Black dots represent different measurements. Picture modified from Lynch-Stieglitz et al. (2007).

has also been found in the sediment's δ^{13} from cores off the Brazilian margin (29 °S) (Oppo and Horowitz, 2000; Curry and Oppo, 2005). In addition, ^{231}Pa/^{230}Th measurements from the western Atlantic and accompanied model simulations suggest that this shallow return flow occupied depths of around 2,000 m being as vigorous as NADW transport today (Lippold et al., 2012). GNAIW could have acted as an effective barrier preventing the subjacent nutrient rich AABW to mix with the uppermost ocean layers. In conclusion, large-scale mixing processes between greatly shallowed AABW and surface water during major climate events seem not to be a viable candidate for stimulating coral growth along the continental slope off Brazil.

6.6.1 Mesoscale eddies and coastal upwelling

A viable candidate for supplying nutrient-rich water from intermediate depths (SACW, AAIW) to the surface ocean are eddies occurring in the Campos Basin. The continuously flowing BC is birthplace of relatively cold cyclonic mesoscale eddies, which owe their existence to strong instabilities of the meandering BC facilitated through topographically induced shearing and exfoliation at the projection of Cabo São Tomé (Garfield, 1990; Viana et al., 1998). Eddies, once tied off, were advected by the BC in southwestward direction along the Brazilian slope and shelf region reaching velocities between 4−35 cm/s (see Viana et al. (1998) and references therein). Present-day eddies show diameters between 50 to more than 100 km being able to affect the water column up to a depth of ∼800 m. By raising the thermocline at the continental slope, SACW and AAIW are caused to upwell bringing relatively nutrient rich water to the surface (Silva et al., 1994; Campos et al., 2000; de Mahiques et al., 2002) thereby stimulating surface productivity. Considering that during periods of apparent coral growth glacial sea level was reduced by up to ∼130 m during the LGM (see de Mahiques et al. (2010) and references therein), all cores could have been easily within the reach of the eddy activity. Their average life expectancy is on the order of days to a month (Viana et al., 1998). This local phenomenon could therefore be a promising candidate to realize mixing processes across the thermocline, which otherwise would be quite suppressed. It can be speculated that during periods of enhanced coral growth (during the

YD and Heinrich stadials) the BC was probably more vigorous than today and as a result less stable, which promoted exfoliation of more eddies. During the LGM, however, eddy activity might have been strongly reduced, which would explain the lack of coral samples during this period. A second unrelated process operating in this region during austral summer also lead to upwelling of colder, nutrient-rich waters at the Brazilian slope around the Campos and Santos Basin. The dominant wind system in this area during austral summer is the northeast trade wind as a consequence of a shifting ITCZ below the equator. Due to the abrupt break in the physiographic orientation of the Brazilian coast between the Cabo S. Tomé and Cabo Frio (Fig. 6.14), both, the coastal orientation and trade winds are becoming parallel aligned. As a consequence Ekman transport demands a displacement of the immediate coastal water towards the open ocean which lead to upwelling of the subjacent colder thermocline SACW (de Mahiques et al., 2005). The more constant the wind blows the more intense this phenomenon is. As a result of the Ekman transport the sea level near the coast is lowered generating a pressure gradient, which drives a geostrophically balanced coastal current carrying the upwelled water towards more southern regions. Fig. 6.14 shows the SST in the Campos and Santos Basin derived from a satellite-born AVHRR during an austral summer upwelling event together with two eddies. Today, this phenomenon is quasi-seasonal controlled and might have been much more pronounced during episodic shifts of the ITCZ farther south during glacial times as indicated in Fig. 6.12 Arz (1998) during Heinrich stadials, YD, and during the early Holocene Haug et al. (2001). Micropaleontological and geochemical analyses conducted on assemblages of calcareous nannoplankton and planktonic foraminifera of a sediment core covering the past 25 ka BP taken off southeast Brazil

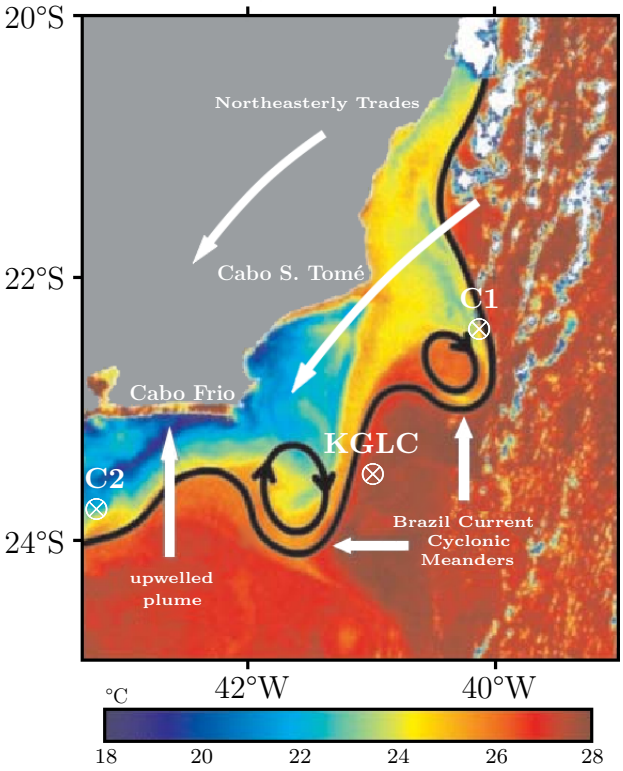

Fig. 6.14: AVHRR measurements showing the typical situation during austral summer: the meandering BC and the southward shifted northeasterly trades are causing broad upwelling of colder and nutrient rich water in the inner and outer shelf region. Crosses mark core locations. Curved arrows indicate the direction of austral trade wind flow. Image modified from de Mahiques et al. (2005).

[1]AVHRR: Advanced Very High Resolution Radiometer.

documented significant changes in the surface productivity (Toledo et al., 2007). This core is directly aligned between the KGLC and C2 cores (not shown in Fig. 6.12). These findings corroborate the idea of pronounced changes in the surface hydrography as a consequence of intense north-south shifts of the ITCZ instigated by major climate events. Two further mechanisms should be briefly mentioned here for the sake of completeness but are regarded as improbable scenarios. After Kumar et al. (1995), amplified winds from Patagonia have promoted the input of iron-rich lithospheric material into the South Atlantic during the glacial period compared to the Holocene. Aeolian dust, rich in iron, is expected to have had a fertilizing effect on the marine ecosystems. As a possible explanation attempt this approach is getting along without any complex upwelling mechanism. But the reconstructed proxy data indicating an increased export production lack the appropriate timing and correlation with the indicated climate events in Fig. 6.11. Furthermore, augmented input of aoelian dust was assessed only on sediment cores between ∼40−55 °S (Subantarctic zone). The prevailing westerlies have carried the Patagonian dust from the South American continent far into the eastern South Atlantic. Whether this dust has also reached the Brazilian core sites several thousand kilometers farther north remains elusive. Last but not least, areas with pockmarks actively venting hydrocarbon-rich fluids usually host a rich benthic-dwelling ecosystem. It is thought that bacteria-based food webs nourishing from hydrocarbon seepage have stimulated formation of such biological ecosystems (Dando et al., 1991). As a side product, cold-water corals off Brazil might have benefited as they consume redundant organic material coming from such communities in the immediate neighborhood. This is highly speculative, since nothing is known about past seepage activity around pockmarks off Brazil until today. Besides, cores KGLC and C1 from Campos Basin have been retrieved from an area devoid of any pockmark activity.

6.6.2 The potential density hypothesis

In this subsection a hypothesis put forward by Dullo et al. (2008) is tested. Observations of living cold-water coral reefs of species *L. pertusa* settling along the Celtic and Norwegian margins have shown an apparent connection between reef occurrences in intermediate-depths and the potential density anomaly of the ambient seawater. Though other environmental parameters are widely changing at these locations, the potential density anomaly (hereafter PDA), however, is found to be constant within a narrow range. It has been proposed that the PDA might constitute an important physical boundary condition for the spreading of *L. pertusa* and thus for the reef growth in these regions. Investigated *L. pertusa* frameworks occur within a certain density envelope of ∼27.35 to 27.65 kg/m^3. The PDA is defined as $\sigma_\Theta = \rho_{(S,\Theta,p)} - 1000$ kg/m^3, where $\rho_{(S,\Theta,p)}$ is the adiabatically corrected density a water parcel would obtain after brought to a certain pressure (depth) level (the pressure reference level is chosen to be the sea surface). By way of analogy, Θ is the potential temperature a water parcel would acquire if brought to the sea surface as well. It has been speculated that larvae transport preferentially occurs along those isopycnals encompassing the observed density range of ∼27.35−27.65 kg/m^3 (Dullo et al., 2008). This seems to

be a viable mechanism if coral larvae behave neutral buoyant, that is, stays submerged, while spreading along the related isopycnals. This has already been observed for some shallow-water corals but is not yet confirmed for deep-water corals. Even though data on larvae densities from *L. pertusa* are not available to test the hypothesis for the southwestern subtropical Atlantic off Brazil, the question arises in which depths these isopycnal range can be found at the Brazilian margin and if this depth corresponds to the *L. pertusa* occurrences found at the core locations investigated in this thesis. Fig. 6.15 is depicting different potential temperature and salinity profiles from MUC[2], CTD, and bottle measurements collected from the continental slope of the Santos Basin and one profile from the São Paulo plateau as part of the WOCE hydrographic program. The gray lines are isopycnals calculated for given temperatures and salinities. The reddishly dashed lines show the density range proposed by Dullo et al. (2008), which are found on the middle to lower slope region off Brazil in depths between ∼1,547 m and ∼1,000 m. This is much deeper than the locations of the recovered *L. pertusa* fossils. A lower sea level stand during glacial times has most likely reduced the potential density at the core sites even further. Assessing paleo-isopycnals is difficult and beyond the scope of this discussion. Correcting for a likely sea level change of 100−130 m off Brazil (de Mahiques et al., 2010) and under the assumption that glacial seawater and salinity profiles in this area were comparable to today the PDA for the shallower and deeper cores are placed well above the present-day density envelope for *L. pertusa* as suggested by Dullo et al. (2008) (see crosses in Fig. 6.15). The yellow cross marks the PDA for the shallower cores C1 and KGLC, green represents the deeper cores C2 and MXL and red is the single modern *L. pertusa* specimen from the Campos Basin from a depth of 606 m. Adjusting today's water mass characteristic in such a way that the colored crosses fall within Dullo's proposed density envelope would imply

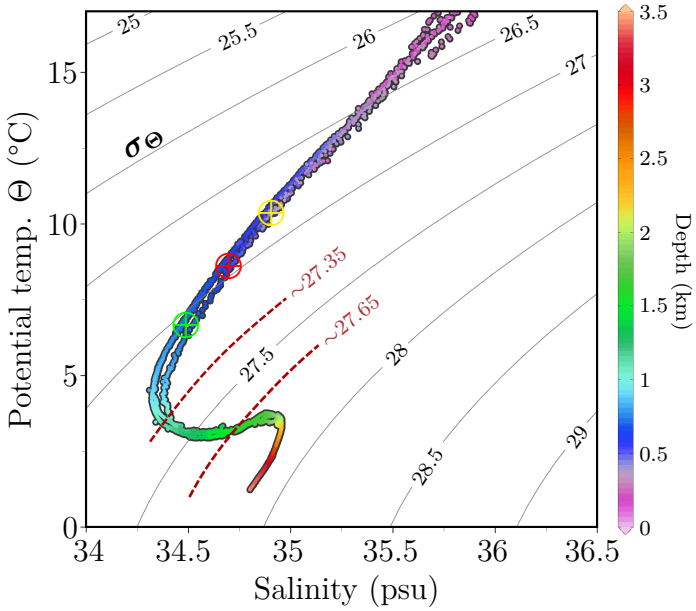

Fig. 6.15: Θ-S plot showing the potential water density at the Brazilian slope reconstructed from MUC, CTD and bottle measurements together with the proposed density range from Dullo et al. (2008) (dashed lines). ⊕ Modern *L. pertusa* (606 m), ⊕ and ⊕ are the shallower cores from Campos Basin and deeper cores from Santos Basin, respectively, corrected for a 100−130 m glacial sea level change.

[2]MUC: Multicorer, CTD: Conductivity, Temperature, and Depth.

unrealistically large variations in either the salinity, temperature or both. The investigated glacial *L. pertusa* corals in this thesis, therefore, seem to have thrived well beyond the proposed density envelope. A captured living *L. pertusa* coming from the immediate vicinity of core C1 (Campos Basin) from depths not deeper than ∼750 m (Goff-Vitry et al., 2004) supports my conclusions. Nevertheless, it cannot be ruled out that living *L. pertusa* reefs do exist in the deeper parts of the Brazilian slope and are well situated in the expected density range, but up to date no living *L. pertusa* reef has been found in this region. Due to the scarcity of the dataset the potential density of a water mass as a basic prerequisite for *L. pertusa* reef growth and distribution off Brazil cannot be verified.

7

Results and Discussion: ^{14}C

7.1 ^{14}C measurements

Thirty four coral samples have been chosen for ^{14}C dating after careful assessment of their quality based on the previous investigations. $^{14}C/^{12}C$ isotope ratios have been measured on the coralline material after carbon has been extracted by using standard hydrolysis methods. After preceding sample preparation (physical cleaning and chemical leaching with weak HNO_3) all samples were individually dissolved in 7M HCl to convert the carbonate into carbon dioxide gas. The CO_2 was subsequently catalytically reduced to graphite following the methodology already described in my diploma thesis covering also information about the sample treatment (Ruckelshausen, 2009). Target pretreatments for Zurich and Mannheim were conducted at the IUP. Except for two graphite targets that have been measured on the Mini Carbon Dating System (MICADAS) at ETH-Zurich, the remainder has been conducted either on the compact AMS (NEC 0.5 MV 1.5 SDH-2) at Keck-CCAMS facility at the University of California, Irvine or at the MICADAS at the Curt-Engelhorn-Center for Archaeometry in Mannheim. Individual samples were counted for 50,000 ^{14}C events and 10,000−30,000 at Keck-CCAMS and ETH-Zurich and Mannheim, respectively.

All results have been corrected for isotopic fractionation according to the conventions of Stuiver and Polach (1977) with $\delta^{13}C$ values simultaneously measured on the graphite targets using the AMS spectrometer. These $^{13}C/^{12}C$ ratios can differ from the original material if fractionation occurs during graphitization or during AMS measurements. All uncertainties were calculated based on the counting statistics from multiple runs on each sample, together with propagated uncertainties from blank corrections (based on measurements of ^{14}C free material), $\delta^{13}C$ corrections, and normalization, see Eq. 4.3.4.1 for isotopic fractionation corrections. Tab. E.3 depicts ^{14}C blank measurements from the Keck-CCAMS facility. One coral subset comprising samples exclusively from the MXL core has been blank corrected by using the ^{14}C value returned from a coral sample (M-385) from the same

core thought to be ^{14}C-free according to its ^{230}Th/U age (∼90 ka BP). Because calcite is "structurally speaking" cleaner than a coral (consisting of aragonite), it does normally return lower backgrounds. A sufficiently old coral sample ($\geqslant$ 60 ka) from the same core should provide a more realistic blank. The relatively young ^{14}C age of sample M-385 indicates that this coral had probably suffered from in-situ alterations which chemical pre-treatments were not capable to remove. Since diagenetic alterations cannot be ruled out for the whole coral subset the same blank correction was applied for these samples. All ^{14}C results shifted slightly toward older ages. The samples not measured at the Keck-CCAMS facility were background corrected by using the in-house calcite blanks of the different laboratories since no representative old coral samples from the other sediment cores were available for blank correction. More information about the differently used AMS techniques as well as the instrumental and offline data analysis can be found elsewhere (e.g. Unkel, 2006; Santos et al., 2007; Wacker et al., 2010). ^{14}C results are listed in Tab. E.1 and E.2.

7.2 Data representation

Before getting to the results and starting the discussion and comparison with other ^{14}C datasets from the literature, a few words need to be said about the chosen form of illustrating the data. As can be seen in Fig. 7.1 the reconstructed atmospheric Δ^{14}C from IntCal09 (Reimer et al., 2009) exhibits short-term variations superimposed by a steadily long-term decline. Δ^{14}C have been higher by as much as ∼73% with respect to the modern ^{14}C/^{12}C isotope ratio (AD 1950 $\widehat{=}$ 0 a BP) during several stages in the past. Albeit these high-end values lasted just a short amount of time, the atmosphere's ^{14}C activity was generally enriched by at least 35% during the whole period between ∼45 ka BP until the end of the LGM. Thus, for a better comparison, the deviations in Δ^{14}C between the corals and the contemporaneous atmosphere are a more reasonable measure to look at, rather than comparing the Δ^{14}C of the coral alone. In the following, all outcomes are presented as $\Delta\Delta^{14}$C following the equation:

$$\Delta\Delta^{14}\mathrm{C} = \Delta^{14}\mathrm{C}_{\mathrm{seawater}} - \Delta^{14}\mathrm{C}^{\mathrm{contemporaneous}}_{\mathrm{atmosphere}} \tag{7.1}$$

The $\Delta\Delta^{14}$C obtained can be interpreted as offsets between the two considered carbon reservoirs, namely the atmosphere and the intermediate-depth water off Brazil (Fig. 7.1). Another possibility is to assign these reservoir offsets a corresponding ^{14}C age. But because there is no real benefit for doing so, I will stick to the first notation. The reader is referred to annex B.3 where a overview plot is given in ^{14}C ages as well. For the sake of completeness, a third and widely used alternative to illustrate marine ^{14}C data is to make use of the projection ages concept first proposed by Adkins and Boyle (1997) and Mangini et al. (1998). As outlined in section 4.3.5 this idea involves counting back the Δ^{14}C (starting) value of a sample in time until this "backtrack" intercepts the atmospheric Δ^{14}C record (Fig. 7.1).

The difference between the calendar age of the atmospheric intersect and the sample's $^{230}Th/U$ age yields the so-called projection age, following the underlying equation:

$$T = 8266 \cdot \ln\left(\left(\frac{C^{pipn}}{C^{past}_{inter} \cdot F^{ML_{past}}}\right) e^{^{14}C\ age/8033}\right) - {}^{230}Th/U\ age \tag{7.2}$$

Because the backtrack is calculated until its intercept with the atmosphere the factor $F^{ML_{past}}$ (Mixed Layer), controlling the surface reservoir effect, is set to one. Today, the mean surface reservoir offset amounts to roughly 0.95 corresponding to a ∼400 ^{14}C year offset from the atmosphere. C^{pipn} denotes the $^{14}C/^{12}C$ isotopic ratio of the radiocarbon standard. C^{past}_{inter} is the ratio of the intersect between the backtrack and the atmospheric $\Delta^{14}C$ record. A more appropriate approach would be to backtrack the $\Delta^{14}C$ starting value to the surface's $\Delta^{14}C$ from which the water mass supposedly gained its initial $^{14}C/^{12}C$ imprint. Ages obtained in this way are called ventilation ages. Unfortunately, the surface reservoir ages are badly constrained as has been shown by many studies exhibiting large variations in time and space making a reasonable correction for the surface water virtually impossible. Hence, projection ages always overestimate the real ventilation ages by up to several thousand years depending on the magnitude of the surface reservoir effect. There are additional requirements which need to be fulfilled (see section 4.3.5) in order to make the projection or ventilation ages a reliable measure for the true age of a water mass. Usually these requirements are strictly speaking not satisfied. Though, this concept is tempting, I am waiving to use projection ages in this thesis.

However, for illustration purposes projection ages for the whole dataset (old and new coral data) are shown anyway without discussing the results (Fig. 7.2). Again, no surface reservoir correction afterwards or directly backtracking to the Marine IntCal09 (which tries to model the surface reservoir effect) was applied. For those readers interested in calculating projection ages see appendix C for a Monte Carlo based Python script used to calculate these ages and plotting them as 2σ covariance ellipses using Matplotlib. The script does not consider the 2σ uncertainties in the $\Delta^{14}C$ from the IntCal09 record, as indicated in Fig. 7.1 (yellow $\Delta\Delta^{14}C$ intercept points at the end of the backtracks). Implementing these errors should not pose any major difficulties but was not the focus of this thesis. However, for all calculated $\Delta\Delta^{14}C$ values in this thesis also a Monte Carlo approach came in handy. Generating normally distributed numbers (1,000) meeting the requirements of having the same mean and 2σ uncertainty as obtained from the ^{14}C and $^{230}Th/U$ measurement of a coral sample, the $\Delta^{14}C$ is calculated according to Eq. 7.3 returning an ellipse-shaped scatter diagram (Fig. 7.1) from which the error ellipse parameters can easily be deduced (blue ellipses). In order to find the reservoir offset for each scatter point to the atmospheric $\Delta^{14}C$ record it is more appropriate to find the nearest atmospheric $\Delta^{14}C$ value in the IntCal09 table for each scatter point rather than to interpolate an atmospheric $\Delta^{14}C$ value. Determine the next calendar age neighbor allowed to implement the IntCal09 uncertainty

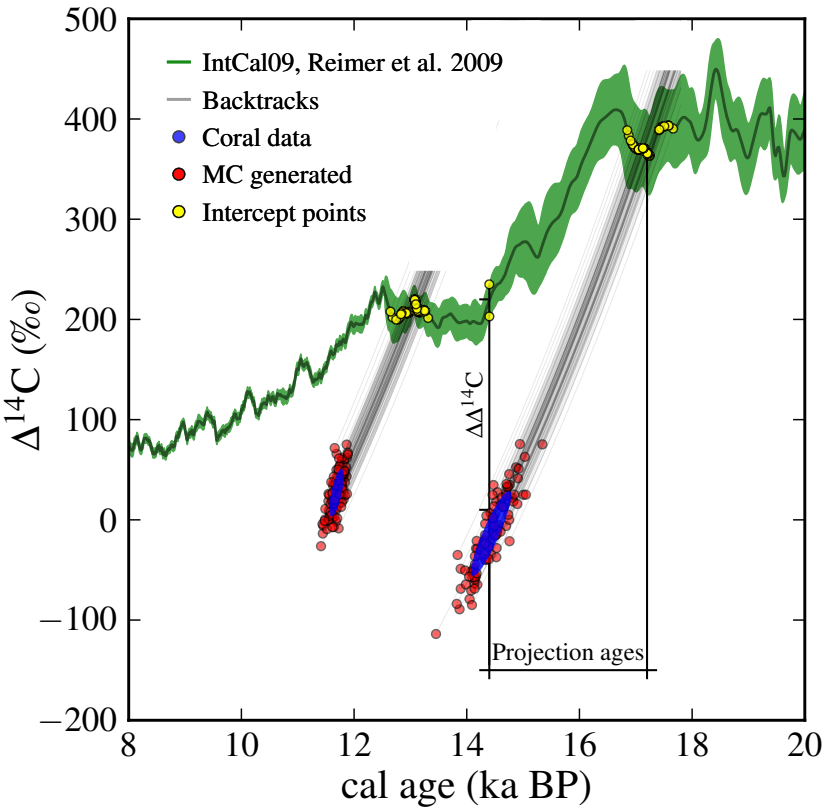

Fig. 7.1: Visualization of projection ages and $\Delta\Delta^{14}$C. For each sample 1,000 Monte Carlo Δ^{14}C values (red) were generated. The blue ellipses are 2σ error ellipses deduced from the MC generated scatter. Backtracks were calculated in order to find the projection ages as illustrated. The 2σ errors of the atmospheric Δ^{14}C were not considered. $\Delta\Delta^{14}$C were calculated for each of the 1,000 MC points with respect to the next corresponding atmospheric value using a next-neigbor approach, see text. For $\Delta\Delta^{14}$C, however, the 2σ Δ^{14}C errors of the IntCal09 were taken into account. To avoid clutter only 100 MC points are shown.

as well. This would otherwise be difficult since it is not clear how to assign an appropriate Δ^{14}C error for an interpolated atmospheric value. Once a next atmospheric Δ^{14}C value for a scatter point was found its associated atmospheric 2σ uncertainty was used as a starting point for a new set of normally distributed numbers (meeting the requirements of having the specific atmospheric Δ^{14}C and its corresponding 2σ error) from which one is chosen every time the next-neighbor-approach results in the same 2σ uncertainty looked up in the IntCal09 table. This method ensures that in this statistically approach the 2σ error of the IntCal09 is taken into account for the $\Delta\Delta^{14}$C calculations. Interpolating the IntCal09, however, is mandatory to find a sufficiently exact intercept for determining projection ages which has been done in the Python script. All error ellipses in Fig. 7.3, which lie 50%

(arbitrarily chosen threshold) above the atmospheric $\Delta^{14}C$ are omitted for the projection age calculation. If the percentage is smaller, only the points above the atmosphere are omitted, but a projection age is calculated anyway, knowing well that error ellipses with projection ages smaller than, say, about 300 years are very likely distorted in their shapes. It would be more reasonable to set the threshold value much smaller than the chosen 50% to get more realistic error estimates.

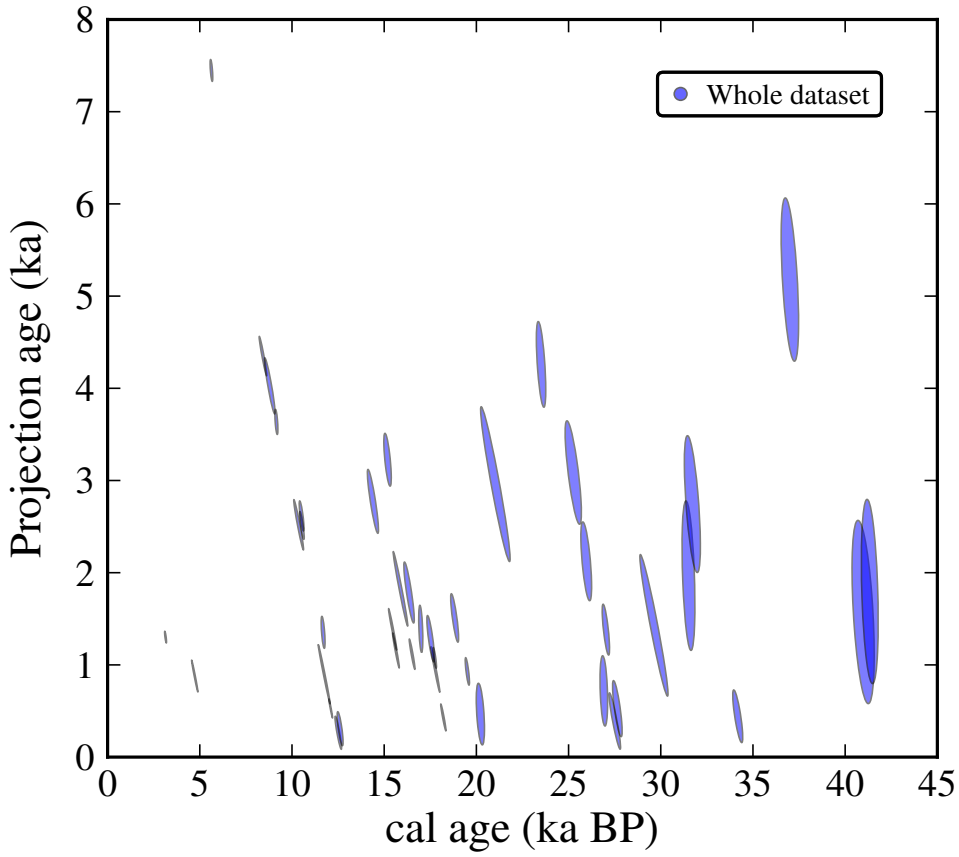

Fig. 7.2: If possible calculated projection ages are shown as 2σ error ellipses for the dataset. The ages range between several hundred years extending as far as ~7.5 ka. By definition projection ages are calculated back to the known atmospheric $\Delta^{14}C$ instead to the ocean surface $\Delta^{14}C$, which is mostly not known. Usually, initial surface-ocean reservoir ages are afflicted with large variations in time and space making a precise correction nearly impossible to get true ventilation ages. Furthermore, the possibility of mixing multiple intermediate- and deep-water sources with different ventilation histories can already lead to faulty projection ages (Adkins and Boyle, 1997). Neither projection nor ventilation ages are further discussed in this thesis.

7.3 Δ^{14}C reconstruction

By using the following equation, introduced in section 4.7

$$\Delta^{14}C_{dw} = \left(\frac{e^{\text{cal age}/8266}}{e^{^{14}\text{C age}/8033}} - 1 \right) \cdot 1000‰ \tag{7.3}$$

combining the uncalibrated ^{14}C age with the age obtained from ^{230}Th/U dating, the Δ^{14}C of a coral sample can be calculated. Δ^{14}C is the relative deviation of the ^{230}Th/U age corrected ^{14}C/^{12}C ratio of a sample to the ^{14}C/^{12}C of the radiocarbon standard given in per mille. As no fractionation between the seawater's ^{14}C-isotopic ratio and the coral carbon-

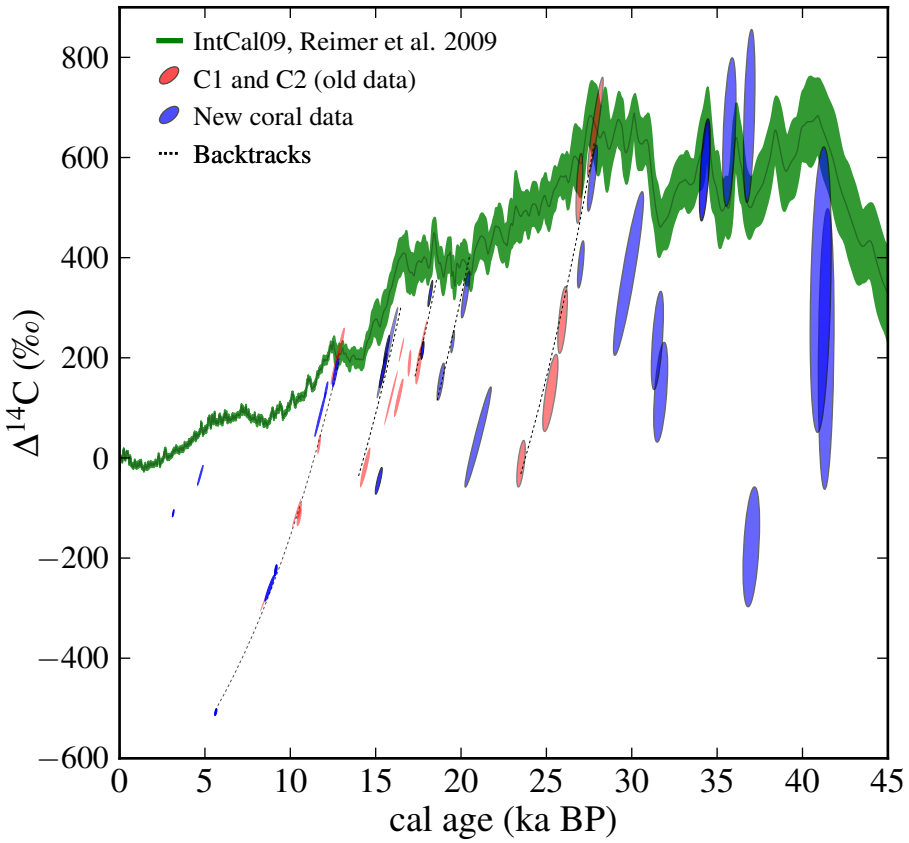

Fig. 7.3: Overview of the new coral data investigated in this thesis depicted as blue 2σ covariance ellipses together with the already published coral data from sediment cores C1 and C2 (red). The whole dataset now encompasses ~40 ka BP reaching from the late Holocene to the last third of the glacial period of the Pleistocene. The green curve is the atmospheric Δ^{14}C from Reimer et al. (2009) with corresponding 2σ uncertainties. The dashed lines represent ^{14}C decay curves, which will be discussed later.

ate occurs, the reconstructed $\Delta^{14}C$ directly reflect the radiocarbon value of the DIC of the (deep)water in which the coral grew (Adkins et al., 2002a). Fig. 7.3 summarizes the new coral $\Delta^{14}C$ dataset together with the already published measurements from my diploma thesis (Ruckelshausen, 2009) revealing amazing variations in the ^{14}C history in the intermediate-depth water of the Brazilian slope for the last ∼40 ka BP. Depletions are exceeding −500‰ at times. Another remarkable feature is that depletions in $\Delta^{14}C$ apparently follow the ^{14}C decay curve, which hints to a closed system behavior of the water mass bathing the coral sites (dashed lines (backtracks) in Fig. 7.3). I will discuss this observation in-depth later on.

7.4 Hydrocarbon seepage activity and coral $\Delta^{14}C$

The reliability of the presented ^{14}C data is potentially marred by hydrocarbon seepage activity, which might have occurred at the Brazilian margin. As outlined in sections 5.1 and 6.4 the Brazilian slope around the core locations is littered with pockmarks, the legacies of catastrophic expulsions of hydrocarbon-rich fluids in the past. Hydrocarbon fluids are often abundant in dissolved methane, which is partly oxidized by microbial anaerobic processes to CO_2 within the sediment. CO_2, once liberated to the above seawater, is subject to the carbonate chemistry forming carbonate ions among others. Since the escaping methane is geologically old and thus free of radiocarbon the resultant carbonate species could have distorted the ^{14}C dating of the corals making them apparently older in ^{14}C than they actually are.

To test this hypothesis coral samples from species *L. pertusa* from cores C1 and C2 have been measured for the stable isotope ratios $^{13}C/^{12}C$ and $^{18}O/^{16}O$. The idea is to compare the carbon isotopic compositions (expressed as $\delta^{13}C$) of the corals with the C isotopic signature of the allegedly released methane. Depending on the provenance of the methane its $\delta^{13}C$ signature exhibits a wide range from roughly −110‰ to −50‰ when biogenically derived and from −50‰ to −20‰ when the origin is thermogenic (e.g. Whiticar, 1999; Peckmann et al., 2001; Stott et al., 2009; Wirsig, 2010). Reported $\delta^{13}C$ from authigenic carbonates from the Campos Basin range between ∼−22‰ to −3‰ featuring unusually elevated values than typically found in such marine carbonates but have been shown to be the result of post-depositional diagenetic effects (Wirsig et al., 2012). The $\delta^{13}C$ and $\delta^{18}O$ coral results exhibit large variations (∼8‰ for the carbon and ∼5‰ for the oxygen isotopes) revealing a linear relationship between these two quantities (Fig. 7.4, Tab. G), which is attributed to vital effects occurring during the calcification process caused by the polyps of a coral, see Freiwald and Roberts (2005) and references therein. Possible variations in $\delta^{18}O$ due to glacial sea level changes are much smaller than due to vital effects and can be neglected. The stable isotope data are compared to a compilation of stable C and O isotope measurements from *L. pertusa* from the northeast Atlantic region, which is thought to be devoid of seepage activity. Carbonate samples (this study) were obtained

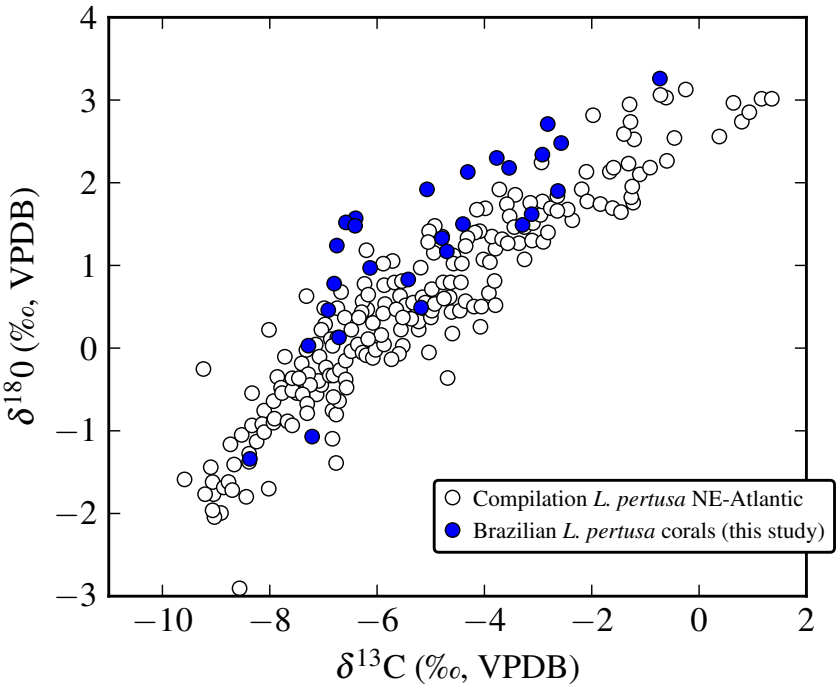

Fig. 7.4: Comparison of measured $\delta^{13}C$ and $\delta^{18}O$ of *L. pertusa* from the Brazilian slope and *L. pertusa* from the northeast Atlantic region. 2σ uncertainties are equal or smaller than dot sizes. Atlantic coral data are from Freiwald and Roberts (2005).

using the dental drill method. Measurements were provided by M. Segl on a conventional mass spectrometer type Finnigan MAT 251/252 at the Center for Marine Environmental Sciences (Marum), Bremen. The findings agree well with the data from the North Atlantic suggesting that escaping methane has played, if ever, a neglectable role in the large ^{14}C depletions observed in the intermediate depth off Brazil. A more quantitative approach indicates a possible methane release at the Brazilian slope region in the past would have had little or no effect on the radiocarbon ages of the corals. On the basis of some simplified assumptions (such as the released methane's $\delta^{13}C$ ranged between $-110‰$ to $-40‰$, low coral radiocarbon ratios were solely the result of ^{14}C-free methane, and a present-day DIC concentration of the intermediate water (before altered by input of methane) of $\sim$2.2$-$2.3 mmol/kg) the impact of a potential methane release on the skeletal $\delta^{13}C$ can be estimated. To illustrate this effect, coral C2-36 (age $\sim$5.6 ka BP) has a $\Delta^{14}C$ of $\sim-430‰$ (corrected for a mean modern reservoir offset of $\sim$85‰ for the core locations), it would be necessary to inject an additional $\sim$1.2 mmol/kg ^{14}C-dead carbon into the intermediate-depth water to explain the huge drop in its $\Delta^{14}C$. The outcome would be a relatively large negative $\delta^{13}C$ anomaly in the surrounding seawater, which should also stand out in the coral carbonate. Calculated $\delta^{13}C$ values for the coral skeletons range between $\sim2‰$ to $-44‰$ depending on how depleted the methane originally was and considering

that the water $\delta^{13}C$ can become fractionated during the aragonite precipitation (vital effect), which amounts up to ~10‰ in $\delta^{13}C$ (Fig 7.4). Unfortunately, no ^{13}C measurement has been performed for this specific sample. The maximum $\delta^{13}C$ range expected to be observed in the skeletons affected by radiocarbon-dead methane is shown as gray bar in Fig. 7.5.

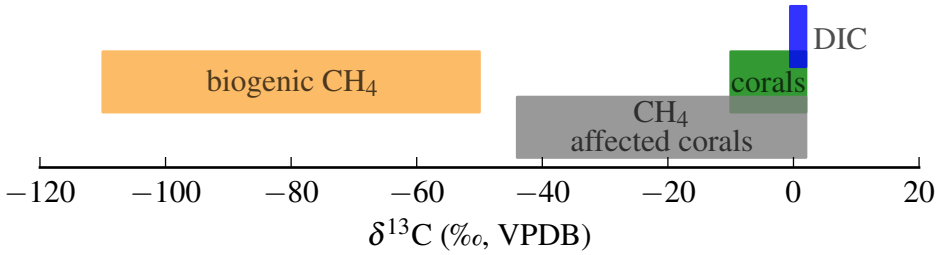

Fig. 7.5: Possible impact of biogenic methane on coral carbonate $\delta^{13}C$. The gray bar overlaps partly with the normal range in $\delta^{13}C$ observed in the cold-water corals of species *L. pertusa*. A discrimination in this range is, however, not possible.

This bar overlaps with the normal (non-methane affected) section (green) rendering a discrimination between these two possibilities impossible. However, for corals featuring large depletions in ^{14}C their stable isotopic composition should clearly stick out beyond the green bar indicating a potential influence from methane. Nevertheless, none of the investigated *L. pertusa* samples from cores C1 and C2 indicate such a behavior (Fig. 7.4). All measurements are in accordance with the results from the northeast Atlantic showing the expected variability in $\delta^{13}C$ and $\delta^{18}O$. Besides, very little is known about cold seep activity off Brazil, not to mention the timing and duration of the fluid venting at this location. Therefore, the conclusion is drawn that seeping methane did not have an impact on the progressively ^{14}C ageing of the water off Brazil. A oceanographic origin of the depleted water is a more likely scenario rather than just a local geologic phenomenon.

7.5 Intermediate-water $\Delta\Delta^{14}C$ between 0−14 ka BP

For readability reasons the whole dataset in Fig. 7.3 is divided into three sections. The first period covers the last quarter of the deglaciation and the Holocene epoch, the second comprises the deglaciation and LGM, and the last section encompasses the LGM up to the scope of radiocarbon dating. Every part will be individually discussed and compared with the available datasets from the literature. To constrain the wealth of other datasets only ^{14}C results from shallow to intermediate and deep waters, respectively, from the Atlantic Ocean are used with two exceptions: the ^{14}C datasets from the Chilean continental slope at the

eastern South Pacific from de Pol-Holz et al. (2010) and the eastern tropical North Pacific data from Marchitto et al. (2007). Fig. 7.6 depicts the coral data in the section between 0−14 ka BP. The gray contour lines give the reader an impression how the $\Delta\Delta^{14}C$ offsets have changed due to changes in the radiocarbon inventory of the atmosphere with time. Because atmospheric ^{14}C concentrations were higher in the past $\Delta\Delta^{14}C$ offsets translate into smaller ^{14}C age offsets than they do today. Thus, all contour lines are somewhat tilted towards larger calendar ages. Associated ^{14}C ages for each plotted contour line are shown ditto. Fig. 7.6 reveals a short period of highly ventilated water ∼13,000 a BP at the end of the Bølling-Allerød (BA) interstadial, immediately before the start of the YD cold snap. Intermediate water activities declined and subsequently attained modern values during the middle of the 1,200 year lasting YD. For comparison, the small rectangle on the left-hand side in Fig. 7.6 marks the preindustrial reservoir offset for the depths between 600−800 m obtained in the immediate vicinity of the cores. Fig. 7.7 shows a $\Delta\Delta^{14}C$ water profile from the WOCE hydrographic program (WHP) from the São Paulo Plateau. AAIW can be identified either by its distinct salinity or $\Delta\Delta^{14}C$ minimum. The horizontally dashed lines in Fig. 7.7 depict the approximate extent of AAIW. The pronounced decline in $\Delta\Delta^{14}C$ in Fig. 7.6 further continues beyond the end of the YD reaching an absolute minimum of about −580‰ during the mid-Holocene, which equates to an ^{14}C age offset from the atmosphere

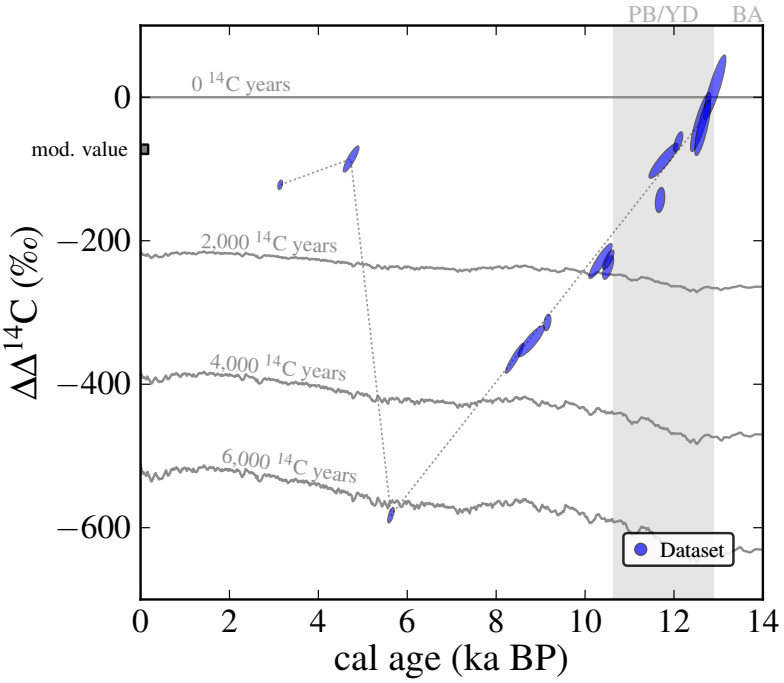

Fig. 7.6: The $\Delta\Delta^{14}C$ data reveal a large excursion in the ^{14}C activity lasting several millennia until the mid-Holocene. The gray contour lines indicate how the reservoir ages have changed in these depths due to shifts in the atmospheric radiocarbon inventory. Also plotted is the duration of the Younger Dryas and the Preboreal.

of ∼6,000 years! However, this conclusion may be marred by the fact that the specific coral sample at 5,600 a BP displays an anomalously high ^{238}U content of nearly 7 ppmw, which may be indicative for some diagenetic alteration. Though the $\delta^{234}U$ is within acceptable range an additional XRD measurement was made to determine the aragonite content but nothing suspicious has been found. The sample consists of 100% aragonite with no traces of calcite or any other mineral phases within detection limit of the used XRD method (Tab. G.2). This specific coral is thus regarded trustworthy despite its elevated uranium content. Otherwise it would be difficult to understand why the ^{14}C measurement came out with the "right age" to be on the decay curve as the older samples show. If this coral has experienced an open system behavior one would expect the carbon atoms inside the skeleton have exchanged with the seawater or pore waters within the sediment as well. Thus, an arbitrary ^{14}C age can be expected which would result in $\Delta^{14}C$ values above or below the backtrack of Fig. 7.3. But this is not the case, which can be regarded as a further proof for the integrity of the coral's aragonite. The huge drop in ^{14}C ended abruptly and activities rebounded within no more than several hundred years to modern values at about 4,700 a BP. No relapse to such depleted $\Delta\Delta^{14}C$ values seem to have happened again until today. The most striking feature, however, is that radiocarbon depletion supposedly followed the rate of ^{14}C decay (Fig. 7.3). The error ellipses between ∼5−14 ka BP line up like a string of pearls following the dashed backtrack curve. This pattern seems to repeat more or less regularly with further pronounced dips in $\Delta^{14}C$ during the deglaciation and between ∼23−27 ka BP. Such a behavior can only be expected for a mass of water that remained closed over a long period of time to allow ^{14}C to decay significantly as reconstructed. Just for clarification, plotting reservoir offsets ($\Delta\Delta^{14}C$), as in Fig. 7.6, eliminates this feature, however. The lowest $\Delta^{14}C$ values observed in the modern ocean are found in the North Pacific (at ∼2 km) with depletions of ∼240‰ relative to the preindustrial atmosphere. Depletions off Brazil were at times more than twice as large and what is really interesting were recorded in depths of only 600−800 m. These findings hint to fundamental changes

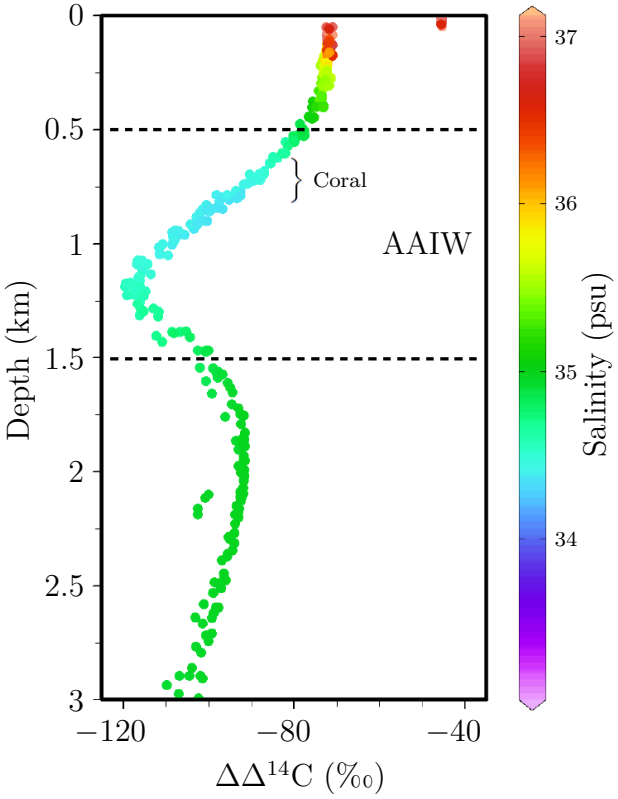

Fig. 7.7: Local preindustrial $\Delta\Delta^{14}C$ seawater profile together with salinity off Brazil. AAIW can be identified either by its distinct salinity or $\Delta\Delta^{14}C$ minimum. The dashed lines give the approximate extent of AAIW. The curly bracket indicates the core/coral depth.

in ocean circulation during that time, which ultimately impacted the intermediate-depth ventilation of the AAIW feeding the core locations. How can these results be explained?

7.5.1 Local ageing hypothesis

As all four core locations are situated in a region directly influenced by the AMOC (the adjacent water mass to AAIW is NADW flowing in south direction, see Fig. 5.7) it is difficult to imagine how AAIW, predominantly bathing the core sites, can become isolated in order to allow ^{14}C to decay. Even if AAIW production had stopped for a longer period of time, in-situ ageing would have been very improbable. In absence of lateral advection of water by AAIW, the diapycnal mixing timescale is set by turbulence across the thermocline, which follows above the AAIW (Viana et al., 1998). Diapycnal mixing is usually quite suppressed across the thermocline owing to the strong density gradients within. According to the diffusion equation the time to overcome a layer of water by diffusion alone can be estimated with:

$$t = \frac{x^2}{4 \cdot K_z} \tag{7.4}$$

where K_z is the vertical eddy diffusion coefficient, which is usually on the order of $\sim 10^{-5}$ m^2/s for an open ocean setting but has been shown to vary locally, for instance, above the abyssal plains in the Brazil basin exhibiting vertical eddy diffusivities of $\sim 10^{-3}$ m^2/s (Polzin et al., 1997). x is the diffusion length which is here set to the depth of the core locations corrected for a potential glacial to Holocene sea-level change of 100 m. The resultant mixing time is a rough estimate between 2 and 520 years depending on which vertical eddy diffusivity is used. From this admittedly very simplistic view it follows already that in-situ ageing of a resting water mass for several thousand years seems to be an unlikely scenario.

7.5.2 Production of AAIW in the Southern Ocean during glacial times

There is by now a large array of evidences, which indicate Atlantic AAIW production and its subsequent northward transport were quite variable during the last glacial and deglacial period. For example opal flux reconstructions from ^{231}Pa/^{230}Th from an equatorial Atlantic sediment core is interpreted as AAIW replacing a weaker NADW during the glacial period (Bradtmiller et al., 2007). Nutrient proxies as Cd/Ca and δ^{13}C obtained on benthic foraminifera corroborate the idea of AAIW penetrating the Atlantic far into high latitudes during the last glacial period (Rickaby and Elderfield, 2005). Authigenic $\varepsilon_{\mathrm{Nd}}$ measurements from intermediate-depth sediment cores from the Brazilian margin, Tobago Basin, and from the Florida Straits suggest abrupt changes of the neodymium source composition of AAIW for at least the past 25,000 years. The data from Pahnke et al. (2008) indicate

enhanced export of AAIW during HS1 and the YD visible by more radiogenic Nd values (Fig. 7.8). However, controversy persists as to whether the northward flow of AAIW was enhanced during these abrupt cold events. ε_{Nd} data from Xie et al. (2012) from Florida Straits sediments, however, exhibit much more negative values during HS1 and the YD indicating only a small to no intrusion of AAIW into the subtropical North Atlantic region during these time periods. The discrepancies can be reconciled by considering the cores' different water depths. It was argued that the Tobago core site lies beneath the modern AAIW depth range and actually failed to record a deglacial AAIW signal (Xie et al., 2012). Nonetheless, there is no evidence that AAIW came to a halt or was in any way significantly reduced during the last glacial or the Holocene. The idea of a resting water mass, which stayed isolated for several thousand years to explain the continuous drop in ^{14}C ($\Delta^{14}C$) must be discarded.

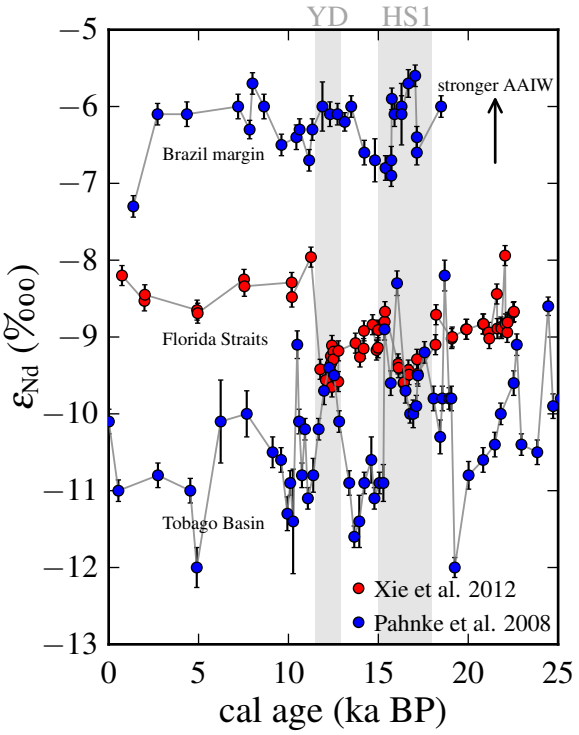

Fig. 7.8: Sediment authigenic ε_{Nd} measurements from intermediate-depths core sites exhibit vividly waxing and waning contributions of AAIW during glacial times. There are no indications that AAIW transport came to a halt for at least the last 25 ka BP.

7.5.3 The oxygen conundrum at the Brazilian slope

Another problem, which needs to be addressed concerns the water's oxygen content during the phases of (very) low Δ^{14}C ($\Delta\Delta^{14}$C). Both quantities are tightly coupled in the present-day ocean in such a way that $\Delta\Delta^{14}$C correlates linearly with the dissolved oxygen concentrations in the same water parcel. The older the water the lower is the expected oxygen concentration due to ongoing respiration and decomposition of organic mater within the water column (Fig. 7.9). Measurements of the oxygen utilization rate (OUR) in the modern Pacific Ocean yield values of $\sim 14 \pm 9$ mmol/m^3/100 a due to remineralization below 1,500 m. Mean values from the modern Atlantic Ocean below ~2,000 m give 12 mmol/m^3/100 a (Broecker, 1991). The oxygen consumption owing to remineralization alone ($\Delta[O_2]_{remin} = [O_2]_{observed} - [O_2]_{preformed}$) correlates with $\Delta\Delta^{14}$C (Fig. 7.9). The slope is equal to the OUR. This relationship allows to estimate the duration for a certain oxygen level to be completely consumed by remineralization. Southern Component Water (SCW), encompassing AAIW and AABW, usually has a mean dissolved oxygen concentration of 250 mmol m^{-3}. An ecophysiological study conducted by Dodds et al. (2007) on the coral *L. pertusa* suggests that the species is incapable to live in an environment with an oxygen level permanently below ~3 ml l^{-1} ≙ 134 mmol m^{-3}. Applying the above OUR for the present-day Atlantic gives that the ambient oxygen level would have dropped below 3 ml l^{-1} after around 1,000 years of isolating the water mass, which makes it impossible for a *L. pertusa* polyp to sustain its aerobic metabolic activity. Since the OUR is generally not known for the past ocean nor for the location off Brazil the result can only be regarded as an educated guess. The fact that corals grew during periods of extreme ^{14}C depletions indicates that dissolved ^{14}C and oxygen must have been decoupled, which is not achievable for a locally resting water mass.

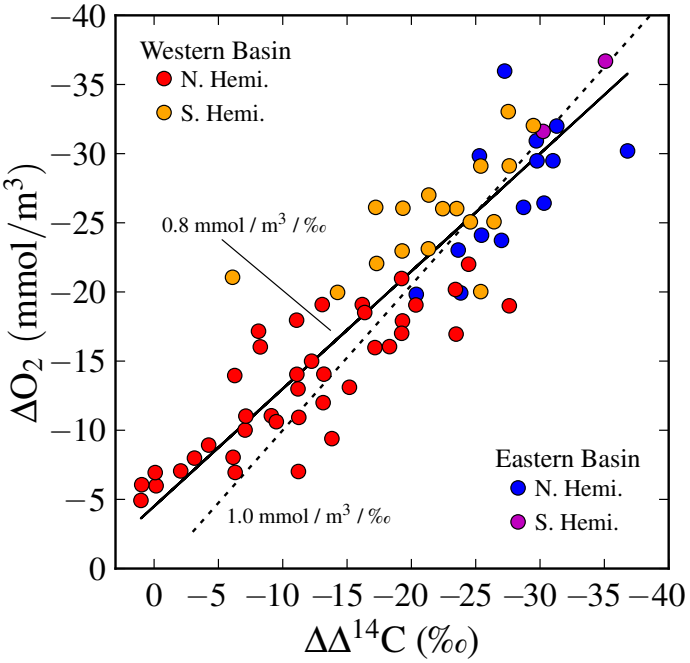

Fig. 7.9: This plot illustrates the measured oxygen versus radiocarbon deficiency obtained from different ocean basins. The slope of the regression line yields the oxygen utilization rate (OUR). Image modified from Sarmiento and Gruber (2006).

7.6 Isolated abyssal water hypothesis

A much more likely scenario to explain the reconstructed $\Delta\Delta^{14}$C depletions off Brazil and to reconcile the oxygen constraint is to invoke advection, rather than in-situ ageing of a static water mass. A viable mechanism proposed by Ninnemann and Charles (1997) and picked up later by Spero and Lea (2002) to explain observed carbon δ^{13}C minimum events recorded in thermocline-dwelling foraminifera from various core sites at the beginning of glacial terminations suggests a common origin of the water. The nearly simultaneous distribution of this isotopic signal spanning the Indo-Pacific, sub-Antarctic, and South Atlantic basin also supposes that the source of this signal very likely originated in the Southern Ocean as it is the only region directly connecting the different basins. According to this idea deglacial events caused the stratified Southern Ocean to upwell poorly ventilated water with a low isotopic δ^{13}C to the surface. The outcropping deep water was subsequently converted to AAIW within the convergence zone of the subantarctic front thereby transporting the distinct isotopic signature throughout the intermediate depth of the Southern Hemisphere (see Fig. 7.10, depicting today's water mass conversion from deep (Circumpolar Deep Water) to thermocline and intermediate water). Besides these δ^{13}C observations, several studies from intermediate depths have reported strong radiocarbon age anomalies during the course of the last glacial and deglacial period (eg. Marchitto et al., 2007; Stott et al., 2009; Bryan et al., 2010; Mangini et al., 2010), suggesting a similar mechanism must have been prevailed. To reconcile the δ^{13}C measurements and the strong depletions in ^{14}C an isolated deep water reservoir has been proposed within the Southern Ocean (Spero and Lea, 2002; Marchitto et al., 2007). This hypothesis requires that radiocarbon renewal from the upper ocean and the atmosphere was greatly suppressed and lasted up to several thousand years. An increasing number of studies indicate the Southern Ocean might indeed have played a key role in the sequestering and releasing of carbon on a glacial-interglacial timescale (Francois et al., 1997; Sigman and Boyle, 2000). This is founded in part on records showing a tight relationship between Antarctic temperature and

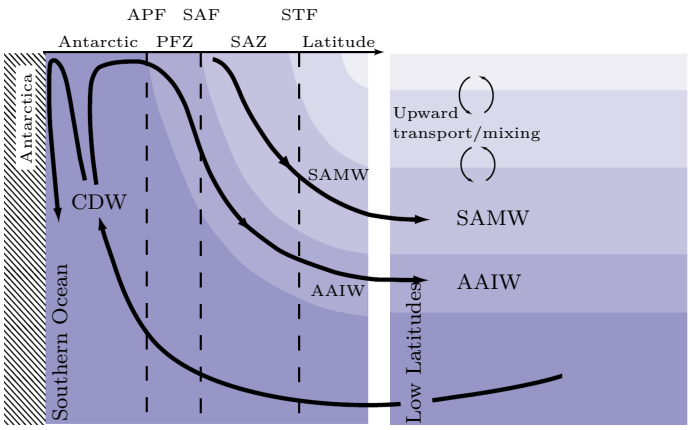

Fig. 7.10: Conceptual diagram modified from (Sarmiento et al., 2004) depicting today's water mass conversion in the Southern Ocean. Upper Circumpolar Deep Water (CDW) upwells to the surface and is entrained into the different Antarctic Frontal Zones where AAIW and SAMW is formed, which spreads throughout the entire Southern Hemisphere (Sloyan and Rintoul, 2001).

deglacial carbon cycle changes favoring a Southern Ocean control (Monnin et al., 2001; Siegenthaler et al., 2005). CO_2 sequestration during the last glacial period might have been promoted during phases of extended sea-ice cover around the Antarctic continent, which could have impeded physical exchange of CO_2 between the air-sea interface (Gersonde et al., 2003). In this regard, measured chloride concentrations reconstructed on sediment pore fluids imply the Southern Ocean contained the saltiest water in the deep ocean during the LGM as the result of sea ice formation and brine rejection at the locations of deep-water formation (Adkins et al., 2002b). Such elevated salinities point to a highly stratified water column, which could have "stabilized" a suppositious deep-water reservoir. Opal burial rates obtained from sediment cores of this region revealed changes in ocean circulation causing enhanced upwelling, which coincides with periods of rising atmospheric CO_2 (Anderson et al., 2009).

Fig. 7.11 summarizes some important deglacial records: measured atmospheric CO_2 stems from an Antarctic ice core and reveals a stepwise rise in CO_2 by as much as ∼80 ppmv with a plateau phase lasting the bigger part of the Antarctic Cold Reversal (ACR), deuterium and $\delta^{18}O$ data from an Antarctic ice core show a similar stepwise rise in atmospheric temperature, while atmospheric $\Delta^{14}C$ declined by about 190‰ within the mystery interval (∼17.5−14.5 ka BP). Variations in cosmogenic ^{14}C-production have been reconstructed and show no important changes during this time (e.g Laj et al., 2002; Muscheler et al., 2004; Broecker and Barker, 2007) and during times of large $\Delta\Delta^{14}C$ depletions discussed in this thesis. Rather, elevated opal burial rates hint to enhanced upwelling of nutrient rich water in the Southern Ocean, which coincided with the end of HS1 and the beginning of the YD. Proposing an "isolated" abyssal reservoir located in the Southern Ocean seems to appear reasonable considering the similar deglacial records from this area. Such a reservoir would not only have accumulated remineralized organic carbon during times of isolation, which could have helped modulating atmospheric CO_2 variability, it also would allow ^{14}C to decay significantly. If mixed back to the atmosphere, CO_2 would have increased while atmospheric $\Delta^{14}C$ declined. Former attempts to locate an old abyssal reservoir in the Pacific Ocean to explain the ∼190‰ drop in atmospheric and ocean surface $\Delta^{14}C$ during the mystery interval have not been met with success. Radiocarbon differences for glacial and deglacial age benthic-planktic pairs covering various core sites in different depths yielded ^{14}C depletions similar to or only slightly greater than in today's Pacific (e.g. Shackleton et al., 1988; Broecker et al., 2004a,b; Broecker et al., 2007; Galbraith et al., 2007; Broecker et al., 2008; Broecker, 2009). Even though precautions have been taken to choose only suitable cores, that is, cores with sufficiently high sedimentation rates to avoid effects of bioturbation, interpretation of B-P-offsets are additionally marred by the fact that surface reservoir ages could have substantially varied over time masking real changes in ocean ventilation and associated water residence times. Apart from that, measuring the $^{13}C/^{12}C$ composition on benthic-planktic tests from the same Pacific sediment cores places a hypothesized abyssal reservoir in depths lower than 4.4 km. Such a deep reservoir, however, appears to have been too small to explain the ∼190‰ drop during the mystery interval. Radiocarbon evidence from corals and benthic-planktic foraminifera from the glacial North Atlantic,

however, indicate strong depletions in ^{14}C by as much as $\sim 200-300‰$ compared to the contemporaneous atmosphere (e.g. Keigwin and Schlegel, 2002; Keigwin, 2004; Skinner and Shackleton, 2004; Robinson et al., 2005). But again, the ^{14}C deficiencies are not large enough to explain the 190‰ during the mystery interval. Until today, a large deep water reservoir responsible for the observed deglacial anomalies has not been found.

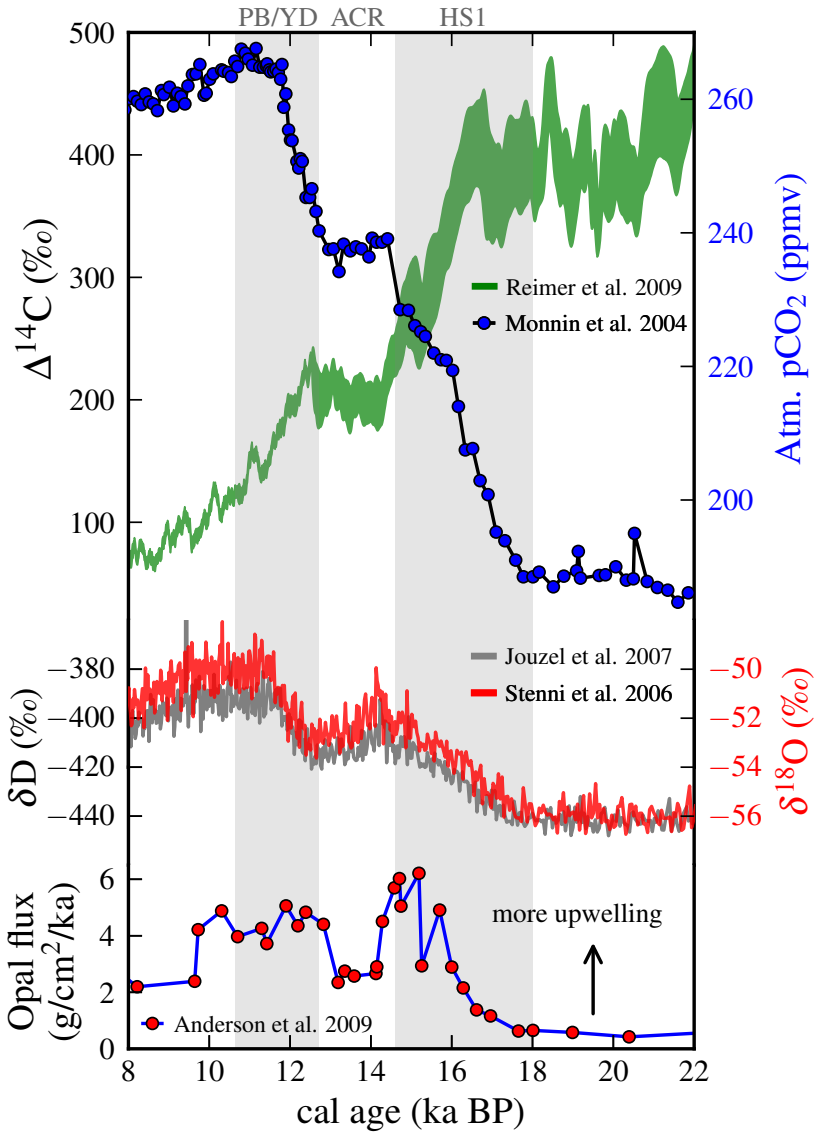

Fig. 7.11: Deglacial records showing a similar stepwise rise in CO_2 and δD from Antarctic ice cores favoring a Southern Ocean control. The coeval drop in $\Delta^{14}C$ suggests that the released $^{14}CO_2$ was quite depleted pointing to poorly ventilated deep water. Enhanced opal fluxes from the Southern Ocean indicate that deep water masses have experienced enhanced upwelled during the same time periods.

7.6.1 Reconciling the oxygen conundrum

Here I set forth the hypothesis wherein the recorded large drops in the radiocarbon activity off Brazil are best explained with the assumption of one or more isolated deep-water reservoirs, which existed in the South Atlantic/Southern Ocean region during the course of the last glacial period especially during HS2, HS1, and the YD/mid-Holocene. As outlined previously, the demise of such an abyssal reservoir, instigated by renewal of deep convection or upwelling events in the Southern Ocean might have led to conversion of ageing deep water to AAIW reaching the Santos and Campos Basin offshore Brazil. This explanation attempt has the advantage of reconciling the oxygen conundrum described in section 7.5.3. The isotopic equilibration time for ^{14}C at the ocean surface is much different from that of gaseous oxygen (O_2). Atmospheric ^{14}C ($\Delta^{14}C$) requires about 10 years to equilibrate with a 80 m thick surface mixed layer, whereas oxygen only needs several weeks to months for equilibration, depending slightly on the used gas exchange model (Broecker and Peng, 1974; Sarmiento and Gruber, 2004). Surface water in the present-day Southern Ocean region has residence times much lower than needed for $\Delta^{14}C$ to equilibrate, but are on the other hand long enough for oxygen to be completely renewed. This decoupling process occurs up to a certain point in today's AAIW formation regions, where ^{14}C does not equilibrate with the atmosphere but oxygen renews to saturation (Ostlund et al., 1987; Key et al., 2004). This may provide an explanation why the Brazilian corals have been bathed in water, which was quite depleted in ^{14}C, while on the other side had enough oxygen for the corals to thrive.

7.6.2 Distribution of hypothesized deep-water reservoirs

The blurry red circles in Fig. 7.12 illustrate how these deep-water reservoirs might have distributed during the last glacial period and early Holocene. The green zone ringing the Antarctic continent indicates the region where today's AAIW production primarily takes place (Orsi et al., 1995). It seems reasonable to suppose their locations in the vicinity of the area of (past) AAIW production. The reader is cautioned that this picture is only an artistic view and does not necessarily represent true circumstances. Also the number of shown abyssal reservoirs is arbitrarily chosen. The red lines feature pathways (stable conduits) the water could have used to reach the Brazilian core sites. The observed exponential decline in $\Delta^{14}C$ of the intermediate-depth water off Brazil (Fig. 7.3, dashed lines) strongly suggests that AAIW bathing the core locations must have stayed isolated for the whole time span the deep water reservoir drained. It is conceivable that at times of low $\Delta^{14}C$, AAIW transport was enhanced to such an extent that mixing with the ambient water was quite suppressed. This could have preserved the preformed ^{14}C signature imprinted in the AAIW formation zone, hence the label 'stable conduit' in Fig. 7.12. If the large ^{14}C depletion between 0−14 ka BP (Fig. 7.6) was without interruption, the corresponding conduit must have existed for over 5,000 years or might have existed for only several hundred years if the spilling was occasionally disrupted, which might be possible due to the poor sample coverage for this time span. The gaps between the $^{230}Th/U$ dated coral amount in part to

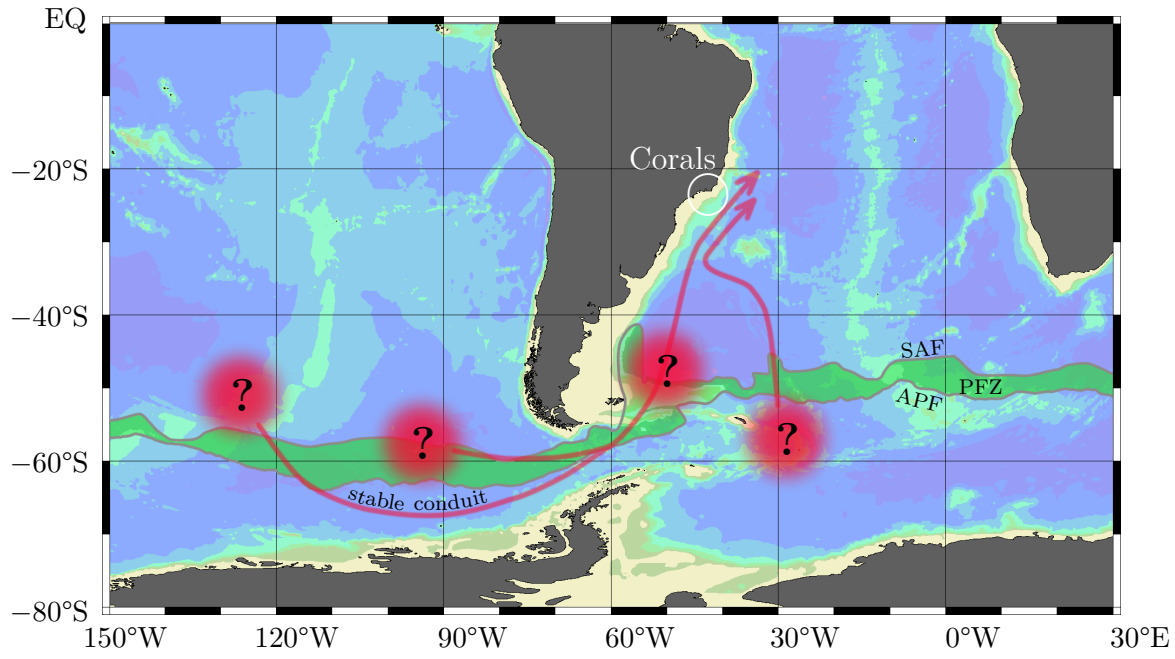

Fig. 7.12: Postulated locations of isolated abyssal water masses, which formed during the last glacial and deglaciation period. The green band marks the area where today's AAIW production takes place (Orsi et al., 1995). The Polar Frontal Zone (PFZ) is stretched by the Subantarctic Front (SAF) and Antarctic Polar Front (APF). After subduction inside the PFZ, portions of newly formed AAIW is transported equatorwards within the subtropical gyres of the South Pacific and Atlantic, some fraction of Pacific AAIW enters also the Atlantic via the Drake Passage. The red lines indicate presumed spilling routes (stable conduits) the ^{14}C-depleted water from the abyssal reservoirs could have taken to reach the Southwest Atlantic coral site.

more than 2,000 years. To clarify matters, the transition time of AAIW from its formation region to the Brazilian continental slope area is almost instantaneous with respect to the ^{14}C half-life and therefore much too short to account for the observed decline in $\Delta^{14}C$. Horizontal water mass transport in the modern Antarctic Circumpolar Current (ACC) and also AAIW is quite vigorous and in the range of several tens of centimeters per second, reaching the coral location only a few decades after formation. Even if assuming a more reduced velocity of say 1 mm/s it will last only several centuries for AAIW to overcome a distance of several thousand kilometers. Proposing stable conduits as the main signal carrier for the extremely radiocarbon-depleted water mass is a bold statement, which poses the question of what may be the mechanisms behind driving their stability and allowed the signal to propagate over such long time periods and distances. The leftmost indicated abyssal reservoir in the Pacific Ocean is between 8,000−9,000 km apart from the coral site off Brazil (Fig. 7.12). No matter how vigorous the spilling via stable conduits might have been during certain time periods an initially low $^{14}C/^{12}C$ signature very likely

would have dissipated away mainly through mixing processes in the Antarctic Circumpolar Current. Modeling work from Hain et al. (2011) suggests that propagation of an extremely radiocarbon-depleted water mass starting from the Southern Ocean to the North Pacific via AAIW is unlikely. The initial ^{14}C signature would be rapidly diluted by mixing with carbon from the ambient water masses. Besides those problems, it is in general not known how these proposed deep water reservoirs came into existence in the first place. Reconstructed chloride concentrations for the LGM on sediment pore fluids suggest the Southern Ocean contained the saltiest water in the deep-glacial ocean, which could have facilitated the formation and stabilization of an isolated abyssal reservoirs. But this kind of investigation has been done only for one sediment core so far, which covers the relatively brief time period around the LGM (Adkins et al., 2002b). Whether such conditions were present during the deglaciation and early to mid-Holocene cannot be decided. There are evidences, however, implying that the eastern South Pacific did not seem to host an isolated reservoir during the late deglacial and Holocene period. This will be discussed in the next section.

7.7 Comparison to other $\Delta\Delta^{14}C$ datasets

Intermediate-water depths between 0−14 ka BP

Fig. 7.13 depicts a compilation of $\Delta^{14}C$ data available in the literature, here presented as $\Delta\Delta^{14}C$. Today, all shown intermediate-depth sites are ventilated directly or indirectly by AAIW but are thought to have been bathed by AAIW during glacial times. It is evident that the different datasets do not show any resemblance compared to the data from off Brazil. While Brazilian corals recorded a strong depletion in $DI^{14}C$ beginning any time during PB, studies from other core sites lack this distinctive pattern. To be more precise, reconstructed radiocarbon from these sites remained relatively confined within a $-50‰$ to $-200‰$ offset from the atmosphere during the most part of the Holocene. Only the landmark study from Marchitto et al. (2007) steps out of line. This core stems from an intermediate depth from the northern edge of the eastern tropical North Pacific and registered marked drops in radiocarbon activity during the YD ($\Delta\Delta^{14}C \sim -400‰$) followed by a sudden return to modern values during the PB and HS1 ($\Delta\Delta^{14}C \sim -500‰$). To explain his data Marchitto et al. (2007) proposed the demise of a carbon reservoir long isolated from the atmosphere located within the deep Southern Ocean. As the result of a progressive resumption in ocean circulation the old water from this reservoir was mixed back to or near the ocean surface and carried by AAIW or its glacial analogue to the lower latitude core site off Baja California. One might expect to see at least parts of this strong radiocarbon-depleted signal also at the different Atlantic locations and in particular at the Chile margin, since Pacific AAIW is transported eastward within the ACC and northward with the counterclockwise rotating subtropical gyre (Hartin et al., 2011). But the available datasets suggest otherwise. During the YD the difference in $\Delta\Delta^{14}C$ between Brazil and the North Pacific amounts to $\sim 350-400‰$ suggesting that no depleted water entered the Atlantic via the Drake Passage. This is corroborated by ^{14}C data obtained on dredged corals from depths between 318−1,750 m from the Drake Passage providing vital informa-

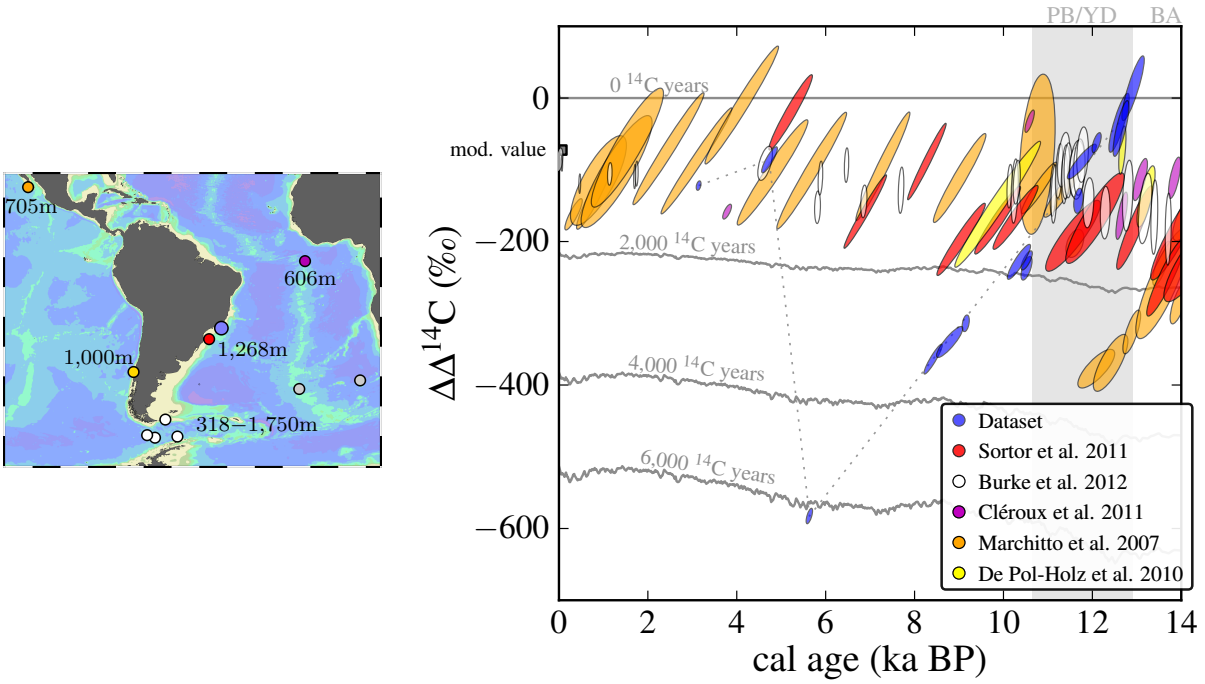

Fig. 7.13: $\Delta\Delta^{14}$C compilation from recent studies from intermediate-depth water primarily covering the South Atlantic and Southern Ocean revealing the ^{14}C water mass histories. Gray dots are study sites from much deeper water and will be discussed in the next section. Numbers denote water depths of the different core sites. All error ellipses represent 2σ uncertainties.

tion regarding a possible transport route of depleted AAIW, which entered the Atlantic Ocean Burke and Robinson (2012). These corals do not only show any large depletions during the YD but also exhibit relatively constant reservoir offsets of around −100‰ throughout the course of the Holocene. $\Delta\Delta^{14}$C are more negative during the Bølling-Allerød period mainly due to changes in the atmospheric ^{14}C reservoir. It may seem odd that the core site of the Chile margin did not record evidence of a low ^{14}C signature during the YD especially as the location is in proximity to modern-day AAIW/SAMW formation. It was argued that water ventilating this site during the deglaciation was subducted north of the subantarctic front, and was, hence, completely free of any Southern Ocean ^{14}C imprint (de Pol-Holz et al., 2010). The datasets presented here give a clear indication that a Pacific origin of the progressively ageing water mass recorded off Brazil can be ruled out. At least the eastern part of the deep South Pacific Ocean quite likely did not host an isolated carbon reservoir, whose water eventually flooded the intermediate-depths shorelines of the Southwest Atlantic between ∼10.8−5.6 ka BP. The study from Sortor and Lund (2011) seems to conflict with this conclusion. The giant gravity core (KNR159−5−36) has been retrieved from the immediate neighborhood to the coral sites from a depth of 1,268 m (Fig. 7.13) only a few hundred kilometers farther south. Today, this core is located within the lower limit of AAIW and inside the transition zone to the underlying deep-water masses

of upper NADW (UNADW) and upper Circumpolar Deep Water (UCDW). UCDW is not shown in Fig. 7.14. Thus, one would expect this location to be sensitive to changes in deep-water mass geometry. Times of enhanced NADW production in the high North Atlantic in the past and subsequent transport as deep western boundary current might have altered the ^{14}C composition of the lower part of the intermediate water towards a more northerly ^{14}C signature or a mixture involving UCDW. There are two leads supporting the idea of a varying water mass geometry. The first comes from $^{231}Pa/^{230}Th$ excess reconstructions of three sediment cores from the western North Atlantic (Fig. 7.15), which are thought to be in direct reach of NADW flow (McManus et al. (2004) and Christner (2011)). The argument runs as follows: after meridional overturning circulation in the North Atlantic virtually ceased at least during the coldest stages of the last deglaciation (during the YD, HS1 with relatively high values in $^{231}Pa/^{230}Th$, see Fig. 7.15), $^{231}Pa/^{230}Th$ values became significantly smaller during the first half of the Holocene proposing a vigorous export of deep water from the North Atlantic to the South Atlantic. The adjustments needed to switch from the glacial circulation pattern, which prevailed until the end of the deglaciation towards a modern circulation state was apparently accompanied by a transient oscillation of the Atlantic circulation system manifesting as a "$^{231}Pa/^{230}Th$-overshoot minimum", which occurred roughly at the middle of the Holocene (Fig. 7.15). Afterwards, $^{231}Pa/^{230}Th$ ratios returned to modern Holocene values. Similar phenomenons have been observed in modeling approaches for the AMOC during the last deglaciation. Barker et al. (2010) reported an AMOC overshoot in his model run at the BA transition from a state of no NADW export at 30 °S to ∼27 Sv within about 200 years while the glacial and modern control runs were characterized by NADW exports of ∼8.5 Sv and ∼14 Sv, respectively. Moreover, a three-dimensional ocean general circulation model has shown that during an overshoot the Atlantic Ocean is dominated by a vertically expanded AMOC cell (Knorr and Lohmann, 2007). If this observation proves true, significant changes in the relative water mass composition at the 1,268 m depth horizon cannot be excluded. The water, which bathed this core site, today dominated by AAIW, could have had a larger influence from upper NADW and/or upper CDW. The second hint that the water-mass geometry could have changed comes from the ^{14}C measurements of the foraminifera from Sortor and Lund (2011) itself. The foraminifera recorded more positive $\Delta\Delta^{14}C$ during the first half of the Holocene, which reached nearly atmospheric $\Delta\Delta^{14}C$ values at ∼5,200 a BP. This can be interpreted to the effect that this location was indeed

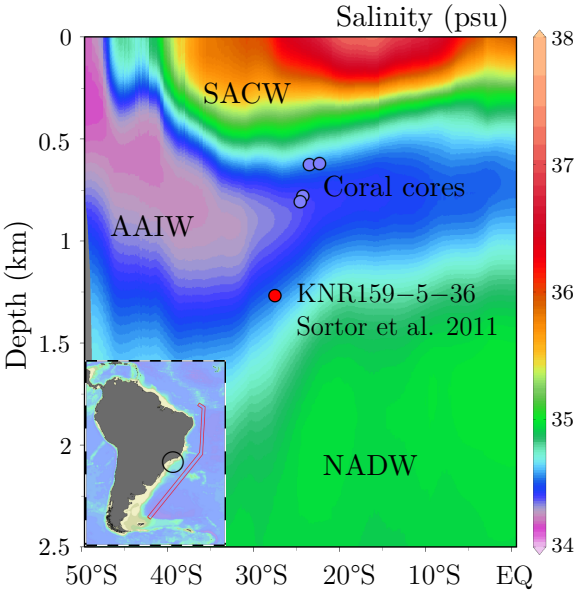

Fig. 7.14: Modern hydrographic setting along the shown transect, which are bathing the core sites indicated by a black circle (inset).

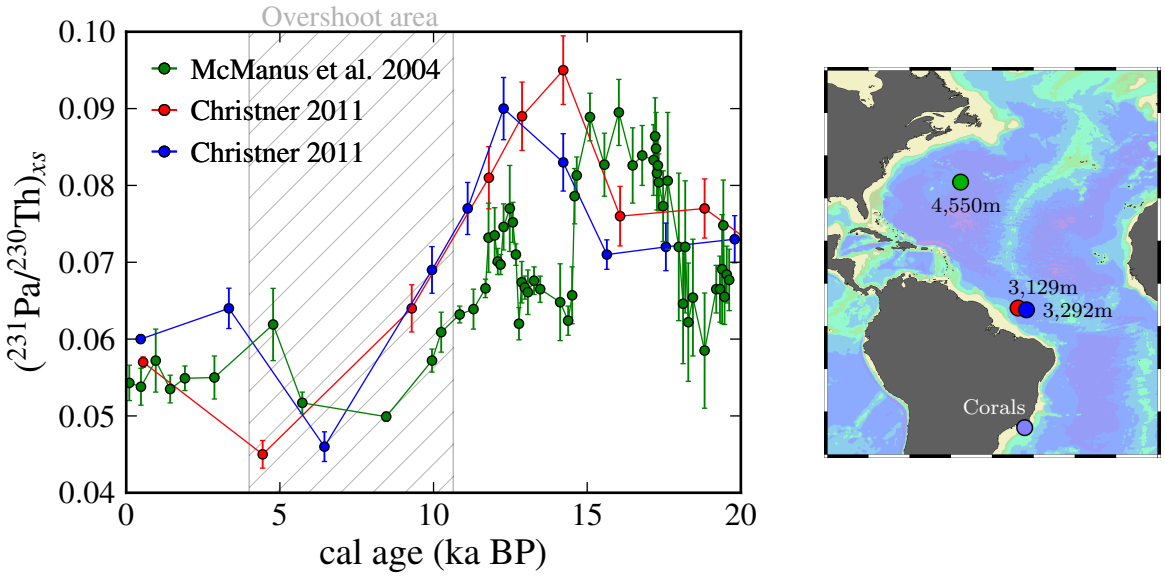

Fig. 7.15: The apparent overshoot period is characterized by $(^{231}Pa/^{230}Th)_{xs}$ that are lower than found today, indicating a vigorous export of North Atlantic deep water during this time period as suggested by several sediment cores. Errors in Pa/Th are 2σ.

affected by water, which gradually became enriched in ^{14}C as a consequence of input from younger water from upper NADW and/or upper CDW. This would imply strong Δ^{14}C gradients existed in the water column between ~800−1,268 m, which needed to be maintained over time periods of up to several thousand years! Another aspect I would like to address briefly is about the almost vanishing reservoir offset for the corals ($\Delta\Delta^{14}C \sim 0‰$) at the climate transition from the BA to YD. During this time the intermediate water off Brazil was obviously highly ventilated, while other core locations just indicate expected reservoir offsets owing to their different depths and core sites (except for Marchitto et al. (2007))(Fig. 7.13). As delineated in section 7.5.2 authigenic neodymium isotope data from Pahnke et al. (2008) from the western tropical Atlantic and the Brazilian margin suggest a vigorous export of AAIW that apparently took place during the Heinrich event 1 and the YD cold snap. To call on enhanced export of AAIW from the Southern Ocean up to the Brazilian core site, however, involves a shortening of the residence time of the upwelled water within the AAIW formation area. Hence, CO_2 isotopic exchange tends to be more reduced than for a more sluggish AAIW flow strength increasing the chances of preservation of the imprinted ^{14}C signal even further. A more vigorous AAIW flow during the YD cannot be held responsible for the almost atmospheric ^{14}C values recorded in depths of ~600−800 m. As shown in section 6.6.1 the continuously flowing BC in this oceanic region is birthplace of relatively cold cyclonic mesoscale eddies which are a consequence of strong instabilities of the meandering BC current in combination with the local bottom topography. These eddies are able to stir up the water column up to depths of several hundred meters

thereby acting like a large blender homogenizing the water column beyond the thermocline. Moreover, seasonal upwelling of coastal water is known to occur in this area during austral summers due to a shift of the ITCZ below the equator that might have been enhanced during the YD as suggested by repeatedly increased accumulation of terrigenous sediments in the coastal areas off northeast Brazil implying a pronounced southward migration of the ITCZ during the YD (Rao et al., 1993; Arz, 1998). Both regionally very localized mechanisms taken together may help to explain why intermediate ^{14}C activities are close to atmospheric values at the beginning of the YD.

7.8 Comparison to other $\Delta\Delta^{14}$C datasets

Deep water between 0−14 ka BP

In the attempt to reconcile the observations made off Brazil with the previously mentioned ^{14}C datasets from the South Atlantic/Southern Ocean two further studies must not be missing. In contrast to the already discussed datasets coming from intermediate depths the two sediment cores from Skinner et al. (2010) and Barker et al. (2010) stem from the deep East Atlantic region from 3,770 m and 4,981 m water depth, respectively. Both sites recorded significant changes in the deep-water circulation during the course of the last deglaciation. But for the last ∼14 ka BP (including the Holocene) no unusual ^{14}C depletions in the marine sediment (foraminifera) were preserved (Fig. 7.16). Reconstructed projection ages from the deeper core site decreased substantially from ∼2,000 years during HS1 to less than 500 years at the end of the BA suggesting an import of well ventilated water masses as a result of an increased influence of NADW in the Southern Ocean during this time period (see Fig. 1 in Barker et al. (2010)).

This is in accordance to several other studies showing a generally better ventilated deep North Atlantic Ocean during the BA period (see Barker et al. (2010) and references therein). Unfortunately, no data from this core are available for the Holocene. At the same time the shallower core from Skinner et al. (2010) from the mid-Atlantic ridge exhibits nearly constant $\Delta\Delta^{14}$C values wiggling around −200‰, which is the expected present-day reservoir offset for this location. Both sites lack significant depletions compared to the coral sites off Brazil. Admittedly, two investigated cores are barely enough to constrain the ^{14}C history for the whole deep eastern South Atlantic and caution is in order not to jump to any conclusions. Nonetheless, there is no indication that the southeast Atlantic has accommodated an isolated deep carbon pool that supplied the AAIW with a steadily ageing water mass. The deep southeast Atlantic might have hosted a putative deep-carbon reservoir during the course of the last deglaciation, especially during HS1 as suggested by Skinner et al. (2010). But there is currently no evidence that such a reservoir existed also during the Holocene epoch. On the basis of the ^{14}C data on-hand between 0−14 ka BP (Fig. 7.16) an isolated carbon reservoir is proposed to have been existed in the deep southwestern Atlantic in order to explain the coral data off Brazil. Of course there is no direct evidence so far to substantiate this contention. Given the properness of all presented ^{14}C data, the

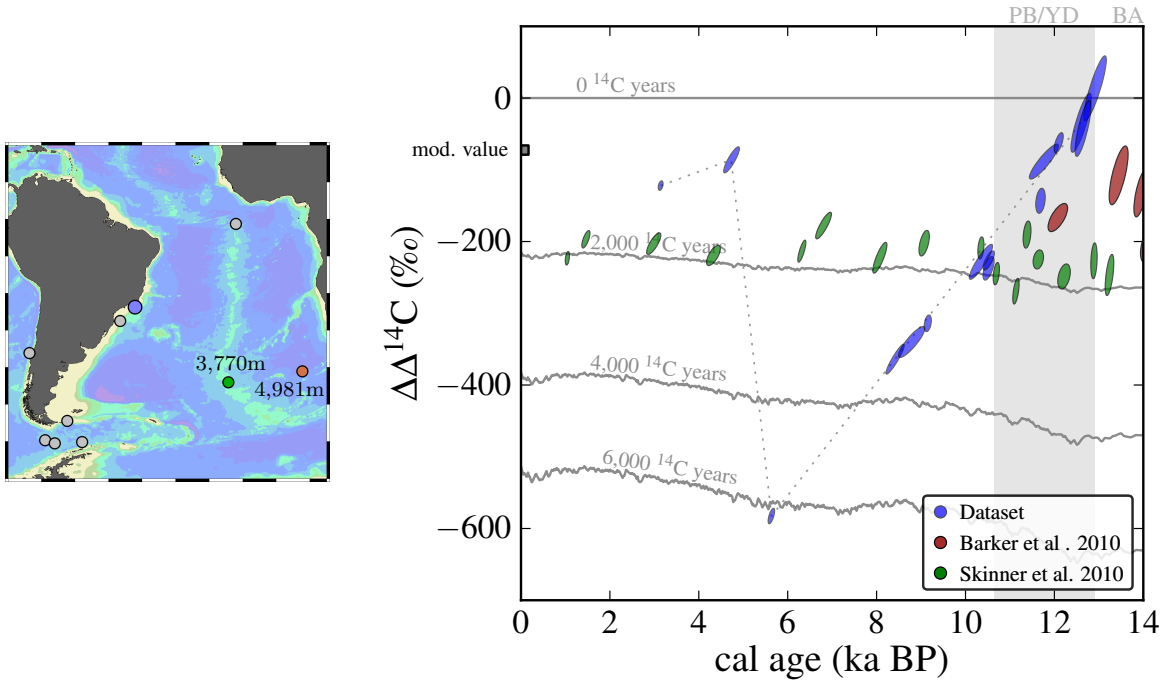

Fig. 7.16: Two benthic radiocarbon studies on foraminifera from the deep southeast Atlantic Ocean reveal no similarities to the intermediate-depth ^{14}C coral record off Brazil between 0−14 ka BP. Though, both locations are situated in a much greater depth the intermediate-depth record from the southwest Atlantic is by far more depleted during the first half of the Holocene which is questioning the southeast Atlantic as a source of a greatly depleted DI^{14}C pool.

Drake Passage as a possible gateway for the intrusion of a very old water mass coming from the Pacific as formerly speculated by Mangini et al. (2010) needs to be reconsidered. The deep southwestern Atlantic seems to be a promising location in pursuing an isolated carbon reservoir. The Argentine Basin as a part of the southwestern Atlantic in particular, spanning the floor off the east coast of Argentina between the mid-Atlantic ridge to the east and the Scotia Basin to the west, shows an average depth of ∼5,000 m hosting the deepest parts of the ocean floor worldwide. The hypothesized location is already indicated in Fig. 7.12.

7.9 $\Delta\Delta^{14}C$ during the glacial between 14−42 ka BP

In the next section encompassing the time span of the last deglaciation (for the most part) and prior reaching back as far as ∼42 ka BP, the coral ^{14}C data are presented for comparative purposes simultaneously with the former deep and intermediate studies from the previously discussed authors. If not stated otherwise all data are given as 2σ error

ellipses. The deglaciation we are now looking at is of special interest since during this time period marked shifts within the atmosphere-ocean climate system occurred, which ultimately paved the way for the transition from a glacial to a interglacial climate state. The Brazilian corals recorded rapid $\Delta\Delta^{14}C$ changes between 14−21 ka BP (Fig. 7.17). Starting with a coral from the LGM at ∼21 ka BP having an offset of ∼−370‰ from the atmosphere (corresponding ^{14}C age ∼2,500 years). $\Delta\Delta^{14}C$ returned to nearly modern values at around 20 ka BP followed by a steadily decrease for the next ∼ 1.4 ka. After a local minimum at around 18.8 ka BP the intermediate water ^{14}C activity rebounds to modern values again near the onset of HS1 (18 ka BP). During HS1 $\Delta\Delta^{14}C$ continuously declined again until another local minimum at ∼15 ka BP, comparable to the LGM value, was attained near the end of HS1. This decline is interrupted by a short excursion at about 15.5 ka BP, indicated by two corals ∼(−90‰ and −115‰) implying the intrusion of ^{14}C enriched water. With the start of the Bølling-Allerød reservoir offsets are getting smaller until the onset of the Younger Dryas. Even if the magnitude of the depletions during the this time span is not that spectacular as during the Holocene, the ^{14}C decline especially during HS1 is apparent. With the onset of HS1 ^{14}C reservoir ages off Brazil did not exceed 450 years being similar to the modern reservoir offset found in this depth (∼500 years; Key et al. (2004)) but rose during the course of HS1 to over 2,300 ^{14}C years.

Some coral data, if plotted in the $\Delta^{14}C$-calendar-age space (Fig. 7.3), apparently line up on ^{14}C decay curves as it is the case for parts of the Holocene and between 23−27 ka BP including Heinrich event 2. Some less obvious backtracks have been plotted during the deglaciation as well to indicate that the ^{14}C recession could also be the result of an ageing water mass flushing the region around the cores during that time. This might have happened several times (Fig. 7.3), albeit it is not evident where to start precisely the backtracks if only two or three corals are lining up on the decay curve. Thus, an unambiguous identification whether the core sites experienced closed system decay cannot be made. This conclusion is corroborated by data from the previously discussed authors summarized in the Figs. 7.17A, B, C, D. As a reminder, when plotting reservoir offsets against calendar age the ^{14}C decay is not showing up as exponential decay anymore as the atmosphere's ^{14}C varies over time. In contrast to the large $\Delta\Delta^{14}C$ deviations in the Holocene compared to the other radiocarbon records from this period, the deglaciation data is in good agreement with the other intermediate-water reconstructions (except for the Marchitto et al. (2007) study). Radiocarbon measurements on the calcite shells of benthic foraminifera from the North Pacific revealed a huge drop in the intermediate-depth ^{14}C activity during HS1 of up to ∼500‰ and over ∼300‰ relative to the modern seawater activity, based on local seawater measurements (Marchitto et al., 2007). There is a certain resemblance between the North Pacific and Brazilian dataset that cannot be questioned. Both start to decline at the onset of HS1, though the decrease in ^{14}C is less steep at the Brazilian slope and features a larger variability during the course of HS1 than the North Pacific site. Mangini et al. (2010) argued that this similarity might be an indication that a common water mass formerly located in the Pacific has fed both locations during this time period. Coral data from Burke and Robinson (2012), however, are suggesting otherwise.

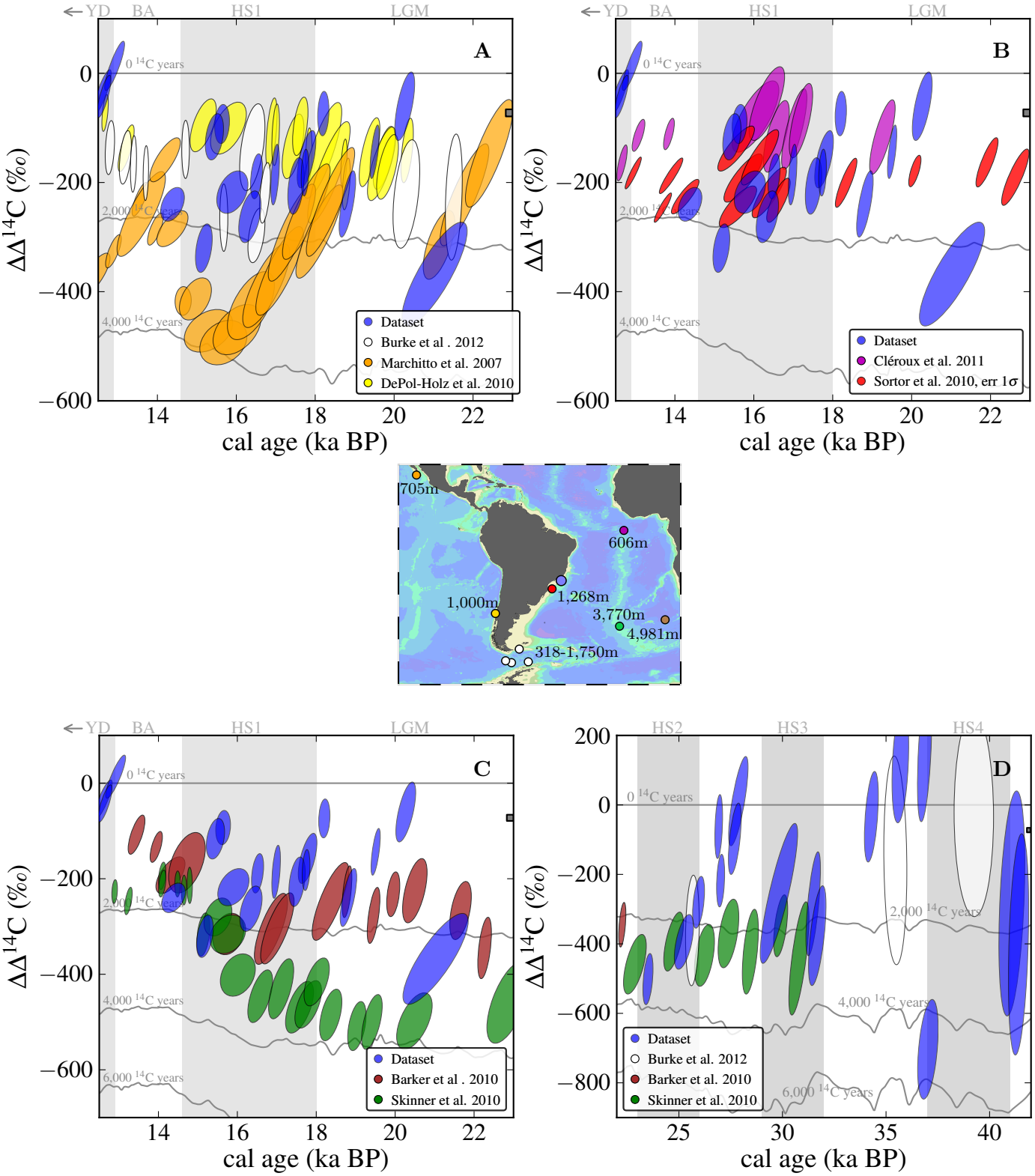

Fig. 7.17: Overview of deglacial radiocarbon data from the Brazilian slope compared to other studies. See picture in the middle for the different locations.

As mentioned for the Holocene, if the core site of Marchitto et al. (2007) was actually ventilated by a very old water mass originated from the Southern Ocean one would expect to see at least parts of this signal had passed the Drake Passage. The corals from Burke and Robinson (2012), thus, should have more or less preserved this ^{14}C signature compared to that recorded by the Brazilian corals several thousand kilometers farther north in the South Atlantic. But this is seemingly not what one finds as depicted in Fig. 7.9A. Both coral sites (Drake Passage and Brazil) have witnessed a similar $\Delta\Delta^{14}C$ history during HS1 implying that no single coherent water mass with a low ^{14}C activity has ventilated the North Pacific site and the intermediate-depth southwest Atlantic simultaneously. The radiocarbon data from Sortor and Lund (2011) (Fig. 7.9B) are promoting this observation by featuring similar depletions during HS1 as at the Brazilian margin. As elucidated earlier, this record failed to trace the true AAIW signal during the "overshoot-period" of the NADW in the early to mid-Holocene. Further Pa/Th overshoots during the last glacial termination do not seem to have occurred (Fig. 7.15). It is therefore believed that both records have been bathed by AAIW during this period, though the characteristic "sawtooth pattern" in $\Delta\Delta^{14}C$ found at the Brazilian coral sites did not show up at the Sortor and Lund (2011) core site. ^{14}C data from foraminifera of the equatorial eastern Atlantic indicate well ventilated water during HS1 in ∼600 m, which is devoid of a southern-sourced ^{14}C imprint (Fig. 7.9B). Cléroux et al. (2011) speculated that depleted water from an alleged deep-water reservoir probably took another purging route. Alternatively, strong ^{14}C gradients in the water column prevented mixing of the deeper and depleted water with the shallower water.

By comparing my dataset with the studies from Barker et al. (2010) and Skinner et al. (2010) from the deep eastern South Atlantic, during most of the glacial termination both sites exhibit much stronger depletions as the intermediate-depth location off Brazil. This is in contrast with the observation I have discussed earlier during the Holocene where ^{14}C depletions were much stronger in intermediate depth (Fig. 7.16). Both deep-water sites propose significant changes in the ^{14}C activity, which occurred during HS1 and the BA. The radiocarbon study presented by Skinner et al. (2010) is of special interest as it is the first one that presumably found direct evidence of a massively depleted deep-water reservoir in the Southern Ocean. According to this, a deep-water reservoir enriched in dissolved inorganic carbon formed during the LGM and subsequently decayed during the course of the deglaciation thereby releasing its excess CO_2 depleted in ^{14}C into the upper ocean and atmosphere. Though the extent of this abyssal reservoir is uncertain it might have played a role in the pulsed rise of atmospheric CO_2 (Skinner et al., 2010). The ^{14}C ages decreased significantly during HS1 from almost 4,000 years to roughly 2,000 years near the beginning of the BA. Under the assumption that this depleted water mass extended much farther to the west occupying also parts of the western basin of the South Atlantic it might have provided the depleted water necessary to explain the moderate ^{14}C decline observed in the shallow depth off the Brazilian shoreline. From an oceanographic point of view internal mixing of lower circumpolar deep water (LCDW) upward into UCDW and the subsequent conversion of UCDW into sub-thermocline water (especially in the southwest Atlantic- and southeast Pacific sectors of the Southern Ocean) allows water to find its

way into Antarctic Intermediate Water via upwelling south of the Subantarctic Front and subsequent subduction within the Polar Frontal Zone (see Fig. 7.12) (Iudicone et al., 2008; Skinner et al., 2010). These mixing processes would have diluted the original ^{14}C signature of the aged LGM reservoir to the extent that only a fraction reached the Brazilian shoreline during HS1. The postulated abyssal reservoir at best would have to have had a zonal expansion reaching from the eastern flank of the mid-Atlantic ridge (the location of the Skinner core) up to the southwest Atlantic region encompassing the Argentine Basin. If such a large coherently connected isolated deep reservoir did really exist cannot for sure be decided from the data at hand. Further investigations to come, conducted in the Southern Ocean region and especially in the southwest Atlantic, will shed light on this issue.

Based on the reversed $\Delta\Delta^{14}C$ data between the shallow North Pacific and the marine site at the deep eastern flank of the mid-Atlantic ridge during HS1, (Skinner et al., 2010) argued that the supposedly aged abyssal reservoir could have remained partially intact and persisted until the end of the YD. The observed radiocarbon decline off Brazil during parts of the Holocene could, thus, be caused by a remnant of this formerly "large" reservoir which has substantially withdrawn from the Atlantic sector of the deep Southern Ocean towards the western Atlantic basin. The characteristic sawtooth pattern repeatedly emerging in the ^{14}C activity (between $\sim$18.5$-$20 ka BP, and $\sim$15.5 ka BP) in the coral record off Brazil (cf. Fig. 7.9A) are presumably the result of enhanced mesoscale eddy activity in combination with upwelling events occurring due to shifts of the ITCZ below the equator as already explained further above for the YD (see section 6.6.1). In the last time slice, encompassing the glacial ages between $\sim$23$-$42 ka BP, the coral data continue to unveil a vigorous ^{14}C history in the intermediate depth off Brazil. Phases of well and significantly less ventilated water are alternating ranging from zero per mille offsets up to depletions exceeding $-600‰$.

Radiocarbon dating of such old samples is often difficult because they could easily become contaminated with modern or ancient ^{14}C during sample preparation (pretreatment, hydrolysis, reduction to graphite or diagenetic effects), which can obscure ^{14}C ages. For example, contamination with ancient and/or modern carbon making up 5‰ of the initially present ^{14}C atoms would render an actually 50 ka old sample $\sim$10 ka younger! Both contaminations (modern or ancient), however, make the radiocarbon age always younger (not older) thereby increasing the corresponding $\Delta^{14}C$ and lower $\Delta\Delta^{14}C$. But any processing contamination associated with the coral samples presented are regarded unlikely. All sample sets are followed by two calcite blanks, which returned appropriate ages of $\gtrsim$53 ka BP, and one FIRI-C turbidite standard and the IAEA-C2 standard (Tab. E.3). Samples and blanks were processed together as one batch and graphitized on the same day using a vacuum line that accommodates 12 targets in one go (G. Santos 2011, pers. comm.). In addition, such relative old samples have a much lower ^{14}C content ($\Rightarrow$ lower counting statistic), which translates into relatively large uncertainties hampering interpretation of the data. Nonetheless, the most striking feature in Fig. 7.9 is the continuous drop of the ^{14}C activity during the timespan between $\sim$23$-$27 ka BP. This decline coincide partly with HS2, the period in which the second documented iceberg discharge (HE2) occurred in the North

Atlantic. $\Delta\Delta^{14}C$ are depleted by as much as $\sim$−500‰ during this time, corresponding to an ^{14}C reservoir age of $\sim$3,200 years BP. Moreover, this decline apparently follows the ^{14}C decay curve as in the case of the huge drop in ^{14}C during the YD/Holocene (Fig. 7.3). In both periods an underlying common mechanism seems to have prevailed. Unlike during the deglaciation the number of samples available in the course of HS2 and prior is sufficing to propose the existence of a deteriorating isolated water reservoir, which must have existed for several thousand years in order to grasp this particular decline. There are only few datasets covering the glacial time between $\sim$23−42 ka BP. One coral from the Drake Passage exhibits similar ^{14}C depletions in dissolved inorganic carbon during the beginning of HS2 (Fig. 7.9). As already discussed for the Holocene decline, transport via the Drake Passage is considered highly improbable. The data from Skinner et al. (2010) suggest that a largely depleted water mass existed already before the LGM in the eastern deep South Atlantic. During the deglacial period an "extended" version of this old abyssal water occupying also the western part of the South Atlantic is called on again to explain the varying ^{14}C data. But this time the situation is different. It is tempting to use the findings of Skinner et al. (2010) again to explain the ^{14}C drop in the coral data as it has been done for the deglaciation. But this would imply very special circumstances to work, because the relatively old deep water mass, assuming it has also occupied the western South Atlantic during this time, has to admix in an elaborate way with the upper water layers to mimic the impression of ^{14}C decay along the decay curve. Maintaining such an "exponential" admixture over thousand of years is considered doubtful if not impossible.

Therefore, a large coherent and old reservoir filling the abyssal South Atlantic from east to west pretty likely did not exist. Instead, as previously claimed for the Holocene, the ageing intermediate water observed off Brazil during HS2 presumably stems from a deep water reservoir located somewhere in the southwest Atlantic where deep to intermediate water conversion took place. The data beyond 27 ka BP do not allow to draw any detailed conclusions. There are moderate depletions during HS3 and also one at the end of H4 ($\sim$37 ka BP), but the considerably larger uncertainties and the limited number of measurements in this time range do not permit to draw any reasonable conclusions. Taken together, the picture that emerges on the ventilation of the intermediate-depth of the glacial South Atlantic/Southern Ocean and adjacent regions during the early Holocene and glacial period is considerably more complex than initially envisioned. Interpretation of the available ^{14}C data from deep and intermediate depths are often not unequivocal, hampering the efforts in giving a unified picture. The existence of multiple isolated deep water reservoirs in the Atlantic Ocean/Southern Ocean cannot be ruled out and more importantly are not a phenomenon limited to the late Pleistocene glacial-interglacial transition. Rather, they seem to be a common feature of the glacial ocean. Isolated reservoirs probably formed during major deep-water mass reorganizations in the Atlantic Ocean probably triggered by Heinrich events and events, which lead to the Younger Dryas cold snap. However, the precise circumstances of how these deep reservoirs came into existence and maintained their "isolation" state while they are purged over centuries or several millennia remains elusive.

7.10 $\Delta\Delta^{14}C$ versus deep North Atlantic $^{231}Pa/^{230}Th$

At this point it is instructive to compare the radiocarbon data from off Brazil with the excess $^{231}Pa/^{230}Th$ (hereafter Pa/Th) measurements from the deep western North Atlantic (Bermuda Rise) from McManus et al. (2004) and Lippold et al. (2009) comprising the last 35 ka BP. Over the course of the last glacial cycle AMOC strength, especially during HS1 and HS2 was strongly diminished if not completely ceased as indicated by high sedimentary Pa/Th ratios during that time (Fig. 7.18), which is thought to be the result of massive iceberg discharges in the North Atlantic region as explained in section 2.5. This assumption is supported by sediment data from various locations in the Atlantic Ocean (e.g. Keigwin et al., 1994; Keigwin and Lehman, 1994; Sarnthein et al., 1994; Elliot, 2002). The resemblance between the Pa/Th and coral ^{14}C data (Fig. 7.18) is striking considering their different locations and depths (∼700 m (Brazil) vs. ∼4,500 m (Bermuda Rise)) suggesting a tight coupling between these two oceanic regions at times of glacial stadials. Cessation of deep-water formation in the North Atlantic is apparently accompanied by the advance of a progressively ageing intermediate water in the South Atlantic off Brazil. Starting ∼27 ka BP the coral $\Delta\Delta^{14}C$ significantly declined before the onset of HS2 while Pa/Th increased sharply to near production ratios (note the reversed axis of the Pa/Th plot!). The precise timing of the onset of the ^{14}C depletion cannot be firmly established, though. Two corals centered at ∼27 ka BP and ∼26 ka BP seem to indicate that the water's ^{14}C activity started to decline in between by the intrusion of water from the postulated deep-water reservoir.

The steep rise in Pa/Th coincides with a cooling incident at ∼26.5 ka BP recorded off northeast Brazil (Fig. 6.12), which has been related to a precursor event that preceded the sediment pulses of HE2 by 1.5 ka (Jaeschke et al., 2007). It is presumed that this precursor event has its origin in enhanced iceberg calving from the Fennoscandian and Icelandic ice sheet rather than the Laurentide ice sheet (Grousset et al., 2000) and might have impacted the strength of the Atlantic MOC at this early point of time. Whether the Pa/Th and ^{14}C observations are a direct consequence of major water mass changes in the remote North Atlantic caused by enhanced iceberg discharge from a precursor event before HS2 is a matter of debate. A recent study from Gutjahr and Lippold (2011) raises doubts about the chronological sequence of the marine events that took place in the glacial Atlantic around HE2. Bottom water neodymium isotope ratios ($^{143}Nd/^{144}Nd$) extracted from sediment Fe-Mn oxyhydroxide coatings from Bermuda Rise covering the time period of the early Marine Isotope Stage 2 (including HS2) suggest that major deep water mass reorganizations predated Northwest European Ice Sheets derived IRD deposition by ∼2 ka Gutjahr and Lippold (2011). According to the authors ice rafting from the Northwest European Ice Sheets might have been a consequence of advancing Southern Source Water (SSW) partly replacing NADW at ∼27 ka BP rather than being the cause of the circulation changes of the AMOC at that time. There is indeed increasing evidence, which hints at the possibility that intense ice rafting during Heinrich stadials may be the result of preceding

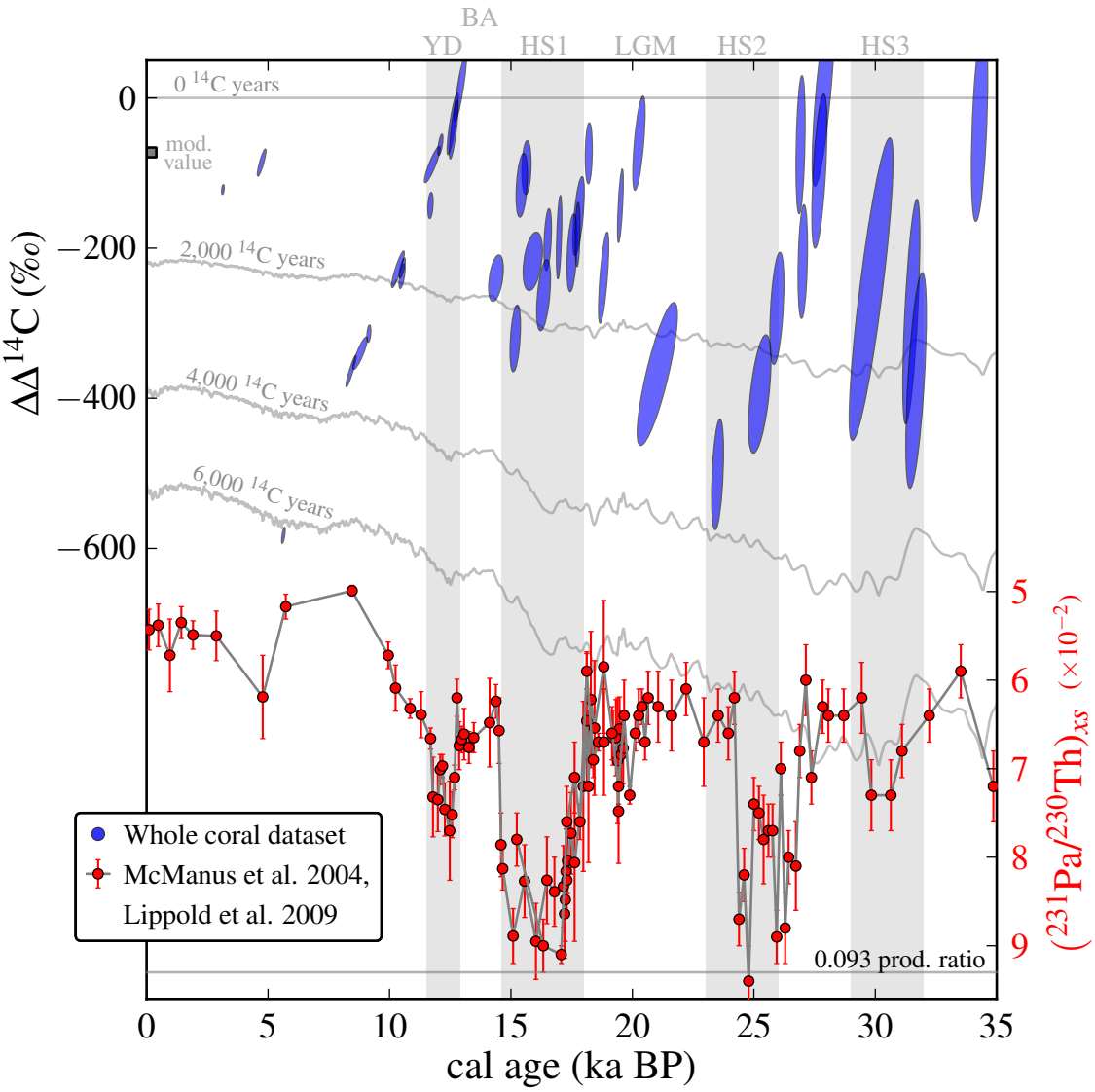

Fig. 7.18: The striking resemblance between the coral $\Delta\Delta^{14}$C and the sedimentary excess ^{231}Pa/^{230}Th data for the most part of the last 35 ka BP suggest a tight coupling among the large-scale changes in deep-ocean circulation of the North Atlantic and the responding intermediate-depth water in the western South Atlantic. At times NADW formation weakened or even collapsed (YD and Heinrich events) progressively ageing AAIW from the South Atlantic/Southern Ocean flushed the intermediate-depth of the Brazilian slope. Deviations exist for the first half of the Holocene when ^{231}Pa/^{230}Th attained modern values while the radiocarbon activity went on to great depletions. ^{14}C observations are reasonably explained through the existence of isolated deep-water reservoirs forming during major deep-water reorganizations.

water mass changes (see Gutjahr and Lippold (2011) and references therein). Combined with an intensified inflow of AAIW, as suggested by more radiogenic Nd ratios (Fig 7.8) at that time could have provided the necessary heat required to initiate accelerated basal melting of marine-based continental ice sheets in the North Atlantic (Gutjahr and Lippold, 2011). Unfortunately, due to the scarcity of coral samples in his time range the data do not allow to make a distinct decision for or against this hypothesis before the time period of HS2.

This intrusion of SSW lasted at least until the end of HS2 at both locations when intermediate water (AAIW) $\Delta\Delta^{14}C$ reached a minimum of $-500‰$ at ∼23.6 ka BP. Pa/Th, however, exhibit values of around 0.06, which are only slightly higher than during the Holocene and persisted throughout the LGM (Fig. 7.18). This discrepancy in the timing between the coral and the Pa/Th data might be reconciled by the neodymium data from Gutjahr and Lippold (2011). The Nd isotope measurements from Bermuda Rise at the end of HS2 clearly indicate the presence of SSW (AABW) at this deep-water location (see Fig. 2 in Gutjahr and Lippold (2011)), while very old water was still swamping the intermediate depth off Brazil. Both observations indicate a vigorous export of water with a southern origin, which continued at least until the end of HS2. The low Pa/Th at the end of HS2, however, seem to contradict with the relatively high radiogenic Nd ratios (ε_{Nd} of about -11) compared to the present-day Atlantic NADW ranging between ε_{Nd} of -13.5 to -14.5 (Piepgras and Wasserburg, 1987). The NADW end-member composition of neodymium did not change during the course of the last glacial cycle noteworthy (van de Flierdt et al., 2006). This obvious mismatch in the Pa/Th and neodymium data can be explained with the very recent Pa/Th study from Lippold et al. (2012) demonstrating that the flow strength of the relatively shallow GNAIW (glacial counterpart to NADW) during the LGM might have been increased rather than weakened as previously thought. This would imply that the Pa/Th signal has been predominantly derived by the vigorously southward flowing GNAIW rather than being the uniformly integrated signal over the whole water column, whereas the more radiogenic Nd ratios at that time reflect mainly the bottom water signature of the intruded SSW.

HS1 was also preceded by a precursor event (∼19.5 ka BP) Jaeschke et al. (2007) coinciding with a small increase in Pa/Th and an almost simultaneous decrease in the ^{14}C activity from nearly atmospheric values to values exceeding $-200‰$, which hint to a tight connection and sensitivity between both locations capable of responding even to small perturbations. But this time the situation is no that clear. The neodymium data suggest no significant changes during the whole LGM and the precursor event. It seem therefore more likely that during the precursor event of HS1 iceberg discharges from the non-Laurentide ice sheet (Fennoscandian and Icelandic) as described by Grousset et al. (2000) have caused a short-term weakening of the AMOC before it came to a halt during HE1. The formerly made proposition that the observed $\Delta\Delta^{14}C$ drop during this precursor event could be the result of enhanced mesoscale eddy activity is thereby called into question and cannot be decided by means of the coral data. Paleo-$\Delta\Delta^{14}C$ at the end of HS1 indicate that the intermediate water is still depleted (by around $-220‰$), while Pa/Th rebounded to approx-

imate LGM values during the brief BA. Neodymium measurements at this time obtained on benthic foraminifera from the Bermuda Rise indicate the presence of NADW water with ε_{Nd} of about -13.5 (Roberts et al., 2010). This is the first time that the apparent tight connection between the deeper component of the SSW, namely AABW, and AAIW (shallow component of SSW), which probably persisted the previous ∼12 ka (encompassing the larger part of the deglaciation and the beginning of HS2), finally decoupled at the end of HS1. This becomes evident during the YD, when Pa/Th of the deep North Atlantic increased once again but only with half the magnitude than observed during HS1. After the ∼1.2 ka lasting cold snap of the YD, Pa/Th decreased rapidly until near Holocene values established as early as ∼10 ka BP. The intermediate-depth ^{14}C activity in contrast still decreased for another ∼4,200 years showing great depletions of over $-500‰$in $\Delta\Delta^{14}C$. For the sake of completeness it is mentioned that also some Pa/Th measurements have been performed in this thesis on the sediment of the cores C1 and C2 in an attempt to reconstruct the Pa/Th history for the slope region off Brazil. Unfortunately, dominant boundary scavenging processes, which are present in these shallow depths, render this tool impractical as a proxy for circulation strength and are of no further interest here. The reader is referred to the annex B.2 and Tab. G.3 for the results and some remarks.

7.11 The missing increase in atmospheric CO_2

Isolation of a deep-water reservoir as described in section 7.6 over several thousand years would have resulted in accumulation of excess metabolic CO_2 dissolved in the water. If this water is brought back to the ocean surface via upwelling it would have released its surplus CO_2 to the atmosphere thereby raising the CO_2 concentration. There are a few radiocarbon studies from intermediate depth so far documenting large negative excursions in $\Delta^{14}C$ at times of increasing atmospheric CO_2 and decreasing atmospheric $\Delta^{14}C$ (e.g. Marchitto et al., 2007; Stott et al., 2009; Bryan et al., 2010) indicating enhanced flux of aged carbon to the upper ocean and atmosphere from below. The data presented in this thesis do not allow to draw this conclusion. The increase in atmospheric CO_2 does not seem to correlate with the large negative $\Delta\Delta^{14}C$ excursions found offshore Brazil. While the radiocarbon coral record declined continuously during the Holocene, atmospheric CO_2 concentrations have already reached a maximum of ∼265 ppmv at the end of the Younger Dryas and even declined slightly during the first half of the Holocene by about 5−10 ppmv (Fig. 7.19). During the middle of the Holocene CO_2 rose again by ∼20 ppmv to reach preindustrial values of ∼280 ppmv.

This is peculiar since one would expect water this age is saturated with excess CO_2, previously sequestered, which should have been partly liberated during the recoupling of the alleged deep reservoir with the surface and the subsequent water mass conversion within the Antarctic's PFZ. It is hard to imagine why atmospheric CO_2 has not changed and even decreased slightly during the course of the Holocene. One possibility could be that

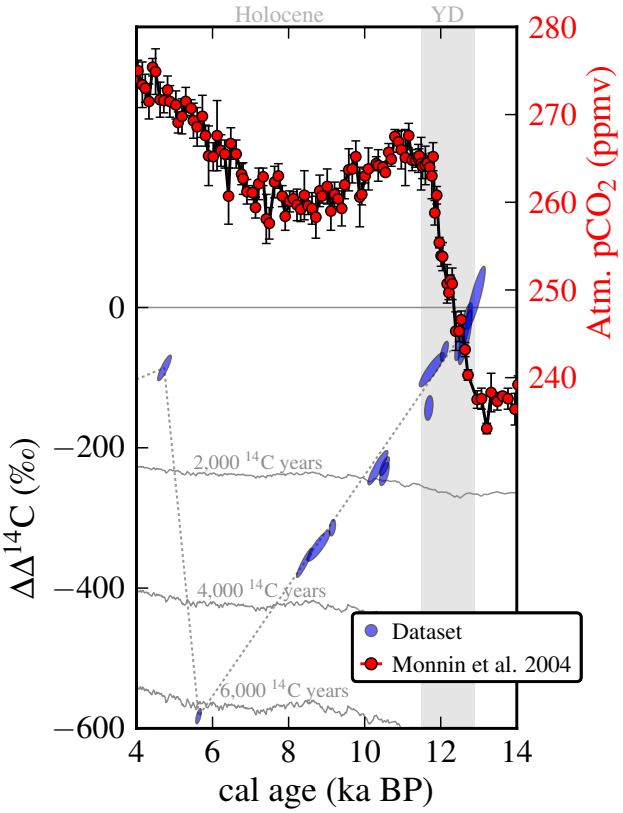

Fig. 7.19: Development of atmospheric CO_2 and coral $\Delta\Delta^{14}C$ over the course of the first half of the Holocene, see text for information.

the proposed isolated reservoir was simply too small in size to had a noticeable affect of atmospheric CO_2. Estimates of the released amount of CO_2 require the precise knowledge of the reservoir's volume, which is not known. Concurrently, atmospheric $\Delta^{14}C$ exhibits only a small decrease in this time period and cannot be used to constrain the amount of CO_2 released. It seems reasonable that a multitude of processes in Earth' carbon cycle operated simultaneously to draw down atmospheric CO_2 during the Holocene compensating the CO_2 release as suggested from the corals. The carbon reservoir size of the land biosphere, for example, increased during the first half of the Holocene as indicated by increasing atmospheric $\delta^{13}C$ measurements on Antarctic ice cores from Dome C and Taylor Dome (Ciais et al., 2012; Schmitt et al., 2012). Though, carbon was probably released concurrently from the ocean in response to carbonate compensation of the terrestrial uptake during the termination of the last glacial (Elsig et al., 2009) these processes combined could have overcompensated the alleged CO_2 release from the purging deep reservoir during the early Holocene. A similar phenomenon is observed during HS2 when intermediate water $\Delta\Delta^{14}C$ exhibit also large negative excursions, while atmospheric CO_2 reconstructions revealed no significant changes (Indermühle et al., 2000; Monnin et al., 2004) (Fig. 7.20). Changes in

the terrestrial biosphere are unlikely to have happened during that time when full glacial conditions prevailed, which favors the idea of a relatively small reservoir size. Depending on the amount of dissolved CO_2 in the deep water, once the nutrient-rich water was brought back to or near the euphotic zone, it could have boosted phytoplankton production largely compensating the surplus of dissolved CO_2. During the deglaciation depletions in $\Delta\Delta^{14}C$ are anticorrelated with the famous rise in atmospheric CO_2 during HS1. Whether the proposed reservoir contributed to the observed rise in CO_2 during the deglacial period, however, is doubtful given the lack of an atmospheric rise in CO_2 between the early to mid-Holocene and during HS2. The circumstances behind this remain enigmatic. It is important to note at the end of this chapter that obviously old isolated deep-water reservoirs existed, which, at times, formed and decayed without contributing to the atmospheric CO_2 concentration.

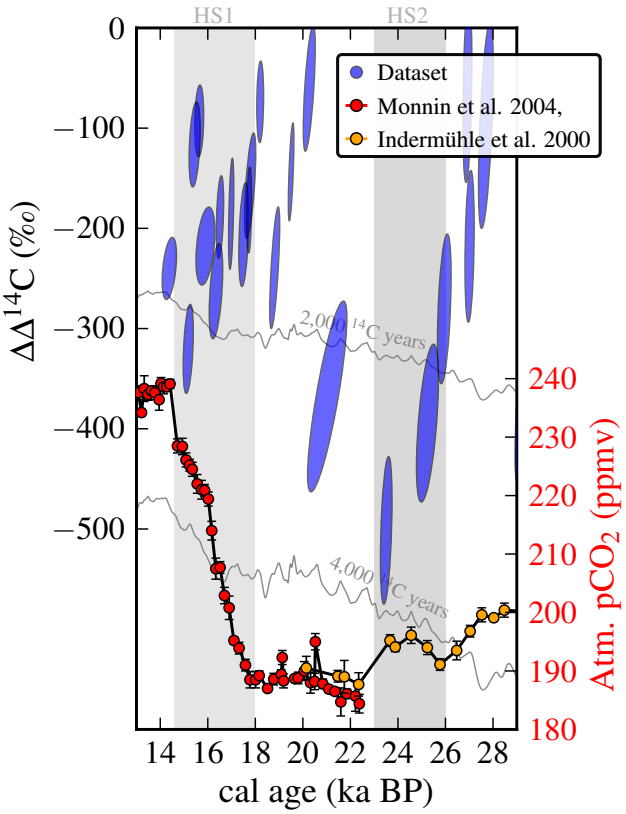

Fig. 7.20: History of atmospheric CO_2 and coral $\Delta\Delta^{14}C$ during the glacial period between 14−28 ka BP.

8

Results and discussion: ε_{Nd}

8.1 $^{143}Nd/^{144}Nd$ measurements

Thirty five measurements of $^{143}Nd/^{144}Nd$ have been performed on coral samples from the four sediment cores. For three samples, neodymium was extracted from the wash solution of the U-series anion exchange chemistry conducted earlier. For the remainder, neodymium was directly purified from the dissolved aragonite samples using the chromatographical method described in the following section 8.2. Most samples have been analyzed on a MC-ICPMS and six of them on a TIMS at the Laboratoire des Sciences du Climat et de l'Environnement (LSCE) in Gif-sur-Yvette, France. For the investigations on the TIMS (Finnigan MAT 262) purified Nd samples were loaded onto single degassed rhenium filaments by using the H_3PO_4/silica gel method. Neodymium was subsequently measured as metal-oxide $Nd^{16}O^+$, $Nd^{17}O^+$, and $Nd^{18}O^+$ using dynamic multiple collection on six Faraday cups. Metal-oxide masses ranged between 157−163. The typical $^{144}Nd^{16}O^+$ signal was larger than 500 mV during data acquisition for each sample. Since separation of Nd from Pr is less efficient using the Ln-Spec resin than for Ce, La, and Sm possible PrO^+ isobaric interferences can be expected, which have been corrected line by line during off-line analysis by means of $^{141}Pr^{16}O^+$ (mass 157). Also Ce, Sm were continuously monitored during Nd oxide measurements and were found to be negligible (Copard et al., 2010). All Nd isotope ratios were corrected for mass fractionation relative to $^{146}Nd/^{144}Nd = 0.7219$ using a power law. Concentrations of Nd blanks were negligible. ε_{Nd} was calculated using a CHUR of 0.512638 (Jacobsen and Wasserburg, 1980).

Replicates have been measured for different samples. Coral pieces for replication from a single coral were not identical but from the adjacent coralline material integrating no more than ∼10 years of growth. Furthermore, ε_{Nd} from the two leftmost samples in Fig. 8.1 stem from the wash solution of the U-series anion exchange chemistry, which were stored for six month in a PP-beaker before Nd chemistry. The reproducibility for the different samples

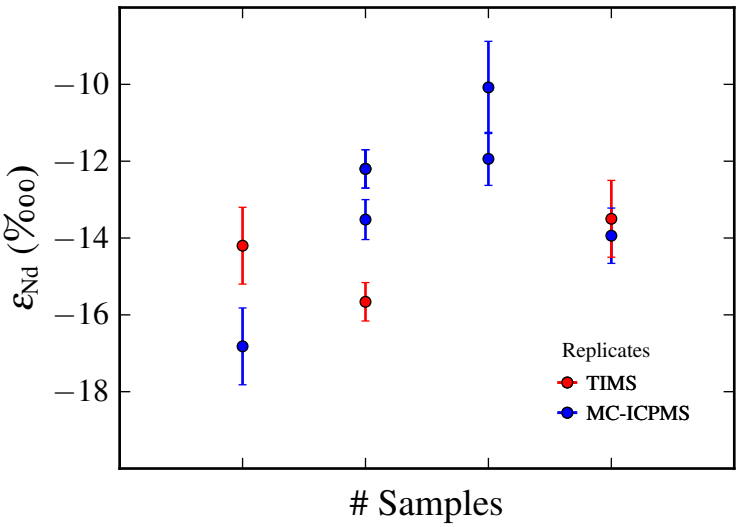

Fig. 8.1: Coral pieces for replication from a single coral were not identical. Reproducibility was relatively poor and only agree for two samples within their respective 2σ uncertainties.

from core C1 is relatively poor and only agree for two samples within their respective 2σ uncertainties. The reason for the relatively large offsets is unclear. Nd concentration analyses on samples from the shallower core sites revealed concentrations of < 10 ppbw, which are low for fossil cold-water corals (see section 8.4). All samples chosen for replication could have been easily influenced by residual contaminants or undetected small cavities filled with sediment the cleaning procedure was not able to remove. However, the possibility of a machine offset between the TIMS and ICPMS of any kind whatsoever is regarded unlikely since many measurements of a Nd standard were run in between the samples of each mass spec session and yielded reproducible results.

The Nd isotope procedure used for the MC-ICPMS data acquisition at LSCE has not been published yet. In principle, a static multi-collection mode was used and sample measurements were bracketed with various standards (La Jolla, JNdi-1, Rennes and Annie Michard (AM)). Internally, an exponential fraction law was used, but ultimate data reduction was performed using an average linear fractionation based on mass ratios 145/144 and 146/144. 142/144 could not be used given the samples variable 142/144 ratio due to minor residues of ^{142}Ce. However, the use of this mean fractionation avoided residual linear mass dependence of the corrected isotope ratios and provided a perfect match between the standard measurements performed on the TIMS and MC-ICPMS. In addition, daily standard variability as observed using an exponential fractionation law was dramatically reduced. Fig. 8.2 highlights absolute deviations of various neodymium standard MC runs from their respective reference value at variable concentration (signal intensities) compared to the previous TIMS analysis. Standard values are on average smaller than the respective

reference value. For low Nd concentrations (< 1 ppbw) statistical uncertainties increases exponentially and Nd isotope ratio become useless. Therefore, the standard dilution experiments clearly impose an analytical limit of at least 200 mV signal on mass 142 to obtain reasonable standard reproducibility at ±0.5 epsilon (2σ). Sample measurements with signal height below this critical value were no longer considered (N. Frank 2013, pers. comm.).

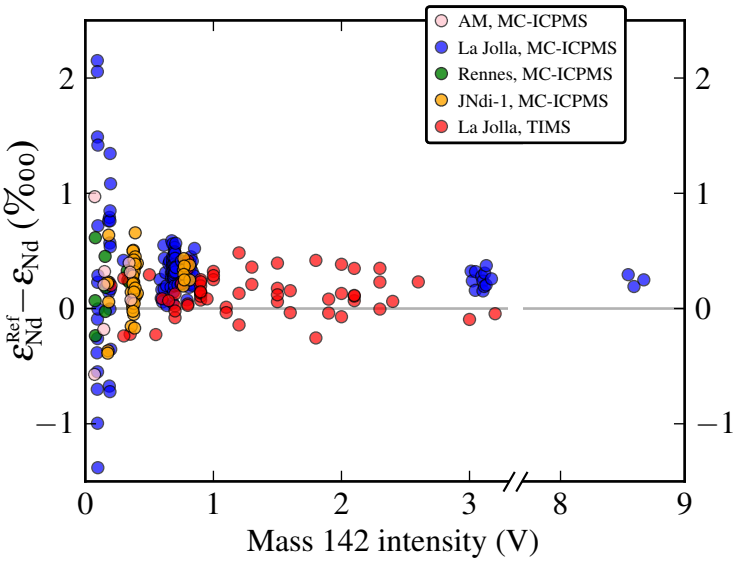

Fig. 8.2: Deviation of various Nd standard measurements from their respective reference values highlighting that the observed mean offset from reference is independent of isotopic ranges (here −10 to −30 epsilon for JNdi-1 and Annie Michard standards). TIMS NdO^+ and MC-ICPMS Nd^+ measurements (using a desolvating system - here the Apex HF) yielded approximately similar reproducibility of 0.3−0.5 epsilon unit. Data provided by N. Frank.

8.2 Chemical purification of neodymium

All samples were subject to a rigorous physical and chemical cleaning to remove contaminants usually adhering at the inner and outer surface of each coral. The applied mechanical cleaning procedure was the same as used for the $^{230}Th/U$ and ^{14}C preparations and can be looked up in my diploma thesis (Ruckelshausen, 2009). Oxidative and reductive cleaning steps as suggested by van de Flierdt et al. (2010) are regarded to have minor effects and were omitted. In general, pretreatment of coral samples is essential in order to extract the pristine neodymium signature present only in small traces within the coralline skeleton. Smallest residues could alter the measured $^{143}Nd/^{144}Nd$ isotopic ratios, which must be

avoided. After mechanical cleaning, samples were leached in diluted HNO_3 for 20 seconds to remove further potential residues like Fe-Mn coatings. Used carbonate masses varied between 200-600 mg. The following Nd purification was conducted in the labs at the Laboratoire des Sciences du Climat et de l'Environnement (LSCE) in Gif-sur-Yvette.

For that 83 mg of Eichrom TRU-Spec resin (transuranic-element specific resin, mesh size 100−150 μm) was used to prepare the columns for the first step in the ion exchange chemistry. This specific chromatographic resin allows selective sorption and extraction of different (radio)elements among them are also the light rare earth elements (LREE). After the columns were loaded with the resin by using 0.05 M HNO_3, they were rinsed a further 2−4 times with 2 ml 0.05 M HNO_3 and subsequently preconditioned with 2 ml 1 M HNO_3. Before, samples were dissolved in 1 ml 1 M HNO_3 and transferred into (previously HCl-cleaned and Mill-Q-rinsed) centrifuge tubes and centrifuged for ∼5 min at 11,000 rpm to segregate potentially insoluble contaminants within a sample from the soluble part. The sample were loaded onto the preconditioned TRU-Spec columns in steps of 0.5 ml without the residuum at the bottom of each centrifuge tube. Columns were subsequently gently rinsed 5 times with 0.5 ml 1 M HNO_3 separating the bulk LREE from the carbonate matrix and other major and trace elements within the samples. Before eluting the retained LREE from the TRU-Spec columns a second set of columns, which were used to extract the neodymium from the suite of other LREEs, was prepared in the meanwhile.

These columns were already loaded with the resin Ln-Spec and for preservation reasons stored in a dilute HCl bath (0.5 M HCl). In order to use them they needed to be cleaned with 1 ml 6 M HCl (a lower molarity is also possible) and were next rinsed with Milli-Q water until pH 7 was reached! The next step was to change the resins' molarity for both column sets (TRU-Spec and Ln-Spec) with 0.25 ml 0.05 M HNO_3 for the TRU-Spec columns and 1ml 0.05 M HNO_3 for the Ln-Spec columns, respectively. Thereafter, the TRU-Spec columns are placed over the Ln-Spec columns and the LREE were eluted from the upper columns using 7 portions of 0.1 ml of 0.05 M HNO_3. After 700 μl 0.05 M HNO_3 passed through the TRU-Spec columns they are no longer needed. The REE are now withhold in the lower Ln-Spec columns. After decoupling from the TRU-Specs, the Ln-Spec columns are rinsed with 3.1 ml 0.25 M HCl in steps of 2×100, 2×200, 500, $2 \times 1,000$ μl. This will mostly flush out the individual LREE, namely La, Ce, and Pr. Labelled beakers were placed under the columns and subsequently eluted with 2.5 ml 0.25 M HCl in steps of 500, $2 \times 1,000$ μl in order to catch the Nd fraction. It is crucial to use only the specified quantities of acid. For example, eluting with more than 2.5 ml in the last step will cause more Pr, Sm, and Eu to strip from the Ln-Spec columns leading to isobaric interferences with the Nd isotopes during mass spectrometer analysis. Finally, a droplet of 10 μl H_3PO_4 was added to each Nd beaker to ensure the liquid narrows down at one point during the subsequent evaporation. This Nd-purification scheme is a modified version of the original method described by (Pin and Zalduegui, 1997).

8.3 Coral ε_{Nd} from the continental slope off Brazil

A first overview of the neodymium data is provided in Fig. 8.3 featuring the ε_{Nd} isotopic composition of the samples against their respective core depths. For comparison a present-day neodymium seawater profile from the nearest available station from Jeandel (1993) is shown as well as a measurement of a modern *L. pertusa* from van de Flierdt et al. (2010) from the Brazilian margin. The plot already reveals a large variability in ε_{Nd} for the last ~37 ka BP comprising a range of ~11 ε_{Nd} units! This is surprising as all four cores are located today within the northward flowing AAIW, with the upper two cores bathing in the

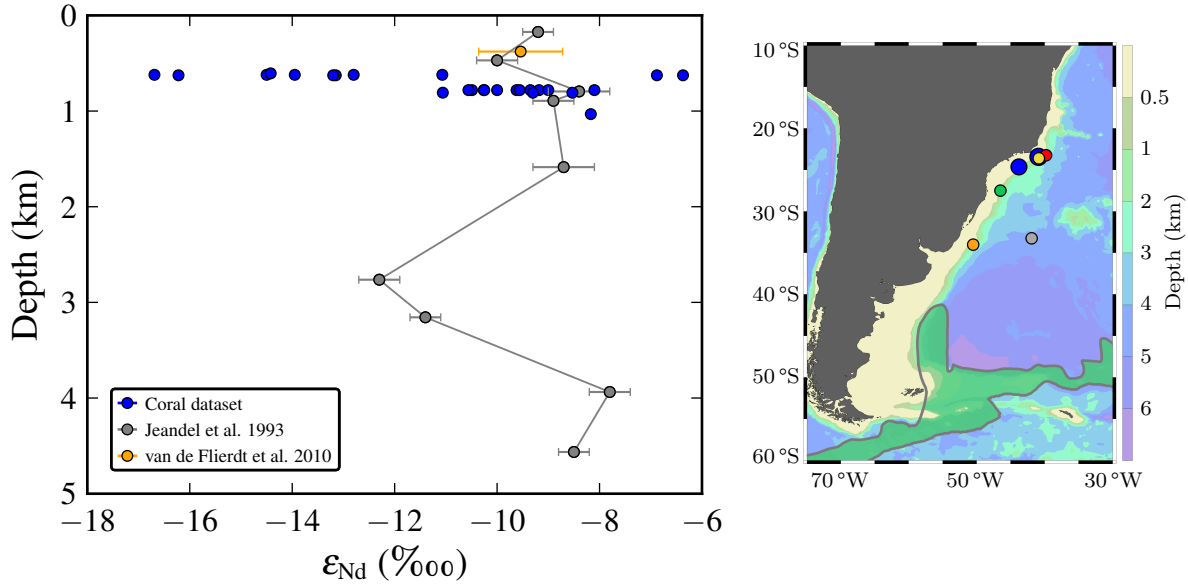

Fig. 8.3: Overview of all ε_{Nd} plotted against core depth compared with two present-day water sample ε_{Nd} from Jeandel (1993) and a single coral specimen from van de Flierdt et al. (2010). To avoid clutter, the errors of the coral data have been omitted. The right figure shows the different locations discussed in this chapter.

transition zone to SACW. Reported modern seawater ε_{Nd} for AAIW range between −6 to −9 (Jeandel, 1993; von Blanckenburg, 1999), whereas mature NADW in the North Atlantic exhibits a range between −13.5 to −14.5 ε_{Nd} (Piepgras and Wasserburg, 1987; Gutjahr and Lippold, 2011) and is still traceable off Brazil (see Fig. 8.3 in a depth ~ 2.7 km). Differentiating between the shallower and the deeper core sites it becomes apparent that the deeper cores C2 and MXL (781 m and 808 m) recorded a significantly different coral aragonite Nd isotopic ratio than at the shallower cores C1 and KGLC (621 m and 626 m), which I am going to discuss in more detail in the following sections.

8.3.1 ε_{Nd} from cores C2 and MXL

Fig. 8.4 depicts the coral Nd isotope record from the deeper cores sites from the Santos Basin encompassing the last ∼37 ka BP. Corals between ∼37−23.4 ka BP show a relatively constant ε_{Nd} with values ranging between −10.2 and −8.5 with a mean of around −9.2. The most radiogenic value is observed at ∼16.3 ka BP with an epsilon Nd of −8.1, which is similar to the nearby modern seawater measurement at 795 mbsl from Jeandel (1993). This elevated epsilon Nd coincides with relatively higher authigenic Nd values reconstructed from the sediment from Pahnke et al. (2008) during HS1 (Fig. 7.8 for a better resolved plot

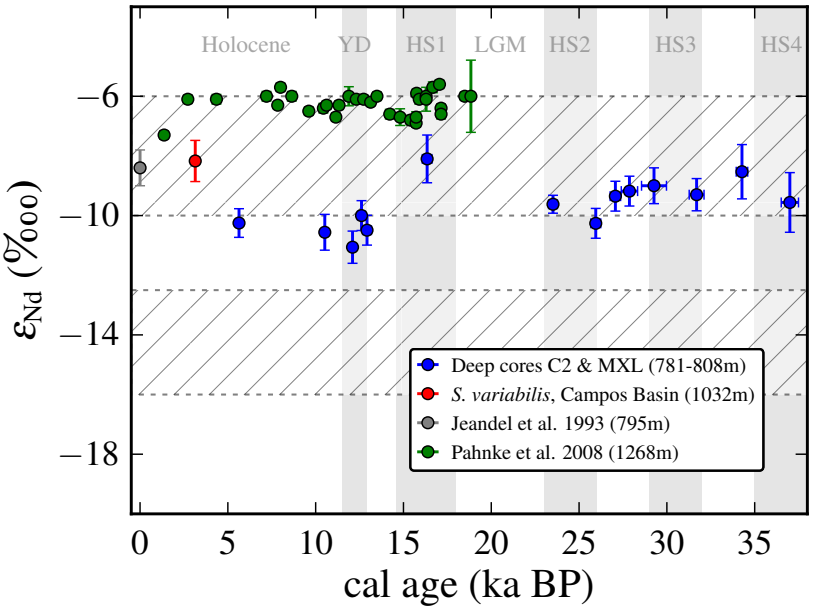

Fig. 8.4: Neodymium results for the deeper cores C2 and MXL (Santos Basin) for the last ∼37 ka BP. The data coverage is incomplete especially during the deglaciation. The red single coral from Campos Basin (this study) is also shown together with the dataset from Pahnke et al. (2008). All errors are 2σ.

of the neodymium sediment data) suggesting a larger contribution of deeper more radiogenic AAIW as a result of an increase in AAIW flow strength during HS1. Future investigations will substantiate this observation. After that, less radiogenic values were preserved between ∼12.9−5.6 ka BP with an average of about −10.4. The single *S. variabilis* specimen with a ^{230}Th/U age of ∼3.1 ka BP from the Campos Basin (depth 1032 mbsl) recorded an epsilon Nd which is in good agreement with the modern value found for the open ocean AAIW (São Paulo Plateau) from Jeandel (1993). The sediment data from Pahnke et al. (2008) from a depth of 1,268 m are additionally plotted. As indicated by the present-day seawater profile in Fig. 8.3 ε_{Nd} varies largely in between the transition zone from AAIW to SACW amounting to ∼2.6 ε_{Nd} units considering the largest possible range of the 2σ

uncertainties of the seawater measurements between 470−795 m. Under the assumption that this present-day change in the Nd isotopic composition was valid also in the past, coral ε_{Nd} from the two deeper cores can be explained by varying contributions from the shallower northward flowing SACW and the adjacent northward flowing AAIW alone. Whether the Nd isotopic composition of AAIW for this depth has changed over the course of the ∼37 ka BP is thus difficult to assess. Even in the absence of any water mass mixing the large uncertainties associated with the Nd measurements would prevent a clear detection. Variations in ε_{Nd} of AAIW for the last 25 ka BP have been reported from a deeper sediment core from farther showing only small changes (< 1 epsilon unit) occurred within the last ∼25 ka BP (Pahnke et al., 2008) (see Fig. 8.4). Unfortunately, no detrital ε_{Nd} is available from the coral sites. Reported detrital ε_{Nd} from Pahnke et al. (2008) (core KNR159−5−36GGC from the Brazil margin) exhibit values between −10 to −9.5‰ and do not co-vary with the authigenic ε_{Nd} signal from the Fe-Mn hydroxide coatings (Pahnke et al., 2008). These values are similar to that found in the ambient seawater recorded in the corals from Santos Basin farther north. A possible input or exchange of neodymium with a similar isotopic ratio mediated by boundary exchange processes at the margin as described in Jeandel et al. (2007) and Wilson et al. (2013), therefore, cannot be ruled out, but is regarded unlikely. Mixing of AAIW with the much deeper flowing NADW (ε_{Nd}∼−13.5) is unlikely to have happened as well. This is not as clear as one might think, because present-day AAIW enters the Brazil Basin between 20−28 °S from the east bifurcating into a northward and southward flowing AAIW branch as it meets the continental break off Brazil (Müller et al., 1998). As AAIW and NADW are flowing in the opposite direction at the coral locations (Fig. 5.7) one would expect diapycnal mixing between these water masses more enhanced than for the southerly located core (30 ° S) from Pahnke et al. (2008), where both flow directions are aligned to each other. Furthermore, the relatively constancy of the ε_{Nd} throughout the last ∼37 ka BP at the deeper coral locations strengthen the assumption that no notable changes occurred even during times when intermediate-water $\Delta\Delta^{14}C$ dropped significantly. For instance, during HS2 intermediate-depth water ^{14}C

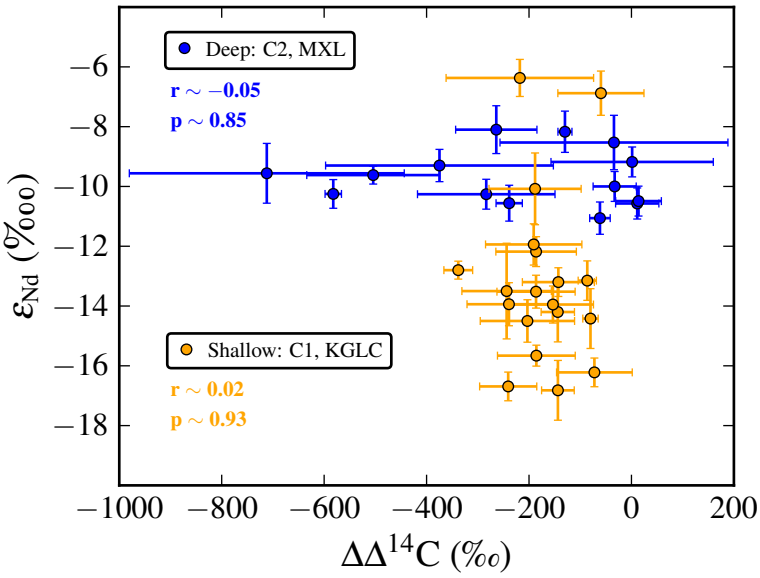

Fig. 8.5: Coral $\Delta\Delta^{14}C$ and ε_{Nd} for the shallower and deeper cores show no correlation suggesting that both tracer are decoupled. This corroborates the idea of a continuously advecting and ageing water mass of a southern origin.

declined by as much as 500‰ at the end of HS2 and by nearly 600‰ during the middle of the Holocene. ε_{Nd}, however, remained quasi constant during these periods suggesting that the neodymium source composition of the ageing intermediate water has not changed. The decoupled behavior of both tracers is illustrated in Fig. 8.5 for the two deeper cores (blue) showing a Pearson's correlation coefficient of ~ -0.05. These results corroborate the idea of a continuously advecting and simultaneously ageing water mass of a southern ocean origin, which flushed the intermediate-depth core sites off Brazil. Furthermore, the relatively stable ε_{Nd} values are in accordance with the hypothesis of an isolated deep water reservoir presumably located in the South Atlantic and/or Southern Ocean region and the concept of stable conduits allowing ^{14}C to decay significantly during the purging events. The alternative option that during times of quite depleted $\Delta\Delta^{14}C$ the epsilon Nd shows pronounced negative values suggesting a northern provenance of the ageing water mass could not be approved. The attempt of tracing back the advective paths or even pinpointing the exact origin of the ageing AAIW by means of the neodymium measurements from the corals, however, is not possible, simply, because the deep- and intermediate-depth waters in the Southern Ocean have similar neodymium isotopic compositions rendering a clear differentiation not feasible yet.

8.3.2 ε_{Nd} from cores C1 and KGLC

The situation regarding Nd is quite different for the shallower two cores C1 and KLC from the Campos Basin. The corals cover the last ~27 ka BP and recorded a much larger variability in the past seawater ε_{Nd} than the deeper cores. With just two samples the time period between ~20−27 ka BP is poorly resolved. Both measurements feature the highest radiogenic values found in all four cores with ε_{Nd} of ~ -6.8 and ~ -6.3, which is about 2 epsilon units more radiogenic than for the samples in cores C2 and MXL. Beginning ~20.2 ka BP the relatively high values dropped steeply to ~ -13.2 at ~19.5 ka BP. During the deglaciation neodymium isotopes exhibit a large scatter encompassing a range of ~ 6 ε_{Nd} units! Values drop to ~ -16.2 at ~18.1 ka BP and subsequently rise sharply until a local maximum is reached at ~16.9 ka BP with a relatively radiogenic value of ~ -11.5. After that, neodymium ratios significantly decline again showing a minimum at the beginning of the Bølling-Allerød period (~ -16.7). Ratios rebound with a further substantial increase at ~10.5 ka BP to ~ -11 and declined during the course of the Holocene. The modern *L. pertusa* retrieved from the Campos Basin (606 mbsl) shows a ε_{Nd} of -14.42 ± 1. Coral ε_{Nd} from cores C1 and KGLC recorded systematically lower values for the last ~20 ka BP than the corals from the deeper cores. Additionally performed epsilon Nd measurements on three sediment samples younger than 20 ka BP from core C1 seem to confirm this observation of large negative values. The chemistry was done at the IUP. The authigenic Nd isotope signal was extracted from the sediment coating by applying a sequential leaching technique, followed by an in-house Nd-purification scheme based on the method from Gutjahr et al. (2007). The neodymium data were provided from M. Gutjahr and J. Lippold on a MC-ICPMS (Neptune) at the department of Earth Sciences at Bristol University. Due

to an amplifier problem during data acquisition 2σ uncertainties can vary by up to 1 ε_{Nd} unit (J. Lippold 2010, pers. comm.). All three radiogenic isotope ratios from authigenic ferromanganese oxides must therefore be regarded with caution. Measurements exhibit quite depleted neodymium isotopic compositions ranging between −14.26 for the core-top sample and −17.16 (∼16 ka BP), and −16.94 (∼18 ka BP) for the glacial age samples (Fig. 8.6). Sediment ages are rough estimates interpolated from Fig. 6.9. The authigenic neodymium results from this core C1 confirm the coral findings that ε_{Nd} have been systematically lower for the shallower core site during the last 20 ka BP than found for the deeper cores. Epsilon Nd for the modern *L. pertusa* and the sediment core top agree well supporting the validity

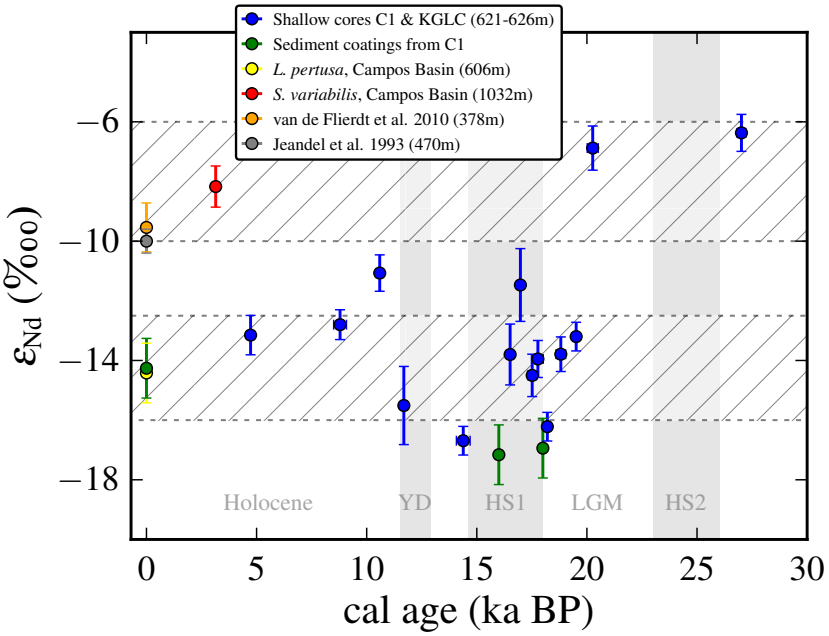

Fig. 8.6: The neodymium results for the shallower cores C1 and KGLC from the Campos Basin exhibiting a large variability in ε_{Nd} comprising ∼11 epsilon units pointing to local processes, which were able to alter the $^{143}Nd/^{144}Nd$ composition of the ambient water significantly. All given uncertainties are 2σ.

of the coral data deviating significantly from the open ocean seawater profile of Jeandel (1993). The mismatch between the seawater station and *L. pertusa* is all the greater amounting to ∼4.4 ε_{Nd} units. The substantially deviating replicates performed on the coral samples from core C1 (Fig. 8.1) are summarized and given as single 2σ error following the method of Birge (1932). The large gap in ε_{Nd} occurring around 20 ka BP is spectacular given the veracity of the data. Even though the uncertainty of each measurement from cores C1 and KGLC would be de facto larger by a further epsilon unit, the large gap at about 20 ka BP (∼7 epsilon units) would still be visible. Largely depleted ε_{Nd} for the shallower core sites continue up to the present day. The single late Holocene aged *S. variabilis* from 1032 mbsl, however, features values of around −8 for the Campos Basin,

which is the expected modern-day value for this depth (Fig. 8.4 and Fig. 8.3) suggesting that a tongue of water of relatively depleted Nd ratios was and still is flowing along the shallower core sites wedged by relatively high radiogenic waters above and below. A totally different water mass, which bathed this site can be precluded since the ^{14}C data highly support the conclusion that the shallower as well as the deeper locations have been flushed by the same ageing water mass. $\Delta\Delta^{14}C$ and ε_{Nd} are nearly uncorrelated (r $\sim$0.02) substantiating the conclusion that no different water mass intruded this depth range. The likelihood that AAIW emerged with this pronounced ε_{Nd} layering from its source region within the Southern Ocean is highly implausible considering the formation process in the Southern Ocean. Besides, the Southern Ocean region is characterized by much more radiogenic ε_{Nd} derived from the Pacific Ocean, which cannot explain the observed depleted values.

An explanation would be that the initial neodymium isotopic composition of AAIW was altered by boundary exchange processes with the continental margin after AAIW hit the Brazilian slope between 20−28 °S and was bifurcated into a northward and southward flowing branch. Similar observations have been made by several authors proposing that significant exchange fluxes of neodymium between the dissolved and particulate fraction exist at ocean margins having the ability to alter the isotopic composition without essentially affecting the Nd concentration of the seawater (e.g Tachikawa et al., 2003; Lacan and Jeandel, 2004, 2005; Wilson et al., 2013). If boundary exchange processes at the continental-ocean interface are a viable candidate to explain the coral data from the Campos Basin, the question is raised, why only the shallower core sites are obviously affected. This observation is probably related to the high hydrodynamic conditions occurring in this region as outlined in section 6.6.1. Seasonal austral upwelling events in combination with cyclonic mesoscale eddy activity within the Campos Basin influences the water column up to the depth of the cores thereby favoring resuspension of formerly deposited sediments increasing the chances of sediment remobilization and dissolution as described by Haley et al. (2004). The upwelling events and eddy activities are localized phenomena confined predominantly to the Campos Basin. This might explain why the single *L. pertusa* from van de Flierdt et al. (2010) located much farther south lacks a depleted ε_{Nd}. Furthermore, systematically low Nd concentrations measured within the coral samples from cores C1 and KGLC suggest an enhanced particle flux and associated elevated boundary scavenging as a consequence of the high hydrodynamic conditions in this area. Thus, the Nd isotopic composition within the water column is even more prone to input of neodymium from different sources with different isotopic ratios. What finally caused the ε_{Nd} to drop significantly starting around 20 ka BP cannot be answered within the scope of this thesis. Also, the nature of the supposed boundary exchange processes ultimately influencing the ε_{Nd} at the shallower core sites remain elusive.

8.4 Nd, Mn, Ca measurements

50μl aliquots were taken from ten of the cleaned and dissolved coral samples to measure Nd, Mn, and Ca concentrations as well. These element concentrations are routinely monitored to check the efficiency of the cleaning procedure. A possible contamination of ε_{Nd} from residual Fe-Mn oxyhydroxide surface coatings can thereby be assessed (Colin et al., 2010). The trace element data were provided by E. Douville and C. Colin at LSCE on a quadrupole ICPMS (Xseries II CCT) by measuring the isotopes ^{46}Ca, ^{55}Mn and ^{146}Nd. Fig. 8.7 illustrates the results (see also Tab. G.5). Nd/Ca concentrations range from 4.39−207.31 nmol/mol with eight samples exhibiting values smaller than 35nmol/mol. Reported neodymium-calcium concentration ratios for modern corals have shown values between ∼2−35 nmol/mol (Copard et al., 2010; van de Flierdt et al., 2010). Mn/Ca measurements lie between 0.1−7.54 μmol/mol and exhibit a neglectable correlation with Nd/Ca of ∼0.12. Reported Mn/Ca concentration ratios for modern corals range between 0.05−9.8 μmol/mol (Copard et al., 2010). The outcome underlines that physical cleaning and applied weak leaching with HNO_3 afterwards was sufficient to obtain the pristine Nd

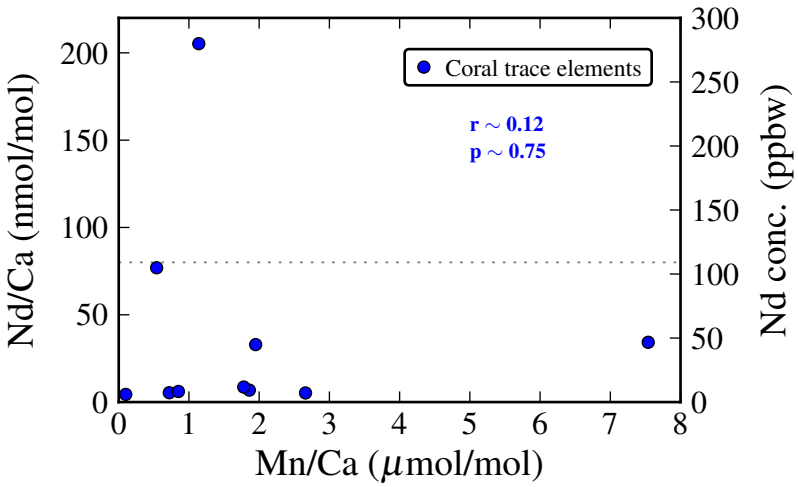

Fig. 8.7: Investigated trace metal concentrations for ten samples show no significant contaminants of incorporated Fe-Mn hydroxides compromising Nd concentrations. The dashed cut-off line is empirically justified from Nd/Ca concentrations on modern corals from Copard et al. (2010). Corals above this line are regarded as not reliable. 2σ errors are smaller than the size of the dots.

not only

concentrations of the samples despite their relatively large calendar ages (∼0−37 ka BP). Only sample C2-94 exhibits a Nd/Ca of over 200 nmol/mol but coincidentally has an insignificant small manganese content of 1.12 μmol/mol suggesting that the elevated Nd concentration was probably derived from a residual contamination introduced from a source

other than Fe–Mn oxyhydroxides. The origin of this excess Nd, however, is unknown. Another sample C1-163 features a higher Mn/Ca concentration (7.54 μmol/mol) but concomitantly shows a relatively low and acceptable Nd/Ca concentration. Corals with a Nd/Ca larger than 80 nmol/mol are considered to be not reliable. This cut-off is empirically justified from Nd/Ca concentrations on modern corals (Copard et al., 2010). This truncation effects only sample C2-94, the oldest coral in the whole Nd dataset. Since the $\varepsilon_{\mathrm{Nd}}$ is similar to the adjacent corals from core C2, this specific sample is shown in Fig. 8.4 anyway. The presented results suggest that the incorporated neodymium concentrations of the corals were derived from the ambient seawater rather than caused by contamination. Thus, $\varepsilon_{\mathrm{Nd}}$ reflect the isotopic composition of the past seawater.

9

Summary and outlook

In this thesis I have presented a set of newly performed ^{230}Th/U measurements on cold-water corals from the Brazilian slope. Corals exhibit large variations in δ^{234}U, even though within acceptable range, the short-term deviations of δ^{234}U from the present-day open ocean seawater value of 146.8‰ is noticeable and normally would point to diagenetic activity. Other indications as concentration measurements of ^{232}Th and U as well as some XRD data from specific samples with conspicuously low or high δ^{234}U have testified the coralline skeletons an impeccable state of preservation questioning the applicability of δ^{234}U as a strict means of quality control. The possibility is raised that observed variations are the result of a local phenomenon and might be linked to fluid seepage activity especially as the Brazilian continental slope in this area is rich in large deposits of petroleum. It is conceivable that corals growing in such a region can directly incorporate δ^{234}U-enriched or -depleted fluids diffusing out of the margins prior to complete mixing with the bulk ocean.

Furthermore, I have shown reconstructed ambient seawater Δ^{14}C extracted from the coral skeletons for the last ∼40 ka BP. The observed depletions are astonishing and exceed several hundred per mille predominantly at times of documented climate changes, which seem to have affected the mid-depth ocean circulation off Brazil. The resemblance between the observed decline in radiocarbon activity and the ^{14}C-decay curve has lead to the idea of an isolated water mass swamping the coral locations for up to several millennia. A hypothetical isolated abyssal reservoir has been postulated to account for these observations boosting the idea of the existence of an aged abyssal reservoir formerly called on to explain the rise in atmospheric CO_2 during the last deglaciation. To rule out any contributions from ^{14}C-dead methane to the ^{14}C dates from possible hydrocarbon seepage activities, stable isotope measurements of ^{13}C and ^{18}O on the coral carbonate have been conducted revealing no noteworthy influence from geological-old methane.

Last but not least, neodymium isotopic compositions on the corals have been measured to gain insights about the provenance of the intermediate-depth water. It has become apparent

that corals from the deeper core sites have $^{143}Nd/^{144}Nd$ ratios suggesting a Southern Ocean origin of the water for at least the last ∼37 ka BP. This is much different for the corals from the shallower-depth sites indicating a much larger variability of the neodymium isotopic compositions. A reasonable explanation is that boundary exchange processes in these shallower depths alter the original Nd composition. What is more, there exists no correlation between the neodymium isotopes and the radiocarbon at times of significant ^{14}C depletions corroborating the idea of just one water mass irrigating the Brazilian slope. The existence of an isolated deep-ocean reservoir formerly located in the Southern Ocean/South Atlantic region has been strongly recommended to reconcile the obtained results. The exact location of this hypothesized reservoir, however, remains elusive.

Up to this date, the coverage of marine $\Delta^{14}C$ reconstructions in time and space is very scarce especially for the glacial and deglacial ocean. Moreover, the few datasets available in the literature give partially conflicting results clearly suggesting that the emerging picture about the mid-depth ocean ventilation during the early Holocene and glacial period is considerably more complex than initially envisioned. Tracing the aged water found off Brazil back to its origin will be difficult. The present-day AAIW is entering the Brazil Basin between 20−28 °S from the east, bifurcating into a northward and southward flowing branch, which irrigate the slope region afterwards (Müller et al., 1998). Before that, AAIW flows only in open ocean regions where no deep-water corals can be expected. The only possibility to map past $\Delta^{14}C$ would be to pick foraminifera from sediment from open ocean regions, which would represent a significant effort.

Mapping Holocene and glacial $\Delta^{14}C$ in the southwest Atlantic slope region of Argentina south of −40 °S by means of cold-water corals would be a more promising area to look at in pursuing the postulated reservoir presumably located in the Argentine Basin. Today's PFZ is stretching out as a tongue following the continental margin up to ∼−40 °S (Fig. 7.12). If water mass conversion from an isolated deep reservoir within the Argentine Basin took place in this part of the PFZ, cold-water corals probably would have recorded these events. Chiefly due to the difficulties and costs of sampling this will probably not happen any time soon. In the meanwhile, the next logical step must be to model these ^{14}C observations found in the intermediate depth at different locations worldwide and to clarify the issue under what circumstances transport of highly depleted water into northern latitudes several thousand kilometers apart is possible. Not least because already conducted model calculations suggest rapid dissipation of extremely ^{14}C-deplete water casting doubt on the reservoir idea and its ability to explain the mid-depth $\Delta^{14}C$ anomalies (Hain et al., 2011).

Appendices

A

Alternative derivation of the ^{230}Th/U age equation

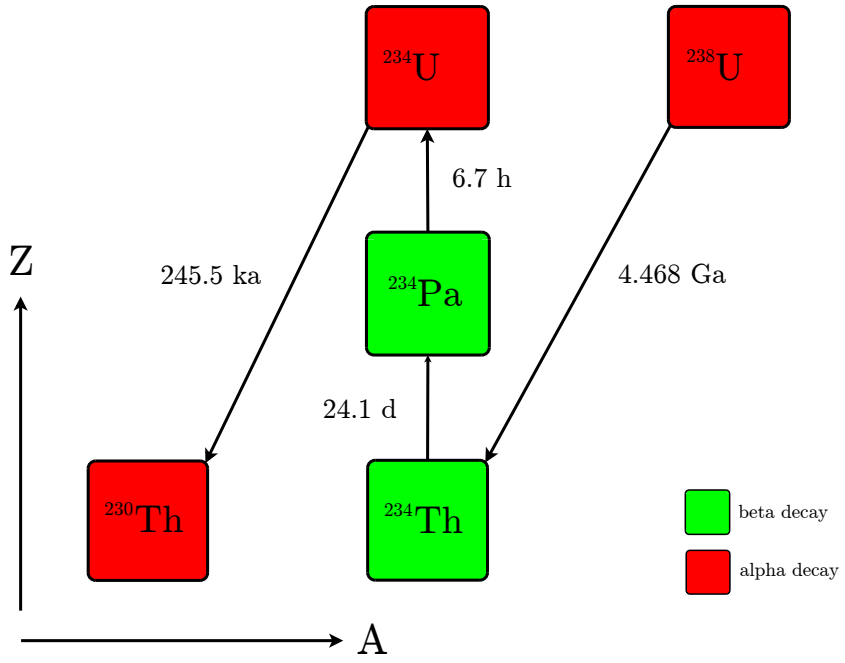

Fig. A.1: Outline of the uranium-radium decay series beginning with ^{238}U ending with ^{230}Th.

In the following derivation of the so-called marine age equation the radionuclides ^{234}Th and ^{234}Pa, daughter and granddaughter products of the ^{238}U decay in the radium series, are relatively short-lived nuclides and will therefore not be taken into account. In this manner the ^{238}U decays directly to ^{234}U and subsequently to ^{230}Th. The equation A.1 governing

the decay from ^{238}U to ^{234}U is mathematically spoken a first-order ordinary differential equation with constant coefficients. This kind of equation can easily be solved with well proven methods which I am going to show for this particular equation. Being more common all equations are denoted in terms of activities instead of number of atoms, $N = A/\lambda$.

$$\frac{d\left(\frac{^{234}U}{\lambda_{234}}\right)}{dt} = {}^{238}U - {}^{234}U \tag{A.1}$$

With ^{238}U being equal to $^{238}U_0 \cdot e^{-\lambda_{238}\cdot t}$. Multiplication of equation A.1 with $e^{\lambda_{234}\cdot t}$ and afterward separation of variables leads to

$$\int e^{\lambda_{234}\cdot t} d\left(\frac{^{234}U}{\lambda_{234}}\right) = \int {}^{238}U_0 \cdot e^{(\lambda_{234}-\lambda_{238})\cdot t} dt - \int {}^{234}U e^{\lambda_{234}\cdot t} dt$$

Partial integration of this expression yields

$$^{234}U e^{\lambda_{234}\cdot t} = \frac{\lambda_{234}}{\lambda_{234}-\lambda_{238}} {}^{238}U_0 \cdot e^{-(\lambda_{238}-\lambda_{234})\cdot t} + C \tag{A.2}$$

The integration constant is determined by the initial condition and set to

$$^{234}U_0 = {}^{234}U, \ {}^{234}U_0 \text{ refers to the initial activity at t} = 0$$

This fixed value C is then put into equation A.2. This now complete term is than divided by $e^{\lambda_{234}\cdot t}$. The next step is to substitute $^{238}U_0 \cdot e^{-\lambda_{238}\cdot t}$ through ^{238}U in the whole equation. Dividing the equation by ^{238}U finally gives

$$\Rightarrow \qquad \frac{^{234}U}{^{238}U} - \frac{\lambda_{234}}{\lambda_{234}-\lambda_{238}} = \left[\frac{^{234}U_0}{^{238}U_0} - \frac{\lambda_{234}}{\lambda_{234}-\lambda_{238}}\right] e^{-(\lambda_{234}-\lambda_{238})\cdot t} \tag{A.3}$$

This term now can be further simplified if one considers that the decay constant of ^{238}U is five orders of magnitudes smaller than ^{234}U, that is

$$\lambda_{234} - \lambda_{238} \cong \lambda_{234}$$

$$\Rightarrow \qquad \left[\left(\frac{^{234}U}{^{238}U}\right) - 1\right] = \left[\left(\frac{^{234}U}{^{238}U}\right)_0 - 1\right] e^{-\lambda_{234}\cdot t} \tag{A.4}$$

$(^{234}U/^{238}U)$ is the activity ratio at the time of measurement, in comparison the ratio $(^{234}U/^{238}U)_0$ refers to the activity ratio at t = 0, which could be the time when the system became closed. To give a more realistic example it could be the time when a coral skeleton was being formed in the seawater thereby incorporating some of the dissolved uranium in the seawater into its skeleton. In the next step, I am going to focus on the equation that governs the decay of ^{234}U in ^{230}Th. Being the same equation with just different radionuclides the solution follows the same scheme as described above.

$$\frac{d\left(\frac{^{230}Th}{\lambda_{230}}\right)}{dt} = {}^{234}U - {}^{230}Th$$

Substitute ^{234}U by the equation A.3 since we now know how the ^{234}U activity evolves with time. Then multiply both sides of the equation with the factor $e^{\lambda_{230}\cdot t}$ as already described above. It is always the same trick to handle this kind of equation.

$$\Rightarrow \left(\frac{1}{\lambda_{230}}\frac{d\,^{230}Th}{dt} + {}^{230}Th\right) e^{\lambda_{230}\cdot t} = \frac{\lambda_{234}}{\lambda_{234}-\lambda_{238}}\,{}^{238}U_0\left(e^{-\lambda_{238}\cdot t} - e^{-\lambda_{234}\cdot t}\right) e^{\lambda_{230}\cdot t} + {}^{234}U_0 \cdot e^{-(\lambda_{234}-\lambda_{230})\cdot t}$$

Separation of variables and then integration by parts yields

$$^{230}Th \cdot e^{\lambda_{230}\cdot t} = \frac{\lambda_{230}\cdot\lambda_{234}}{(\lambda_{234}-\lambda_{238})(\lambda_{230}-\lambda_{238})}\,{}^{238}U_0 \cdot e^{-(\lambda_{238}-\lambda_{230})\cdot t} - \frac{\lambda_{230}\cdot\lambda_{234}}{(\lambda_{234}-\lambda_{238})(\lambda_{230}-\lambda_{234})}\cdot$$

$$^{238}U_0 \cdot e^{-(\lambda_{234}-\lambda_{230})\cdot t} + \frac{\lambda_{230}}{\lambda_{230}-\lambda_{234}}\,{}^{234}U_0 \cdot e^{-(\lambda_{234}-\lambda_{230})\cdot t} + C \tag{A.5}$$

C again is an integration constant which needs to be fixed. The only reasonable choice for the initial condition is

$$^{230}Th_0 = {}^{230}Th,\ {}^{230}Th_0 \text{ is the initial activity at t} = 0,\ \text{the time of the system's closure}$$

$$\Rightarrow C = {}^{230}Th_0 - \frac{\lambda_{230}\cdot\lambda_{234}}{(\lambda_{234}-\lambda_{238})(\lambda_{230}-\lambda_{238})}\,{}^{238}U_0 + \frac{\lambda_{230}\cdot\lambda_{234}}{(\lambda_{234}-\lambda_{238})(\lambda_{230}-\lambda_{234})}\,{}^{238}U_0 -$$

$$\frac{\lambda_{230}}{\lambda_{230}-\lambda_{234}}\,{}^{234}U_0$$

Insert the obtained integration constant in equation A.5 and multiply both sides with $e^{-\lambda_{230}\cdot t}$. The second to last step is to factor out ^{238}U and make use of the fact that it is $\lambda_{234} \wedge \lambda_{230} \gg \lambda_{238}$. This yields

$$\Rightarrow \frac{^{230}Th}{^{238}U} = 1 - \frac{\lambda_{230}}{\lambda_{230}-\lambda_{234}} e^{-\lambda_{234}\cdot t} + \frac{\lambda_{230}}{\lambda_{230}-\lambda_{234}} \left(\frac{^{234}U}{^{238}U}\right)_0 e^{-\lambda_{234}\cdot t} + \left(\frac{^{230}Th}{^{238}U}\right)_0 e^{-\lambda_{230}\cdot t} -$$
$$\frac{\lambda_{230}}{\lambda_{230}-\lambda_{234}} \left(\frac{^{234}U}{^{238}U}\right)_0 e^{-\lambda_{230}\cdot t} - e^{-\lambda_{230}\cdot t} + \frac{\lambda_{230}}{\lambda_{230}-\lambda_{234}} e^{-\lambda_{230}\cdot t}$$

One last substitution of the initial $(^{234}U/^{238}U)_0$ by equation A.4 and the derivation of the marine age equation is complete.

$$\frac{^{230}Th}{^{238}U} = 1 + \left(\left(\frac{^{230}Th}{^{238}U}\right)_0 - 1\right) e^{-\lambda_{230}\cdot t} + \frac{\delta^{234}U}{1000} \left(\frac{\lambda_{230}}{\lambda_{230}-\lambda_{234}}\right) (1 - e^{(\lambda_{234}-\lambda_{230})\cdot t}) \qquad \text{(A.6)}$$

$$\text{with} \qquad \delta^{234}U = \left(\left(\frac{^{234}U}{^{238}U}\right) - 1\right) \cdot 1000$$
$$\text{and} \qquad \frac{^{234}U}{^{238}U} = \left(\left(\frac{^{234}U}{^{238}U}\right)_0 - 1\right) e^{-\lambda_{234}\cdot t} + 1$$

In order to understand the single terms in equation A.6 better, let us rearrange them a little

$$\left(\frac{^{230}Th}{^{238}U}\right)_m = \underbrace{\left(\frac{^{230}Th}{^{238}U}\right)_0 \cdot e^{-\lambda_{230}\cdot t}}_{\text{1. term}} + \underbrace{1 - e^{-\lambda_{230}\cdot t}}_{\text{2. term}} + \underbrace{\frac{\delta^{234}U}{1000} \left(\frac{\lambda_{230}}{\lambda_{230}-\lambda_{234}}\right) (1 - e^{(\lambda_{234}-\lambda_{230})\cdot t})}_{\text{3. term}}$$

The first term in this equation describes the initial, non-in situ produced component of the measured $(^{230}Th/^{238}U)_m$ activity ratio, which was built in during the mineral's precipitation. The second term describes the ingrowth of ^{230}Th independently of the sample's δ^{234}U, that is, regardless of whether the sample's initial $(^{234}U/^{238}U)_0$ were one or uneven one. Since precipitates, however, originating from natural waters like corals show a disequilibrium in the δ^{234}U the third term accounts for this case as well.

Replacing $(^{230}Th/^{238}U)_0$ by $(^{232}Th/^{238}U)(^{230}Th/^{232}Th)_0$ is convenient since the sample's $^{232}Th/^{238}U$ activity can precisely be measured. This reduces the problem to one estimating the initial $^{230}Th/^{232}Th$. The problems associated with assessing the initial thorium content are discussed starting with section 4.2.3.1. Some of the derivations presented here can be found in Ivanovich and Harmon (1992).

Marine ^{230}Th/U age equation:

$$\frac{\mathbf{^{230}Th}}{\mathbf{^{238}U}} = \mathbf{1} + \left(\left(\frac{\mathbf{^{232}Th}}{\mathbf{^{238}U}}\right)\left(\frac{\mathbf{^{230}Th}}{\mathbf{^{232}Th}}\right)_{\mathbf{0}} - \mathbf{1}\right)\mathbf{e}^{-\lambda_{\mathbf{230}}\cdot\mathbf{t}} + \frac{\delta^{\mathbf{234}}\mathbf{U}}{\mathbf{1000}}\left(\frac{\lambda_{\mathbf{230}}}{\lambda_{\mathbf{230}} - \lambda_{\mathbf{234}}}\right)(\mathbf{1} - \mathbf{e}^{(\lambda_{\mathbf{234}} - \lambda_{\mathbf{230}})\cdot\mathbf{t}})$$

B

Plots: ^{230}Th/U blank, ^{231}Pa/^{230}Th results, ^{14}C reservoir ages

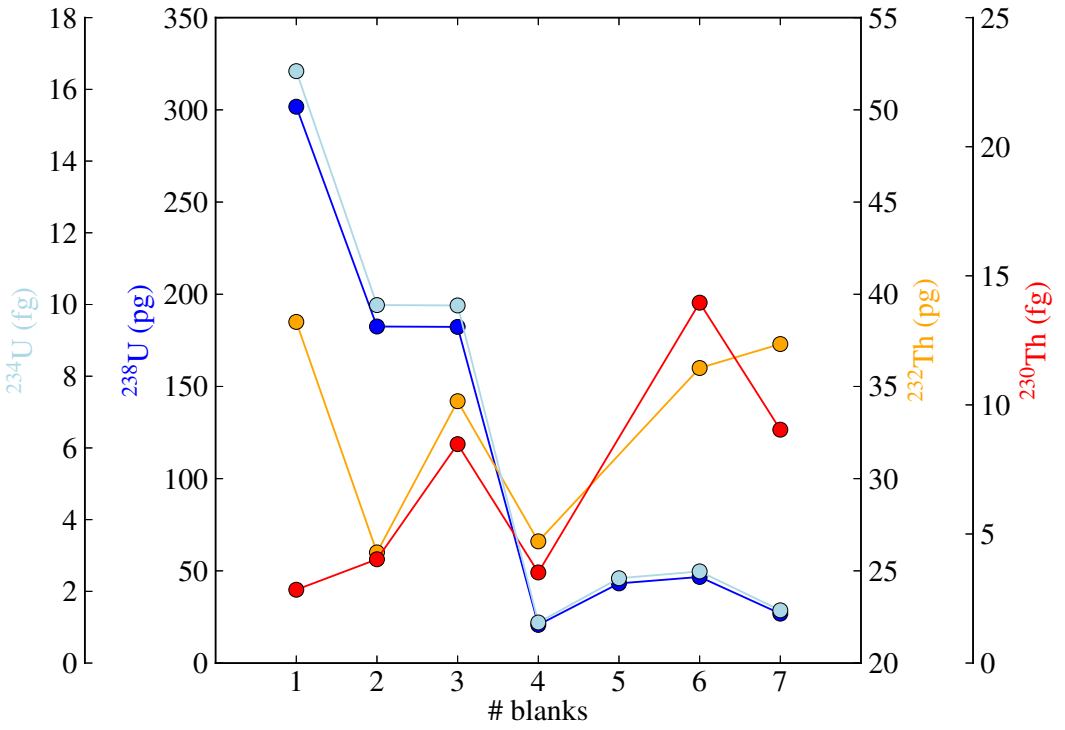

Fig. B.1: Procedural blank development over the course of this work. Though all blank measurements were neglectable, an average blank correction was applied for all the ^{230}Th/U data presented in this thesis (see also Tab. D.3).

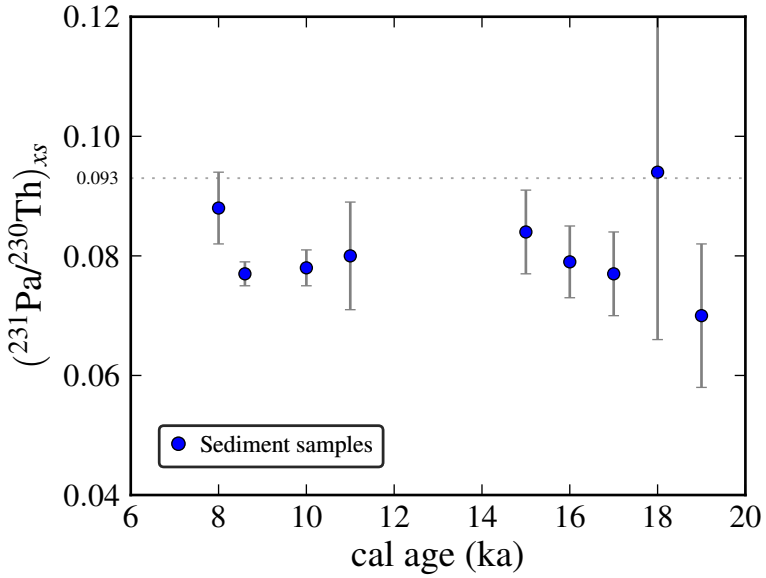

Fig. B.2: Sedimentary $^{231}Pa/^{230}Th$ excess ratios of nine samples from cores C1 and C2 were performed in this thesis following the procedure of Lippold (2008) and Lippold et al. (2009). Sample C1-5cm is not shown due to its large error. $^{231}Pa/^{230}Th$ uncertainties are given in 2σ. All measurements exhibit relatively high values near the production ratio between 8−18 ka BP indicating other processes than circulation alone dominate $^{231}Pa/^{230}Th$ deposition on the Brazilian slope. Often continental margins "suffer" from a higher particle flux and particle composition (e.g. higher biogenic opal production due to upwelling), which quickly removes Pa from the water column rendering the ratio useless as a circulation proxy. This phenomenon is known as boundary scavenging. As described in 6.6.1 the continental slope and shelf region around the core location off Brazil is indeed affected by seasonal upwelling events. Besides this problem it was almost impossible to establish a reliable age model for the sediment cores, which exhibit severe age reversals based on the $^{230}Th/U$ age of the coral rubble within the sediment. Roughly interpolated ages can vary by as much as 2 ka! Taken together, no further investigations on the sedimentary $^{231}Pa/^{230}Th$ have been made.

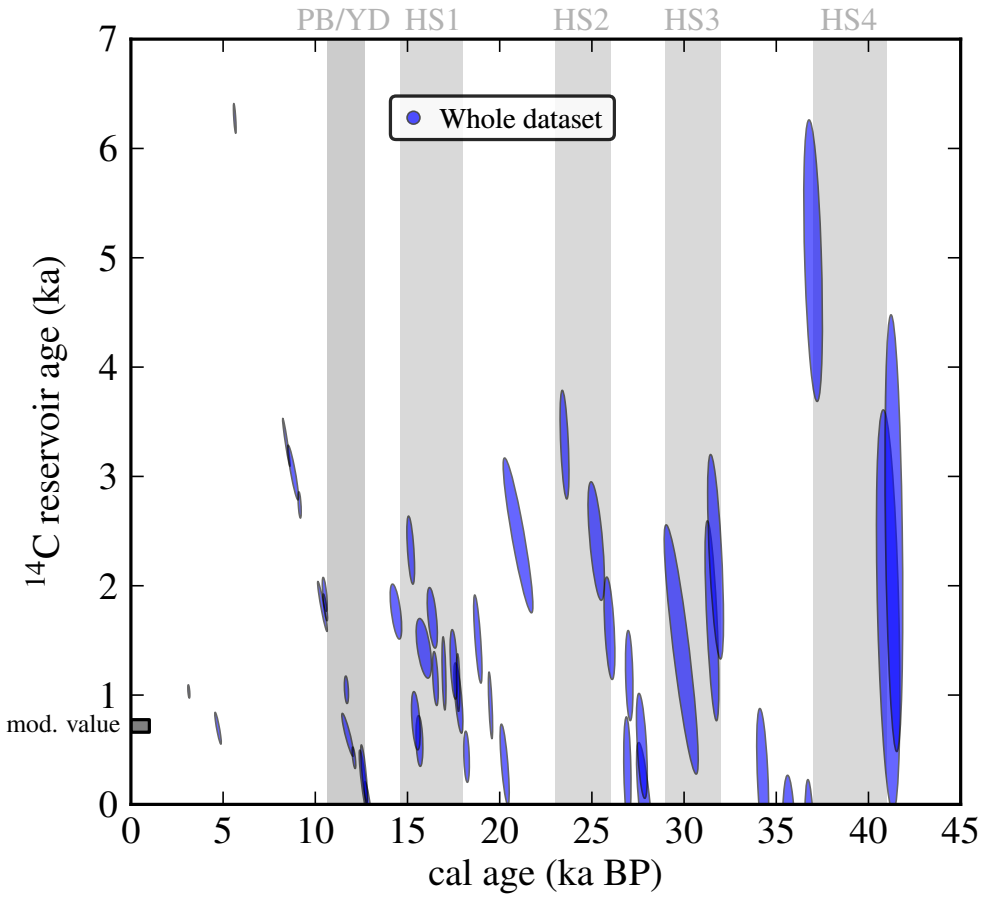

Fig. B.3: For the sake of completeness calculated reservoir offsets between coral samples and respective contemporaneous atmosphere are shown in ^{14}C years between 3−42 ka BP. This quantity is sometimes also called apparent ^{14}C ventilation age. In this thesis, however, all radiocarbon intermediate-depth ^{14}C offsets are presented and discussed as $\Delta\Delta^{14}$C.

C

Python Script (ventilation ages), ^{230}Th/U preparation flowchart

```
#! /usr/bin/python
# -*- coding: utf-8 -*-

from pylab import *
from matplotlib import rc
from matplotlib.patches import Ellipse
from scipy.interpolate import interp1d
import matplotlib.font_manager as font_manager


#Comment out these lines if you do not have LaTeX installed
rc('font',**{'family':'serif','serif':['Times']})
rc('text', usetex=True)


#Creates the canvas on which the final results are plotted
#with Matplotlib (MPL) <- have to be installed too!
fig = plt.figure(1, figsize=(4.5, 4))
ax = fig.add_subplot(111)
ax.set_position(pos = [0.15, 0.14, 0.8, 0.8])


#Read in IntCal09 and sample data file
x, y, yerr = np.loadtxt('intcal09.14c', usecols=[0,3,4], \
delimiter=',', unpack=True)
mittelUTH_list, sigmaUTH_list, mittel14C_list, sigma14C_list = \
np.loadtxt('samples', usecols=[0,1,2,3], unpack=True)


#Sort IntCal09 data file for interpolation
xInt_decr, yInt_decr = np.loadtxt('intcal09.14c', usecols=[0,3] \
, delimiter=',', unpack=True)
Idx = np.argsort(xInt_decr)
xInt = xInt_decr[Idx]
yInt = yInt_decr[Idx]


#Random numbers generated for every U/Th entry in sample list
anzahl = 1000.

for idx_mittelUTH, mittelUTH in enumerate(mittelUTH_list):
    alpha = np.linspace(0.5, 0.8, len(mittelUTH_list))
    xUTHstart_list = mittelUTH + 1000. * \
```

```
sigmaUTH_list[idx_mittelUTH] * np.random.randn(anzahl)
x14C_list = mittel14C_list[idx_mittelUTH] +  2. * \
sigma14C_list[idx_mittelUTH] * np.random.randn(anzahl)

xUTHschnitt_list = []

#Calculating backtrack curve starting from the MC generated points
for idx_xUTHstart, xUTHstart in enumerate(xUTHstart_list):
    xUTH = np.arange(xUTHstart, 45000., 1.)
    ydelta = (np.exp(xUTH/8267.) / \
    exp(x14C_list[idx_xUTHstart]/8033.) - 1.) * 1000.


    #IntCal09 interpolation for the xUTH grid
    f = interp1d(xInt, yInt)
    yInt_interp = f(xUTH)

    #Finding points of intercept between backtrack and IntCal09
    #and throw away points which are above IntCal09
    diffs = yInt_interp - ydelta
    xschnitt = []
    yschnitt = []

    for Idx_Diff, Diff in enumerate(diffs[0:len(diffs)-1]):
        if (diffs[Idx_Diff] > 0 and diffs[Idx_Diff+1] < 0) \
            or (diffs[Idx_Diff] < 0 and diffs[Idx_Diff+1] > 0):
            xschnitt.append(xUTH[Idx_Diff])
            yschnitt.append(ydelta[Idx_Diff])

    if len(xschnitt) == 0:
        xschnitt = [0.]
        yschnitt = [0.]
    xUTHschnitt_list.append(xschnitt[0])

venti = xUTHschnitt_list - xUTHstart_list
a = len([item for item in venti if item < 0.])


#Percentages written out during run of the script illustrate how
#many MC points for an individual error ellipse lie above the
#IntCal09. If too large ventilation age calculation might not be
#useful. Such samples should be taken off from the sample list.
print 'negativ', a/anzahl*100., '%'
```

```
    venti_pos = []
    xuthstart_pos = []
    for idx, item in enumerate(venti):
        if item > 0.:
            venti_pos.append(item)
            xuthstart_pos.append(xUTHstart_list[idx])
    venti = venti_pos
    xUTHstart_list = xuthstart_pos


    #Covariance ellipse calculation
    xx = np.cov(xUTHstart_list, venti, rowvar=0)
    cov_delta = xx[0,1]

    venti_mean =  mean(venti)
    venti_std  =  std(venti)
    xUTHstart_list_mean =  mean(xUTHstart_list)
    xUTHstart_list_std  =  std(xUTHstart_list)


    sigma_x_strich = sqrt( (venti_std**2 + \
    xUTHstart_list_std**2)/2  + sqrt((venti_std**2 - \
    xUTHstart_list_std**2)**2/4 + cov_delta**2) )
    sigma_y_strich = sqrt( (venti_std**2 + \
    xUTHstart_list_std**2)/2 - sqrt((venti_std**2 - \
    xUTHstart_list_std**2)**2/4 + cov_delta**2) )

    theta = 0.5 * arctan( 2*cov_delta / (xUTHstart_list_std**2 - \
    venti_std**2) )
    if cov_delta < 0 and (xx[0,0] - xx[1,1]) < 0:
        theta = theta/pi*180 - 90
    if cov_delta < 0 and (xx[0,0] - xx[1,1]) > 0:
        theta = theta/pi*180


#Printing the final ellipses with MPL
    alpha = np.linspace(0.5, 0.9, len(xUTHstart_list))
    e = Ellipse((xUTHstart_list_mean, venti_mean ), \
    2*sigma_x_strich, 2*sigma_y_strich, theta,
    color = 'b', alpha = alpha[idx_mittelUTH] , zorder=2, lw=0.5)
    e.set_edgecolor('k')
    ax.add_artist(e)
```

```
#Fake point for legend
C1, = plt.plot([10000], 'ob', markersize=0.5, markeredgecolor='k', \
alpha=0.6, lw=0.5)


#Legend upper right
l1 = ax.legend([C1], ['Whole dataset'],
loc=4, shadow=None, fancybox=True,numpoints=1, handletextpad=0.5, \
handlelength=0.8, markerscale=8, \
prop=font_manager.FontProperties(size=9), bbox_to_anchor=[0.95, 0.85])
l1.get_frame().set_alpha(1)
plt.gca().add_artist(l1)


#Setting axes dimensions
ax.axis([0, 45000, 0, 8000])
ax.set_xlabel('cal age (ka BP)', fontsize=14)
ax.set_ylabel(r'Projection age (ka)', fontsize=14, labelpad=8)
ax.set_xticklabels([0,5,10,15,20,25,30,35,40,45])
ax.set_yticklabels([0,1,2,3,4,5,6,7,8])
#savefig('final.pdf')
show()
```

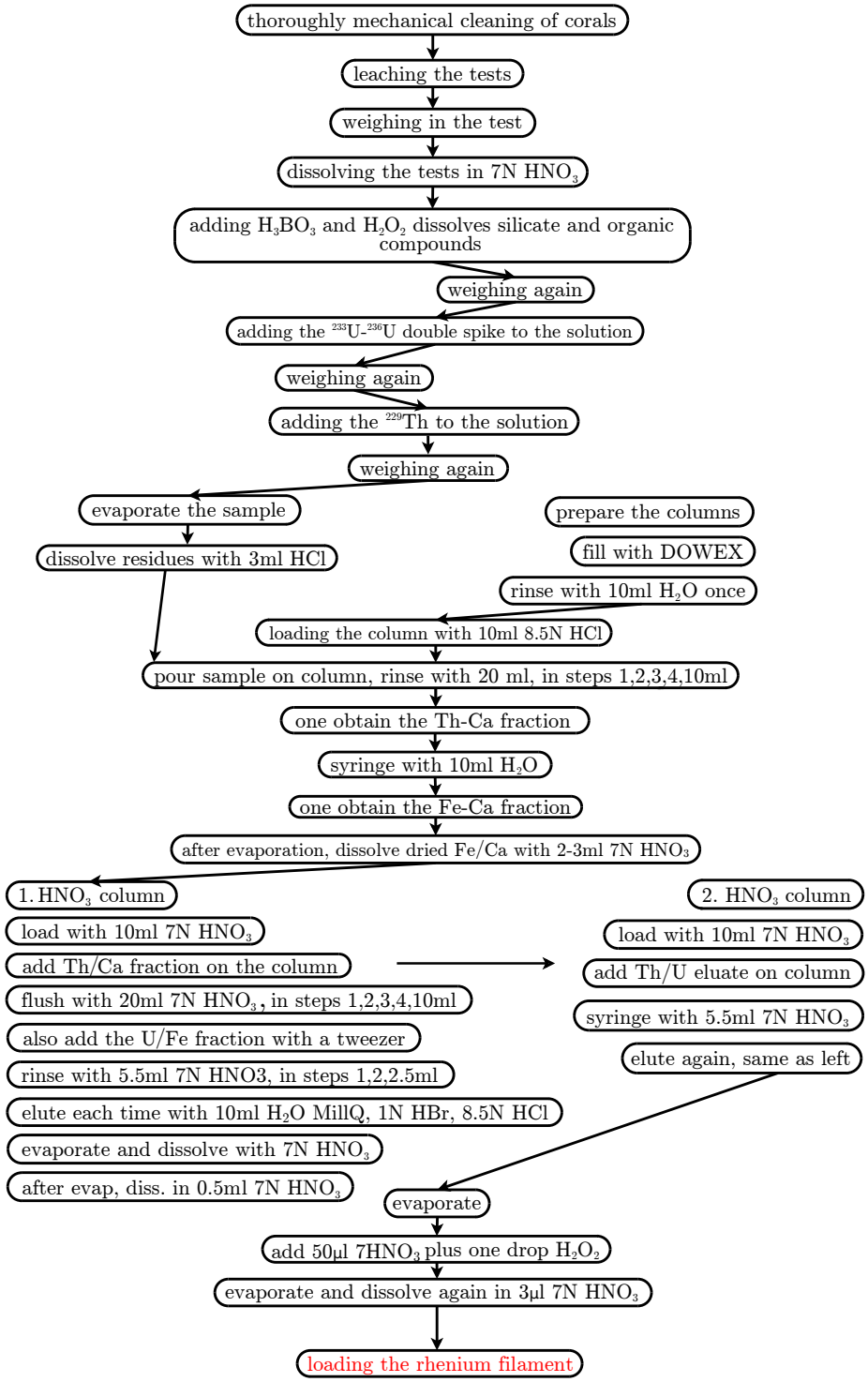
thoroughly mechanical cleaning of corals
leaching the tests
weighing in the test
dissolving the tests in 7N HNO_3
adding H_3BO_3 and H_2O_2 dissolves silicate and organic compounds
weighing again
adding the ^{233}U-^{236}U double spike to the solution
weighing again
adding the ^{229}Th to the solution
weighing again
evaporate the sample
dissolve residues with 3ml HCl
prepare the columns
fill with DOWEX
rinse with 10ml H_2O once
loading the column with 10ml 8.5N HCl
pour sample on column, rinse with 20 ml, in steps 1,2,3,4,10ml
one obtain the Th-Ca fraction
syringe with 10ml H_2O
one obtain the Fe-Ca fraction
after evaporation, dissolve dried Fe/Ca with 2-3ml 7N HNO_3
1. HNO_3 column
load with 10ml 7N HNO_3
add Th/Ca fraction on the column
flush with 20ml 7N HNO_3, in steps 1,2,3,4,10ml
also add the U/Fe fraction with a tweezer
rinse with 5.5ml 7N HNO3, in steps 1,2,2.5ml
elute each time with 10ml H_2O MillQ, 1N HBr, 8.5N HCl
evaporate and dissolve with 7N HNO_3
after evap, diss. in 0.5ml 7N HNO_3
2. HNO_3 column
load with 10ml 7N HNO_3
add Th/U eluate on column
syringe with 5.5ml 7N HNO_3
elute again, same as left
evaporate
add 50µl 7HNO_3 plus one drop H_2O_2
evaporate and dissolve again in 3µl 7N HNO_3
loading the rhenium filament

D

Table: ^{230}Th/U

lab# HD	tag	^{238}U (ppbw)	2σ	^{232}Th (pptw)	2σ	^{230}Th/^{238}U ($\times10^{-4}$)	2σ	^{232}Th/^{238}U ($\times10^{-6}$)	2σ	$\delta^{234}U_m$ (‰)	2σ	cal age$_u$ (ka)	$2\sigma^*$	**cal age** (ka BP)	**$2\sigma^{**}$**	$\delta^{234}U_i$ (‰)	2σ
5250	M-24	3580.1	3.6	7748.0	51.1	1232.5	17.7	708.3	4.7	149.1	1.8	12.358	0.189	11.761	0.328	154.2	2.4
5466	M-39	3313.6	2.0	165.8	1.1	1255.4	16.2	16.4	0.1	139.7	1.3	12.714	0.180	12.640	0.174	144.8	1.5
5251	M-51	3464.5	3.5	1900.5	5.9	1225.4	6.7	179.5	0.6	148.0	1.6	12.296	0.072	12.100	0.100	153.2	1.7
5465	M-65	2978.5	3.0	192.0	1.9	1189.3	24.3	21.1	0.2	142.3	2.2	11.977	0.251	11.900	0.259	147.2	2.6
5252	M-82	3746.6	1.9	762.1	4.6	1530.9	16.6	66.6	0.4	136.7	1.3	15.749	0.188	15.638	0.185	142.9	1.6
5464	M-86	3854.4	3.5	163.0	1.7	1512.2	20.6	13.8	0.1	138.4	2.1	15.518	0.238	15.447	0.229	144.6	2.4
5463	M-104	3267.4	6.9	394.5	8.7	1540.9	57.7	39.5	0.9	142.0	4.2	15.780	0.627	15.689	0.637	148.5	5.2
5462	M-119	2625.4	8.9	12784	147	2132	44.7	1593	19.1	151.1	6.6	22.267	0.520	20.999	0.808	160.3	8.0
5461	M-142	3231.1	11.3	7742.6	72.0	2785.6	68.7	784.2	7.8	138.3	5.7	30.467	0.911	29.809	0.929	150.4	7.6
5460	M-151	3519.2	3.9	2467.8	15.5	2862.1	31.6	229.5	1.5	123.3	2.0	31.931	0.418	31.693	0.422	134.9	2.9
5293	M-154	2946.0	2.4	420.5	2.5	3061.6	24.3	46.7	0.3	127.6	1.9	34.373	0.318	34.276	0.327	140.6	2.5
5459	M-155	3123.4	2.5	5924.6	29.6	2885.9	20.3	620.8	3.1	129.2	1.8	32.038	0.269	31.500	0.358	141.2	2.5
5458	M-157	3088.6	2.8	48655	2476	3553.0	291	5155	262	144.0	2.4	40.270	3.892	36.257	4.455	159.5	21
5457	M-178	2680.5	5.1	1806.7	19.9	3090.5	63.3	220.6	2.5	127.9	5.3	34.741	0.851	34.511	0.860	141.0	7.0
5456	M-189	2694.9	6.2	634.8	32.9	3083.9	151.3	77.1	4.0	119.0	16.8	34.989	2122	34.869	2.112	131.4	21
5453	M-193	2653.6	2.9	566.4	3.4	3194.1	30.2	69.9	0.4	135.2	2.2	35.828	0.419	35.714	0.408	149.5	3.1
5452	M-209	3630.8	2.2	9438.7	42.5	3619.9	24.0	850.8	3.9	124.2	1.4	42.102	0.336	41.387	0.475	139.6	2.7
5455	M-210	3343.2	3.3	5129.7	42.1	3627.3	38.3	502.2	4.1	128.4	2.1	42.006	0.534	41.562	0.578	144.4	3.6
5451	M-215	2582.6	2.6	3330.7	16.7	4024.5	36.8	422.1	2.2	129.0	2.2	47.679	0.579	47.297	0.579	147.5	3.7
5446	M-222	2543.0	3.1	205.7	1.0	4045.6	24.8	26.5	0.1	137.7	2.1	47.512	0.392	47.431	0.380	157.4	3.0
5450	M-231	2420.0	1.7	1348.8	5.8	3970.3	24.0	182.4	0.8	135.7	1.7	46.528	0.370	46.328	0.366	154.6	2.6
5448	M-245	2343.0	4.2	2401.9	16.8	3603.3	43.0	335.5	2.4	134.6	3.4	41.381	0.598	41.065	0.630	151.2	4.9
5447	M-259	3105.5	1.6	1048.9	4.4	4726.6	25.2	110.5	0.5	122.7	1.3	58.985	0.433	58.839	0.425	144.9	2.6
5449	M-267	3136.6	4.1	7721.0	49.4	4701.4	49.3	805.6	5.3	124.8	2.7	58.415	0.783	57.739	0.881	147.0	5.4
5445	M-270	2808.8	3.9	1268.4	10.3	4840.2	59.0	147.8	1.2	125.8	2.5	60.616	0.965	60.442	0.996	149.3	5.7
5294	M-296	3054.3	2.4	1137.0	8.4	5042.0	49.6	121.8	0.9	123.4	2.3	64.207	0.847	64.053	0.871	147.9	5.2
5531	M-385	3304.9	2.3	9985.5	58.9	6340.8	65.5	988.8	5.9	110.2	1.7	90.747	1.478	89.928	1.505	142.1	8.7
2473[G]	M-142	3094.6	1.6	2986.4	2.6	2816.4	11.8	315.8	0.3	165.6	29.7	29.996	0.910	29.701	0.927	180.1	32
2475[G]	M-189	2727.3	0.3	272.3	0.6	3239.3	13.2	32.7	0.1	121.7	7.1	36.967	0.327	36.881	0.362	135.1	8.1

Tab. D.1: ^{230}Th/U results for core MXL. $2\sigma^*$ indicate uncertainty calculated by a Monte-Carlo approach, double asterisk denote uncertainties obtained by first order Gaussian error propagation. Samples marked with *G* are repetitions and were measured in Gif-sur-Yvette at LSCE; corresponding lab numbers are in-house at LSCE.

lab# HD	tag	^{238}U (ppbw)	2σ	^{232}Th (pptw)	2σ	^{230}Th/^{238}U ($\times10^{-4}$)	2σ	^{232}Th/^{238}U ($\times10^{-6}$)	2σ	$\delta^{234}U_m$ (‰)	2σ	cal age$_u$ (ka)	$2\sigma^*$	**cal age** (ka BP)	**$2\sigma^{**}$**	$\delta^{234}U_i$ (‰)	2σ
5286	K-10	4111.2	4.1	1125.6	16.5	494.2	16.7	89.6	1.3	135.1	3.8	4.857	0.173	4.728	0.172	136.9	3.9
5245	K-25	3443.1	3.4	100.1	0.6	1756.6	12.6	9.5	0.1	136.7	1.6	18.271	0.149	18.203	0.145	143.9	1.8
5246	K-40	3981.3	4.0	184.6	0.5	1713.2	7.9	15.2	0.0	134.9	1.9	17.812	0.100	17.741	0.095	141.8	2.0
5287	K-85	3109.5	2.2	341.9	3.7	1753.2	31.2	36.0	0.4	132.6	1.7	18.305	0.368	18.217	0.355	139.6	2.4
5288	K-124	3419.7	1.7	451.4	1.5	1867.8	9.6	43.2	0.1	132.9	1.3	19.605	0.110	19.512	0.114	140.4	1.4
5469	K-130	2817.0	5.6	6067.8	47.3	1921.2	24.7	704.9	5.7	138.5	3.6	20.106	0.281	19.507	0.397	146.4	4.2
5468	K-133	2748.9	2.7	6237.6	31.8	1965.7	15.5	742.6	3.9	132.4	2.2	20.743	0.182	20.111	0.340	140.1	2.8
5470	K-146	3210.5	3.5	455.4	3.5	1923.3	21.1	46.4	0.4	127.1	2.4	20.360	0.254	20.263	0.250	134.5	2.8
5467	K-162	2962.4	3.9	222.7	2.1	1919.2	25.6	24.6	0.2	131.0	2.6	20.233	0.307	20.153	0.301	138.7	3.1
5289	K-180	3123.5	1.6	271.1	3.7	2459.7	38.9	28.4	0.4	124.9	3.0	26.817	0.507	26.735	0.485	134.7	3.9
5530	K-208	2923.7	2.0	333.1	2.5	2442.2	27.2	37.3	0.3	126.8	1.6	26.550	0.343	26.460	0.336	136.7	2.3
5529	K-260	3154.0	3.2	1012.0	6.2	2496.2	19.1	105.0	0.6	127.8	1.6	27.186	0.233	27.044	0.243	138.0	2.1
5290	K-286	3398.8	1.7	334.8	2.4	2537.0	23.6	32.2	0.2	124.6	2.0	27.781	0.296	27.697	0.299	134.8	2.6
5291	K-322	3083.4	3.1	234.7	1.1	2501.3	18.4	24.9	0.1	131.0	2.2	27.159	0.232	27.080	0.235	141.4	2.6
5248	K-358	3153.3	3.2	332.5	2.5	2523.8	28.9	34.5	0.3	125.9	1.9	27.580	0.354	27.493	0.362	136.1	2.7
5249	K-394	3233.1	3.2	407.2	1.8	2496.1	15.7	41.2	0.2	130.5	1.6	27.108	0.201	27.017	0.198	140.9	2.0
5136	C1-33	3860.9	5.4	494.1	8.5	886.3	27.8	41.9	0.7	132.9	2.7	8.883	0.292	8.791	0.291	136.2	3.1
5244	C1-33	3897.2	3.9	293.5	1.2	925.4	7.7	24.6	0.1	140.1	1.6	9.229	0.078	9.150	0.082	143.7	1.7
5137	C1-42	3237.0	3.2	241.0	2.1	1064.6	15.6	24.4	0.2	141.5	1.8	10.670	0.167	10.592	0.165	145.8	2.0
5182	C1-42a	3396.2	4.9	962.6	10.6	1061.5	28.2	92.8	1.0	139.1	2.7	10.661	0.302	10.530	0.300	143.3	3.1
4673	C1-295^{D}	3172.3	3.2	1351.4	6.5	1808.2	18.2	139.4	0.7	129.9	2.4	18.980	0.206	18.815	0.219	137.0	2.7
4679	C2-36^{D}	6977.6	7.0	590.9	4.0	577.9	7.0	27.7	0.2	132.4	1.9	5.715	0.070	5.635	0.072	134.5	1.9
4502	C2-47^{D}	3871.2	3.9	5103.1	24.0	1515.4	12.1	431.4	2.1	137.4	2.1	15.570	0.131	15.182	0.214	143.4	2.4
5196	C2-84	4611.0	4.7	11899.0	77.0	1875.2	26.9	844.5	5.5	124.8	2.3	19.849	0.304	19.135	0.455	131.7	3.1
4504	C2-87	5982.1	6.0	10493.2	77.6	1598.7	17.7	574.1	4.3	129.4	2.1	16.619	0.2075	16.119	0.300	135.4	2.6
5183	C2-94	3807.6	10.3	10435.0	44.5	3313.1	22.5	896.9	4.5	126.9	4.2	37.751	0.342	37.003	0.492	140.9	5.3
4872	L606	3439.4	3.4	53.5	0.5	3.8	0.3	5.1	0.1	142.7	1.8	0.037	0.004	-0.026	0.004	142.7	1.8
4871	S612	3185.9	3.2	243.6	3.2	11.7	1.2	25.0	0.3	144.3	2.3	0.112	0.011	0.034	0.015	144.3	2.3
5197	S1032	4647.7	4.6	1354.6	6.0	338.2	3.8	95.4	0.4	143.6	1.6	3.276	0.038	3.143	0.052	144.9	1.6

Tab. D.2: ^{230}Th/U results for core KGLC, C1, C2 and three single specimens of *Lophelia pertusa* and *Solenosmilia variabilis*. $2\sigma^*$ indicate uncertainty calculated by a Monte-Carlo approach, double asterisk denote uncertainties obtained by first order Gaussian error propagation. *D*: already measured ^{230}Th/U in my diploma thesis but ^{14}C in this thesis, see Tab. E.2.

	lab#	^{238}U (ng)	2σ	^{234}U (fg)	2σ	^{232}Th (ng)	2σ	^{230}Th (fg)	2σ
	4648	0.3017	0.0006	16.508	0.030	0.0385	0.0004	2.84	1.14
	4680	0.1825	0.0004	9.984	0.020	0.0260	0.0005	4.02	2.61
	4686	0.1823	0.0005	9.974	0.030	0.0342	0.0014	8.48	4.66
	5253	0.0207	0.0001	1.131	0.007	0.0266	0.0004	3.51	1.55
	5295	0.0432	0.0020	2.365	0.110	/	/	/	/
	5454	0.0467	0.0001	2.556	0.005	0.0360	0.0009	13.96	4.33
	5471	0.0268	0.0002	1.470	0.010	0.0373	0.0006	9.04	2.08
$\bar{x}$		0.1149		6.284		0.0331		6.97*	

Tab. D.3: Measured ^{230}Th/U blanks used for underground correction. In red: used mean values.

E

Table: ^{14}C

#	lab	lab# HD	tag	cal age (ka BP)	1σ	Fm	1σ	D^{14}C (‰)	1σ	^{14}C age (ka BP)	1σ	Δ^{14}C (‰)	1σ
90143	UCIAMS	5286	K-10	4.728	0.086	0.5447	0.0010	-455.3	1.0	4.880	0.020	-34.9	10.2
90144	UCIAMS	5245	K-25	18.203	0.073	0.1469	0.0007	-853.1	0.7	15.410	0.040	328.2	13.7
90145	UCIAMS	5246	K-40	17.741	0.047	0.1421	0.0007	-857.9	0.7	15.675	0.045	215.2	9.7
90146	UCIAMS	5288	K-124	19.512	0.057	0.1163	0.0007	-883.7	0.7	17.285	0.050	232.1	11.4
14722	MAMS	5470	K-146	20.263	0.125	0.1143	0.0011	-885.7	1.1	17.426	0.077	325.9	23.8
90147	UCIAMS	5290	K-286	27.697	0.150	0.0547	0.0006	-945.3	0.6	23.350	0.100	558.8	34.3
90148	UCIAMS	5249	K-394	27.017	0.100	0.0528	0.0006	-947.2	0.6	23.630	0.100	386.6	24.0
90149	UCIAMS	5250	M-24	11.762	0.164	0.2620	0.0008	-738.0	0.8	10.760	0.025	87.0	21.8
14716	MAMS	5466	M-39	12.641	0.087	0.2534	0.0013	-746.6	1.3	11.027	0.042	169.4	13.5
90150	UCIAMS	5251	M-51	12.101	0.050	0.2628	0.0008	-737.2	0.8	10.735	0.025	136.0	7.7
90151	UCIAMS	5252	M-82	15.639	0.093	0.1833	0.0009	-816.7	0.9	13.625	0.040	216.3	14.5
94254	UCIAMS	5464	M-86	15.447	0.115	0.1812	0.0009	-818.8	0.9	13.720	0.045	174.5	17.2
94255	UCIAMS	5463	M-104	15.689	0.319	0.1814	0.0009	-818.6	0.9	13.715	0.045	210.1	46.7
94256	UCIAMS	5462	M-119	21.000	0.404	0.0821	0.0009	-917.9	0.9	20.080	0.100	41.7	53.9
94257	UCIAMS	5461	M-142	29.809	0.465	0.0371	0.0009	-962.9	0.9	26.450	0.200	368.3	85.8
94258	UCIAMS	5460	M-151	31.694	0.211	0.0244	0.0009	-975.6	0.9	29.810	0.310	131.2	52.1
90152	UCIAMS	5293	M-154	34.276	0.164	0.0249	0.0006	-975.1	0.6	29.660	0.210	575.3	51.4
94259	UCIAMS	5459	M-155	31.501	0.179	0.0273	0.0009	-972.7	0.9	28.920	0.280	234.6	50.6
94260	UCIAMS	5456	M-189	34.869	1.056	0.0194	0.0009	-980.6	0.9	31.660	0.390	319.3	177.7
94261	UCIAMS	5453	M-193	35.715	0.204	0.0219	0.0009	-978.1	0.9	30.680	0.340	651.0	81.0
94262	UCIAMS	5452	M-209	41.388	0.238	0.0082	0.0009	-991.8	0.9	38.640	0.930	217.5	145.4
94263	UCIAMS	5451	M-215	47.297	0.290	0.0073	0.0009	-992.7	0.9	39.510	1.030	1,233	297
94264	UCIAMS	5446	M-222	47.432	0.190	0.0086	0.0009	-991.4	0.9	38.170	0.870	1,681	297
94265	UCIAMS	5450	M-231	46.329	0.183	0.0057	0.0009	-994.3	0.9	41.500	1.320	550.5	257.0
94266	UCIAMS	5448	M-245	41.065	0.315	0.0093	0.0009	-990.7	0.9	37.580	0.810	336.1	143.6

Tab. E.1: ^{14}C results for cores KGLC and MXL

#	lab	lab# HD	tag	cal age (ka BP)	1σ	Fm	1σ	$D^{14}C$ (‰)	1σ	^{14}C age (ka BP)	1σ	$\Delta^{14}C$ (‰)	1σ
14721	MAMS	5136	C1-33	8.791	0.146	0.2554	0.0013	-744.6	1.3	10.965	0.042	-260.3	13.5
11673	MAMS	5244	C1-33	9.150	0.041	0.2564	0.0015	-743.6	1.5	10.934	0.046	-224.5	6.0
11674	MAMS	4673	C1-295	18.814	0.110	0.1183	0.0012	-881.7	1.2	17.145	0.080	152.4	19.2
11671	MAMS	4679	C2-36	5.635	0.036	0.2490	0.0014	-751.0	1.4	11.170	0.045	-507.8	3.5
14717	MAMS	4502	C2-47	15.182	0.109	0.1521	0.0012	-847.9	1.2	15.130	0.061	-45.8	14.5
90153	UCIAMS	5183	C2-94	37.003	0.246	0.0094	0.0006	-990.6	0.6	37.530	0.550	-177.6	62.0
14723	MAMS	5197	S1032	3.143	0.026	0.6027	0.0019	-397.3	1.9	4.068	0.025	-118.5	3.9
90154^{R}	UCIAMS	5197	S1032	3.143	0.026	0.6083	0.0014	-391.7	1.4	3.995	0.020	-110.5	3.6
35341	ETH	4872	L606	-0.026	0.019	0.9957	0.0024	-4.3	2.4	0.035	0.019	-7.5	2.4
15420^{R}	MAMS	4872	L606	-0.026	0.019	1.0056	0.0027	5.6	2.7	-0.045	0.021	2.4	2.6
35342	ETH	4871	S612	0.034	0.008	0.9939	0.0024	-6.1	2.4	0.049	0.019	-2.1	2.5
15421^{R}	MAMS	4871	S612	0.034	0.008	0.9853	0.0026	-14.7	2.6	0.119	0.022	-10.8	2.8

Tab. E.2: ^{14}C results for cores C1, C2, and three single specimens of species *L. pertusa* and *S. variabilis* from Campos Basin. *R* denote ^{14}C replicate measurements.

material	#	lab	Fm	1σ	$D^{14}C$ (‰)	1σ	^{14}C age (ka BP)	1σ	tag	cal age (ka BP)	1σ
Calcite	94739	UCIAMS	0.0014	0.000047840	-998.6	0.0	52.910	0.280	/	/	/
Calcite	94740	UCIAMS	0.0011	0.000044512	-998.9	0.0	55.040	0.340	/	/	/
Calcite	94253	UCIAMS	0.0012	0.000035615	-998.8	0.0	53.910	0.240	/	/	/
Calcite	94267	UCIAMS	0.0010	0.000039756	-999.0	0.0	55.490	0.320	/	/	/
FIRI-C	94268	UCIAMS	0.1039	0.000527573	-896.1	0.5	18.190	0.045	/	/	/
IAEA C-2	94269	UCIAMS	0.4111	0.000908994	-588.9	0.9	7.140	0.020	/	/	/
Aragonite	94737	UCIAMS	0.0027	0.000073320	-997.3	0.1	47.620	0.230	M-385	89.928	0.773
Aragonite	94738	UCIAMS	0.0029	0.000082576	-997.1	0.1	46.970	0.230	M-385	89.928	0.773

Tab. E.3: Measured ^{14}C blanks used for background correction.

F

Table: $^{143}Nd/^{144}Nd$

lab# Gif	tag	cal age (ka BP)	2σ	$^{143}Nd/^{144}Nd$	2σ	ε_{Nd} (‰)	2σ	mass spectrometer
2033	C1-33	8.791	0.291	0.511982	0.000015	-12.80	0.30	TIMS
3170	C1-42	10.592	0.165	0.512071	0.000031	-11.07	0.61	ICP-MS
2032	C1-54	11.687	0.111	0.511910	0.000051	-14.20	1.00	TIMS
3168	C1-54	11.687	0.111	0.511776	0.000051	-16.82	1.00	ICP-MS
3173	C1-113	14.385	0.311	0.511782	0.000025	-16.69	0.48	ICP-MS
3160^{R}	C1-163	16.513	0.156	0.511945	0.000028	-13.52	0.55	ICP-MS
n/a ^{R}	C1-163	16.513	0.156	0.511835	0.000018	-15.66	0.35	TIMS
2038^{R}	C1-163	16.513	0.156	0.512014	0.000026	-12.18	0.50	ICP-MS
3166^{R}	C1-193	16.980	0.108	0.512026	0.000036	-11.94	0.69	ICP-MS
2039^{R}	C1-193	16.980	0.108	0.512121	0.000062	-10.08	1.20	ICP-MS
3163	C1-235	17.774	0.242	0.511923	0.000032	-13.95	0.62	ICP-MS
3161	C1-247	17.515	0.205	0.511895	0.000036	-14.50	0.71	ICP-MS
3165^{R}	C1-295	18.815	0.219	0.511923	0.000037	-13.94	0.72	ICP-MS
2034^{R}	C1-295	18.815	0.219	0.511946	0.000082	-13.50	1.60	TIMS
2045	C2-5	12.611	0.227	0.512125	0.000026	-10.00	0.50	ICP-MS
3171^{R}	C2-17	12.925	0.249	0.512096	0.000027	-10.57	0.52	ICP-MS
2040^{R}	C2-17	12.925	0.249	0.512100	0.000026	-10.49	0.50	ICP-MS
3175	C2-36	5.635	0.072	0.512113	0.000025	-10.25	0.48	ICP-MS
2035	C2-44 old	16.348	0.273	0.512223	0.000041	-8.10	0.80	TIMS
2042	C2-44 new	10.520	0.127	0.512097	0.000031	-10.56	0.60	ICP-MS
2046	C2-58	27.868	0.465	0.512168	0.000026	-9.18	0.50	ICP-MS
2056	C2-59	27.068	0.298	0.512159	0.000026	-9.35	0.50	ICP-MS
2047	C2-63	25.950	0.285	0.512112	0.000026	-10.26	0.50	ICP-MS
n/a	C2-68 new	23.515	0.250	0.512145	0.000015	-9.62	0.30	TIMS
3174	C2-94	37.003	0.492	0.512148	0.000051	-9.56	1.00	ICP-MS
3172	K-10	4.728	0.172	0.511964	0.000034	-13.15	0.66	ICP-MS
3154	K-25	18.203	0.145	0.511807	0.000025	-16.22	0.48	ICP-MS
3164	K-124	19.512	0.114	0.511961	0.000025	-13.20	0.48	ICP-MS
3162	K-146	20.263	0.250	0.512285	0.000038	-6.88	0.74	ICP-MS
3156	K-394	27.017	0.198	0.512312	0.000032	-6.37	0.62	ICP-MS
3159	M-51	12.100	0.100	0.512071	0.000028	-11.06	0.54	ICP-MS
3167	M-151	31.693	0.422	0.512161	0.000028	-9.30	0.54	ICP-MS
3157	M-154	34.276	0.327	0.512201	0.000046	-8.53	0.91	ICP-MS
3169	S1032	3.143	0.052	0.512219	0.000035	-8.17	0.69	ICP-MS
3155	L606	-0.026	0.004	0.511899	0.000051	-14.42	1.00	ICP-MS

Tab. F.1: Nd results from all four sediment cores and single specimens from the Campos Basin. *R* denote Nd replicate measurements.

G

Table: δ^{13}C, δ^{18}O, XRD, ^{231}Pa/^{230}Th, trace elements (Mn, Nd)

lab# HD	tag	lab# MARUM	δ^{13}C (‰, VPDB)	$1\sigma^*$ $\leqslant$	δ^{18}O (‰, VPDB)	$1\sigma^*$ $\leqslant$
5136	C1-33	104555	-7.21	0.05	-1.07	0.07
5137	C1-42	104556	-5.18	0.05	0.49	0.07
4676	C1-54	104557	-8.37	0.05	-1.34	0.07
4674	C1-113	104558	-6.71	0.05	0.13	0.07
4647	C1-163	104559	-6.91	0.05	0.46	0.07
4645	C1-193a	104560	-4.40	0.05	1.50	0.07
4645	C1-193b	104562	-4.79	0.05	1.33	0.07
4645	C1-193c	104563	-2.57	0.05	2.48	0.07
4646	C1-235	104564	-2.82	0.05	2.71	0.07
4699	C1-247	104565	-4.70	0.05	1.17	0.07
4673	C1-295	104566	-2.92	0.05	2.34	0.07
4499	C2-5	104567	-3.29	0.05	1.49	0.07
4413	C2-17	104569	-3.12	0.05	1.62	0.07
4681	C2-44a	104571	-2.63	0.05	1.90	0.07
4501	C2-44b	104572	-3.77	0.05	2.30	0.07
4502	C2-47a	104573	-3.54	0.05	2.18	0.07
4502	C2-47b	104574	-0.73	0.05	3.26	0.07
4683	C2-55	104576	-5.42	0.05	0.83	0.07
4414	C2-58	104577	-6.40	0.05	1.57	0.07
4677	C2-59	104578	-4.31	0.05	2.13	0.07
4682	C2-63	104579	-6.58	0.05	1.52	0.07
4684	C2-65	104580	-5.07	0.05	1.92	0.07
4678	C2-68	104581	-6.75	0.05	1.24	0.07
4503	C2-68a	104583	-6.41	0.05	1.48	0.07
4503	C2-68b	104584	-6.13	0.05	0.97	0.07
4685	C2-74	104585	-6.80	0.05	0.78	0.07
4504	C2-87	104655	-7.28	0.05	0.03	0.07

Tab. G.1: Measured δ^{13}C and δ^{18}O isotopes on *L. pertusa* corals from off Brazil. Asterisk denotes long term reproducibility of the in-house carbonate standard.

lab# HD	tag	recog. minerals	mass fraction (wt%)	1σ	further candidates	mass fraction (wt%)	1σ
5136	C1-33	aragonite	100	1	/	/	/
4679	C2-36	aragonite	100	1	/	/	/
4684	C2-65	aragonite	100	1	/	/	/
4678	C2-68	aragonite	100	1	/	/	/
5183	C2-94	aragonite	100	1	/	/	/
5470	K-146	aragonite	100	1	/	/	/
5290	K-286	aragonite	100	1	/	/	/
5250	M-24	aragonite	100	1	/	/	/
5251	M-51	aragonite	100	1	/	/	/
5460	M-151	aragonite	98	1	anatase	1	1
5293	M-154	aragonite	97	1	monazite-(Ce)	3	1
5451	M-215	aragonite	100	1	/	/	/
5446	M-222	aragonite	96	1	quartz low, anatase	4	1

Tab. G.2: XRD measurements on thirteen coral samples of all four cores showing no signs of calcite.

lab# HD	tag	material	cal age (ka BP approx.)	$(^{231}Pa/^{230}Th)_{xs}$	2σ
620	C1-5	sediment	0	0.079	0.132
622	C1-47	sediment	10	0.078	0.003
624	C1-70	sediment	15	0.084	0.007
625	C1-150	sediment	16	0.079	0.006
626	C1-177	sediment	17	0.077	0.007
627	C1-230	sediment	18	0.094	0.028
628	C1-280	sediment	19	0.070	0.012
629	C2-7	sediment	8	0.088	0.006
621	C2-25	sediment	8.6	0.077	0.002
630	C2-35	sediment	11	0.080	0.009

Tab. G.3: Sedimentary $(^{231}Pa/^{230}Th)_{xs}$ results from cores C1 and C2. All calendar ages are rough estimates, interpolated from the coral's age-depth-relationships of cores C1 and C2 (see Fig. 6.9 and 6.10).

material	lab# HD	tag	cal age (ka BP approx.)	$^{143}Nd/^{144}Nd$	2σ	ε_{Nd} (‰)	2σ
sediment	J191	C1-5	core top	0.511907	0.000010	-14.26	0.20
sediment	J194	C1-150	16	0.511758	0.000011	-17.16	0.21
sediment	J195	C1-230	18	0.511769	0.000012	-16.94	0.24

Tab. G.4: Due to an amplifier problem during the data aquisition 2σ uncertainties can vary by up to one ε_{Nd} unit (J. Lippold 2010, pers. comm.). Results must be regarded with caution.

lab# Gif	tag	Mn/Ca (μmol/mol)	Nd/Ca (nmol/mol)	Nd (ppbw)
3160	C1-163	7.54	34.24	49.34
3160	C1-163	7.37	34.51	49.73
3166	C1-193	1.78	8.61	12.41
3166	C1-193	1.79	7.80	11.24
3175	C2-36	1.95	32.91	47.43
3174	C2-94	1.14	205.27	295.82
3174	C2-94	1.12	207.31	298.76
3159	M-51	0.54	76.92	110.85
3159	M-51	0.48	76.14	109.73
3157	M-154	2.66	5.23	7.54
3164	K-124	0.85	6.08	8.76
3164	K-124	0.78	5.99	8.63
3162	K-146	0.72	5.36	7.72
3156	K-394	1.86	6.86	9.89
3156	K-394	1.92	6.76	9.74
3155	L606	0.10	4.39	6.33

Tab. G.5: Trace element measurements on some coral samples from all four cores. Note, many entries are replicate measurements. Internal reproducibility for Nd on the JCp-1 standard was five percent (2σ) for Nd and Mn and one percent for Ca.

List of Figures

List of Tables

Acknowledgments

First and foremost, I would like to express my gratitude to my supervisor Augusto Mangini who allowed me to work in this fascinating research field of deep-sea corals. His expertise and patience added considerably to the success of this thesis.

Furthermore, I would like to thank Prof. Dr. Werner Aeschbach-Hertig for reviewing this thesis with its seemingly never-ending pages. Sorry for that!

A very special thank goes out to Renato Kowsmann from Petrobras, without him this thesis would not have come into being in the first place as he provided the Brazilian corals. It is owing to his persistence that the Brazilian custom, withdrawing the samples, allowed further shipment after a few days.

Cordial thanks to all who contributed to the measurements on the various mass specs and for their help in the clean labs (in alphabetical order): Benny Antz, Patrick Blaser, Evelyn Böhm, Emmanuel Christner, Christophe Colin, Eric Douville, Rene Eichstädter, Jens Fohlmeister, Norbert Frank, Marcus Gutjahr, Bernd Kromer, Jörg Lippold, Paolo Montagna, Jean-Carlos Montero-Serrano, Guaciara Macedo dos Santos, Monika Segl, Andrea Schöder-Ritzrau, Christoph Vogt.

Appreciation also goes out to Evelyn Böhm, Michael Deininger, Jörg Lippold and especially Jens Fohlmeister, Norbert Frank (for proof-reading and providing a small text fragment on Nd MC-measurements), Andrea Schröder-Ritzrau, and my partner Gabriele Maier for proof-reading some of the chapters.

A warm thanks also goes out to Nicole Vollweiler, Sophie Winterhalder, and Anne Stempel (formerly Wackerbarth), Karoline Thomas, and Christian Wirsig for their moral support and many moments of hearty laugh.

Of course no acknowledgments would be complete without giving thanks to my parents. Without their support during my physics study and beyond, this endeavor would not have come to fruition.

Last but not least, thanks to my newborn son Emil who always held me awake with his unbearable screaming attacks allowing me to write on my thesis even at 3 am.

This thesis was funded by Deutsche Forschungsgemeinschaft (DFG), file reference MA-821/39-1.

References

Adkins J. (**1998**). "Deep-Sea Corals: A New Oceanic Archive." Ph.D. thesis, Massachusetts Institute of Technology.

Adkins J.F. and Boyle E.A. (**1997**). "Changing atmospheric Δ^{14}C and the record of deep water paleoventilation ages." *Paleoceanographic Currents*, 12(3): 337–344.

Adkins J.F., Cheng H., Boyle E.A., Druffel E.R.M. and Edwards R.L. (**1998**). "Deep-Sea Coral Evidence for Rapid Change in Ventilation of the Deep North Atlantic 15,400 Years Ago." *Science*, 280: 725–728.

Adkins J.F., Griffin S., Kashgarian M., Cheng H., Druffel E., Boyle E.A., Edwards R.L. and Shen C.C. (**2002**a). "Radiocarbon Dating of Deep-Sea Corals." *Radiocarbon*, 44(2): 567–580.

Adkins J.F., Henderson G.M., Wang S., O'Shea S. and Mokadem F. (**2004**). "Growth rates of the deep-sea scleractinia Desmophyllum cristagalli and Enallopsammia rostrata." *Earth and Planetary Science Letters*, 227: 481–490.

Adkins J.F., McIntyre K. and Schrag D.P. (**2002**b). "The Salinity, Temperature, and δ^{18}O of the Glacial Deep Ocean." *Science*, 298: 1769–1773.

Al-Rousan S., Felis T., Manasrah R. and Al-Horani F. (**2007**). "Seasonal variations in the stable oxygen isotopic composition in Porites corals from the northern Gulf of Aqaba, Red Sea." *Geochemical Journal*, 41: 333–340.

Andersen M.B., Stirling C.H., Zimmermann B. and Halliday A.N. (**2010**). "Precise determination of the open ocean ^{234}U/^{238}U composition." *Geochemistry, Geophysics, Geosystems*, 11: 1–8.

Anderson E.C. and Libby W.F. (**1951**). "World-Wide Distribution of Natural Radiocarbon." *Physical Review*, 81(1): 64–69.

Anderson R.F., Ali S., Bradtmiller L.I., Nielsen S.H.H., Fleisher M.Q., Anderson B.E. and Burckle L.H. (**2009**). "Wind-Driven Upwelling in the Southern Ocean and the Deglacial Rise in Atmospheric CO_2." *Science*, 323: 1443–1448.

Anderson R.F., Bacon M.P. and Brewer P.G. (**1983**). "Removal of ^{230}Th and ^{231}Pa from the open ocean." *Earth and Planetary Science Letters*, 62: 7–23.

Anderson R.F. and Carr M.E. (**2010**). "Uncorking the Southern Ocean's Vintage CO_2." *Science*, 328: 1117–1118.

Andrews A.H., Cordes E.E., Mahoney M.M., Munk K., Coale K.H., Cailliet G.M. and Heifetz J. (**2002**). "Age, growth and radiometric age validation of a deep-sea, habitat-forming gorgonian (Primnoa resedaeformis) from the Gulf of Alaska." *Hydrobiologia*, 471: 101–110.

Andrews J.T., Erlenkeuser H., Tedesco K., Aksu A.E. and Jull A.J.T. (**1994**). "Late Quaternary (Stage 2 and 3) Meltwater and Heinrich Events, Northwest Labrador Sea." *Quaternary Research*, 41: 26–34.

Arantes R.C.M., Castro C.B., Pires D.O. and Seoane J.C.S. (**2009**). "Depth and water mass zonation and species associations of cold-water octocoral and stony coral communities in the southwestern Atlantic." *Marine Ecology Progress Series*, 397: 71–79.

Arz H. (**1998**). "Correlated Millennial-Scale Changes in Surface Hydrography and Terrigenous Sediment Yield Inferred from Last-Glacial Marine Deposits off Northeastern Brazil." *Quaternary Research*, 50: 157–166.

Asmus T., Frank M., Kochschmieder C., Frank N., Gersonde R., Kuhn G. and Mangini A. (**1999**). "Variations of biogenic particle flux in the south ern Atlantic section of the Subantarctic zone during the late Quaternary: Evidence from sedimentary $^{231}Pa_{ex}$ and $^{230}Th_{ex}$." *Marine Geology*, 159: 63–78.

Bacon M.P. and Anderson R.F. (**1982**). "Distribution of thorium isotopes between dissolved and particulate forms in the deep ocean." *Journal of Geophysical Research*, 87 (C3): 2045–2056.

Bard E., Rostek F., Turon J.L. and Gendreau S. (**2000**). "Hydrological Impact of Heinrich Events in the Subtropical Northeast Atlantic." *Science*, 289: 1321–1324.

Barker S., Diz P., Vautravers M.J., Pike J., Knorr G., Hall I.R. and Broecker W.S. (**2009**). "Interhemispheric Atlantic seesaw response during the last deglaciation." *Science*, 457: 1097–1102.

Barker S., Knorr G., Vautravers M.J., Diz P. and Skinner L.C. (**2010**). "Extreme deepening of the Atlantic overturning circulation during deglaciation." *Nature Geoscience*, 3: 567–571.

Barnes J.W., Lang E.J. and Potratz H.A. (**1956**). "Ratio of Ionium to Uranium in Coral Limestone." *Science*, 124: 175–176.

Bateman H. (**1910**). "The solution of a system of differential equations occurring in the theory of radio-active transformations." *Proc. Cambridge Phil. Soc*, 15: 423–427.

Baumgartner A. and Reichel E. (**1975**). "Die Weltwasserbilanz. Niederschlag, Verdunstung und Abfluss über Land und Meer sowie auf der Erde im Jahresdurchschnitt." *R. Oldenbourg-Verlag.*

Bayon G., German C.R., Burton K.W., Nesbitt R.W. and Rogers N. (**2004**). "Sedimentary Fe-Mn oxyhydroxides as paleoceanographic archives and the role of aeolian

flux in regulating oceanic dissolved REE." *Earth and Planetary Science Letters*, 224: 477–492.

Begemann F., Ludwig K.R., Lugmair G.W., Min K., Nyquist L.E., Patchett P.J., Renne P.R., Shih C.Y., Villa I.M. and Walker R.J. (**2001**). "Call for an improved set of decay constants for geochronological use." *Geochimica et Cosmochimica Acta*, 65: 111–121.

Bett B.J. (**2001**). "UK Atlantic Margin Environmental Survey: Introduction and overview of bathyal benthic ecology." *Continental Shelf Research*, 21: 917–956.

Birge R.T. (**1932**). "The Calculation of Errors by the Method of Least Squares." *Phys. Rev.*, 40: 207–227.

Board on Health Care Services (**1999**). "Exposure of the American People to Iodine-131 from Nevada Nuclear-Bomb Tests." *National Academy Press*.

Bollhöfer A. (**1996**). "Uranreihen-Datierung diagenetischer Manganknollen mittels Thermionen-Massenspektroskopie (TIMS)." Ph.D. thesis, Ruprecht-Karls-Universität Heidelberg.

Bond G., Broecker W., Johnsen S., McManus J., Labeyrie L., Jouzel J. and Bonani G. (**1993**). "Correlations between climate records from North Atlantic sediments and Greenland ice." *Nature*, 365: 143–147.

Bond G., Heinrich H., Broecker W.S., Labeyrie L., MacManus J., J.Andrews, Huon S., Jantschik R., Clasen S., Simet C., Tedesco K., Klas M., Bonani G. and Ivy S. (**1992**). "Evidence for massive discharges of icebergs into the North Atlantic ocean during the last glacial period." *Nature*, 360: 245–251.

Bourdon B., Henderson G.M., Lundstrom C.C. and Turner S. (**2003**). "Introduction to U-series Geochemistry." *Reviews in Mineralogy and Geochemistry*, 52: 1–21.

Boyle E.A. and Keigwin L. (**1987**). "North Atlantic thermohaline circulation during the past 20000 years linked to high-latitude surface temperature." *Nature*, 330: 35–40.

Boynton W.V. (**1975**). "Fractionation in the solar nebula - Condensation of yttrium and the rare earth elements." *Geochimica et Cosmochimica Acta*, 39: 569–584.

Bradtmiller L.I., Anderson R.F., Fleisher M.Q. and Burckle L.H. (**2007**). "Opal burial in the equatorial Atlantic Ocean over the last 30 ka: Implications for glacial-interglacial changes in the ocean silicon cycle." *Paleoceanography*, 22: 4216.

Broecker W. (**1982**). "Glacial to interglacial changes in ocean chemistry." *Progress in Oceanography*, 11: 151–197.

Broecker W. (**2009**). "The Mysterious ^{14}C Decline." *Radiocarbon*, 51(1): 109–119.

Broecker W. and Barker S. (**2007**). "A 190‰ drop in atmosphere's Δ^{14}C during the 'Mystery Interval'(17.5 to 14.5 kyr)." *Earth and Planetary Science Letters*, 256: 90–99.

Broecker W., Barker S., Clark E., Hajdas I., Bonani G. and Stott L. (**2004**a). "Ventilation of the Glacial Deep Pacific Ocean." *Science*, 306: 1169–1172.

Broecker W., Bond G., Klas M., Clark E. and McManus J. (**1992**). "Origin of the northern Atlantic's Heinrich events." *Climate Dynamics*, 6: 265–273.

Broecker W., Clark E. and Barker S. (**2008**). "Near constancy of the Pacific Ocean surface to mid-depth radiocarbon-age difference over the last 20 kyr." *Earth and Planetary Science Letters*, 274: 322–326.

Broecker W., Clark E., Barker S., Hajdas I., Bonani G. and Moreno E. (**2007**). "Radiocarbon age of late glacial deep water from the equatorial Pacific." *Paleoceanography*, 22: 2206+.

Broecker W.S. (**1991**). "The Great Ocean Conveyor." *Oceanography*, 4(2): 79–89.

Broecker W.S. (**1994**). "Massive iceberg discharges as triggers for global climate change." *Nature*, 372: 421–424.

Broecker W.S., Clark E., Hajdas I. and Bonani G. (**2004**b). "Glacial ventilation rates for the deep Pacific Ocean." *Paleoceanography*, 19: PA2002.

Broecker W.S. and Peng T.H. (**1974**). "Gas exchange rates between air and sea." *Tellus*, 26: 21.

Broecker W.S. and Takahashi T. (**1966**). "Calcium carbonate precipitation on the Bahama Banks." *Journal of Geophysical Research*, 71(6): 1575 – 1602.

Brooke S. and Young C.M. (**2009**). "In situ measurement of survival and growth of *Lophelia pertusa* in the northern Gulf of Mexico." *Marine Ecology Progress Series*, 397: 153–161.

Brown J., Colling A., Park D., Phillips J., Rothery D. and Wright J. (**1989**). "Ocean Circulation." *Pergamon Press, Milton Keynes.*

Bryan S.P., Marchitto T.M. and Lehman S.J. (**2010**). "The release of ^{14}C-depleted carbon from the deep ocean during the last deglaciation: Evidence from the Arabian Sea." *Earth and Planetary Science Letters*, 298: 244–254.

Buddemeier R.W. and Kienze R.A. (**1976**). "Coral growth." *Oceanography and Marine Biology: Annual Review*, 14: 183–225.

Burke A. and Robinson L.F. (**2012**). "The Southern Ocean's Role in Carbon Exchange During the Last Deglaciation." *Science*, 335: 557–561.

Cainelli C., and Mohriak W.U. (**1999**). "Some remarks on the evolution of sedimentary basins along the eastern Brazilian continental margin." *Journal of International Geoscience*, 22: 206–216.

Cairns S.D. (**2007**). "Deep-water corals: an overview with special reference to diversity and distribution of deep-water scleractinian corals." *Bulletin of Marine Science*, 81(3): 311–322.

Cairns S.D. and Stanley G.D.J. (**1981**). "Ahermatypic coral banks: Living and fossil counterparts." *Proceedings of the Fourth International Coral Reef Symposium*, 1: 611–618.

Campos E.J.D., Velhote D. and da Silveira I.C.A. (**2000**). "Shelf break upwelling driven by Brazil Current Cyclonic Meanders." *Geophysical Research Letters*, 27: 751–754.

Chase Z., Anderson R.F., Fleisher M.Q. and Kubik P.W. (**2002**). "The influence of particle composition and particle flux on scavenging of Th, Pa and Be in the ocean." *Earth and Planetary Science Letters*, 204: 215–229.

Chen J.H., Edwards R. and Wasserburg G. (**1986**). "^{238}U, ^{234}U and ^{232}Th in seawater." *Earth and Planetary Science Letters*, 80: 241–251.

Cheng H., Adkins J., Edwards R.L. and Boyle E.A. (**2000**a). "U-Th dating of deep-sea corals." *Geochimica et Cosmochimica Acta*, 64(14): 2401–2416.

Cheng H., Edwards R.L., Hoff J., Gallup C.D., Richards D.A. and Asmerom Y. (**2000**b). "The half-lives of uranium-234 and thorium-230." *Chemical Geology*, 169(1-2): 17–33.

Christner E. (**2011**). "Deglaziale Beschleunigung der Zirkulation und koinzidenter Wassermassenwechsel im äquatorialen Atlantiknull." Master's thesis, Fakultät für Physik und Astronomie, Ruprecht-Karls-Universität Heidelberg.

Ciais P., Tagliabue A., Cuntz M., Bopp L., Scholze M., Hoffmann G., Lourantou A., Harrison S.P., Prentice I.C., Kelley D.I., Koven C. and Piao S.L. (**2012**). "Large inert carbon pool in the terrestrial biosphere during the Last Glacial Maximum." *Nature Geoscience*, 5: 74–79.

Cléroux C., deMenocal P. and Guilderson T. (**2011**). "Deglacial radiocarbon history of tropical Atlantic thermocline waters: absence of CO_2 reservoir purging signal." *Quaternary Science Reviews*, 30: 1875–1882.

Colin C., Frank N., Copard K. and Douville E. (**2010**). "Neodymium isotopic composition of deep-sea corals from the NE Atlantic: implications for past hydrological changes during the Holocene." *Quaternary Science Reviews*, 29: 2509–2517.

Copard K., Colin C., Douville E., Freiwald A., Gudmundsson G., De Mol B. and Frank N. (**2010**). "Nd isotopes in deep-sea corals in the North-eastern Atlantic." *Quaternary Science Reviews*, 29: 2499–2508.

Craig H. (**1953**). "The geochemistry of the stable carbon isotopes." *Geochimica et Cosmochimica Acta*, 3: 53–92.

Currie L.A. (**2004**). "The Remarkable Metrological History of Radiocarbon Dating [II]." *Journal of Research of the National Institute of Standards and Technology*, 109(2): 185–217.

Curry W.B. and Oppo D.W. (**2005**). "Glacial water mass geometry and the distribution of δ^{13}C of ΣCO_2 in the western Atlantic Ocean." *Paleoceanography*, 20: 1–12.

Cutler K.B., Edwards R.L., Taylor F.W., Cheng H., Adkins J., Gallup C.D., Cutler P.M., Burr G.S. and Bloom A.L. (**2003**). "Rapid sea-level fall and deep-ocean temperature change since the last interglacial period." *Earth and Planetary Science Letters*, 206: 253–271.

da Silveira I.M.O. (**1999**). "Phosphor in den Sedimenten der brasilianischen Mangroven- und Schelfgebiete zwischen 15 °S und 20 °S." Ph.D. thesis, Universität Hamburg.

Damon P.E., Lerman J.C. and Long A. (**1978**). "Temporal Fluctuations of Atmospheric ^{14}C: Causal Factors and Implications." *Annual Review Earth Planetary Science*, 6: 457–494.

Dando P.R., Austen M.C., Burker R.A., Kendall M.A., Kennicutt M.C., Judd A.G., Moore D.C., O'Hara S.C.M., Schmaljohann R. and Southward A.J. (**1991**). "Ecology of a North Sea pockmark with an active methane seep." *Marine Ecology Progress Series*, 70: 49–63.

de Mahiques M.M., Bícego M.C., Silveira I.C.A., Sousa S.H.M., Lourenço R.A. and Fukumoto M.M. (**2005**). "Modern sedimentation in the Cabo Frio upwelling system, Southeastern Brazilian shelf." *Anais da Academia Brasileira de Ciências*, 77(3): 535–548.

de Mahiques M.M., de Mello e Sousa S.H., Furtado V.V., Tessler M.G., de Lima Toledo F.A., Burone L., Figueira R.C.L., Klein D.A., Martins C.C. and Alves D.P.V. (**2010**). "The southern Brazilian shelf: general characteristics, Quaternary evolution and sediment distribution." *Brazilian Journal of Oceanography*, 58 (special issue): 25–34.

de Mahiques M.M., Silveira I.C.A., Sousa S.H.M. and Rodrigues M. (**2002**). "Post-LGM sedimentation on the outer shelf-upper slope of the northernmost part of the São Paulo Bight, southeastern Brazil." *Marine Geology*, 181: 387–400.

de Pol-Holz R., Keigwin L., Southon J., Hebbeln D. and Mohtadi M. (**2010**). "No signature of abyssal carbon in intermediate waters off Chile during deglaciation." *Nature Geoscience*, 3: 192–195.

de Vries H.L. (**1958**). "Variation in concentration of radiocarbon with time and location on Earth." *Royal Netherlands Academy of Arts and Sciences*: 94–102.

Delanghe D., Bard E. and Hamelin B. (**2002**). "New TIMS constraints on the uranium-

238 and uranium-234 in seawaters from the main ocean basins and the Mediterranean Sea." *Marine Chemistry*, 80: 79–93.

DeMol B.S.G., van Rensbergen P., Pillen S., van Herreweghe K., Rooij D.V., McDonnell A., Huvenne V.A.I., Ivanov M.K., Swennen R. and Henriet J.P. (**2002**). "Large deep-water coral banks in the Porcupine Basin, southwest of Ireland." *Marine Geology*, 188: 193–231.

Denton G.H., Anderson R.F., Toggweiler J.R., Edwards R.L., Schaefer J.M. and Putnam A.E. (**2010**). "The Last Glacial Termination." *Science*, 328: 1652–1656.

DePaolo D.J. and Wasserburg G.J. (**1976**). "Nd Isotopic Variations and Petrogenetic Models." *Geophysical Research Letters*, 3(5): 249–252.

Dickson R.R. and Brown J. (**1994**). "The production of North Atlantic Deep Water: Sources, rates, and pathways." *Journal of Geophysical Research*, 99: 12319–12342.

Dodds L.A., Roberts J.M. and Marubini A.C.T.F. (**2007**). "The cold-water coral Lophelia pertusa (Scleractinia) reveals metabolic tolerance to temperature and dissolved oxygen change." *Journal of Experimental Marine Biology and Ecology*, 349: 205–214.

Druffel E.R.M., King L.L., Belastock R.A. and Buesseler K.O. (**1990**). "Growth rate of a deep-sea coral using ^{210}Pb and other isotopes." *Geochimica et Cosmochimica Acta*, 54: 1493–1499.

Dullo W.C., Flögel S. and Rüggeberg A. (**2008**). "Cold-water coral growth in relation to the hydrography of the Celtic and Nordic European continental margin." *Marine Ecology Progress Series*, 371: 165–176.

Duplessy J.C., Shackleton N., Fairbanks R.G., Labeyrie L.., Oppo D. and Kallel N. (**1988**). "Deepwater Source Variations During The Last Climate Cycle And Their Impact On The Global Deepwater Circulation." *Paleoceanography*, 3(3): 343–360.

Edwards R.L., Chen J.H. and Wasserburg G.J. (**1986/87**). "^{238}U, ^{234}U, ^{232}Th systematics and the precise measurement of time over the past 500,000 years." *Earth and Planetary Science Letters*, 81: 175–192.

Elliot M. (**2002**). "Changes in North Atlantic deep-water formation associated with the Dansgaard Oeschger temperature oscillations (10−60 ka)." *Quaternary Science Reviews*, 21: 1153–1165.

Elsig J., Schmitt J., Leuenberger D., Schneider R., Eyer M., Leuenberger M., Joos F., Fischer H. and Stocker T.F. (**2009**). "Stable isotope constraints on Holocene carbon cycle changes from an Antarctic ice core." *Nature*, 461: 507–514.

Emiliani C. (**1955**). "Pleistocene Temperatures." *The Journal of Geology*, 63(6): 538–577.

Epstein S., Buchsbaum R., Lowenstam H. and Urey H.C. (**1953**). "Revised

carbonate-water isotopic temperature scale." *Geological Society of America Bulletin*, 64: 1315–1326.

Ericson D.B. and Wollin G. (**1968**). "Pleistocene Climates and Chronology in Deep-Sea Sediments." *Science*, 162: 1227–1234.

Esat T.M. and Yokoyama Y. (**2006**). "Variability in the uranium isotopic composition of the oceans over glacial interglacial timescales." *Geochimica et Cosmochimica Acta*, 70: 4140–4150.

Evans D.L., Signorini S.R. and Miranda L.B. (**1983**). "A Note on the Transport of the Brazil Current." *Journal of Physical Oceanography*, 13: 1732–1738.

Ferrell R.E. and Aharon P. (**1994**). "Mineral assemblages occurring around hydrocarbon vents in the northern Gulf of Mexico." *Geo-Marine Letters*, 14: 74–80.

Figueiredo A.G.J., Brehme I., Barbosa K.F., Neto J.A.B. and Silva C.G. (**1999**). "Sea-floor depressions in Parana continental shelf, Santos Basin." *6th International Congress of the Brazilian Geophysical Society Extended Abstracts, Rio de Janeiro*: 5pp.

Francois R., Altabet M.A., Yu E.F., Sigman D.M., Bacon M.P., Frank M., Bohrmann G., Bareille G. and Labeyrie L.D. (**1997**). "Contribution of Southern Ocean surface-water stratification to low atmospheric CO_2 concentrations during the last glacial period." *Nature*, 389: 929–935.

Frank M. (**2002**). "Radiogenic Isotopes: Tracers of Past Ocean Circulation and Erosional Input." *Reviews of Geophysics*, 40(1): 1–38.

Frank N. (**1997**). "Anwendung der Thermionen-Massenspektrometrie zur Uranreihen-Datierung pleistozäner, mitteleuropäischer Travertinvorkommen." Ph.D. thesis, Ruprecht-Karls-Universität Heidelberg.

François R. (**2007**). "Paleoflux and Paleocirculation from Sediment ^{230}Th and ^{231}Pa/^{230}Th." *publ. in Proxies in Late Cenozoic Paleoceanography (Developments in Marine Geology), Elsevier*, 1: 681–716.

Freiwald A. (**2002**). "Reef-forming cold-water corals. In: Ocean Margin Systems (eds. G. Wefer, D. Billett, D. Hebbeln, B. B. Jørgensen, M. Schlüter, T. C. E. van Weering)." *Springer, Heidelberg*: 365–385.

Freiwald A., Fosså J.H., Grehan A., Koslow T. and Roberts J.M. (**2004**). "Cold-water coral reefs." *UNEP World Conservation Monitoring Centre (WCMC).*

Freiwald A. and Roberts J.M. (**2005**). "Cold-Water Corals and Ecosystems." *Springer-Verlag, Heidelberg.*

Froehlich K. (**2010**). "Environmental Radionuclides, Tracers and Timers of Terrestrial Processes." *Radioactivity in the Environment Series Editor M.S. Baxter*, 16.

Fukamachi Y., Rintoul S.R., Church J.A., Aoki S., Sokolov S., Rosenberg M.A. and M.Wakatsuchi (**2010**). "Strong export of Antarctic BottomWater east of the Kerguelen plateau." *Nature Geoscience*, 3: 327–331.

Galbraith E.D., Jaccard S.L., Pedersen T.F., Sigman D.M., Haug G.H., Cook M., Southon J.R. and Francois R. (**2007**). "Carbon dioxide release from the North Pacific abyss during the last deglaciation." *Nature*, 449: 890–894.

Gallup C.D., Edwards L.R. and Johnson R.G. (**1994**). "The timing of high sea levels over the past 200,000 years." *Science*, 263: 796–800.

Ganachaud A. and Wunsch C. (**2000**). "Improved estimates of global ocean circulation, heat transportandmixing from hydrographic data." *Nature*, 408: 453–457.

Garfield N. (**1990**). "The Brazil Current at Subtropical Latitudes." Ph.D. thesis, University of Rhode Island.

Gattuso J.P., Allemand D. and Frankignoulle M. (**1999**). "Photosynthesis and calcification at cellular, organismal and community levels in coral reefs: A review on interactions and control by carbonate chemistry, 39, 160–183, 1999." *American Zoologist*, 39: 160–183.

Geibert W. and Usbeck R. (**2004**). "Adsorption of thorium and protactinium onto different particle types: experimental findings." *Geochimica et Cosmochimica Acta*, 68: 1489–1501.

Gersonde R., Abelmann A., Brathauer U., Becquey S., Bianchi C., Cortese G., Grobe H., Kuhn G., Niebler H.S., Segl M., Sieger R., Zielinski U. and Fütterer D.K. (**2003**). "Last glacial sea surface temperatures and sea-ice extent in the Southern Ocean (Atlantic-Indian sector): A multiproxy approach." *Paleoceanography*, 18: 1061.

Geyh M.A. and Schleicher H. (**1990**). "Absolute age determination. Physical and chemical dating methods and their application." *Springer-Verlag. Berlin.*

Gherardi J.M., Labeyrie L., Nave S., Francois R., McManus J.F. and Cortijo E. (**2009**). "Glacial-interglacial circulation changes inferred from ^{231}Pa/^{230}Th sedimentary record in the North Atlantic region." *Paleoceanography*, 24: 1–14.

Goff-Vitry M.C.L., Rogers A.D. and Baglow D. (**2004**). "A deep-sea slant on the molecular phylogeny of the Scleractinia." *Molecular Phylogenetics and Evolution*, 30: 167–177.

Goldstein S.L. and Hemming S.R. (**2003**). "Long-lived Isotopic Tracers in Oceanography, Paleoceanography, and Ice-sheet Dynamics." *Elsevier, Treatise on Geochemistry, Editor: Henry Elderfield*, 6: 453–489.

Grootes P.M., Stuiver M., White J.W.C., Johnsen S. and Jouzel J. (**1993**).

"Comparison of oxygen isotope records from the GISP2 and GRIP Greenland ice cores." *Nature*, 366: 552–554.

Grousset F.E., Pujol C., Labeyrie L., Auffret G. and Boelaert A. (**2000**). "Were the North Atlantic Heinrich events triggered by the behavior of the European ice sheets?" *Geology*, 28: 123–126.

Gutjahr M., Frank M., Stirling C.H., Klemm V., van de Flierdt T. and Halliday A.N. (**2007**). "Reliable extraction of a deepwater trace metal isotope signal from Fe–Mn oxyhydroxide coatings of marine sediments." *Chemical Geology*, 242: 351–370.

Gutjahr M. and Lippold J. (**2011**). "Early arrival of Southern Source Water in the deep North Atlantic prior to Heinrich event 2." *Paleoceanography*, 26(26): PA2101.

Gvirtzman G., Friedman G.M. and Miller D.S. (**1973**). "Control and distribution of Uranium in coral reefs during diagenesis." *Journal of Sedimentary Research*, 43(4): 985–997.

Hain M.P., Sigman D.M. and Haug G.H. (**2011**). "Shortcomings of the isolated abyssal reservoir model for deglacial radiocarbon changes in the mid-depth Indo-Pacific Ocean." *Geophysical Research Letters*, 38: 4604.

Haley B.A., Klinkhammer G.P. and McManus J. (**2004**). "Rare earth elements in pore waters of marine sediments." *Geochimica et Cosmochimica Acta*, 68: 1265–1279.

Harkness D.D. (**1970**). "Artificial carbon-14, a tracer for carbon in the atmosphere and biosphere." Ph.D. thesis, University of Glasgow.

Harkness D.D. and Wilson H.W. (**1979**). "Scottish Universities Research and Reactor Centre Radiocarbon Measurements III." *Radiocarbon*, 21(2): 203–256.

Hartin C.A., Fine R.A., Sloyan B.M., Talley L.D., Chereskin T.K. and Happell J. (**2011**). "Formation rates of Subantarctic mode water and Antarctic intermediate water within the South Pacific." *Deep Sea Research Part I: Oceanographic Research*, 58: 524–534.

Haug G.H., Hughen K.A., Sigman D.M., Peterson L.C. and Röhl U. (**2001**). "Southward Migration of the Intertropical Convergence Zone Through the Holocene." *Science*, 293: 1304–1308.

Heinrich H. (**1988**). "Origin and Consequences of Cyclic Ice Rafting in the Northeast Atlantic Ocean during the Past 130,000 Years." *Quaternary Research*, 29: 142–152.

Hemming S.R. (**2004**). "Heinrich Events: Massive Late Pleistocene Detritus Layers of the North Atlantic and their Global Climate Imprint." *Reviews of Geophysics*, 42: 1–43.

Henderson G., Cohen A. and O'Nions R. (**1993**). "$^{234}U/^{238}U$ ratios and ^{230}Th ages for Hateruma Atoll corals: implications for coral diagenesis and seawater $^{234}U/^{238}U$ ratios." *Earth and Planetary Science Letters*, 115: 65–73.

Henderson G.M. (**2002**). "Seawater $^{234}U/^{238}U$ during the last 800 thousand years." *Earth and Planetary Science Letters*, 199: 97–110.

Henderson G.M., Heinze C., Anderson R.F. and Winguth A.M.E. (**1999**). "Global distribution of the ^{230}Th flux to ocean sediments constrained by GCM modelling." *Deep-Sea Research Part I*, 46: 1861–1893.

Henrich R., Freiwald A. and the Shipboard Party (**1997**). "The Lophelia reef of Sula ridge, mid-Norwegian shelf." *Cruise report No 228/97, Bremerhaven*: 12pp.

Hovland M. (**2008**). "Deep-water Coral Reefs: Unique Biodiversity Hot-Spots." *Springer, Heidelberg*: 300pp.

Hovland M., Judd A.G. and Jr. R.A.B. (**1993**). "The Global Flux Of Methane From Shallow Submarine Sediments." *Chemosphere*, 26(1-4): 559–578.

Hovland M., Vasshus S., Indreeide A., Austdal L. and Øivind Nilsen (**2002**). "Mapping and imaging deep-sea coral reefs off Norway, 1982–2000." *Hydrobiologia*, 471: 13–17.

Indermühle A., Monnin E., Stauffer B., Stocker T.F. and Wahlen M. (**2000**). "Atmospheric CO_2 concentration from 60 to 20 kyr BP from the Taylor Dome ice core, Antarctica." *Geophysical Research Letters*, 27(5): 735–738.

Iudicone D., Speich S., Madec G. and Blanke B. (**2008**). "The Global Conveyor Belt from a Southern Ocean Perspective." *Journal of Physical Oceanography*, 38: 1401.

Ivanovich M. and Harmon R. (**1992**). "Uranium-series disequilibrium." *Clarendon Press.*

Jacobsen S.B. and Wasserburg G.J. (**1980**). "Sm-Nd isotopic evolution of chondrites." *Earth and Planetary Science Letters*, 50: 139–155.

Jaeschke A., Rühlemann C., Arz H., Heil G. and Lohmann G. (**2007**). "Coupling of millennial-scale changes in sea surface temperature and precipitation off northeastern Brazil with high-latitude climate shifts during the last glacial period." *Paleoceanography*, 22: 1–10.

Jeandel C. (**1993**). "Concentration and isotopic composition of Nd in the South Atlantic Ocean." *Earth and Planetary Science Letters*, 117: 581–591.

Jeandel C., Arsouze T., Lacan F., Téchiné P. and Dutay J.C. (**2007**). "Isotopic Nd compositions and concentrations of the lithogenic inputs into the ocean: A compilation, with an emphasis on the margins." *Chemical Geology*, 239: 156–164.

Jeandel C., Bishop J.K. and Zindler A. (**1995**). "Exchange of neodymium and its isotopes between seawater and small and large particles in the Sargasso Sea." *Geochimica et Cosmochimica Acta*, 59: 535–547.

Johnson D.A. (**2007**). "Regional Oceanographic Setting of the Southwestern Atlantic." *Deep Sea Drilling Project Reports and Publications*, LXXII: 15–35.

Jouzel J., Masson-Delmotte V., Cattani O., Dreyfus G., Falourd S., Hoffmann G., Minster B., Nouet J., Barnola J.M., Chappellaz J., Fischer H., Gallet J.C., Johnsen S., Leuenberger M., Loulergue L., Luethi D., Oerter H., Parrenin F., Raisbeck G., Raynaud D., Schilt A., Schwander J., Selmo E., Souchez R., Spahni R., Stauffer B., Steffensen J.P., Stenni B., Stocker T.F., Tison J.L., Werner M. and Wolff E.W. (**2007**). "Orbital and Millennial Antarctic Climate Variability over the Past 800,000 Years." *Science*, 317: 793–796.

Keigwin L.D. (**2004**). "Radiocarbon and stable isotope constraints on Last Glacial Maximum and Younger Dryas ventilation in the western North Atlantic." *Paleoceanography*, 19: 1–15.

Keigwin L.D. and Boyle E.A. (**2008**). "Did North Atlantic overturning halt 17,000 years ago?" *Paleoceanography*, 23: 1–5.

Keigwin L.D., Curry W.B., Lehman S.J. and Johnsen S. (**1994**). "The role of the deep ocean in North Atlantic climate change between 70 and 130 kyr ago." *Nature*, 371: 323–326.

Keigwin L.D. and Lehman S.J. (**1994**). "Deep circulation change linked to HEINRICH Event 1 and Younger Dryas in a middepth North Atlantic Core." *Paleoceanography*, 9: 185–194.

Keigwin L.D. and Schlegel M.A. (**2002**). "Ocean ventilation and sedimentation since the glacial maximum at 3 km in the western North Atlantic." *Geochemistry Geophysics Geosystems*, 3(6): 1–14.

Keller N.B. (**1976**). "The deep-sea madreporarian corals of the genus Fungiacyathus from the Kurile-Kamchatka, Aleutian trenches and other regions of world oceans. Trudy Instituta Okeanologii, 99, pp. 31-." *Trudy Instituta Okeanologii*, 99: 31–44.

Key R.M., Kozyr A., Sabine C.L., Lee K., Wanninkhof R., Bullister J.L., Feely R.A., Millero F.J., Mordy C. and Peng T. (**2004**). "A global ocean carbon climatology: Results from Global Data Analysis Project (GLODAP)." *Global Biogeochemical Cycles*, 18: 1–23.

Kigoshi K. (**1971**). "Alpha-Recoil Thorium-234: Dissolution into Water and the Uranium-234/Uranium-238 Disequilibrium in Nature." *Science*, 173: 47–48.

Killworth P.D. (**1983**). "Deep Convection in the World Ocean." *Reviews of Geophysics nad Space Physics*, 21(1): 1–26.

Kirby M.E.. and Andrews J.T. (**1999**). "Mid-Wisconsin Laurentide Ice Sheet growth and decay: Implications for Heinrich events 3 and 4." *Paleoceanography*, 14(2): 211–223.

Kitahara M.V. (**2007**). "Species richness and distribution of azooxanthellate scleractinia in Brazil." *Bulletin of Marine Science*, 81(3): 497–518.

Knorr G. and Lohmann G. (**2007**). "Rapid transitions in the Atlantic thermohaline circulation triggered by global warming and meltwater during the last deglaciation." *Geochemistry, Geophysics, Geosystems*, 8: 12006.

Koczy F.F., Picciotto E., Poulaert G. and Wilgain S. (**1957**). "Mesure des isotopes du thorium dans l'eau de mer." *Geochimica et Cosmochimica Acta*, 11: 103–129.

Korff S.A. and Clarke E.T. (**1942**). "The Production of Neutrons and Protons by the Cosmic Radiation at 14,125 Feet." *Physical Review*, 61: 422–427.

Kretschmer S., Geibert W., Schnabel C., Rutgers van der Loeff M. and Mollenhauer G. (**2008**). "Distribution of ^{230}Th, ^{10}Be and ^{231}Pa in sediment particle classes." *Geochimica et Cosmochimica Acta Supplement*, 72: 498.

Kroopnick P. (**1980**). "The distribution of ^{13}C in the Atlantic Ocean." *Earth and Planetary Science Letters*, 49: 469–484.

Kroopnick P. (**1985**). "The distribution of ^{13}C of ΣCO_2 in the world oceans." *Deep Sea Research Part I: Oceanographic Research*, 32: 57–84.

Ku T. (**1977**). "Uranium in open ocean: concentration and isotopic composition." *Deep Sea Research Part II: Topical Studies in Oceanography*, 24: 1005–1017.

Ku T.L. (**1965**). "An Evaluation of the ^{234}U/^{238}U Method as a Tool for Dating Pelagic Sediments." *Journal of Geophysical Research*, 70: 3457–3474.

Kuhlbrodt T., Griesel A., Montoya M., Levermann A., Hofmann M. and Rahmstorf S. (**2007**). "On The Driving Processes Of The Atlantic Meridional Overturning Circulation." *Reviews of Geophysics*, 45: 1–32.

Kumar N., Anderson R.F., Mortlock R.A., Froelich P.N., Kubik P., Dittrich-Hannen B. and Suter M. (**1995**). "Increased biological productivity and export production in the glacial Southern Ocean." *Nature*, 378: 675–680.

Labeyrie L. (**1992**). "Changes in the vertical structure of the North Atlantic Ocean between glacial and modern times." *Quaternary Science Reviews*, 11: 401–413.

Lacan F. and Jeandel C. (**2004**). "Denmark Strait water circulation traced by heterogeneity in neodymium isotopic compositions." *Deep Sea Research Part I: Oceanographic Research*, 51: 71–82.

Lacan F. and Jeandel C. (**2005**). "Neodymium isotopes as a new tool for quantifying exchange fluxes at the continent ocean interface." *Earth and Planetary Science Letters*, 232: 245–257.

Laj C., Kissel C., Mazaud A., Michel E., Muscheler R. and Beer J. (**2002**).

"Geomagnetic field intensity, North Atlantic Deep Water circulation and atmospheric Δ^{14}C during the last 50 kyr." *Earth and Planetary Science Letters*, 200: 177–190.

Lal D. and Peters B. (**1967**). "Cosmic ray produced radioactivity on the Earth." *In Handbook of physics, Springer*, 46/2: 551–612.

Langmuir D. (**1978**). "Uranium Solution-Mineral Equilibria at low Temperatures with Applications to Sedimentary Ore Deposits." *Geochimica et Cosmochimica Acta*, 42: 547–569.

Lazar B., Enmar R., Schossberger M., Bar-Matthews M., Halicz L. and Stein M. (**2004**). "Diagenetic effects on the distribution of uranium in live and Holocene corals from the Gulf of Aqaba." *Geochimica et Cosmochimica Acta*, 68: 4583–4593.

Lazier A.V., Smith J.E., Risk M.J. and Schwarcz H.P. (**1999**). "The skeletal structure of Desmophyllum cristagalli: the use of deepwater corals in sclerochronology." *Lethaia*, 32: 119–130.

Levin I. and Hesshaimer V. (**2000**). "Radiocarbon – A Unique Tracer Of Global Carbon Cycle Dynamics." *Radiocarbon*, 42(1): 69–80.

Lima J.A.M. (**1992**). "Modelo de circulação oceânica da Bacia de Campos." *PETROBRAS Internal Report Cenpes/Supen/Sepron 051/92, Rio de Janeiro*: 70pp.

Lippold J. (**2008**). "Die Anwendung des ^{231}Pa/^{230}Th Verhältnisses zur Rekonstruktion der Atlantischen Zirkulation." Ph.D. thesis, Ruprecht-Karls-Universität Heidelberg.

Lippold J., Grützner J., Winter D., Lahaye Y., Mangini A. and Christl M. (**2009**). "Does sedimentary ^{231}Pa/^{230}Th from the Bermuda Rise monitor past Atlantic Meridional Overturning Circulation?" *Geophysical Research Letters*, 36: 1–6.

Lippold J., Luo Y., Francois R., Allen S.E., Gherardi J., Pichat S., Hickey B. and Schulz H. (**2012**). "Strength and geometry of the glacial Atlantic Meridional Overturning Circulation." *Nature Geoscience*, 5: 813–816.

Lomitschka M. (**1999**). "Untersuchungen zur Th/U und Pa/U Datierbarkeit von Tiefseekorallen und Pteropoden: Berechnung von Tiefenwasseralter im Nordatlantik." Ph.D. thesis, Universität Heidelberg.

Lomitschka M. and Mangini A. (**1999**). "Precise Th/U-dating of small and heavily coated samples of deep sea corals." *Earth and Planetary Science Letters*, 170: 391–401.

Lynch-Stieglitz J., Adkins J.F., Curry W.B., Dokken T., Hall I.R., Herguera J.C., Hirschi J.J.M., Ivanova E.V., Kissel C., Marchal O., Marchitto T.M., McCave I.N., McManus J.F., Mulitza S., Ninnemann U., Peeters F., Yu E.F. and Zahn R. (**2007**). "Atlantic Meridional Overturning Circulation During the Last Glacial Maximum." *Science*, 316: 66–69.

MacAyeal D.R. (**1993**). "Binge/Purge Oscillations of the Laurentide Ice Sheet as a Cause of the North Atlantic's Heinrich Events." *Paleoceanography*, 8(6): 775–784.

Manabe S. and Stouffer R.J. (**1993**). "Century-scale effects of increased atmospheric CO2 on the ocean-atmosphere system." *Nature*, 364: 215–218.

Manabe S. and Stouffer R.J. (**1997**). "Coupled ocean-atmosphere model response to freshwater input: Comparison to Younger Dryas event." *Paleoceanography*, 12: 321–336.

Mangini A., Godoy J., Godoy M., Kowsmann R., Santos G., Ruckelshausen M., Schröder-Ritzrau A. and Wacker L. (**2010**). "Deep sea corals off Brazil verify a poorly ventilated Southern Pacific Ocean during H2, H1 and the Younger Dryas." *Earth and Planetary Science Letters*, 293: 269–276.

Mangini A., Lomitschka M., Eichstädter R., Frank N., Vogler S., Bonani G., Hajdas I. and Patzold J. (**1998**). "Coral provides way to age deep water." *Nature*, 392: 347–348.

Mangini A., Sonntag C., Bertsch G. and Müller E. (**1979**). "Evidence for a higher natural uranium content in world rivers." *Nature*, 278: 337–339.

Marchitto T.M., Lehman S.J., Ortiz J.D., Flückiger J. and van Geen A. (**2007**). "Marine Radiocarbon Evidence for the Mechanism of Deglacial Atmospheric CO_2 Rise." *Science*, 316: 1456–1459.

Masarik J. and Beer J. (**2009**). "An updated simulation of particle fluxes and cosmogenic nuclide production in the Earth's atmosphere." *Journal of Geophysical Research (Atmospheres)*, 114: 11103+.

Matsumoto K. and Key R.M. (**2004**). "Natural Radiocarbon Distribution in the Deep Ocean." *Global Environmental Change in the Ocean and on Land, Eds.*

McCrea J.M. (**1950**). "On the Isotopic Chemistry of Carbonates and a Paleotemperature Scale." *The Journal of Chemical Physics*, 18(6): 849–857.

McGregor H.V. and Gagan M.K. (**2003**). "Diagenesis and geochemistry of porites corals from Papua New Guinea - Implications for paleoclimate reconstruction." *Geochimica et Cosmochimica Acta*, 67: 2147–2156.

McManus J.F., Francois R., Gherardi J.M., Keigwin L.D. and Brown-Leger S. (**2004**). "Collapse and rapid resumption of Atlantic meridional circulation linked to deglacial climate changes." *Nature*, 428: 834–837.

Mikkelsen N., Erlenkeuser H., Killingley J.S. and Berger W.H. (**1982**). "Norwegian corals: radiocarbon and stable isotopes in Lophelia pertusa." *Boreas*, 11: 163–171.

Miller D.J. and Kowsmann R.O. (**2009**). "Occurrence of Authigenic Carbonate Chimneys and Crusts in the Campos Basin Continental Slope - SE Brazil." *Abstract, AAPG International Conference and Exhibition, Rio de Janeiro.*

Mohriak W.U., Mello M.R., Dewey J.F. and Maxwell J.R. (**1990**). "Petroleum geology of the Campos Basin, offshore Brazil." *Geological Society, London, Special Publications*, 50: 119–141.

Monnin E., Indermühle A., Dällenbach A., Flückiger J., Stauffer B., Stocker T.F., Raynaud D. and Barnola J. (**2001**). "Atmospheric CO_2 Concentrations over the Last Glacial Termination." *Science*, 291: 112–114.

Monnin E., Steig E.J., Siegenthaler U., Kawamura K., Schwander J., Stauffer B., Stocker T.F., Morse D.L., Barnola J.M., Bellier B., Raynaud D. and Fischer H. (**2004**). "Evidence for substantial accumulation rate variability in Antarctica during the Holocene, through synchronization of CO_2 in the Taylor Dome, Dome C and DML ice cores." *Earth and Planetary Science Letters*, 224: 45–54.

Mook W.G. and de Vries J.J. (**2000**). "Environmental Isotopes in the Hydrological Cycle, Principles and Applications." *Volume 1: Introduction - Theory, Methods, Review IAEA*.

Moore D.M. and Reynolds R.C.J. (**1989**). "X-ray Diffraction and the Identification and Analysis of Clay Minerals." *Oxford University Press*: 332pp.

Moore W.S. (**1981**). "The thorium isotope content of ocean water." *Earth and Planetary Science Letters*, 53: 419–426.

Moore W.S. and Sackett W.M. (**1964**). "Uranium and Thorium Series Inequilibrium in Sea Water." *Journal of Geophysical Research*, 69: 5401–5405.

Moran S.B., Charette M.A., Hoff J.A., Edwards R.L. and Landing W.M. (**1997**). "Distribution of ^{230}Th in the Labrador Sea and its relation to ventilation." *Earth and Planetary Science Letters*, 150: 151–160.

Mortensen P.B. and Rapp H.T. (**1998**). "Oxygen and carbon isotope ratios related to growth line patterns in skeletons of Lophelia pertusa (L) (Anthozoa, Scleractinia): Implications for determination of linear extension rates." *Sarsia*, 83: 433–446.

Müller T.J., Ikeda Y., Zangenberg N. and Nonato L.V. (**1998**). "Direct measurements of western boundary currents off Brazil between 20 °S and 28 °S." *Journal of Geophysical Research*, 103: 5429–5438.

Mursula K. and Usoskin I. (**2003**). "Heliospheric Physics and Cosmic Rays." *Lecture notes*: 1–168.

Muscheler R., Beer J., Wagner G., Laj C., Kissel C., Raisbeck G.M., Yiou F. and Kubik P.W. (**2004**). "Changes in the carbon cycle during the last deglaciation as indicated by the comparison of ^{10}Be and ^{14}C records." *Earth and Planetary Science Letters*, 219: 325–340.

Neff U. (**2001**). "Massenspektrometrische Th/U-Datierung von Höhlensintern aus dem

Oman: Klimaarchive des asiatischen Monsuns." Ph.D. thesis, Ruprecht-Karls-Universität Heidelberg.

Nier A.O. (**1950**). "A redetermination of the relative abundances of the isotopes of carbon, nitrogen, oxygen, argon and potassium." *Physical Review*, 77: 789–793.

Ninnemann U.S. and Charles C.D. (**1997**). "Regional differences in quaternary Subantarctic nutrient cycling: Link to intermediate and deep water ventilation." *Paleoceanography*, 12: 560–567.

Nozaki Y., Yang H.S. and Yamada M. (**1987**). "Scavenging of thorium in the ocean." *Journal of Geophysical Research*, 92 (C1): 772–778.

Olson D.B., Podesta G., Evans R.H. and Brown O.B. (**1988**). "Temporal variations in the separation of Brazil and Malvinas currents." *Deep-Sea Research*, 35(12): 1971–1990.

O'Nions R.K., Carter S.R., Evensen N.M. and Hamilton P.J. (**1979**). "Geochemical and cosmochemical applications of Nd isotope analysis." *Annual Review Earth Planetary Science*, 7: 11–38.

Oppo D.W. and Horowitz M. (**2000**). "Glacial deep water geometry: South Atlantic benthic foraminiferal Cd/Ca and δ^{13}C evidence." *Paleoceanography*, 15(2): 147–160.

Orsi A., Whitworth T. and Nowlin W. (**1995**). "On the meridional extent and fronts of the Antarctic Circumpolar Current." *Deep Sea Research Part I: Oceanographic Research*, 42: 641–673.

Ostlund G., Craig H., Broecker W.S. and Spencer D. (**1987**). "GEOSECS Atlantic, Pacific and Indian Ocean Expeditions, Shorebased Data and Graphics." *U.S. Government Printing Office, Washington, DC*, vol. 7.

O'Brien K. (**1979**). "Secular variations in the production of cosmogenic isotopes in the Earth's atmosphere." *Journal of Geophysical Research*, 84: 423–431.

Pahnke K., Goldstein S.L. and Hemming S.R. (**2008**). "Abrupt changes in Antarctic Intermediate Water circulation over the past 25,000 years." *Nature Geoscience*, 1: 870–874.

Peckmann J., Reimer A., Luth U., Luth C., Hansen B.T., Heinicke C., Hoefs J. and Reitner J. (**2001**). "Methane-derived carbonates and authigenic pyrite from the northwestern Black Sea." *Marine Geology*, 177: 129–150.

Piepgras D.J. and Wasserburg G.J. (**1980**). "Neodymium Isotopic Variations In Seawater." *Earth and Planetary Science Letters*, 50: 128–138.

Piepgras D.J. and Wasserburg G.J. (**1987**). "Rare earth element transport in the western North Atlantic inferred from Nd isotopic observations." *Geochimica et Cosmochimica Acta*, 51: 1257–1271.

Pilcher R. and Argent J. (**2007**). "Mega-pockmarks and linear pockmark trains on the West African continental margin." *Marine Geology*, 244: 15–32.

Pin C. and Zalduegui J.F.S. (**1997**). "Sequential separation of light rare-earth elements, thorium and uranium by miniaturized extraction chromatography: Application to isotopic analyses of silicate rocks." *Analytica Chimica Acta*, 339(1-2): 79–89.

Polzin K.L., Toole J.M., Ledwell J.R. and W.Schmitt R. (**1997**). "Spatial Variability of Turbulent Mixing in the Abyssal Ocean." *Science*, 276(5309): 93–96.

Rahmstorf S. (**1996**). "On the freshwater forcing and transport of the Atlantic thermohaline circulation." *Climate Dynamics*, 12: 799–811.

Rahmstorf S. (**2002**). "Ocean circulation and climate during the past 120,000 years." *Nature*, 419: 207–214.

Randall D.A., Wood R.A., Bony S., Colman R., Fichefet T., Fyfe J., Kattsov V., Pitman A., Shukla J., Srinivasan J., fer R.J.S., Sumi A. and Taylor K.E. (**2007**). "Cilmate Models and Their Evaluation." *In: Climate Change 2007: The Physical Science Basis. Contribution of Working Group I to the Fourth Assessment Report of the Intergovernmental Panel on Climate Change*, Cambridge University Press: 589–662.

Rao V.B., de Lima M.C. and Franchito S.H. (**1993**). "Seasonal and Interannual Variations of Rainfall over Eastern Northeast Brazil." *Journal of Climate*, 6: 1754–1763.

Reeder R.J., Nugent M., Tait C.D., Morris D.E., Heald S.M., Beck K.M., Hess W.P. and Lanzirotti A. (**2001**). "Coprecipitation of Uranium(VI) with Calcite: XAFS, micro-XAS, and luminescence characterization." *Geochimica et Cosmochimica Acta*, 65: 3491–3503.

Reid J.L. (**1989**). "On the total geostrophic circulation of the South Atlantic Ocean: Flow patterns, tracers, and transports." *Prog. Oceanog.*, 23: 149–244.

Reid J.L., Nowlin W.D. and Patzert W.C. (**1977**). "On the Characteristics and Circulation of the Southwestern Atlantic Ocean." *Journal of Physical Oceanography*, 7: 62–91.

Reimer P.J., Baillie M.G.L., Bard E., Bayliss A., Beck J.W., Blackwell P.G., Ramsey C.B., Buck C.E., Burr G.S., Edwards R.L. and ... M.F. (**2009**). "IntCal09 and Marine09 radiocarbon age calibration curves, 0–50,000 years cal BP." *Radiocarbon*, 51(4): 1111–1150.

Rickaby R.E.M. and Elderfield H. (**2005**). "Evidence from the high-latitude North Atlantic for variations in Antarctic Intermediate water flow during the last deglaciation." *Geochemistry Geophysics Geosystems (G^3)*, 6(5): 1–12.

Risk M.J., Heikoop J.M., Snow M.G. and Beukens R. (**2002**). "Lifespans and growth patterns of two deep-sea corals: Primnoa resedaeformis and Desmophyllum cristagalli." *Hydrobiologia*, 471: 125–131.

Robert P.J., Miranda C.F. and Muxard R. (**1969**). "Mesure de la période du protactinium 231 par microcalorimétrie." *Radiochimica Acta*, 11: 104–108.

Roberts J.M., Wheeler A., Freiwald A. and Cairns S. (**2009**). "Cold-Water Corals, The Biology and Geology of Deep-Sea Coral Habitats." *Cambridge University Press*.

Roberts J.M., Wheeler A.J. and Freiwald A. (**2006**). "Reefs of the Deep: The Biology and Geology of Cold-Water Coral Ecosystems." *Science*, 312: 543–547.

Roberts N.L., Piotrowski A.M., McManus J.F. and Keigwin L.D. (**2010**). "Synchronous Deglacial Overturning and Water Mass Source Changes." *Science*, 327: 75–78.

Robinson L. and Siddall M. (**2012**). "Palaeoceanography: motivations and challenges for the future." *Phil. Trans. R. Soc. A*, 370: 5540–5566.

Robinson L.F., Adkins J.F., Fernandez D.P., Burnett D.S., Wang S.L., C.Gagnon A. and Krakauer N. (**2006**). "Primary U distribution in scleractinian corals and its implications for U series dating." *Geochemistry Geophysics Geosystems (G^3)*, 7(5): 1–20.

Robinson L.F., Adkins J.F., Keigwin L.D., Southon J., Fernandez D.P., Wang S.L. and Scheirer D.S. (**2005**). "Radiocarbon Variability in the Western North Atlantic During the Last Deglaciation." *Science*, 310: 1469–1473.

Robinson L.F., Belshaw N.S. and Henderson G.M. (**2004**). "U and Th concentrations and isotope ratios in modern carbonates and waters from the Bahamas." *Geochimica et Cosmochimica Acta*, 68(8): 1777–1789.

Robinson L.F., Henderson G.M., Hall L. and Matthews I. (**2004**). "Climatic Control of Riverine and Seawater Uranium-Isotope Ratios." *Science*, 305: 851–855.

Roche D., Paillard D. and Cortijo E. (**2004**). "Constraints on the duration and freshwater release of Heinrich event 4 through isotope modelling." *Nature*, 432: 379–382.

Rogers A.D. (**1999**). "The biology of Lophelia pertusa (Linnaeus, 1758) and other deep-water reef-forming corals and impacts from human activities." *International Review of Hydrobiology*, 84: 315–406.

Rollion-Bard C., Blamart D., Cuif J.P. and Dauphin Y. (**2010**). "In situ measurements of oxygen isotopic composition in deep-sea coral, Lophelia pertusa: Re-examination of the current geochemical models of biomineralization." *Geochimica et Cosmochimica Acta*, 74: 1338–1349.

Roy-Barman M., Chen J.H. and Wasserburg G.J. (**1996**). "^{230}Th-^{232}Th systematics in the central Pacific Ocean: The sources and the fates of thorium." *Earth and Planetary Science Letters*, 139: 351–363.

Ruckelshausen M. (**2009**). "Rekonstruktion von Tiefenwasseraltern während der Heinrich-Ereignisse H1 und H2 anhand von Tiefseekorallen vor Brasilien." Master's thesis, Ruprecht-Karls-Universität Heidelberg.

Rudge J.F., Kleine T. and Bourdon B. (**2010**). "Broad bounds on Earth's accretion and core formation constrained by geochemical models." *Nature Geoscience*, 3: 439–443.

Russell A.D., Emerson S., Mix A.C. and Peterson L.C. (**1996**). "The use of foraminiferal uranium/calcium ratios as an indicator of changes in seawater uranium content." *Paleoceanography*, 11: 649–664.

Russell A.D., Emerson S., Nelson B.K., Erez J. and Lea D.W. (**1994**). "Uranium in foraminiferal calcite as a recorder of seawater uranium concentrations." *Geochimica et Cosmochimica Acta*, 58: 671–681.

Santos G.M., Moore R.B., Southon J.R., Griffin S., Hinger E. and Zhang D. (**2007**). "AMS ^{14}C sample preparation at the KCCAMS/UCI facility: status report and performance of small samples." *Radiocarbon*, 49: 255–269.

Saraceno M., Provost C., Piola A.R., Bava J. and Gagliardini A. (**2004**). "Brazil Malvinas Frontal System as seen from 9 years of advanced very high resolution radiometer data." *Journal of Geophysical Research (Oceans)*, 109: 5027.

Sarmiento J.L. and Gruber N. (**2004**). "Ocean Biogeochemical Dynamics." *Princeton University Press (In preparation)*: 1–275.

Sarmiento J.L. and Gruber N. (**2006**). "Ocean Biogeochemical Dynamics." *Princeton University Press*: 503pp.

Sarmiento J.L., Gruber N., Brzezinski M.A. and Dunne J.P. (**2004**). "High-latitude controls of thermocline nutrients and low latitude biological productivity." *Nature*, 427: 56–60.

Sarnthein M., Winn K., Jung S.J.A., Duplessy J.C., Labeyrie L., Erlenkeuser H. and Ganssen G. (**1994**). "Changes in east Atlantic deepwater circulation over the last 30,000 years: Eight time slice reconstructions." *Paleoceanography*, 9(2): 209–267.

Schiff J.L. (**1999**). "The Laplace Transform: Theory and Applications." *Springer-Verlag, Heidelberg*: 1–245.

Schimel D., Enting I., Heimann M., Wigley T., Raynaud D., Alves D. and Siegenthaler U. (**1995**). "The global carbon cycle. In: Houghton et al., editors. Climate change 1994: radiative forcing of climate change and an evaluation of the IPCC IS92 emission scenarios." *Cambridge University Press*: 35–71.

Schlitzer R. (**2012**). "Ocean Data View." *http://odv.awi.de*.

Schmid C., Schäfer H., Zenk W. and Podestá G. (**1995**). "The Vitória Eddy and Its Relation to the Brazil Current." *Journal of Physical Oceanography*, 25: 2532–2546.

Schmitt J., Schneider R., Elsig J., Leuenberger D., Lourantou A., Chappellaz J., Köhler P., Joos F., Stocker T.F., Leuenberger M. and Fischer H. (**2012**).

"Carbon Isotope Constraints on the Deglacial CO_2 Rise from Ice Cores." *Science*, 336: 711–.

Scholz D. (**2005**). "U-series dating of diagenetically altered fossil reef corals and the application for sea level reconstructions." Ph.D. thesis, Universität Heidelberg.

Shackleton N.J. (**1974**). "Attainment of isotopic equilibrium between ocean water and benthonic foraminifera genus Uvigerina: isotopic changes in the ocean during the last glacial." *Les Méth Quant Étude Variation Climat Au Cours Du Pleistocène, Coll Int CNRS*, 219: 203–209.

Shackleton N.J., Duplessy J.C., Arnold M., Maurice P., Hall M.A. and Cartlidge J. (**1988**). "Radiocarbon age of last glacial Pacific deep water." *Nature*, 335: 708–711.

Shen G.T. and Boyle E.A. (**1988**). "Determination of lead, cadmium and other trace metals in annually-banded corals." *Chemical Geology*, 67: 47–62.

Shen G.T. and Dunbar R.B. (**1995**). "Environmental controls on uranium in reef corals." *Geochimica et Cosmochimica Acta*, 59(10): 2009–2024.

Sherwood O.A., Scott D.B., Risk M.J. and Guilderson T.P. (**2005**). "Radiocarbon evidence for annual growth rings in the deep-sea octocoral Primnoa resedaeformis." *Marine Ecology Progress Series*, 301: 129–134.

Shirai K., Kusakabe M., Nakai S., Ishii T., Watanabe T., Hiyagon H. and Sano Y. (**2005**). "Deep-sea coral geochemistry: Implication for the vital effect." *Chemical Geology*, 224: 212–222.

Siegenthaler U., Stocker T.F., Monnin E., Lüthi D., Schwander J., Stauffer B., Raynaud D., Barnola J.M., Fischer H., Masson-Delmotte V. and Jouzel J. (**2005**). "Stable Carbon Cycle-Climate Relationship During the Late Pleistocene." *Science*, 310: 1313–1317.

Sigman D.M. and Boyle E.A. (**2000**). "Glacial/interglacial variations in atmospheric carbon dioxide." *Nature*, 407: 859–869.

Signorini S. (**1978**). "On the circulation and the volume transport of the Brazil Current between the Cape of São Tomé and Guanabara Bay." *Deep Sea Research Part II: Topical Studies in Oceanography*, 25: 481–490.

Silva C.L., Lorenzzetti J., Rosa S.M., Stech J.L. and Araujo C.E.S. (**1994**). "An analysis of AVHRR thermal images of cold oceanic eddies in Cabo Frio region." *Symposium Resource and Environmental Monitoring, Rio de Janeiro, Annals.*

Skinner L.C., Fallon S., Waelbroeck C., Michel E. and Barker S. (**2010**). "Ventilation of the Deep Southern Ocean and Deglacial CO_2 Rise." *Science*, 328: 1147–1151.

Skinner L.C. and Shackleton N.J. (**2004**). "Rapid transient changes in northeast Atlantic deep water ventilation age across Termination I." *Paleoceanography*, 19: 2005.

Sloyan B.M. and Rintoul S.R. (**2001**). "Circulation, Renewal, and Modification of Antarctic Mode and Intermediate Water." *Journal of Physical Oceanography*, 31: 1005–1030.

Smith S.D., Muench R.D. and Pease C.H. (**1990**). "Polynyas and leads: An overview of physical processes and environment." *Journal of Geophysical Research*, 95: 9461–9479.

Sortor R.N. and Lund D.C. (**2011**). "No evidence for a deglacial intermediate water Δ^{14}C anomaly in the SW Atlantic." *Earth and Planetary Science Letters*, 310: 65–72.

Spero H.J. and Lea D.W. (**2002**). "The Cause of Carbon Isotope Minimum Events on Glacial Terminations." *Science*, 296: 522–525.

Spiro B., Roberts M., Gage J. and Chenery S. (**2000**). "^{18}O/^{16}O and ^{13}C/^{12}C in an ahermatypic deep-water coral Lophelia pertusa from the North Atlantic: a case of disequilibrium isotope fractionation." *Rapid Communications in Mass Spectrometry*, 14: 1332–1336.

Starik I.E. and Kolyadin L.B. (**1957**). "The occurrence of uranium in ocean water." *Geochemistry*, 3: 245–256.

Stein M., Wasserburg G.J., Lajoie K.R. and Chen J.H. (**1991**). "U-series ages of solitary corals from the California coast by mass spectrometry." *Geochimica et Cosmochimica Acta*, 55(12): 3709–3722.

Stirling C.H., Esat T.M., McCulloch M.T. and Lambeck K. (**1995**). "High-precision U-series dating of corals from Western Australia and implications for the timing and duration of the Last Interglacial." *Earth and Planetary Science Letters*, 135: 115–130.

Stocker T.F. and Wright D.G. (**1991**). "Rapid transitions of the ocean's deep circulation induced by changes in surface water fluxes." *Nature*, 351: 729–732.

Stommel H. (**1961**). "Thermohaline Convection with Two Stable Regimes of Flow." *Tellus*, 13(2): 225–230.

Stott L., Southon J., Timmermann A. and Koutavas4 A. (**2009**). "Radiocarbon age anomaly at intermediate water depth in the Pacific Ocean during the last deglaciation." *Paleoceanography*, 24: 1–10.

Stuiver M. (**1961**). "Variations in Radiocarbon Concentration and Sunspot Activity." *Journal of Geophysical Research*, 66(1): 273–276.

Stuiver M. and Polach H.A. (**1977**). "Radiocarbon." *Radiocarbon*, 19(3): 355–363.

Stuiver M. and Quary P.D. (**1980**). "Changes in Atmospheric Carbon-14 Attributed to a Variable Sun." *Science*, 207: 11–19.

Sumida P.Y.G., Yoshinaga M.Y., Madureira L.A.S.P. and Hovland M. (**2004**). "Seabed pockmarks associated with deepwater corals off SE Brazilian continental slope, Santos Basin." *Marine Geology*, 207: 159–167.

Sverdrup H.U., Johnson M.W. and Hemming R.H. (**1942**). "The Oceans." *Prentice-Hall, Englewood Cliffs, N.J.*: 1087pp.

Swart P.K. and Hubbard J.A.E.B. (**1982**). "Uranium in Scleractinian Coral Skeletons." *Coral Reefs*, 1: 13–19.

Szabo B.J., Ludwig K.R., Muhs D.R. and Simmons K.R. (**1994**). "Thorium-230 ages of corals and duration of the last interglacial sea-level high stand on Oahu, Hawaii." *Science*, 266: 93–96.

Tachikawa K., Athias V. and Jeandel C. (**2003**). "Neodymium budget in the modern ocean and paleo-oceanographic implications." *Journal of Geophysical Research (Oceans)*, 108: 3254+.

Taviani M., Freiwald A. and Zibrowius H. (**2005**). "Deep coral growth in the Mediterranean Sea: an overview. In: A. Freiwald & J. M. Roberts (eds). Cold-water corals and Ecosystems." *Springer-Verlag*: 137–156.

Taylor R.E. (**1987**). "Radiocarbon dating. An Archaeological Perspective." *Academic Press, London*: 224.

Taylor S.R. and McLennan S.M. (**1985**). "The continental crust: its composition and evolution." *Scientific Publication, Oxford.*

Teichert B.M.A., Eisenhauer A., Bohrmann G., Haase-Schramm A., Bock B. and Linke P. (**2003**). "U/Th systematics and ages of authigenic carbonates from Hydrate Ridge, Cascadia Margin: recorders of fluid flow variations." *Geochimica et Cosmochimica Acta*, 67: 3845–3857.

Toledo F.A.L., Cachao M., Costa K.B. and Pivel M.A.G. (**2007**). "Planktonic foraminifera, calcareous nannoplankton and ascidian variations during the last 25 kyr in the Southwestern Atlantic: A paleoproductivity signature?" *Marine Micropaleontology*, 64: 67–79.

Torres L.C., Jeck I.K., Alberoni A.A.L. and Villena H.H. (**2010**). "Brazilian Southern Margin: An example of the Identification of the Base of the Slope on a Passive Continental Margin." *session paper*: 12pp.

Tucker M. (**1988**). "Techniques in Sedimentology." *Blackwell Scientific, Publications, Oxford*: 394pp.

Turekian K.K. and Chan L.H. (**1971**). "The marine geochemistry of the uranium isotopes ^{230}Th and ^{2}31Pa." *Activation Analysis in Geochemistry and Cosmochemistry, edited by A. O. Brunfelt and E. Steinnes, Oslo Univerity Press*: 69–102.

Unkel I. (**2006**). "AMS-^{14}C-Analysen zur Rekonstruktion der Landschafts- und Kulturgeschichte in der Region Palpa (S-Peru)." Ph.D. thesis, Universität Heidelberg.

van de Flierdt T. and Frank M. (**2010**). "Neodymium isotopes in paleoceanography." *Quaternary Science Reviews*, 29: 2439–2441.

van de Flierdt T., Robinson L.F. and Adkins J.F. (**2010**). "Deep-sea coral aragonite as a recorder for the neodymium isotopic composition of seawater." *Geochimica et Cosmochimica Acta*, 74: 6014–6032.

van de Flierdt T., Robinson L.F., Adkins J.F., Hemming S.R. and Goldstein S.L. (**2006**). "Temporal stability of the neodymium isotope signature of the Holocene to glacial North Atlantic." *Paleoceanography*, 21(26): 4102+.

van der Loeff M.M.R. and Berger G.W. (**1993**). "Scavenging of ^{230}Th and ^{231}Pa near the Antarctic Polar Front in the South Atlantic." *Deep-Sea Research I*, 40(2): 339–357.

Viana A., Faugeres J.C., Kowsmann R.O., Lima J.A.M., Caddah L.F.G. and Rizzo J.G. (**1998**). "Hydrology, morphology and sedimentology of the Campos continental margin, offshore Brazil." *Sedimentary Geology*, 115: 133–157.

Viana A.R. (**1994**). "Deep water coral mounds along the southeastern Brazilian continental slope." *paper presented at 14th Int. Sedimentol. Congr., Int. Assoc. Sedimentol.*

Vogler S., Scholten J., van der Loeff M.R. and Mangini A. (**1998**). "^{230}Th in the eastern North Atlantic: the importance of water mass ventilation in the balance of ^{230}Th." *Earth and Planetary Science Letters*, 156: 61–74.

Vogt C., Lauterjung J. and Fischer R.X. (**2002**). "Investigation of the clay fraction (< 2 μm) of the clay mineral society reference clays." *Clays and Clay Minerals*, 50(3): 388–400.

von Blanckenburg F. (**1999**). "Tracing Past Ocean Circulation?" *Science*, 286(5446): 1862–1863.

Wacker L., Christl M. and Synal H.A. (**2010**). "Bats: A new tool for AMS data reduction." *Nuclear Instruments and Methods in Physics Research B*, 268: 976–979.

White W.M. (**2003**). "Geochronology III, The Sm-Nd system." *Geol. 655 Isotope Geochemistry Lecture, http://www.geo.cornell.edu/geology/classes/Geo656/656notes03/656%2003Lecture07.pdf*: 46–50.

Whiticar M.J. (**1999**). "Carbon and hydrogen isotope systematics of bacterial formation and oxidation of methane." *Chemical Geology*, 161: 291–314.

Wilson D.J., Piotrowski A.M., Galy A. and Clegg J.A. (**2013**). "Reactivity of neodymium carriers in deep sea sediments: Implications for boundary exchange and paleoceanography." *Geochimica et Cosmochimica Acta*, 109: 197–221.

Wilson J.B. (**1979**a). "Distribution of the coral Lophelia pertusa (L.) [L. prolifera (Pallas)] in the north-east Atlantic." *Journal of the Marine Biological Association of the United Kingdom*, 59(1): 149–164.

Wilson J.B. (**1979**b). "'Patch' development of the deep-water coral Lophelia Pertusa (L.) on Rockall Bank." *Journal of the Marine Biological Association of the United Kingdom*, 59(1): 165–177.

Wirsig C. (**2010**). "Uran-Thorium Datierung authigener Carbonate von Cold Seeps aus dem Campos Becken, Brasilien." Master's thesis, Ruprecht-Karls-Universität Heidelberg.

Wirsig C., Kowsmann R.O., Miller D.J., de Oliveira Godoy J.M. and Mangini A. (**2012**). "U/Th-dating and post-depositional alteration of a cold seep carbonate chimney from the Campos Basin offshore Brazil." *Marine Geology*, 329–331: 24–33.

Worthington L.V. (**1976**). "On the North Atlantic Circulation." *Johns Hopkins University Press*, 6: 110pp.

Xie R.C., Marcantonio F. and Schmidt M.W. (**2012**). "Deglacial variability of Antarctic Intermediate Water penetration into the North Atlantic from authigenic neodymium isotope ratios." *Paleoceanography*, 27: 3221.

Yu E.F., Francois R. and Bacon M.P. (**1996**). "Similar rates of modern and last-glacial ocean thermohaline circulation inferred from radiochemical data." *Nature*, 379: 689–694.